Volume 8 • No 2 • Dec 2020 • ARO ISSN: 2410-9355 • DOI: 10.14500/2307-549X

ARO

The Scientific Journal of Koya University

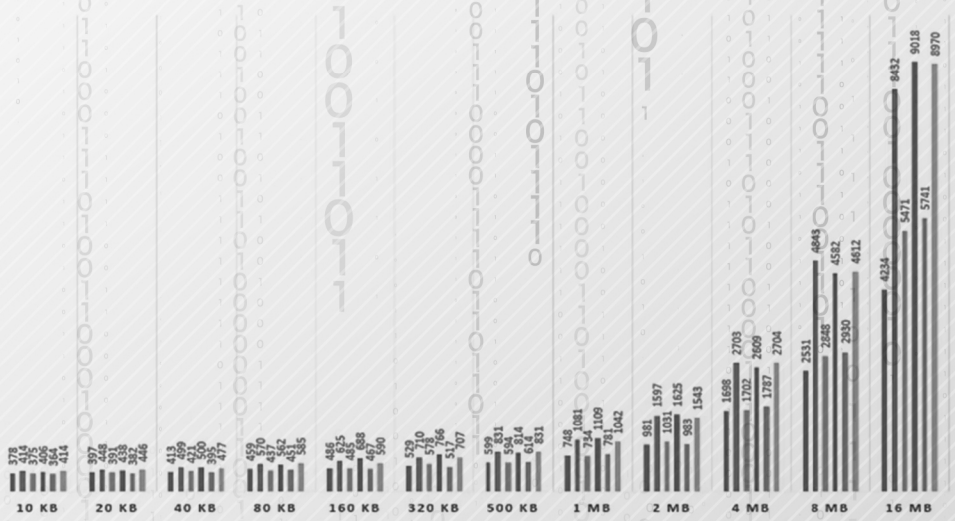

Extraction and Determination of Oxymatrine Pesticide in Environmental Sample and in its Formulation using High-Performance Liquid Chromatography . Spectrophotometric Indirect Determination of Captopril through Redox Reaction with n-bromosuccinimide and RB dye in Pharmaceutical Products . Land Surface Temperature Anomalies Detection for the Strong Earthquakes in 2018 . Calculation of Electron Swarm Parameters in Tetrafluoromethane . Mechanical Response of PbSSe, PbSTe Ternary and PbSnSTe Quaternary Alloys at High Pressure . Integrating Enterprise Resource Planning with the Organizations' Management Structure for Decision-Making . Cloud Storage Protection Scheme Based on Fully Homomorphic Encryption . Assessment of Curing Exposures Effect on the Long-term Engineering Properties of Novel Lightweight Aggregate Concrete . Influence of Natural Fibers on the Performance of Hot Mix Asphalt for the Wearing Course of Pavement . Bacterial Profile and Antimicrobial Susceptibility of Isolates Recovered from Lower Respiratory Tract Infection for Patients in Rizgary Hospital, Erbil . An Area-efficient Microstrip Diplexer with a Novel Structure and Low Group Delay for Microwave Wireless Applications . The Effects of Amine Type and Lean Amine Temperature on Gas Sweetening Processes . New Fluorescence Quenching Approach for Determination of Valsartan in Certain Tablets and Spiked Biological Fluids .

KOYA UNIVERSITY

ISSN: 2410-9355 (printed version) ISSN: 2307-549X (electronic version)
ARO - DOI: 10.14500/2307-549X

ARO-The Scientific Journal of Koya University

The ARO ("Today" in Hewramí Kurdish), is an international scientific journal published by the Koya University with p-ISSN: 2410-9355, e-ISSN: 2307-549X and DOI: 10.14500/2307-549X. ARO is a journal of original scientific research, global news, and commentary. The ARO Scientific Journal is a peer-reviewed, open access journal that publishes original research articles as well as review articles in areas of Science, Engineering and Technology.

ARO the Scientific Journal Office

Koya University, University Park
Danielle Mitterrand Boulevard, Koya KOY45
Kurdistan Region - F.R. Iraq

Tel.: +964 (0) 748 012 7423
Mobile: +964 (0) 750 187 5489
E-mail: aro.journal@koyauniversity.org
url: aro.koyauniversity.org

December 2020

ARO

The Scientific Journal of Koya University

Vol VIII, No 2(2020)

Contents

DOI: 10.14500/2307-549X ARO p-ISSN: 2410-9355, e-ISSN: 2307-549X

ARO Editorial Words

Dear readers,

Aro, the Scientific Journal of Koya University, is closing its issue fifteenth (Vol VIII, No 2, 2020). It has been an exciting and yet dynamic season for our journal. Aro is publishing its 15th issue as an internationally listed Scientific Journal in Kurdistan Region of Iraq. Notably, Aro has been accepted for indexing in the Emerging Sources Citation Index (ESCI), a new edition of Web of Science™ as of Feb 2016. Content in this index is under consideration by Clarivate Analytics to be accepted in the Science Citation Index Expanded™ (SCIE). Aro's individual articles are currently listed by Web of Science™ core collection using articles unique DOI numbers which is a historical achievement for our academic community. Aro is starting its seven-year journey in leading the quality of regional scientific publications with global impact. The editorial team have been working tirelessly to keep the novel mission and sustain Aro's future publications with greater impacts and citations. It is exciting that Aro has been awarded to DOAJ Seal listing which is an indication of a trusted high standard open access scientific work. The upcoming new season will be an even more exciting period in Aro's life as Thomson Reuters will examine our journal for a full permanent listing.

Aro continues its mission to provide resources, support and advice for researchers in the process of publishing their scientific papers, while at the same time offering free public access to scientific research by open online access. This is a daunting task which we hope to advance in the years to come. Thus, in the sections to follow, we would like to share and elaborate on the core elements that constitute Aro. However, finding reliable and skilled reviewers remain a big challenge for us.

Aro was created with a long-term vision of becoming accessible to all researchers in Kurdistan and beyond, and covering a wide range of scholarly disciplines in sciences. Aro is a peer-reviewed, open access journal that publishes original scientific research articles, global news, letters and commentary as well as review articles in areas of natural sciences and technology. In this issue, you will have access to original research papers in a variety of areas, such as Physics, Chemistry, Biology, Material Science, Civil Engineering, Software Engineering, Electrical and Electronics Engineering.

The great responses from researchers, academics and professionals in the past seven years have made us create a wider Editorial Board which serves the wider submitted scientific manuscripts. However, it is clear that having a dedicated and well-organised editorial board for the journal is only one side of the coin. The other is the ability to attract submissions of quality research and scholarly work. We are thankful to all of those who put their trust in Aro and presented their original research work for publication in Vol VIII, No 2 (2020) of the journal, as well as, our thanks are extended to the 30 peer-reviewers from the Universities worldwide for their efforts in reviewing and enabling this issue of Aro.

Your support and feedback are invited and appreciated.

Dilan M. Rostam
Editor-in-Chief

Wali M Hamad
Executive Publisher

Dilan M. Rostam, Salah I. Yahya, Basim M. Fadhil, Fahmi F. Muhammad, Mohammed H. Zangana, Jorge Correia, Fouad Mohammed, Jacek Binda Nadhir Al-Ansari, Howri Mansurbeg, Tara F. Tahir and Yazen A. Khaleel
Executive Editorial Board

DOI: 10.14500/2307-549X ARO p-ISSN: 2410-9355, e-ISSN: 2307-549X

Extraction and Determination of Oxymatrine Pesticide in Environmental Sample and in its Formulation using High-Performance Liquid Chromatography

Ihsan M. Shaheed[1] and Saadiyah A. Dhahir[2]

[1]Department of Chemistry, Faculty of Science, University of Baghdad, Baghdad, Iraq

[2]Department of Chemistry, Faculty of Science for Women, University of Baghdad, Baghdad, Iraq

***Abstract*—The quinolizidine alkaloid compound, oxymatrine pesticide, was analysis in the river water samples collected from different agriculture areas in the Iraqi city of Kerbala and also in its formulation using developed reverse-phase high-performance liquid chromatography method. Acetonitrile:methanol (60:40 v/v) was chosen as mobile phase at pH (7.0), flow rate 0.5 mL/min, and 20 μL as volume injection. Modified ecological-friendly method, dispersive liquid-liquid microextraction, was used for the extraction of oxymatrine from water samples. Linearity study was constructed from 0.1 to 70 μg/mL at λ_{max} 205 nm. The limit of detection and limit of quantification were 0.025 and 0.082 μg/mL, respectively, and the relative standard deviation (RSD) % was 0.518%. Three spiked levels of concentration (20.0, 40.0, and 70.0 μg/mL) were used for the validation method. The percentage recovery for the three spiked samples was ranged between 98.743 and 99.432 and the RSD% was between 0.051 and 0.202%, the formulation studies of oxymatrine between 99.487 and 99.798, and the RSD% was ranged from 0.045 to 0.057%. The developed method can be used accurately and selectively for the determination of oxymatrine in environmental samples and in the formulation.**

***Index Terms*—Dispersive, Oxymatrine, Reverse-phase high-performance liquid chromatography, UV visible.**

I. Introduction

Alkaloids are compound which have low molecular weight which consist of nitrogen atom in its structure. Quinolizidine alkaloids are a type which can be found in 20% of plants. These quinolizidine alkaloids play an important role as a pesticides and in biological activity as starting material instead of acetylcholine to treat senile dementia due to its binding to cholinergic receptors called nicotinic and muscarinic respecters (John, et al., 2014).

Oxymatrine, tetracycloquinolizidine (7aS,13aR,13bR,13cS) dodecahydro-1H,5H,10H-dipyrido[2,1-f:3′,2′,1′-ij][1,6] naphthyridin-10-one 4-oxide, as shown in Fig. 1, is a new extracted insecticide from the roots of *Sophora flavescens* Aiton which used as Chinese herbal to treat cooling and as an antichloristic (Li and Wang, 2004). Oxymatrine regarded as a new biopesticide, under the name Levo2.4, instead of chemical pesticides to overcome the aggregation of residual in environment (Gu, et al., 2012; Zhang, et al., 2015a; Gholam and Sadeghi, 2016). Patient who suffers from hepatitis B can sever form liver damage when they exposed to high dose of oxymatrine (Izdebska, et al., 2019).

Many techniques were reported for the analysis and determination of oxymatrine in plant as residual and in pharmaceutical preparations. Several techniques were used for the determination of oxymatrine, some of these techniques are high-performance liquid chromatography (HPLC) (Izdebska, et al., 2019; Bao, et al., 2019; Zhang, et al., 2016), liquid chromatography–mass spectroscopy (Zhang, et al., 2008; Fan, et al., 2013; Sabatino, et al., 2015; Jong, et al., 2006), capillary electrophoresis (Chen, et al., 2009; Zhang and Chen, 2013), flow injection (Cheng, et al., 2004), and microwave-assisted aqueous two-phase extraction (Zhang, et al., 2015b).

The aim of this study is to provide accurate, selective, and rapid method to the determined of oxymatrine in water samples and in its formulations used in agriculture areas under study because there is no such study which was reported in those areas for the determination of oxymatrine in spite of using this pesticide widely and repeatedly in those areas.

II. Materials and Methodologies

A. Reagent and Solutions

Oxymatrine standard (purity >99%) was purchased from Dr. Ehrenstorfer GmbH Company. All solvents (methanol,

ARO-The Scientific Journal of Koya University
Vol. VIII, No.2 (2020), Article ID: ARO.10666, 7 pages
DOI: 10.14500/aro.10666
Received 22 April 2020; Accepted 06 July 2020
Regular research paper: Published 01 September 2020
Corresponding author's e-mail: Ihsan.aldahan@uokerbala.edu.iq

 http://dx.doi.org/10.14500/aro.10666

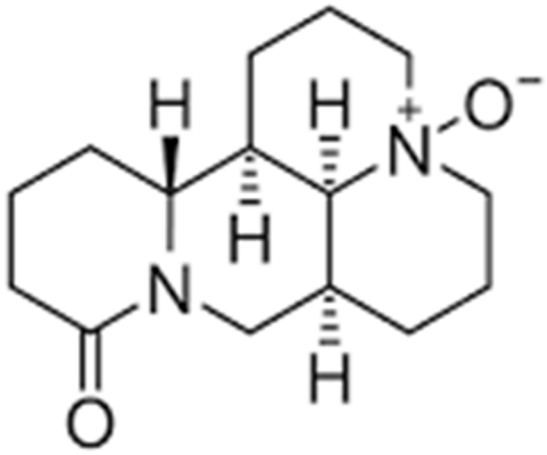

Fig. 1. Structure of oxymatrine.

acetonitrile, and water) for HPLC analysis were used from Sigma-Aldridge Company. Oxymatrine formulation (Levo2.4%) was supplied from Karbala Agriculture Department, Iraq.

B. Preparation of Standard Solutions

Oxymatrine stock standard solution 1000 μg/mL was prepared by dissolving 0.1 g in methanol with sonication and completed to the mark in 100 mL volumetric flask, then filtered through 0.45 μm Millipore filter. A series of solutions ranged from 0.1 to 200 μg/mL were prepared for calibration study. All solutions kept in 4°C until the time of analysis.

C. Preparation of Oxymatrine Formulation

A 1.0 mL of oxymatrine formulation (Levo 2.4%) was diluted to 100 mL, form this solution, further 1.0 mL was diluted to 100 mL, from the final solution, a different concentrations of formulation were prepared by diluting the calculated volumes of solution in 100 mL methanol.

D. Preparation of Sodium Hydroxide 0.1 M

Sodium hydroxide 0.1 M was prepared by dissolving 0.4 g in distilled water, then completed to 100 mL volumetric flask.

E. Preparation of Orthophosphoric Acid 0.1 M

Orthophosphoric acid was prepared by diluting 0.680 mL of concentrated orthophosphoric acid in distilled and completed the volume to 100 mL volumetric flask.

F. Preparation of Sodium Chloride (5%)

A 5.0 g of sodium chloride was dissolved in distilled water and completed to the mark in 100 mL volumetric flask.

III. Sampling

Water samples were collected from agriculture ears in Iraqi city – Kerbala at six different locations: Site I (Center of Kerbala), two agriculture eras were chosen (Al-Kadhy -8 and Al-Kamaliyah), site II (Al-Hindyia), two locations chosen (South and North Al-Manfahan), and from site III (Al-Khairat), two locations (Abu-Ruwayah and Zubaid) were collected chosen, then samples were transported in dark amber glass bottles to the laboratory under cooling conditions (4°C). All samples were filtered through 0.45 μm Nylon filter (Millipore filter) to remove any suspended particles or matrix in water samples, then the samples were stored at 4°C in the dark until the time of analysis.

IV. Modified Dispersive Liquid-Liquid Microextraction

A 5.0 mL from each water samples collected from different agriculture areas in Kerbala city, Iraq (reserved in standard conservation condition) were filtered and the supernatants were separated and transferred to a glass centrifuge test tube with screw. Each sample spiked with different concentration of oxymatrine standard (20.0, 40.0, and 60.0 μg/mL). Sodium chloride (5%) was added as salting-out agent, then a mixture of 100 μL chloroform, as dispersant agent, and 1.0 mL acetonitrile, as extraction solvent, were added, respectively. The final solution was vortexed for 1.0 min and further 10.0 min shaking by hand, then centrifuged at 5000 rpm for 15.0 min. Two phases will have separated; upper aqueous phase removed by microsyringe and organic phase contain extracted oxymatrine as fine droplets diluted with 2.0 mL methanol for HPLC analysis after filtration through 0.45 μm Millipore filter paper. Same procedure was maintained for water samples collected from different agriculture areas for Kerbala city, Iraq, without spiking to use as controller (Albaseera, et al., 2011).

V. Instrumentation

HPLC 20A equipped with UV–visible detector. Ultrasonic cleaner with heating controller, KQ200E. Shimadzu double-beam UV-spectrophotometer-1800. Digital balance, Denver-TP-214. pH meter, Hanna-pH211. Centrifuge, C2series.

VI. Method Validation

A. Wavelength Selection

From the stock solution of standard oxymatrine, 20.0 μg/mL solution was prepared for UV–visible scanning from 190 to 800 nm. It was found that standard oxymatrine has maximum absorption at 205 nm, Fig. 2.

B. Chromatographic Conditions

Analysis of oxymatrine in samples and formulation was applied using HPLC supplied with ODS-C18 column (250 cm×4.6 mm, 5 μm) and UV–visible detector. The mobile phase was acetonitrile:methanol (60:40 v/v) at pH (7). The flow rate was 0.5 mL/min and the volume of injection was 20.0 μL. The measurements were maintained at 205 nm.

VII. Results and Discussion

A. Preliminary Study

Different composition of solvents was tested as mobile phase for the best separation, good resolution, and acceptable

peak shape. Acetonitrile, methanol, and water are used alone and as a mixture with composition from 90:10 v/v to 50:50 v/v to achieve an acceptable separation, Fig. 3. The mobile phase with the ratio (60:40 v/v) was chosen for optimization due to the best separation and high response. All investigations were being under flow rate 1 mL/min and volume injection 20.0 µL at λ_{max} 205 nm. Chromatogram for blank, Fig. 4, was explained for comparison with chromatogram of oxymatrine standard.

B. Effect of pH

Mobile phase was buffered with different pH to improve the peak shape and efficiency of alkaloid (oxymatrine) separation, for that, selected mobile phase (acetonitrile:methanol 60:40 v/v) was eluted under pH ranged from 3.0 to 8.0 using 0.1 M H_3PO_4/and or 0.1 M NaOH for adjusting. Results obtained were illustrated in Table 1 and Fig. 5 for standard oxymatrine under optimized condition (pH = 7.0). In general, oxymatrine regarded as weak basic and its protonation can be altered in acidic and basic media, it was found that pH 7.0 was the best media for its separation.

Results in Table 1 and Fig. 5 explained that the separation of oxymatrine in acidic medium or high basic medium gave low intensity than in neutral medium depends on the properties of oxymatrine, for that pH (7.0) was chosen for optimization due to good resolution and acceptable values of capacity and tailing factors.

C. Effect of Flow Rate

A 20.0 µL of 20.0 µg/mL oxymatrine standard at pH (7.0) was injected to HPLC system (n=3) at various flow rates ranged from 0.3 to 1.5 mL/min.

TABLE I
EFFECT OF PH

pH	Peak area	Resolution (R)	Capacity (k)	Tailing factor (TF)
3.0	18,544	20.897	2.260	1.122
4.0	17,499	18.560	1.645	1.134
5.0	20,270	20.943	2.230	1.124
6.0	23,251	20.232	2.133	1.031
7.0	25,960	13.051	1.231	1.041
8.0	22,132	17.238	1.521	1.105

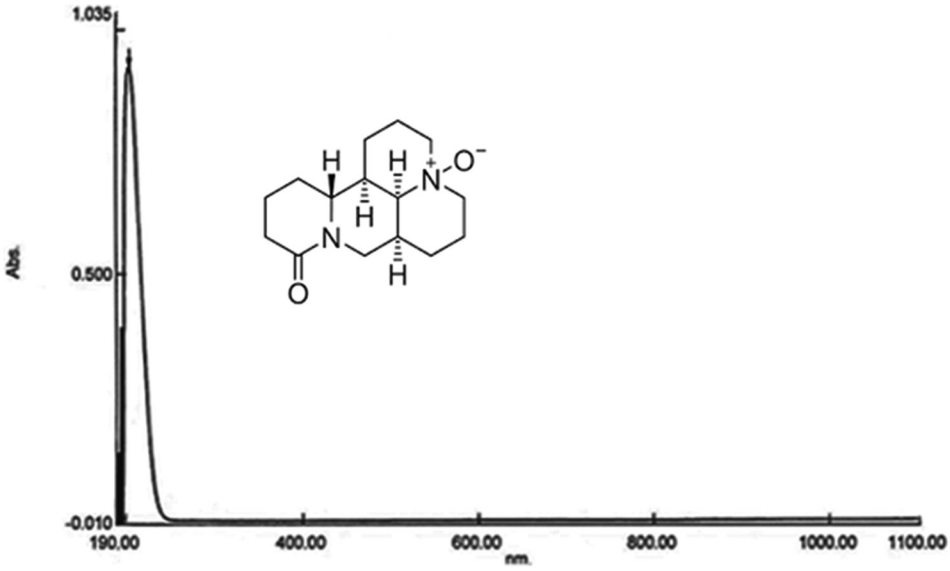

Fig. 2. UV–visible spectra for standard oxymatrine.

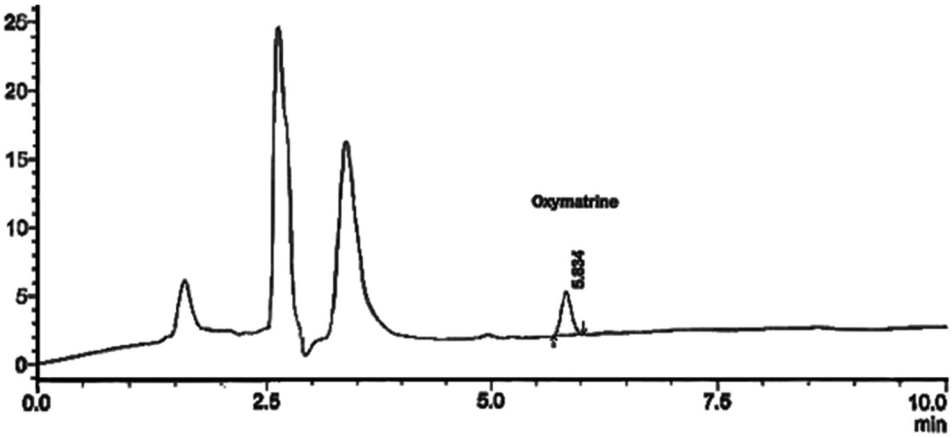

Fig. 3. Chromatogram of oxymatrine standard.

http://dx.doi.org/10.14500/aro.10666

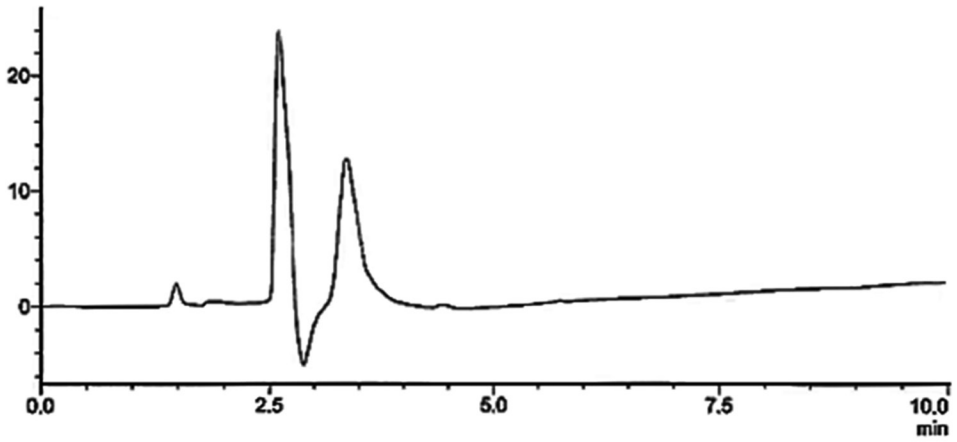

Fig. 4. Chromatogram of Blank.

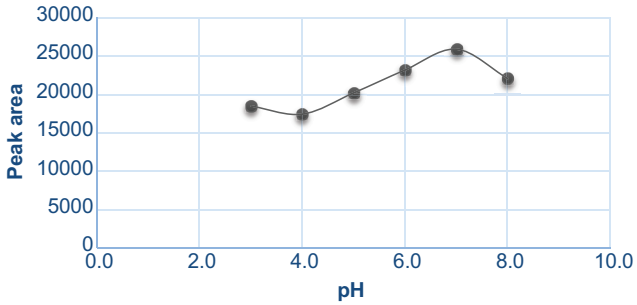

Fig. 5. Effect of pH.

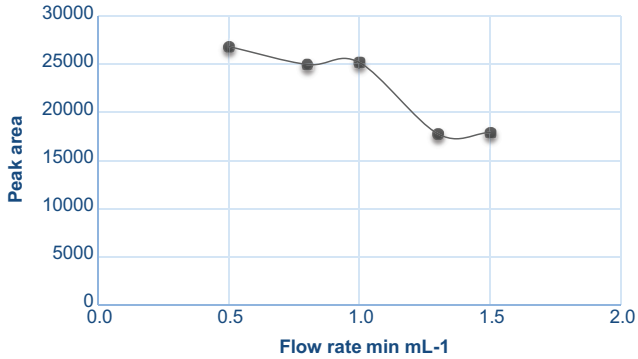

Fig. 6. Effect of flow rate.

Injection of oxymatrine standard into HPLC system at different flow rate explained that at 0.3 mL/min too long time for analysis was required (Table 2 and Fig. 6). Flow rate at 0.5 mL/min maintained high response with good capacity factor and low tailing factor after that the response decreases up to 1.5 mL/min. For that, 0.5 mL/min was chosen for oxymatrine determination.

D. Effect of Volume Injection

A 20.0 µL of 20.0 µg/mL of oxymatrine standard under optimized conditions of pH and flow rate was injected (n=3) to achieve the best separation.

From results shown in Table 3 and Fig. 7, increasing the injected volume of oxymatrine standard up to 20.0 µL led to increase the response systematically without overloaded of the column and without affecting the capacity factor of the shape of chromatogram.

TABLE II
Effect of Flow Rate

Flow rate mL/min	Peak area	Resolution (R)	Capacity	Tailing factor (TF)
0.3	No detection till 20 min			
0.5	26,048	10.643	2.963	1.123
0.8	25,001	9.953	2.787	1.129
1.0	25,193	8.983	1.196	1.135
1.3	17,783	8.179	1.614	1.152
1.5	17,931	7.421	1.648	1.182

TABLE III
Effect of Volume Injection

Volume injection (µL)	Area	Resolution (R)	Capacity (k)	Tailing factor (TF)
5	9502	9.117	3.061	1.100
10	15,348	9.043	3.008	1.132
15	20,771	8.681	2.993	1.119
20	26,855	10.643	2.963	1.023

TABLE IV
Statistical Data Analysis of Determination of Oxymatrine

Parameter	Results
λ max (nm)	205
Correlation coefficient	0.9999
Linearity range (µg/mL)	0.1–70
Limit of detection[a] (µg/mL)	0.024
Limit of quantification[b] (µg/mL)	0.082
Regression equation	y=1219.6x+1853.1
Slope	1219.6
Recovery %	100.002%
RSD%	0.518
C.L[c] for 0.5 µg/mL	0.498±0.004
C.L for 10.0 µg/mL	10.134±0.013
C.L for 50.0 µg/mL	49.757±0.020

[a]LOD=(SD/S)×3. [b]LOQ=(SD/S)×10. Where, SD is the standard deviation, S is the slope of calibration curve (Li, et al., 2016). [c]CL=$\bar{X}$±t (SD/(n)$^{(1/2)}$). Where, $\bar{X}$ is rate of measurement, t is the t-test at n-1 from degree of freedom at 95%, *N* number of sample (number of degree of freedom) (19). [d]RSD%=(SD/$\bar{X}$)×100. LOD: Limit of detection, LOQ: Limit of quantification, SD: Confidence limit, RSD: Relative standard deviation

E. Linearity Curve

A series of solution with different concentration ranged from 0.1 to 200 µg/mL were prepared for the calibration study at optimized conditions. The calibration curve obtained by plotting the peak area of injected solutions (n=3) against the concentration. Linearity was achieved in the range from 0.1 to 70 µg/mL, Fig. 8, after that increasing the concentration led to deviation from Beer's low. All results related to calibration curve study are sorted in Table 4.

VIII. Validation Method

Validation of method was a proved in term of accuracy and precision. Accuracy was represented by recovery percentage value and precision by relative standard deviation (RSD) %. Three different concentrations of prepared oxymatrine standards were injected (n=5) into HPLC system under optimized condition for validation studies. Results are illustrated in Table 5.

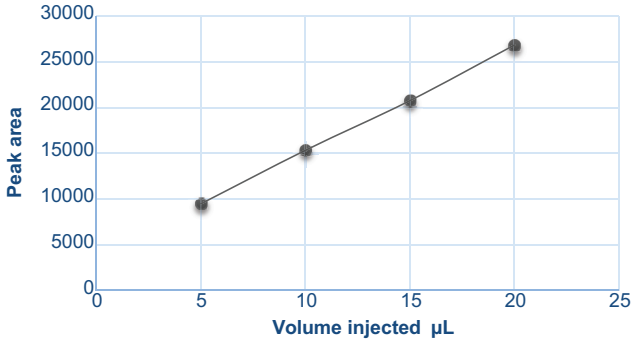

Fig. 7. Effect of volume injection.

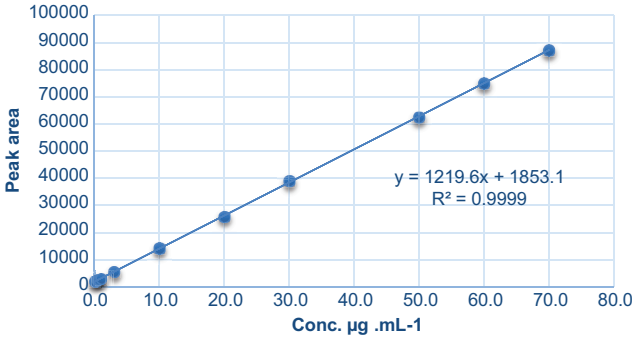

Fig. 8. Calibration curve of oxymatrine.

IX. Applications

The proposed method was applied for the determination of oxymatrine in spiked water samples with different concentration and also its formulation. The results are shown in Tables 6, 7 and Figs. 9-13. Values of recoveries (98.745–99.432) and RSD% (0.202–0.064) obtained for the determination of oxymatrine in spiked water samples in addition to the acceptable values of recovery and RSD% for oxymatrine in its formulation approved that the method was prices and accurate.

Results in Tables 6, 7 and Figs. 9, 10 explained that the applied method was accurate and selective for the

TABLE V
Accuracy and Precision of Determination of Oxymatrine Standards

Concentration (µg/mL)	Found (µg/mL) (n=5)	Recovery% (n=5)	RSD% (n=5)
0.5	0.465	93.096	0.698
10.0	10.109	101.078	0.107
50.0	49.752	99.505	0.033

TABLE VI
Determination of Oxymatrine in Spiked Samples

Added (µg/mL)	Found (µg/mL) (n=5)	Recovery % (n=5)	RSD% (n=5)
20	19.748	98.745	0.202
40	39.772	99.432	0.051
70	69.236	98.908	0.064

TABLE VII
Determination of Oxymatrine in Formulation

Added (µg/mL)	Found (µg/mL)	Recovery % (n=5)	RSD% (n=5)
30	29.846	99.487	0.057
60	59.879	99.798	0.045

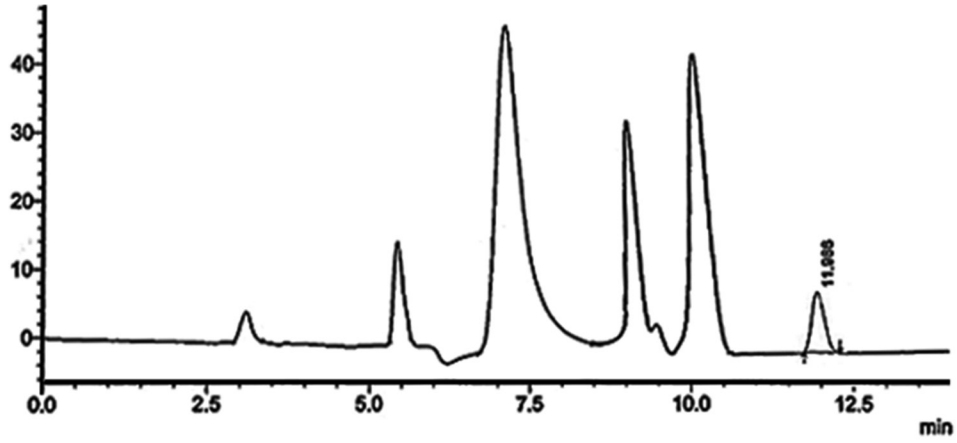

Fig. 9. Chromatograms for spiked water samples with 20.0 µg/mL oxymatrine.

http://dx.doi.org/10.14500/aro.10666

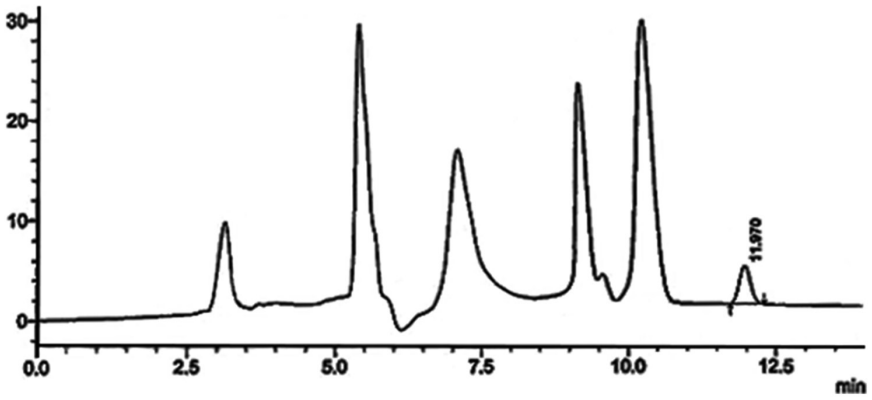

Fig. 10. Chromatograms for spiked water samples with 40 µg/mL oxymatrine.

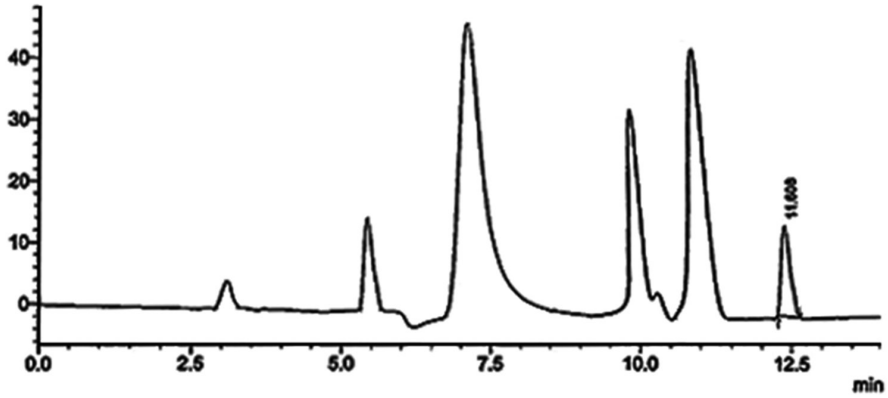

Fig. 11. Chromatograms for spiked water samples with 40.0 µg/mL oxymatrine.

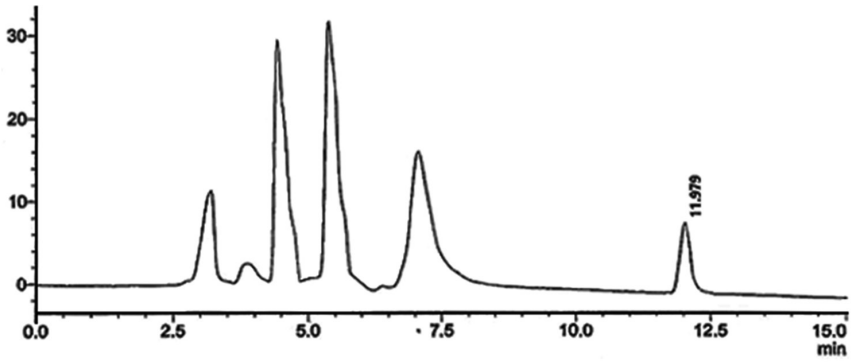

Fig. 12. Chromatograms for 30.0 µg/mL oxymatrine formulations.

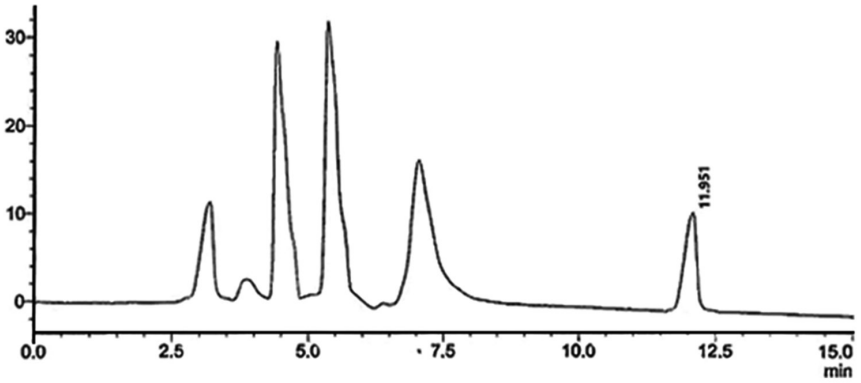

Fig. 13. Chromatograms for 60.0 µg/mL oxymatrine formulations.

determination of oxymatrine in spiked water samples and formulation.

X. Conclusion

Although this pesticide is widely and repeatedly used in the treatment of crops in the regions from which the samples collected, which may cause the accumulation of oxymatrine in water samples, leading to influence farmers in those areas, the applied method explained that there is no high level of oxymatrine residual in all water samples collected from those different agriculture areas in Kerbala city, Iraq. On the other hand, high accuracy was obtained for the determination of oxymatrine in spiked water samples and also in the formulation of oxymatrine that used in the field, as a result this method can be used successfully to follow up oxymatrine residual in the environmental samples.

Acknowledgment

The authors are grateful for the facilities provided by department of chemistry, college of science for women and thank Kerbala department of agriculture, Iraq, for providing information about the agriculture area in which oxymatrine used as pesticides against insects.

References

Albaseera, S.S., Raob, R.N., Swamyc, Y. and Mukkantia, K., 2011. Optimization of dispersive liquid liquid microextraction of pyrethroid insecticides from aqueous samples for determination by reversed-phase high performance liquid chromatography. *Global Journal of Analytical Chemistry*, 2(5), pp.224-231.

Bao, H., Chi, J., Yang, H., Liu, F., Fang, K. and Xu, Y., 2019. Simultaneous determination of six active components in danggui kushen pills via quantitative analysis of multicomponents by single marker. *Journal of Analytical Methods in Chemistry*, 2019, p.9620571.

Chen, Q., Li, P., Cheng, F., Li, B., Wu, S. and He, J., 2009. Nonaqueous CE for rapid and sensitive determination of matrine and oxymatrine in *Sophora flavescens* and its medicinal preparations. *Chromatographia*, 69, pp.1443-1446.

Cheng, Y., Chen, H., LI, Y., Chen, X. and Hu, Z., 2004. Separation and determination of aloperine, sophoridine, matrine and oxymatrine by combination of flow injection with microfluidic capillary electrophoresis. *Talanta*, 63, pp.491-496.

Fan, R., Liu, R., Ma, R., Bi, K. and Li, Q., 2013. Determination of oxymatrine and its active metabolite matrine in human plasma after administration of oxymatrine oral solution by high-performance liquid chromatography coupled with mass spectrometry. *Fitoterapia*, 89, pp.271-277.

Gholam, Z. and Sadeghi, A., 2016. Management strategies for western flower thrips in vegetable greenhouses in Iran: A review. *Plant Protection Science*, 52, pp.87-98.

Gu, X.B., Yang, X.J., Zhong, H., Lu, Z.H., Zhang, B., Zhu, Y.F., Wu, H.Y., Jiang, Y.M., Chen, H.K. and Hao, P., 2012. Effect of oxymatrine on specific cytotoxic T lymphocyte surface programmed death receptor-1 expression in patients with chronic hepatitis B. *Chinese Medical Journal*, 125, pp.1434-1438.

Izdebska, M., Zielińska, W., Hałas-Wiśniewska, M., Mikołajczyk, K. and Grzanka, A., 2019. The cytotoxic effect of oxymatrine on basic cellular processes of A549 non-small lung cancer cells. *Acta Histochemica*, 121, pp.724-731.

John, B., Sulaiman, C., George, S. and Reddy, V., 2014. Spectrophotometric estimation of total alkaloids in selected Justicia species. *International Journal of Pharmacy and Pharmaceutical Sciences*, 6, pp.647-648.

Jong, T.T., Lee, M.R., Chiang, Y.C. and Chiang, S.T., 2006. Using LC/MS/MS to determine matrine, oxymatrine, ferulic acid, mangiferin, and glycyrrhizin in the Chinese medicinal preparations Shiau-feng-saan and Dang-guei-nian-tong-tang. *Journal of Pharmaceutical and Biomedical Analysis*, 40, pp.472-477.

Li, J., Lin, D., J.I., R., Yao, K., Deng, W.Q., Yuan, H., Wu, Q., Jia, Q., Luo, P. and Zhou, K., 2016. Simultaneous determination of β-cypermethrin and its metabolite 3-phenoxybenzoic acid in microbial degradation systems by HPLC-UV. *Journal of Chromatographic Science*, 54, pp.1584-1592.

Li, K. and Wang, H., 2004. Simultaneous determination of matrine, sophoridine and oxymatrine in *Sophora flavescens* Ait. by high performance liquid chromatography. *Biomedical Chromatography*, 18, pp.178-182.

Sabatino, L., Scarangella, M., Lazzaro, F., Scordino, M., Picariello, G., Leotta, C., Traulo, P. and Gagliano, G., 2015. Matrine and oxymatrine in corroborant plant extracts and fertilizers: HPLC/MS-MS method development and single-laboratory validation. *Journal of Environmental Science and Health, Part B*, 50, pp.862-870.

Zhang, J. and Chen, Z., 2013. Determination of matrine and oxymatrine in *Sophora flavescens* by nonaqueous capillary electrophoresis-electrospray ionization-ion trap-mass spectrometry. *Analytical Letters*, 46, pp.651-662.

Zhang, R., Hu, S., Chen, X. and Bai, X., 2016. Dispersive liquid liquid microextraction combined with high-performance liquid chromatography for the simultaneous analysis of matrine alkaloids in traditional Chinese medicine. *Journal of Chromatographic Science*, 54, pp.1687-1693.

Zhang, T.Z., Qiang, F., Tong, C. and Shi-Ping, M., 2015a. Anti-asthmatic effects of oxymatrine in a mouse model of allergic asthma through regulating CD40 signaling. *Chinese Journal of Natural Medicines*, 13, pp.368-374.

Zhang, W., Xiang, B.R. and Ma, P.C., 2008. Determination of oxymatrine in human plasma by LC-MS and study on its pharmacokinetics. *Journal of Chromatographic Science*, 46, pp.529-533.

Zhang, W., Zhu, D., Fan, H., Liu, X., Wan, Q., Wu, X., Liu, P. and Tang, J.Z., 2015b. Simultaneous extraction and purification of alkaloids from *Sophora flavescens* Ait. by microwave-assisted aqueous two-phase extraction with ethanol/ammonia sulfate system. *Separation and Purification Technology*, 141, pp.113-123.

http://dx.doi.org/10.14500/aro.10662

Spectrophotometric Indirect Determination of Captopril through Redox Reaction with n-bromosuccinimide and RB dye in Pharmaceutical Products

Dashne M. Kokhasmail[1], Tara F. Tahir[2] and Kurdistan F. Azeez[1]

[1]Department of Chemistry, Faculty of Science and Health, Koya University, Koya KOY45, Kurdistan Region - F.R. Iraq

[2]Department of Medical Microbiology, Faculty of Science and Health, Koya University, Koya KOY45, Kurdistan Region - F.R. Iraq

***Abstract*—A simple, accurate, and sensitive method for the spectrophotometric determination of captopril in bulk and dosage forms is reported. The method is based on the bromination of captopril with excess solution of n-bromosuccinimide (NBS) in HCl acid medium. The excess NBS is pursued by the assessment of the residual NBS based on its ability to bleach the rhodamine B dye and measuring the absorbance at 555 nm. The amount of NBS reacted coincides to the drug content. The different experimental parameters influencing the development and stability of the color are precisely studied and optimized. Beer's law is valid within a concentration range of 0.3–1.0 μg/mL with a correlation coefficient R^2 = 0.991. The limit of detection 0.169 μg/mL is attained and relative standard deviation values for five replicated measurements of 0.3, 0.7, and 1.0 μg/mL captopril were between 0.53% and 2.03%. No interference is detected from prevalent additives found in pharmaceutical preparations. The proposed method is profitably put on to the determination of captopril in the tablet formulations with mean recoveries 98.91–101.27% and the results were statistically confronted with those of a reference method by applying Student's t-and F-test.**

***Index Terms*—Captopril, Indirect determination, n-bromosuccinimide, Rhodamine B, Spectrophotometer.**

I. Introduction

Hypertension takes place with two-fold the recurrence in the diabetic community in comparison with the non-diabetic community, and more than 50% of patients with type 2 diabetes mellitus develop into hypertensive (Parving, et al., 1983). Besides, enduring a large risk cause for atherosclerosis in large blood vessels, hypertension in diabetes contributes to mini-vessel disease and is a danger cause for diabetic nephropathy and probably for diabetic retinopathy. Investigations have presented that angiotensin-converting enzyme (ACE) inhibitors can sluggish the development of diabetic nephropathy in patients with type 1 or type 2 diabetes with microalbuminuria or macroalbuminuria (Phillip and Hall, 2006).

A main thing whither toward preserve the kidney from the complexity of diabetes is to manage elevated blood pressure destructively, despite the antihypertensive drug types utilized. Literature stated that patients with type 1 diabetes and antihypertensive drugs such as diuretics, beta-blockers, and hydralazine were taken, demonstrating that decreasing blood pressure diminishes proteinuria and sluggish the dismiss of renal work (Lewis, et al., 1993). A predominance of clue records that ACE inhibitors preserve the kidney more than undertake other blood pressure suppressing medications, apparently because ACE inhibitors particularly reduce the intrarenal pressure.

Patients with type 1 diabetes, albuminuria, and mildly impaired creatinine clearance were exposed to a milestone study. The ACE inhibitor captopril was diminished the risk of a decline in renal function more effectively than did other antihypertensive regimens (Lewis, et al., 1993). It has been found that captopril is powerful in lowering blood pressure and also lowering the risk of macrovascular end points. It was confirmed that captopril does not develop any important differences in the blood levels of ionized calcium or phosphorous ions and that it does not modify the serum levels of parathyroid hormone (PTH) and metabolites of Vitamin D (Florentin, et al., 2004).

Captopril (1-[(2S)-2-methyl-3-sulfanylpropanoyl]-L-proline) is an inhibitor of ACE, acting directly on the adrenal gland to activate the release of aldosterone (Fig. 1). It inhibits elevated blood pressure by preventing the enzymatic alteration of angiotensin I to angiotensin II. It is a white crystalline powder ($C_9H_{15}NO_3S$, molar mass 217.29 g/mol)

ARO-The Scientific Journal of Koya University
Vol. VIII, No.2 (2020), Article ID: ARO.10662, 7 pages
DOI: 10.14500/aro.10662
Received 12 April 2020; Accepted 27 July 2020
Regular research paper: Published 01 September 2020
Corresponding author's e-mail: tara.fuad@koyauniversity.org

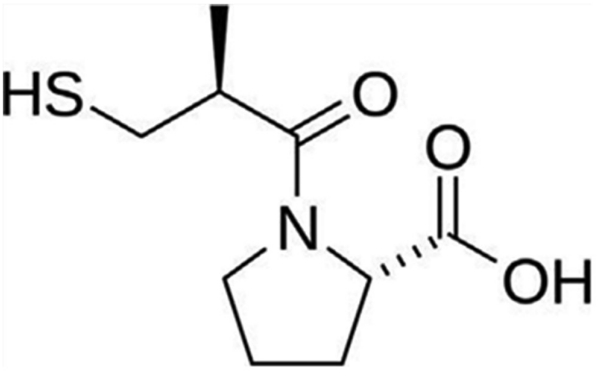

Fig. 1. Chemical structure of captopril.

having an essence sulfide-like odor and a melting point between 105 and 108°C. Captopril is plainly soluble in water or diluted solutions of alkali hydroxides, in alcohols, in methylene chloride, or in chloroform (Milan, et al., 2015).

Many methods were available for the determination of captopril in various samples including pharmaceutical products. The first approaches to captopril determination in biological matrix were made by liquid chromatography (LC) and mass spectrometry (Salem, et al., 2005, Vancea, et al., 2009).

Captopril is determined in blood, plasma, and urine using an investigate method of high-performance LC (HPLC). Nevertheless, determination methods of low concentration levels of captopril based on oxidation reaction are pursued three different oversights: Apply of extra sensitive detection method as an alternative to ultraviolet (UV) method such as electrochemical method without any derivatization of the analyte; detection of a derivatized product of captopril that is identified before or after chromatographic separation using the UV or fluorescent method; and utilize of pre-concentration techniques such as liquid-liquid extraction and multicolumn switching setup (Florentin, et al., 2004).

Despite the fact that captopril is non-toxic, but appropriate caution must be taken because it can cause hypotension when overdosed. This result is only expected following ingestion of quantities >450 mg/day. Taking medicines of captopril level above the accepted value can be harmful to the patient (Jia, et al., 2001). Accordingly, there is a sustaining demand for the development of new analytical procedures for the determination of captopril in pharmaceutical products (Lima, et al., 2016).

HPLC is recognized as a favored analytical technique for identification and quantification of most pharmaceutical products including captopril (Iqbal, et al., 2015). Disregarding that the advantage of HPLC as it is a well-built technology in the pharmaceutical field, offering sensitivity and specificity, it has defects that include high operation costs, the demand for large amounts of samples and solvents, and the formation of hazardous wastes such as organic solvents that are costly to relinquish and can have significant environmental impacts (Safila, et al., 2013).

In the published works, different methods were reported for the determination of captopril which include atomic absorption spectrometry, spectrophotometry, chemiluminescence, LC, amperometry, electrophoresis, and HPLC techniques (El-reis, et al., 2000; El-Shanawany, et al., 2014; Zhaofu, et al., 2017; Fu, et al., 2017, Shafi, et al., 2015; Marcolino-Junior, et al., 2009; Tomas, et al., 2006; Iqbal, et al., 2015, Zhang, et al., 2020).

The use of spectrophotometry provides a simple and inexpensive technique for the determination of drugs in pharmaceutical products. Sensitivity is another important characteristic of molecular absorption technique. Besides, the large linear concentration ranges make the method interesting and versatile for routine analysis of drugs in quality control laboratories (Rao, et al., 2012). Most of the reported methods were based on the redox reaction of captopril with an excess of an oxidizing agent (El-Didamony and Erfan, 2010; Skowron and Ciesielski, 2011).

The aim of the present work was, therefore, to use a convenient, low cost but sensitive analytical method as spectrophotometer for quantification of captopril in pharmaceuticals based on redox reaction with n-bromosuccinimide (NBS) and rhodamine B dye (RB). The results were compared with the recommended method described in the literature.

II. EXPERIMENTAL

A. Apparatus

Molecular absorption spectra were measured using UV-1000 CECIL 1021 spectrophotometer, UK, with a glass cell of 1.0 cm optimal path length. LW Scientific Digital Water Bath, US, was used to control the temperature of the solution during the studies. The studies were accomplished using HPLC system of Agilent 1100 controlled by ChemStation Data System. A G 1311A quaternary pump and UV detector (VWD-G1314 A) were supplied with the system. A reverse phase C18 column (Kromasil 100-5-Phenyl®, 300 mm × 4.6 mm, 5 μm) was handling at 25°C and the mobile phase of 0.1 % v/v trifluoroacetic acid and acetonitrile at ratio (80:20 v/v) was provided during the investigation. The flow rate of 1.5 mL/min elute was advised at wavelength 290 nm.

B. Material and Reagent

Captopril was collected from Awamedica Pharmaceutical Company (Kurdistan region, Iraq), used as received, the purity of which was 99.9%. A solution of 100 μg/mL of NBS (from Fluka) was prepared by dissolving 0.1 g of NBS ($C_4H_4BrNO_2$) in small amount of warm water, then diluted to 1000 mL with distilled water, and kept in 5°C refrigerator until further usage. A dye solution of 100 μg/mL of RB (from RIEDEL-DEHAEN) was prepared by dissolving 0.1 g of RB in distilled water and diluted to 1000 mL with distilled water (the solution is stable for at least 2 weeks). Hydrochloric acid, sulfuric acid, nitric acid, and acetic acid (from Scharlau) of 1 mol/L solution were prepared, individually. Interfering solutions of 500 μg/mL of fructose (from BDH), glucose (SCP), lactose (BDH), starch (from Difco), and sucrose (from Difco) were prepared individually by dissolving 0.1 g of solid compound in 100 ml distilled water.

C. Preparation of Standard and Sample Solution

A stock solution of standard captopril 1000 μg/mL was prepared by dissolving 0.1 g of standard captopril powder in

20 mL distilled water with stirring carefully, then the volume was completed to 100 mL volumetric flask with the same solvent and kept in 5°C refrigerator to remain stable for 28 days (Pereira and Tam, 1992). Working standard solutions were prepared daily by proper dilution of the stock standard solution with the same solvent.

All pharmaceutical products of captopril in the local medical store are containing 25 mg and two different companies were used for the determination (captopril Awa, Erbil, Iraq, and Rilcapton, Medochemie-Cyprus). Ten tablets of captopril were weighed and crushed for each pharmaceutical company, and the sample powder of the two companies was accurately weighed individually and placed in a 50.0 mL beaker, then dissolved in 30.0 mL of distilled water. The solution was stirred for 10 min to increase solubility. Insoluble excipient was removed by filtration using Whatman No. 41 membrane filter paper. The filtered solution was diluted to 100 mL in a volumetric flask with the same solvent.

D. Analytical Procedure

In 25.0 mL volumetric flask, 2.5 mL of NBS (100 μg/mL), 0.8 mL of HCl (1 mol/L), and adequate captopril standard or sample (0.3–1.0 μg/mL) of 100 μg/mL solution were added. This mixture was shacked thoroughly and left to stand for 10 min at 25 ± 2°C. Finally, 2.5 mL of RB (100 μg/mL) was added and directly diluted to the mark with distilled water. The absorbance was measured against reagent blank prepared in similar conditions without captopril at 555 nm.

III. Results and Discussion

Captopril is acting as a reducing agent due to the presence of thiol group (- SH) in its structure and the literature explains that captopril in aqueous solution undergoes oxidative degradation at its thiol function to yield captopril-disulfide (Chenl, et al., 1995). In this work, the reaction involves two steps (Fig. 2):

(i) Oxidation of the drug (captopril) by excess of NBS reagent, generated in sedentary by the action of HCl acid solution on captopril-disulfide
(ii) Determination of unreacted oxidant NBS by bleaching the color of RB dye in acidic medium (Abdel-Hady, 2013).

The absorption spectrum of the yielded bleaching 2.5 mL of (100 μg/mL) RB demonstrated the maximum absorbance at 555 nm against the blank solution after 10 min (Fig. 3a). The absorbance of individual 0.7 μg/mL captopril showed dropping at the same wavelength (Fig. 3b), whereas no significant absorbance was recorded for the blank reagent of NBS and RB dye (Fig. 3c).

A. Optimum of Experimental Conditions

The reaction conditions along with the different experimental parameters influencing the color development and stability of the dye were laboriously examined and optimized for the quantitative determination of captopril in bulk and the tablet dosage forms.

Selection of type and acid concentration

The reaction of 0.7 μg/mL captopril with 2.5 mL of (100 μg/mL) solution of each of NBS and RB dye was tested in 1 mol/L of HCl, HNO_3, H_2SO_4, and CH_3COOH solutions, individually. The results demonstrated that the reaction is suitable in hydrochloric acid medium (Fig. 4a). A 1 mol/L HCl solution was found to be sufficient for the oxidation of captopril as well as the bleaching of RB dye. The variation in HCl volumes indicated that highest absorbance was observed with 0.8 mL of 1 mol/L HCl, subsequent studies were performed with this volume and concentration of HCl (Fig. 4b).

Sequence of addition

The sequence of addition of 2.5 mL (100 μg/mL) NBS oxidant, drug solution, 2.5 mL (100 μg/mL) RB dye, and 0.8 mL (1 mol/L) HCl was studied through bleaching the color of RB dye and measuring its absorbance at 555 nm (Fig. 5). Best absorbance was accomplished when the sequence was in the order; drug, NBS, HCl, and then RB. This study is compatible and confirmed with the mechanism of reaction in Fig. 2.

Reagent and dye concentrations

Elementary experiments were achieved to fix the upper limits of RB dye that could be determined spectrophotometrically in acid medium and this was found to be 2.5 mL of 100 μg/mL of RB. This concentration gave stable and high intensity that was the reasonable concentration for this procedure.

A high concentration of oxidant NBS >100 μg/mL was found to destroy the color of RB dye. Under the experimental conditions, different volumes between 0.5 and 3.0 mL of

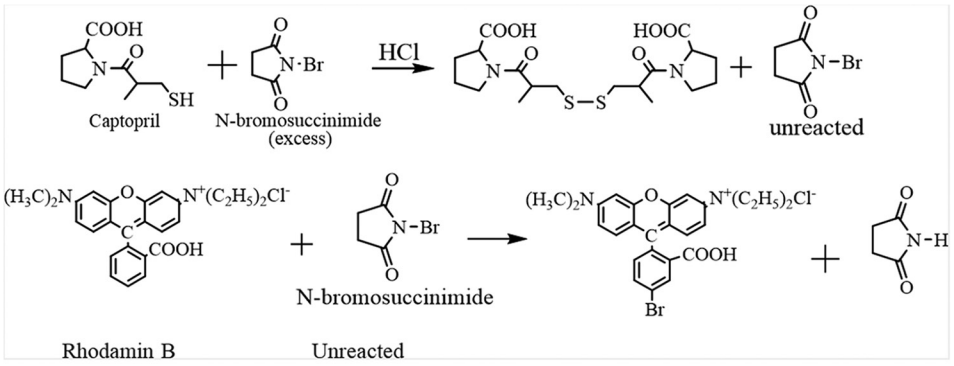

Fig. 2. Mechanism of oxidation of captopril by excess NBS and the latest reaction with RB dye.

100 µg/mL NBS were examined (Table I). Therefore, 2.5 mL of NBS was adopted in the recommended procedure.

Effect of temperature and heating time

The redox reaction of 0.7 µg/mL captopril, 2.5 ml (100 µg/mL) NBS solution, and 2.5 mL (100 µg/mL) RB dye in 0.8 mL (1 mol/L) of HCl acidic medium was examined at various temperatures and heating times through measuring the absorbance (Table II).

TABLE I
AMOUNT OF OXIDANT NBS SOLUTION FOR BLEACHING COLOR OF RB DYE VERSUS ABSORBANCE

Volume of NBS (mL)	Absorbance
0.5	0.982
1.0	0.730
1.5	0.337
2.0	0.183
2.5	0.095
3.0	0.005

NBS: n-bromosuccinimide, RB: Rhodamine B

TABLE II
EFFECT OF TEMPERATURE AND HEATING TIME ON THE ABSORBANCE OF RB DYE

Temperature°C	Absorbance					
	10 min	20 min	30 min	40 min	50 min	60 min
5	0.371	0.372	0.373	0.372	0.375	0.377
10	0.449	0.447	0.445	0.445	0.447	0.449
25	0.587	0.587	0.584	0.588	0.586	0.585
50	0.457	0.459	0.453	0.451	0.450	0.449

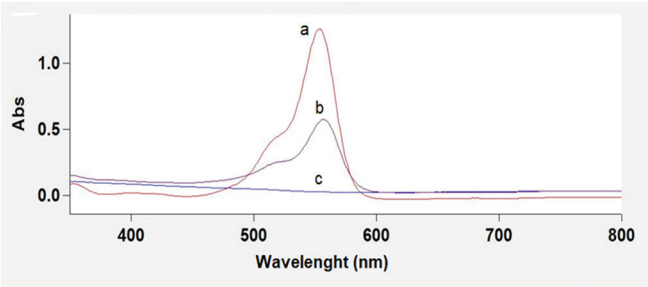

Fig. 3. Absorption spectra of (a) 2.5 mL of (100 µg/mL) rhodamine B, (b) 0.7 µg/mL captopril, 2.5 mL (100 µg/mL) of NSB and RB dye (c) blank reagent of 2.5 mL (100 µg/mL) of NSB and RB solution against distilled water.

As a general rule, increasing the temperature (5–25°C) will increase the reaction rate (for exothermic and endothermic) reactions simply because it means more energy available in the system. However, for the reversible exothermic reaction, there is a range of temperatures where this might not be true (Leenson, 1999). The absorbance was decreased as the temperature rose to 50°C. The results obtained in Table II may be understood in terms of increased quantum yield of the RB dye as the temperature is reduced (Ali, et al., 1991). A 25°C was then applied for further investigation.

Reaction time and stability of dye color

Time is a denoting factor on completing the redox reaction of 0.7 µg/mL captopril with 2.5 mL (100 µg/mL) NBS solution in 0.8 mL (1 mol/L) of HCl acidic medium and bleaching of 2.5 mL (100 µg/mL) RB dye. The maximum absorbance was attained after 10 min at 25 ± 2°C (Fig. 6). The color intensity of RB dye was stable after 25 min for at least 24 h at room temperature.

Interference studies

The effects of common excipients added in pharmaceutical preparations in the form of tablets and capsules were tested for their possible interferences in the assessment of captopril under optimum conditions (El-Didamony and Erfan, 2010). The excipient solutions (500 µg/mL) of lactose, fructose, glucose, starch, and sucrose were mixed with 0.7 µg/mL pure captopril in the final volume of 25 mL, individually. The spectra obtained were compared with the spectrum of 0.7 µg/mL captopril standard solution. A level of interference was considered to be acceptable when the error is not higher than ±5%. No significant levels of interferences were observed in the determination of captopril in the presence of the common excipients (Table III).

B. Analytical Figures of Merit

Determination of captopril was investigated under optimum experimental conditions, when the relative standard deviation (RSD%) was 2.33% as obtained from five replicated measurements of three different concentrations of captopril. In agreement with IUPAC guidelines of the validation of analytical method, the limit of detection value (LOD) = 3.3 SD/P was adopted, in which SD is the standard deviation of

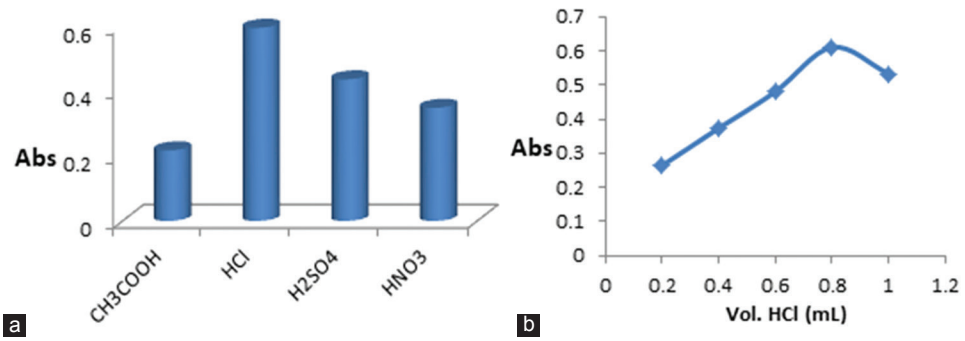

Fig. 4. (a) Absorbance vs. solutions that contain 0.7 µg/mL captopril, 2.5 mL of (100 µg/mL) solution of each of NBS and RB dye with 1 mol/L of CH3COOH, HCl, H2SO4 and HNO3, individually; (b) Absorbance vs. solutions that contain 0.7 µg/mL captopril, 2.5 mL of (100 µg/mL) solution of each of NBS and RB dye with different volumes between (0.2-1.0 mL) of 1 mol/L HCl solution.

http://dx.doi.org/10.14500/aro.10662

five reagent blank measurements and P is the gradient of the calibration curve (Topic Q2 (R1): Validation of Analytical Procedures: Text and Methodology, International Conference on Harmonization (ICH), 2005, Ana, et al., 2014, Tahir, et al., 2019). The linear range was 0.3–1.0 µg/mL with correlation coefficient R^2 = 0.991 and molar absorptivity of 2333 L/mol/cm (Fig. 7). The LOD and limit of quantification were 0.169 µg/mL and 0.304 µg/mL, respectively. The regression equation of standard solutions was Y = 1.0665x - 0.1766 in which x is in µg/mL.

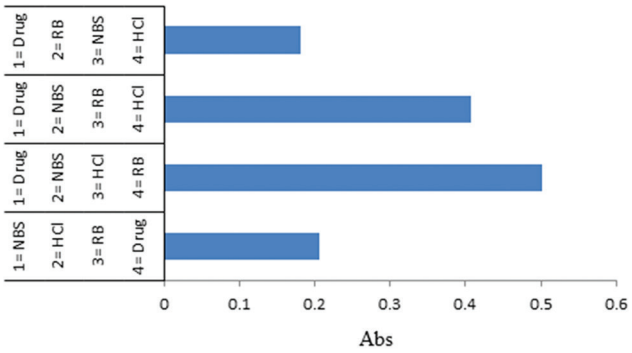

Fig. 5. Absorbance of different sequence of mixing captopril, 2.5 mL (100 µg/mL) NBS, 2.5 mL (100 µg/mL) RB and 0.8 mL (1 mol/L) HCl solution.

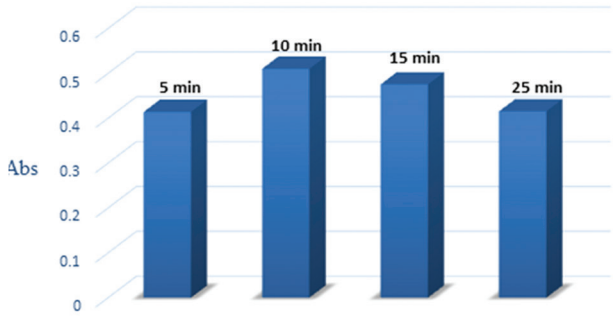

Fig. 6. Absorbance of 0.7 µg/mL captopril, 2.5 mL (100 µg/mL) NBS and 2.5 mL (100 µg/mL) RB solution in 0.8 mL (1 mol/L) of HCl acidic medium at different reaction times.

The accuracy and precision of the proposed procedure was provided by measuring the absorbance of RB dye after bleaching through excess amount of oxidant NBS that was remained after oxidation of three different concentrations of standard captopril (0.3, 0.7, and 1.0 µg/mL), individually in five replicate measurements (Table IV). The values of RSD % and E % were between 0.53%–2.03% and -1.42%–2.00%, respectively, indicating that the proposed procedure is valid and applicative.

C. Application and Comparison

The proposed procedure was successfully bestowed for the determination of captopril in pharmaceutical tables. The ingredients in the pharmaceutical tablets did not interfere in the quantification of captopril. The applicability of the proposed procedure for the analysis of captopril in pharmaceutical formulations was examined by investigating two pharmaceutical tablets and the results are shown in Table V which were compared to the standard captopril assay using HPLC method. HPLC has the capability to detach and determine compounds that are exist in any sample that can

TABLE III
INTERFERENCE STUDIES OF CAPTOPRIL QUANTIFICATION TOWARD SOME COMMON EXCIPIENTS PRESENTED IN THE PHARMACEUTICAL PRODUCTS

Coexisting materials	Allowance concentrations (µg/mL)	E %*
Lactose	500	−1.90
Fructose	500	2.60
Glucose	500	−2.20
Starch	500	2.30
Sucrose	500	2.60

* Average of three determinations

TABLE IV
ACCURACY AND PRECISION DATA FOR THE PROPOSED SPECTROPHOTOMETRIC INDIRECT DETERMINATION OF CAPTOPRIL

Contained amount (µg/mL)	Found by proposed method (µg/mL)	SD	RSD%	E%*
0.3	0.305	0.002	2.030	1.66
0.7	0.690	0.005	0.920	-1.42
1.0	1.020	0.005	0.530	2.00

*Average of five determinations

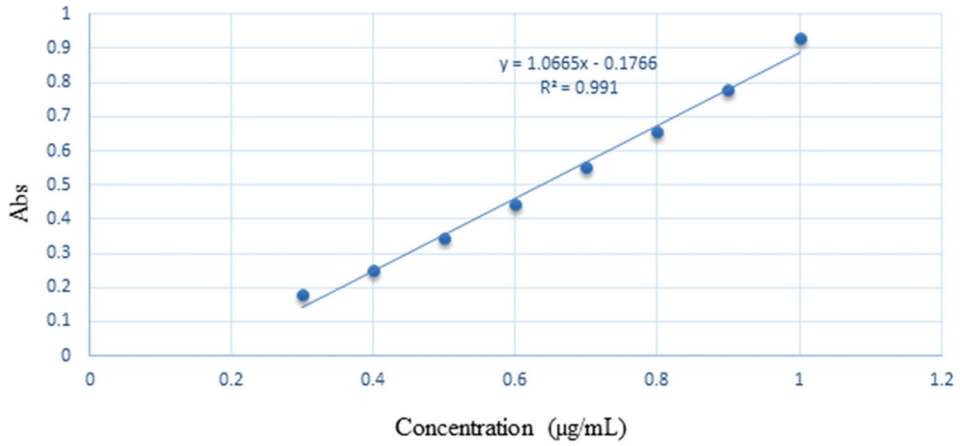

Fig. 7. Calibration curve of spectrophotometric indirect quantitation of captopril via oxidant NBS and RB dye in acidic medium under optimum condition.

TABLE V
Analysis of captopril in pharmaceutical formulations using the proposed method and standard HPLC method

Pharmaceutical tablets	Observed values (mg)	Values from proposed procedure	Values from HPLC	Recovery %	E %*	t and F values**
Captopril awa	25	25.34±1.13	25.02±0.14	101.27	1.27	t = 1.36, F = 1.78
Rilcapton	25	24.71±0.17	24.98±0.08	98.91	-1.08	t = 1.02, F = 1.98

*Average of five determinations, **Theoretical calculation of t and F at 95% confidence level (n=5) was 2.78 and 6.39, respectively, ***The values ± are the standard deviation of the five replication of each sample

TABLE VI
Comparison of determination of captopril using different redox reactions through spectrophotometric technique and the proposed method

Method based on	Ref.	LR (mol/L)	LOD (mol/L)
Reduction of ammonium molybdate	Ribeiro, et al., 2010	4.60×10^{-4} - 1.84×10^{-3}	7.31×10^{-6}
Reduction of potassium dichromate	Moldovan, et al., 2012	3.68×10^{-7} - 1.61×10^{-5}	1.10×10^{-7}
Reaction of O-phthalaldehyde	El-Shanawany, et al., 2014	9.20×10^{-6} - 1.15×10^{-5}	-
Proposed work		1.38×10^{-6} - 4.6×10^{-6}	7.77×10^{-7}

LR: Linear range, LOD: Limit of detection

be dissolved in a liquid in trace concentrations as low as parts per trillion (Iqbal, et al., 2015).

The performance of the proposed procedure was refereed by calculating the Student's t- and F-values. At 95% confidence level, the calculated t- and F-values did not overstep the theoretical values as noticeable from Table V. Consequently, it was concluded that there is no significant difference between the proposed method and the standard method. Moreover, the spectrophotometric method for the determination of captopril in pharmaceutical tablets addressed in this work is simple, fast, inexpensive, precise, and accurate and it may be suitable for routine analysis and quality control laboratories.

In the literature, captopril was quantified using different oxidizing agents through spectrophotometric technique. Table VI views the optimization results of the determination of captopril using different reagent reactions and the proposed method. Despite that some analytical method have lower LOD value and wider linear range, but the proposed method does not need pre-extraction of the sample beside the easy and short time of the reaction.

IV. Conclusion

The proposed method has the expediency of simplicity and rapidity for the determination of captopril in both bulk and dosage forms and interferences free from common tablet excipients. The investigation method comprises less rigorous control of experimental parameters such as the stability of the colored reagent dye, time of reaction, and temperature independence. The reagents applied in the proposed method are low-priced, easily accessible and the procedure does not comprise any laborious sample preparation. These preferences boosted the application of the proposed method in routine quality control of captopril in industrial laboratories.

References

Abdel-Hady, A.M., 2013. Kinetics of oxidative degradation of rhodamine-B by N-bromosuccinimide in aqueous alkaline medium. *European Journal of Chemistry*, 4(3), pp.292-296.

Ali, M.A., Moghaddasi, J., and Ahmed, S.A., 1991. Temperature effects in rhodamine B dyes and improvment in CW dye laser performance. *Laser Chemistry*, 11, pp.31-38.

Ana, B.F.V., Odonírio, A., Roseli, A.S.G., Giancarlo, R.S.B., and Robson, T.S.O., 2014. Electroanalytical determination of captopril in pharmaceutical formulations using boron-doped diamond electrodes. *International Journal of Electrochemical Science*, 9, pp.1044-1054.

Chenl, D., Chen, H., and Ku, H., 1995. Degradation rates of captopril in aqueous medium through buffer-catalysis oxidation. *Drug Development and Industrial Pharmacy*, 21(7), pp.781-792.

El-reis, M.A., Attia, F.A., and Kenawy, I.M.M., 2000. Indirect determination of captopril by AAS. *Journal of Pharmaceutical and Biomedical Analysis*, 23(2), pp.249-254.

El-Didamony, A.M., and Erfan, E.A., 2010. Utilization of oxidation reactions for the spectrophotometric determination of captopril using brominating agents. *Spectrochimica Acta Part A: Molecular and Biomolecular Spectroscopy*, 75(3), pp.1138-1145.

El-Shanawany, A.A., El-Adl, S.M., Abdel-Aziz, L.M., and Hassan, A.F., 2014. Spectrophotometric determination of cefradine and captopril in their bulk and dosage forms using O-phthalaldhyde (OPA). *Asian Journal of Pharmaceutical Analysis*, 4(1), pp.36-41.

Florentin, T., Alexandru, F., Andrei, M., and Victor, D., 2004. Captopril. *Encyclopedia of Endocrine Diseases*, 1, pp.447-450.

Fu, Z., Huang, W., Li, G., and Hu, Y., 2017. A chemiluminescence reagent free method for the determination of captopril in medicine and urine samples by using trivalent silver. *Journal of Pharmaceutical Analysis*, 7(4), pp.252-257.

International Conference on Harmonisation. 2005. *Topic Q2 (R1): Validation of Analytical Procedures: Text and Methodology*. International Conference on Harmonisation, Switzerland.

Iqbal, F.M., Ahmad, M., Zubair, M.M., Tulain, U.R., and Rashid, A., 2015. Determination of captopril in plasma by high-performance liquid chromatography: Application in an *in-vivo* evaluation of drug release from hydrogel. *Latin American Journal of Pharmacy*, 34(5), pp.875-884.

Jia, L., Pei, R., Lin, M., and Yang, X., 2001. Acute and subacute toxicity and efficacy of S-nitrosylated captopril, an ACE inhibitor possessing nitric oxide activities. *Food and Chemical Toxicology*, 39(12), pp.1135-1143.

Leenson, I.A., 1999. Old rule of thumb and the arrihenius equation. *Journal of Chemical Education*, 76(10), pp.1459-1460.

Lewis, I.F., Hunsicker, L.G., Bain, R.P., and Rohde, R.D., 1993. The effect of angiotensin-converting enzyme inhibition on diabetic nephropathy. *The New England Journal of Medicine*, 329(20), pp.1456-1462.

Lima, M.J., Fernandes, R.N., Tanaka, A.A., and Reis, B.F., 2016. Development of a new procedure for the determination of captopril in pharmaceutical formulations employing chemiluminescence and a multicommuted flow analysis approach. *Luminescence*, 31(1), pp.288-294.

Marcolino-Junior, L.H., Bonifacio, V.G., Vicentini, F.C., Janegitz, B.C., and Fatibello-Filho, O., 2009. Amperometric determination of captopril using a carbon paste electrode in flow analysis. *Canadian Journal of Analytical Sciences and Spectroscopy*, 54(1), pp.45-51.

Milan, R., Joanna, B., Anna, R., and Waldemar, M., 2015. Molecular structure and acidity of captopril, zofenopril and their metabolites captopril disulfide and zofenoprilat. *Computational and Theoretical Chemistry*, 1062, pp.50-55.

Moldovan, Z., Badea, I.A., Bunaciu, A.A., and Aboul-Enein, H.Y., 2012. Indirect spectrophotometric method for determination of captopril using Cr(VI) and diphenylcarbazide. *Quimica Nova*, 35(8), pp.1668-1672.

Parving, H.H., Andersen, A.R., Smidt, U.M., Christiansen, J.S., Oxenboll, B., and Svendsen, P.A., 1983. Diabetic nephropathy and arterial hypertension: The effect of antihypertensive treatment. *Diabetes*, 32(2), pp.83-87.

Pereira, C.M., and Tam, Y.K., 1992. Stability of captopril in tap water. *American Journal of Hospital Pharmacy*, 49(3), pp.612-615.

Phillip, M., and Hall, M.D., 2006. Prevention of progression in diabetic nephropathy. *Diabetes Spectrum*, 19(1), pp.18-24.

Rao, K.S., Panda, M., Keshar, N.K., and Yada, S.K., 2012. Simultaneous estimation of captopril and hydrochlorothiazide in combined dosage forms. *Chronicles of Young Scientists*, 3(1), pp.37-41.

Ribeiro, P.R., Pezza, L., and Pezza, H.R., 2010. A simple spectrophotometric method for the determination of captopril in pharmaceutical preparations using ammonium molybdate. *Eclética Química*, 35(3), pp.179-188.

Safila, N., Najma, S., and Saeed, A.M., 2013. Method for the determination of captopril in bulk, pharmaceutical formulations and serum by HPLC using two different system. *American Based Research Journal*, 2(3), pp.8-14.

Salem, I.I., Abu Saif, W., Jmeian, Y., and Al Tamimi, J.I., 2005. A selective and rapid method for the quantification of captopril in human plasma using liquid chromatography/selected reaction monitoring mass spectrometry. *Journal of Pharmaceutical and Biomedical Analysis*, 37(5), pp.1073-1080.

Shafi, N., Siddiqui, F.A., Sultana, N., and Arayne, M.S., 2015. Concurrent determination of diltiazem, lisinopril, captopril, and enalapril in dosage formulations and in human serum by liquid chromatographic technique. *Journal of Liquid Chromatography and Related Technologies*, 38(15). pp.1466-1473.

Skowron, M., and Ciesielski, W., 2011. Spectrophotometric determination of methimazole, D-penicillamine, captopril, and disulfiram in pure form and drug formulations. *Journal of Analytical Chemistry*, 66(8), pp.714-719.

Tahir, T.F., Qader, A.F., Salih, M.I., and Rashid, E.Q., 2019. L-tryptophan as fluorescent probe for determination of folic acid in some pharmaceutical products. *ARO The Scientific Journal*, 7(2), pp.19-26.

Tomas, P., Carmen, M., and Raquel, G., 2006. Development and validation of a capillary electrophoresis method with laser-induced fluorescence detection for the determination of captopril in human urine and pharmaceutical preparations. *Electrophoresis*, 27(12), pp.2310-2316.

Vancea, S., Imre, S., Donath-Nagy, G., Bela, T., Nyulas, M., Muntean, T., and Borka-Balas, R., 2009. Determination of free captopril in human plasma by liquid chromatography with mass spectrometry detection. *Talanta*, 79(2), pp.436-441.

Zhang, P., Wang, L., Zing, J., Tan, J., Long, Y., and Wang, Y., 2020. Colorimetric captopril assay based on oxidative etching-directed morphology control of silver nanoprisms. *Microchim*, 187, pp.107-115.

Zhaofu, F., Wanting, H., Gongke, L., and Yufei, H., 2017. A chemiluminescence reagent free method for the determination of captopril in medicine and urine samples by using trivalent silver. *Journal of Pharmaceutical Analysis*, 7(4), pp.252-257.

Land Surface Temperature Anomalies Detection for the Strong Earthquakes in 2018

Azad Rasul[1] and Luqman W. Omar[2]

[1]Department of Geography, Soran University,
Kawa Street, Soran 44008, Erbil, Kurdistan Region – F.R. Iraq

[2]Department of Geography, Koya University,
Danielle Mitterrand Boulevard, Koya KOY45, Erbil, Kurdistan Region – F.R. Iraq

***Abstract*—Earthquake every year leads to human and material losses and unpredictability of it by now makes this natural disaster worsen. The objective of the current study was to determine the anomalies in land surface temperature (LST) in areas affected by earthquakes. In this research, three earthquakes (M >6) were studied. Moderate Resolution Imaging Spectroradiometer Aqua and Terra day and night LST data used from 2003 to 2018. The interquartile range (IQR) and mean ± 2σ methods utilized to select anomalies. As a result, based on the IQR method, no prior and after anomaly detected in selected cases and data. Based on mean ± 2σ, usually positive anomaly occurred during daytime. However, negative (or positive) anomaly occurred during the nighttime before the Mexico and Bolivia earthquakes. During 10 days after the earthquake, sometimes a negative anomaly detected.**

***Index Terms*—Anomaly detection, Earthquake, Land surface temperature, Remote sensing**.

I. Introduction

One of the most destructive natural disasters is the earthquake which brings enormous losses to humankind (Geiß and Taubenböck, 2013). International seismology and remote sensing community considered utilizing remote sensing (data) for monitoring of earthquake as a promising research area (Tronin, 2009). Ground stations data for earthquakes represent only a small extent. Therefore, compared to traditional approaches of seismic monitoring, satellite data have numerous advantages (Jiao, Zhao and Shan, 2018). During 2018, 134 earthquakes (M >6) occurred around the world (USGS.gov, 2019). However, optical satellite data also have disadvantages, such as cloud cover. Therefore, three examples of them in clear sky atmospheres selected for the current research.

Many signs of earthquake can be monitored by referring to prevailing temperature of underground water, near-surface air temperature, radon, and greenhouse gas. Moreover, the dominant parameters of temporal-spatial magnitude of the earthquake are an anomaly of satellite thermal infrared, temperature, and ionosphere disturbances (Wu and Liu, 2009). Tramutoli, et al. (2001) and Tronin, Hayakawa and Molchanov (2002) detected up to 5°C temperature increase before the earthquakes in Italy, Japan, and China. An increase in land surface temperature (LST) and a decrease in sea surface temperature observed in the Gujarat earthquake in India by Ouzounov and Freund (2004). Furthermore, Ouzounov, et al. (2018) discovered infrared signals such as outgoing longwave radiation (OLR) hotspots several days before some earthquakes near the epicentre. Approximately 7–8 days before the major earthquake, OLR anomaly can increase 30–45 Wm^{-2} around epicentral areas (Rawat, et al., 2011). Zoran Savastru and Savastru (2015) discerned the development of spatiotemporal prior anomaly of LST, OLR, and mean air temperature parameters related to strong earthquakes in Romania.

Despite productive research in this field, still, uncertainty and arguments remain about pre-seismic anomaly detection due to some crucial misinterpretations and failure earthquake forecasting (Geller, 2011; Tronin, 2009). The seismic community still not completely accepted seismic precursor because it is not perfectly formed (Geller, 1997; Geller, et al., 1997). Earthquake prediction to be trusted should be based on scientific methods, the data should be accessible to researchers and earthquake-related signs should be well documented. Besides, the research should specify the spatiotemporal and magnitude window and researcher level of confidence in the prediction and chances of occurring earthquake (Allen, 1976; Geller, 1997). Jiao, Zhao and Shan (2018) suggested that reliability of earthquake forecasting could be intensified by utilizing combined application and multiparameter analysis.

In this research, we utilize both Aqua and Terra LST data of day and night because having an anomaly in many parameters before the earthquakes in the same area, capable to make temperature anomaly that associated with earthquake more trustful and realistic. To save time and efforts in processing LST long time series data, the code script of cloud-based remote sensing platform Google Earth Engine

ARO-The Scientific Journal of Koya University
Vol. VIII, No.2 (2020), Article ID: ARO.10591, 7 pages
DOI:10.14500/aro.10591
Received: 15 November 2019; Accepted: 07 August 2020
Regular research paper: Published: 01 September 2020
Corresponding author's e-mail: azad.rasul@soran.edu.iq

(GEE) was prepared and utilized. In addition, we observed that detecting the earthquake anomaly by utilizing only one statistical method is not robust (Bhardwaj, et al., 2017), in this study, therefore, two methods, namely, interquartile range (IQR) and mean ± 2σ were utilized to improve the efficiency of anomalous difference. This study is important because select LST anomaly in robust technique can have many implications in terms of monitoring earthquakes and its consequences.

The objective of the current study was to determine the earthquake's remote sensing LST anomaly by utilizing GEE with R programming. Three samples of the earthquake in the land transparent sky were considered. The research divided into five sections. The first section is introduction that includes background and literature review. The second section includes explanation of materials and methods used in the research. In the next section, results displayed then we discussed our results compared to other researches. The paper concluded with some conclusion that created from the research.

II. Materials and Methods

A. Data

Moderate Resolution Imaging Spectroradiometer (MODIS) is one of the main sources of earth observation research. Aqua satellite orbits the earth from south to north at 1:30 P.M. local time whereas Terra passes in the opposite direction at 10:30 A.M. local time. Both of them use 36 spectral bands (from 0.415 to 14.235 μm) in senses the surface (Shen, et al., 2013). LST is the radiative temperature of the land surface which typically surveyed by remote sensing. The resolution of selected LST MODIS data is 1 km (Rasul, Balzter and Smith, 2016). In this research, both Aqua and Terra day and night LST data used from 2003 to 2018 (Table I).

B. Study Sites

In this research, three strong earthquakes were assessed which occurred during 2018 around the world (Table II). Included earthquakes are higher than six magnitudes. Because the cloudy condition is a significant problem for active remote sensing, samples were selected in the land with transparent sky situations (Fig. 1).

C. Methodology

C.1. Downloading and processing data

Several studies designate that earthquake anomaly within a few days to a few weeks before the seismic events could be considered as short-term precursors (Jiao, Zhao and Shan, 2018). Therefore, in this study, 20 days before and 10 days after the main shake selected as temporal window. In this study, four overpasses LST data (Table I) processed in GEE (Appendix A) (Gorelick, et al., 2017). The data collection and interested band and interested period selected. One month data selected for each year, the year from 2003 to 2018. Past years' data of 20 days before and 10 days after the main quake have been included in the analyses to characterise anomalies. Images were cropped to study site and LST values are multiplied by a scale factor. Then, the data were exported as CSV file.

C.2. Anomaly detection

Anomaly detected and graphs created in R programming using packages such as "anomalize," "devtools," "coindeskr," "dplyr," and "ggplot2" (Appendix B). To detect anomalies in the time series of the data, two methods were utilized. The first one is the IQR which utilizes a range of 25 the median (Dancho and Vaughan, 2018). In this method, negative anomaly LST outliers are values that smaller than limit lower whereas positive anomaly LST is values that bigger than limit upper. The same as a boxplot, the whiskers are lines ranging from Q1 and Q3 to ends. Limit lower calculated by $Q1 - 1.5 \times IQR$ and upper limit calculated by $Q3 + 1.5 \times IQR$ (Streit and Gehlenborg, 2014).

Moreover, the second method is mean ± 2σ (equation 1). In this rule, 95% of values drop between (mean-2*σ, mean+2*σ) (anomaly.io, 2015). Some researchers (e.g., [Dey and Singh, 2003]) used mean+1.5*σ of parameter as background noise. Besides, Wu, et al. (2016) used "mean±1.5*σ" and "mean±2*σ" for seismic precursor parameters such as soil moisture, soil temperature, and near

TABLE I
Details of the Utilized Data in the Research

Data	Temporal resolution	Spatial resolution	Start date	End date	Image collection ID in GEE	Selected band
Daytime LST (Terra)	1 day	1000 m	January 1, 2003	1 May 2018	MODIS/006/MOD11A1	LST_Day_1 km
Nighttime LST (Terra)	1 day	1000 m	January 1, 2003	1 May 2018	MODIS/006/MOD11A1	LST_Night_1 km
Daytime LST (Aqua)	1 day	1000 m	January 1, 2003	1 May 2018	MODIS/006/MYD11A1	LST_Day_1 km
Nighttime LST (Aqua)	1 day	1000 m	January 1, 2003	1 May 2018	MODIS/006/MYD11A1	LST_Night_1 km

LST: Land surface temperature, MODIS: Moderate Resolution Imaging Spectroradiometer

TABLE II
Details of the Studied Earthquakes

S. No.	Location	Date	Epicentre	Magnitude (USGS)	Focal depth (km, USGS)
1	San Pedro Jicayan, Mexico	Febaury 16, 2018	16.386 N, 97.979 W	7.2	22
2	Carandayti, Bolivia	April 2, 2018	20.659 S, 63.006 W	6.8	559
3	Jarm, Afghanistan	January 31, 2018	36.526 N, 70.851 E	6.2	193.7

Fig. 1. Locations of studied earthquakes. Red stars are the epicentre of the earthquakes.

surface air temperature. In this study, as cautious only two standard deviations considered as anomaly.

$$\text{Anomaly} = \text{mean} \pm (2\sigma) \quad (1)$$

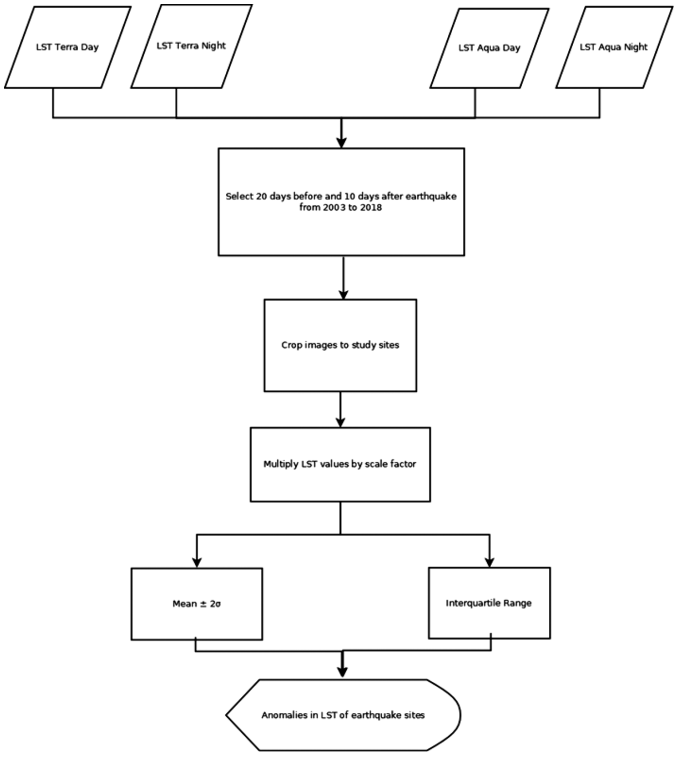

III. Results

LST data of 20 days before and 10 days of data after the quack analyzed for each selected earthquake in Mexico, Bolivia, and Afghanistan during 2018. Both used methods for anomaly detection in LST time series displayed in the following figures. MODIS LST for Aqua and Terra has 4 times passed per day; therefore, they displayed separately in the following in subfigure a, b, c, and d.

A. Mexico Earthquake on Febaury 16, 2018

Based on IQR method, no anomaly detected in LST Aqua and Terra of both day and night data in the Mexico (Fig. 2b), Bolivia (Fig. 3a and b), and Afghanistan earthquakes during 20 days before and 10 days after the earthquakes (Fig. 4a and b). According to mean ± 2σ, in Aqua night, positive anomaly detected. In Terra day LST data, negative anomaly detected 14 and 16 days before the quake (Fig. 2c). Furthermore, positive anomaly occurred 2 days before the Mexico earthquake. After the quake, negative anomaly occurred in Aqua day and Terra night data (Fig. 2a and d). Occurred negative anomaly some days after the quack perhaps explained by returning the area to stability. In Fig. 2d, some values passed lower limits (dotted red lines), but these anomalies occurred during previous years and during 2018, no anomaly detected based on interquartile outliers.

B. Bolivian Earthquake on April 2, 2018

Concerning Bolivian earthquake, no anomaly detected based on IQR. However, based on mean ± 2σ methods in Aqua night (Fig. 3b) and Terra day and night LST (Fig. 3c and d and Table III), prior negative anomaly detected. Duration of detected anomalies is between 5 days and 11 days before the main shake and the degree decreased between −6.9 and −13.1 K. The upper limit in IQR is higher than mean plus two standard deviations. Besides, lower limit based on IQR smaller than lower limit based on mean minus two standard deviations. Therefore, the second method is more capable in detect anomaly in LST time series.

C. Afghanistan Earthquake on January 31, 2018

According to mean ± 2σ method, prior positive anomaly detected 10 and 11 days before Afghanistan earthquake (January 31, 2018) in MODIS Terra daytime (Table III). These

http://dx.doi.org/10.14500/aro.10591

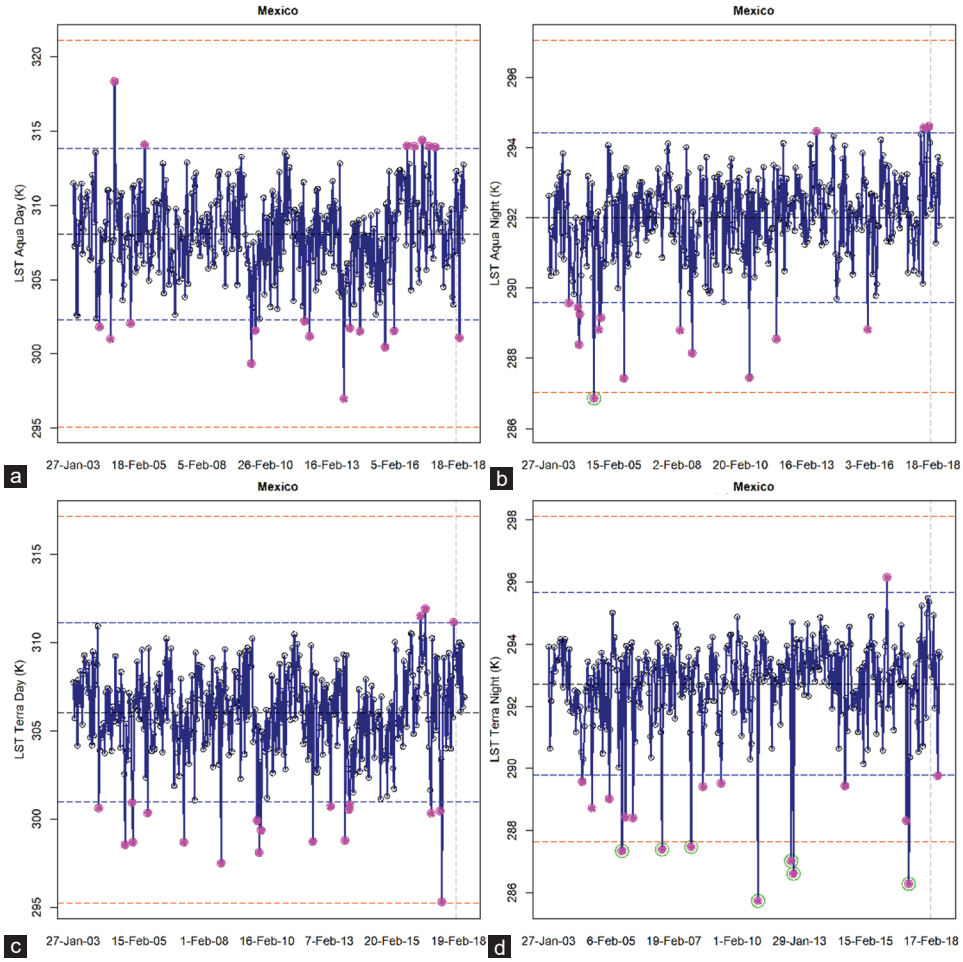

Fig. 2. Temporal anomalies of land surface temperature (LST) Aqua day (a), LST Aqua night (b), LST Terra day (c), LST Terra night (d), in San Pedro Jicayan, Mexico earthquake (February 16, 2018). Gray dashed line: The day of the earthquake, blue dashed lines: Limit upper and limit lower based on mean ± 2σ, red dashed lines: Limit upper and limit lower based on interquartile range (IQR) method, magenta circles: Anomaly based on mean ± 2σ, green circle: IQR-based anomalies, black dashed line: Mean value of the area.

TABLE III
Anomalies in Mexico (February 16, 2018), Bolivia (April 2, 2018), and Afghanistan (January 31, 2018) Earthquakes with the Intensity and Type of Anomaly and How Many Days before or after the Main Quake Anomaly Occurred

Earthquake	Data	IQR method	Mean±2σ method	Type	Compare to mean	Days before
Mexico	Terra night	No	Yes	Post (negative)	−3	(8 after)
	Aqua night	No	Yes	Prior positive	2.6, 2.6, 2.6	2, 3, 8
	Terra day	No	Yes	Prior positive (negative)	5.1, −10.7, −5.6	2, 14, 16
	Aqua day	No	Yes	Post negative	−7.0	(3 after)
Bolivia	Terra night	No	Yes	Prior negative	−6.9	5
	Aqua night	No	Yes	Prior negative	−13.1, −7.8, −9.7	4, 5, 11
	Terra day	No	Yes	Prior negative	−9.8, −9.2	5, 9
	Aqua day	No	No			
Afghanistan	Terra night	No	No			
	Aqua night	No	No			
	Terra day	No	Yes	Prior positive	10.5, 10.2	10, 11
	Aqua day	No	No			

outliers were larger than mean by 10.5 and 10.2 K degrees. In Aqua day and night data, no anomalies detected. Based on quartile outliers, no outliers detected in Aqua and Terra, daytime and nighttime LST data in this case study neither during 2018 nor previous years in the same period (Fig. 4 a-d).

IV. Discussion

Nezammahalleha, et al. (2013) and Saraf, et al. (2008) found more seismic activity occurred in areas with higher LST in Iran and positive anomaly of LST observed in 23 Indian earthquakes. The current research used daytime

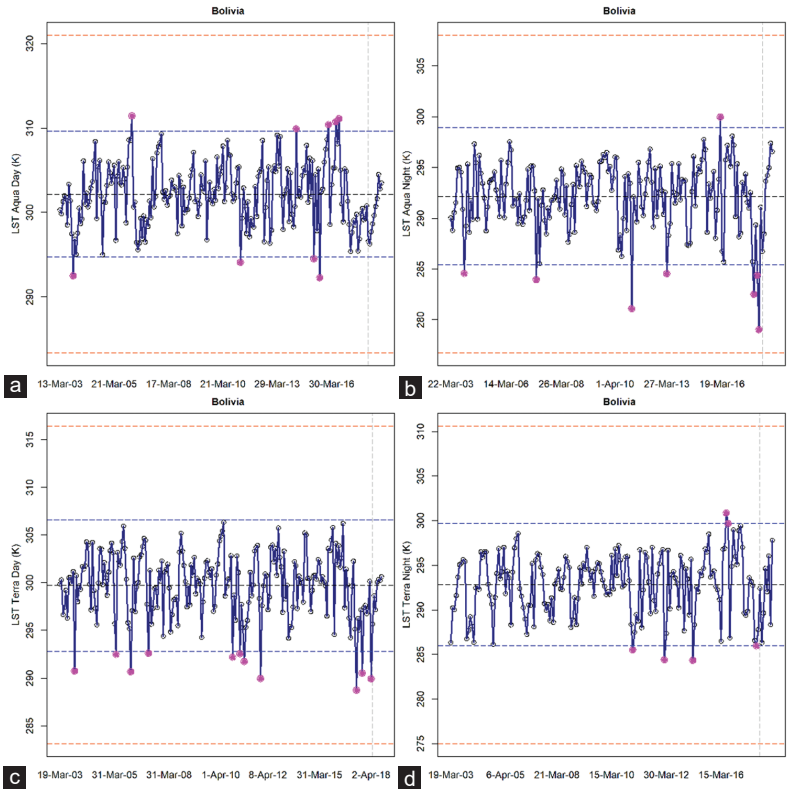

Fig. 3. Temporal anomalies of land surface temperature (LST) Aqua day (a), LST Aqua night (b), LST Terra day (c), LST Terra night (d), in Carandayti, Bolivian earthquake (April 2, 2018). Gray dashed line: The day of the earthquake, blue dashed lines: Limit upper and limit lower based on mean ± 2σ, red dashed lines: Limit upper and limit lower based on interquartile range (IQR) method, magenta circles: Anomaly based on mean ± 2σ, green circle: IQR-based anomalies, black dashed line: Mean value of the area.

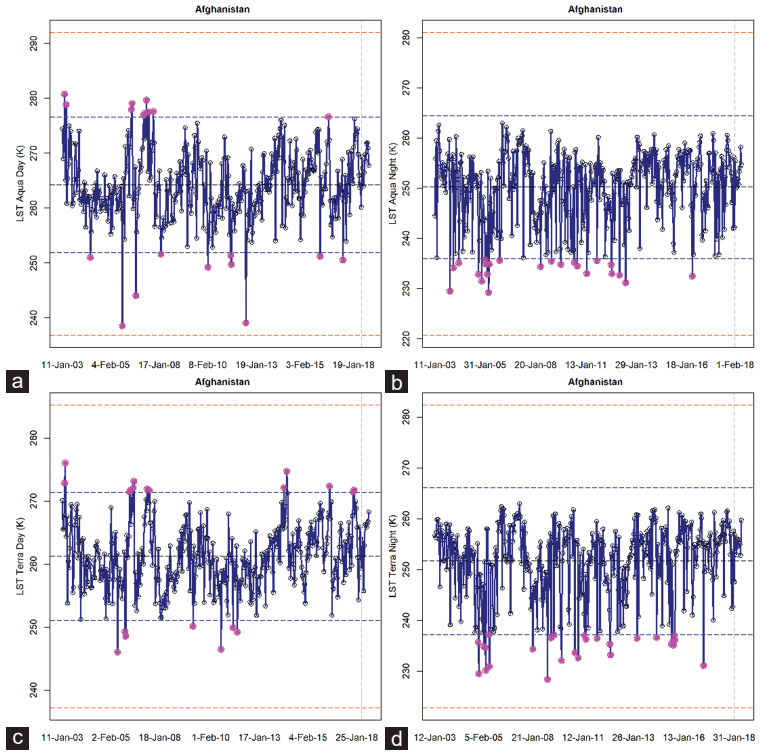

Fig. 4. Temporal anomalies of land surface temperature (LST) Aqua day (a), LST Aqua night (b), LST Terra day (c), LST Terra night (d), in Jarm, Afghanistan earthquake (January 31, 2018). Gray dashed line: The day of the earthquake, blue dashed lines: Limit upper and limit lower based on mean ± 2σ, red dashed lines: Limit upper and limit lower based on on interquartile range (IQR) method, magenta circles: Anomaly based on mean ± 2σ, green circle: IQR-based anomalies, black dashed line: Mean value of the area.

and nighttime MODIS LST data. It found usually positive anomaly of LST during daytime however negative (or positive) anomaly during the nighttime LST data before the earthquakes. After the earthquake during 10 days, a negative anomaly could be anticipated in both Aqua and Terra LST. As a result of investigated three samples of an earthquake during 2018, we observed in some earthquakes, anomaly in more than 1 parameter discerned such as Mexico and Bolivia. Whereas in some earthquake such as Afghanistan earthquake, only prior anomaly occurred in daytime Terra LST.

In LST Terra daytime, positive anomaly was detected in the 20th and 21st of January, which means 10 and 11 days before the earthquake of Afghanistan (Fig. 4c). However, also outliers detected during 2003, 2006, 2007, 2011, 2012, 2014, and 2018. It implies that perhaps occurring anomaly in LST during this period is not completely related to the earthquake. The relationship between longtime data of climatic parameters and dates of earthquakes required more investigations to disclose whether the anomalies related to earthquake or it happened by other factors. Our results confirm that method of mean and two standard deviations is more capable to find anomaly compared to IQR method to select outliers in LST.

V. Conclusions

The current study aimed to determine the earthquake's remote sensing LST temporal anomaly of samples of earthquake occurred during 2018. Samples of the earthquake in the land transparent sky considered. Four times MODIS data that available through GEE used and analyzed using GEE with R programming.

In Bolivian earthquake, based on mean ± 2σ anomaly methods, prior anomaly detected in Aqua night and Terra LST. Based on the IQR method, anomaly of LST not detected in assessed cases. Whereas based on mean ± 2σ anomaly, positive or negative anomaly of LST occurred during daytime and nighttime. However, negative anomaly detected after the Mexico earthquake.

Researches in this field may have some limitations, for instance, some parameters available on the GEE, but they are not real-time data. Some satellite data are available in GEE but they have not high resolution. Besides, some anomaly detected around the earthquake period, may not relate to the occurred earthquake because of anomalies discerned during the same month of previous years. Another problem of earthquake forecasting is false-negative case. Future research should focus on other reliable factors that perhaps related to an earthquake. They should utilize more techniques and statistical methods for discovering robust results that may contribute to forecast an earthquake in the future. Conclusively, use of four LST data from different times of day and night in the current study led to more insight about LST anomaly related to earthquake.

Acknowledgment

The authors would like to acknowledge the GEE program and the R Development Core Team to support and support this freely available program.

References

Allen, C.R., 1976. Responsibilities in earthquake prediction: To the seismological society of America, delivered in Edmonton, Alberta, May 12, 1976. *Bulletin of the Seismological Society of America*. 66(6), pp.2069-2074.

Anomaly.Io., 2015. Anomaly Detection with the Normal Distribution, Anomaly. Available from: https://www.anomaly.io/anomaly-detection-normal-distribution. [Last accessed on 2019 Jul 14].

Bhardwaj, A., Singh, S., Sam, L., Bhardwaj, A., Martín-Torres, F.A., Singh, A., and Kumar, R., 2017. MODIS-based estimates of strong snow surface temperature anomaly related to high altitude earthquakes of 2015. *Remote Sensing of Environment*, 188, pp.1-8.

Dancho, M., and Vaughan, D., 2018. *Anomalize: Tidy Anomaly Detection*. Available from: https://www.cran.r-project.org/package=anomalize. [Last accessed on 2019 Jan 03].

Dey, S., and Singh, R.P. 2003. Surface latent heat flux as an earthquake precursor. *Natural Hazards and Earth System Science*, 3(6), pp.749-755.

Geiß, C., and Taubenböck, H., 2013. Remote sensing contributing to assess earthquake risk: From a literature review towards a roadmap. *Natural Hazards*, 68(1), pp.7-48.

Geller, R.J., 1997. Earthquake prediction: A critical review. *Geophysical Journal International*, 131(3), pp.425-450.

Geller, R.J., 2011. Shake-up time for Japanese seismology. *Nature*, 472, pp.407-409.

Geller, R.J., Jackson, D.D., Kagan, Y.Y., and Mulargia, F., 1997. Earthquakes cannot be predicted. *Science*, 275(5306), pp.1616-1616.

Gorelick, N., Hancher, M., Dixon, M., Ilyushchenko, S., Thau, D., and Moore, R., 2017. Google earth engine: Planetary-scale geospatial analysis for everyone. *Remote Sensing of Environment*, 202, pp.18-27.

Jiao, Z.H., Zhao, J., and Shan, X., 2018. Pre-seismic anomalies from optical satellite observations: A review. *Natural Hazards and Earth System Sciences*, 18(4), pp.1013-1036.

Nezammahalleha, M.A., Noori, A.A., Afsharmanesh, H., Pourhosseini, Z., Rastegar, A., Rezai, H.S.S., and Alavipanah, S.K., 2013. Identification of active areas of earthquake by thermal remote sensing. *International Archives of the Photogrammetry*, *Remote Sensing and Spatial Information Sciences*, 1, pp.295-299.

Ouzounov, D., and Freund, F., 2004. Mid-infrared emission prior to strong earthquakes analyzed by remote sensing data. *Advances in Space Research*, 33(3), pp.268-273.

Ouzounov, D., Pulinets, S., Kafatos, M.C., and Taylor, P., 2018. Thermal radiation anomalies associated with major earthquakes. In: *Pre-Earthquake Processes: A Multidisciplinary Approach to Earthquake Prediction Studies, Geophysical Monograph*. Vol. 234. John Wiley, Hoboken, pp.259-274.

Rasul, A., Balzter, H., and Smith, C., 2016. Diurnal and seasonal variation of surface urban cool and heat Islands in the Semi-Arid City of Erbil, Iraq. *Climate*, 4(3), p.42.

Rawat, V., Saraf, A.K., Das, J., Sharma, K., and Shujat Y., 2011. Anomalous land surface temperature and outgoing long-wave radiation observations prior to earthquakes in India and Romania. *Natural Hazards*, 59(1), pp.33-46.

Saraf, A.K., Choudhury, S., Rawat, V., Banerjee, P., Dasgupta, P., and Das, J.D., 2008. Detecting earthquake precursor: A thermal remote sensing approach. In: *Map India 2008-11th Annual International Conference and Exhibition on Geospatial Information, Technology and Application*. pp.1-10.

Shen, H., Li, X., Zhang, L., Tao, D., and Zeng, C., 2013. Compressed sensing-based inpainting of aqua moderate resolution imaging spectroradiometer band 6 using adaptive spectrum-weighted sparse Bayesian dictionary learning. *IEEE Transactions on Geoscience and Remote Sensing*, 52(2), pp.894-906.

Streit, M., and Gehlenborg, N., 2014. Bar charts and box plots. *Nature Methods*, 11(2), p.117.

Tramutoli, V., Bello, G.D., Pergola, N., and Piscitelli, S. 2001. Robust satellite techniques for remote sensing of seismically active areas. *Annals of Geophysics*, 44, pp.295-312.

Tronin, A., 2009. Satellite remote sensing in seismology. A review. *Remote Sensing*, 2(1), pp.124-150.

Tronin, A.A., Hayakawa, M., and Molchanov, O.A., 2002. Thermal IR satellite data application for earthquake research in Japan and China. *Journal of Geodynamics*, 33(4-5), pp.519-534.

USGS.Gov., 2019. *USGS Earthquake Hazards Program*. Available from: https://www.earthquake.usgs.gov. [Last accessed on 2019 Jul 14].

Wu, L., and Liu, S., 2009. Remote sensing rock mechanics and earthquake thermal infrared anomalies. In: *Advances in Geoscience and Remote Sensing*. Intech Open, London.

Wu, L., Zheng, S., Santis, A.D., Qin, K., Mauro, R.D., Liu, S., and Rainone, M.L., 2016. Geosphere coupling and hydrothermal anomalies before the 2009 Mw 6.3 L'Aquila earthquake in Italy. *Natural Hazards and Earth System Sciences*, 16, pp.1859-1880.

Zoran, M.A., Savastru, R.S., and Savastru, D.M., 2015. Satellite thermal infrared anomalies associated with strong earthquakes in the Vrancea area of Romania. *Open Geosciences*, 7(1), pp.606-617.

Appendixes

APPENDIX A: A sample of process data in the google engine code

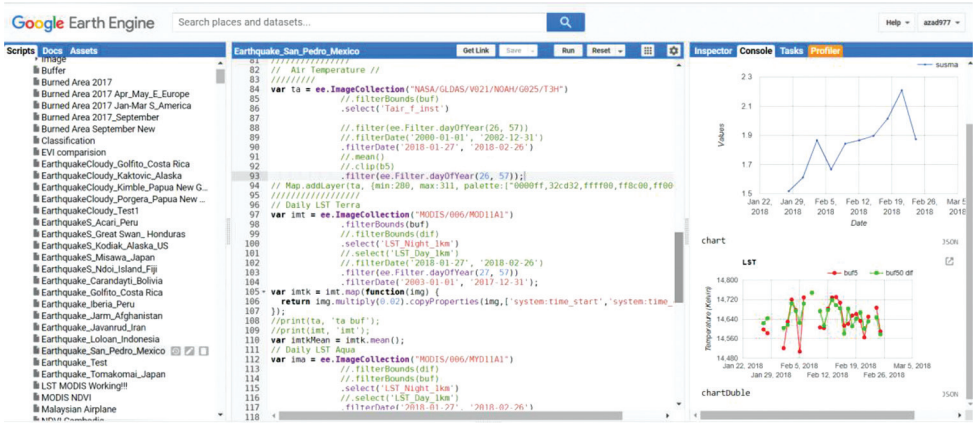

APPENDIX B: A sample of utilized R code in the study

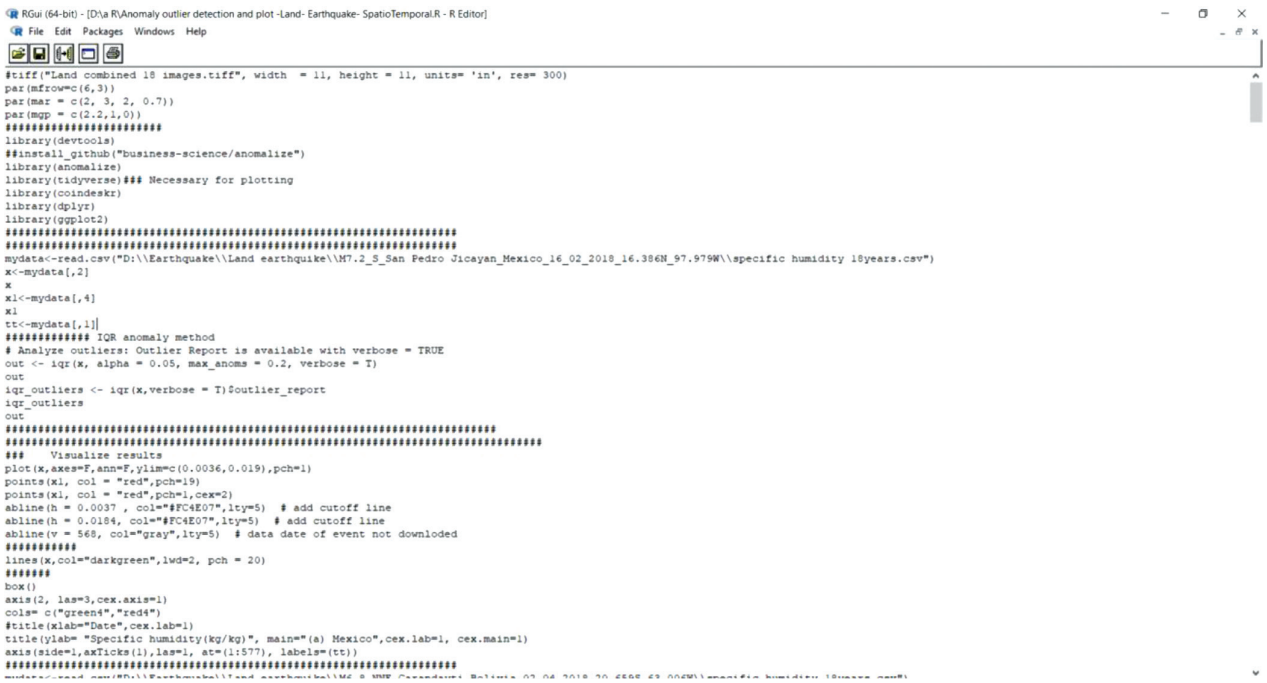

http://dx.doi.org/10.14500/aro.10671

Calculation of Electron Swarm Parameters in Tetrafluoromethane

Idris H. Salih[1], Mohammad M. Othman[2] and Sherzad A. Taha[2]

[1]Tishk International University,
Erbil, Kurdistan Region – F.R. Iraq

[2]Department of Physics, College of Education, Salahaddin University-Erbil,
Erbil, Kurdistan Region – F.R. Iraq

***Abstract*—The electron swarm parameters and electron energy distribution function (EEDF) are necessary, especially on understanding quantitatively plasma phenomena and ionized gases. The EEDF and electron swarm parameters including the reduce effective ionization coefficient (α–η)/N (α and η are the ionization and attachment coefficient, respectively), electron drift velocity, electron mean energy, characteristic energy, density normalized longitudinal diffusion coefficient, and density normalized electron mobility in tetrafluoromethane (CF_4) which was analyzed and calculated using the two-term approximation of the Boltzmann equation method at room temperature, over a range of the reduced electric field strength (E/N) between 0.1 and 1000 Td (1Td=10^{-17} V.cm^2), where E is the electric field and N is the gas density of the gas. The calculations required cross-sections of the electron beam, thus published momentum transfer, vibration, electronic excitation, ionization, and attachment cross-sections for CF_4 were used, the results of the Boltzmann equation in a good agreement with experimental and theoretical values over the entire range of E/N. In all cases, negative differential conductivity regions were found. It is found that the calculated EEDF closes to Maxwellian distribution and decreases sharply at low E/N. The low energy part of EEDF flats and the high-energy tail of EEDF increases with increase E/N. The EEDF found to be non-Maxwellian when the E/N> 10Td, having energy variations which reflect electron/molecule energy exchange processes. In addition, limiting field strength $(E/N)_{limit}$ has been calculated from the plots of (α–η)/N, for which the ionization exactly balances the electron attachment, which is valid for the analysis of insulation characteristics and application to power equipment.**

***Index Terms*—Boltzmann equation, CF4, Electron discharge, Electron swarm parameters, Kinetic and transport theory.**

I. Introduction

Tetrafluoromethane, also known as carbon tetrafluoride or R-14 is the simplest fluorocarbon (CF_4), was first observed as an impurity in krypton by Gassman, 1974, it has a low critical temperature and high critical pressure. The CF_4 is a man-made gas which has an important role in technological applications such as semiconductor, etching plasma for material processing, discharge opening switches, atmospheric physics and chemistry, gaseous dielectrics, and gaseous detector technology (Hunter, et al., 1985; Proshina, et al., 2015). Tetrafluoromethane is combined with oxygen as an etching medium used in the semiconductor industry for etching of dielectric materials, such as SiO_2 and also for deposition of fluorinated polymer films. In combination CF4 with SF_6 produce a less expensive, toxic, and corrosive cryogenic liquid than SF_6 alone (Reinking, et al., 1986).

Tetrafluoromethane (CF_4) is a very powerful greenhouse, it is stable and does not deplete the ozone layer, which strongly absorbs infrared radiation at ~8 μm. The lifetime of CF_4 is 50,000 years, with a global warming potential (GWP) 6500 times greater than that of CO_2 over a 100-year time scale, only about 26.36% of that of SF_6 (Muhle, et al., 2010; Tezcan, et al., 2016).

Tetrafluoromethane, at room temperature and atmospheric pressure, is a colorless, odorless, easy to compress gas, high stability, non-toxic, and non-flammable gas. CF_4 has been used not only in the form of pure but also in mixtures with other gases for much industrial application. In high-voltage technology, CF_4 is used as an admixture for circuit breakers (Duzkaya and Tezcan, 2017).

For example, binary mixtures of CF_4 and Ar are used in microelectronics circuit applications (Cox, et al., 1989), whereas CF_4/Ar mixtures have been also used in the application of capacitively coupled plasma (CCP) (Kitajima, et al., 2000) and possibly even inductively coupled plasma (Hioki, et al., 2000). The mixture of SF_6 and CF_4 has found applications in high-voltage circuit breakers in a cold climate which has greatly reduced the GWP compared with pure SF_6 (Xiao, et al., 2004). A mixture of 50% SF_6–50% CF_4 has been proposed as an insulating gas for electrical equipment, which was successfully utilized for circuit breakers (Wu, et al., 2006).

The electron swarm parameters of CF_4, which are the drift velocity, characteristic energy, mean electron energy, electron mobility, diffusion coefficient ionization, attachment, and effective ionization coefficients, are widely investigated in the

ARO-The Scientific Journal of Koya University
Vol. VIII, No.2 (2020), Article ID: ARO.10671, 7 pages
DOI:10.14500/aro.10671
Received 03 May 2020; Accepted 08 July 2020
Regular research paper: Published 01 September 2020
Corresponding author's e-mail: sherzad.taha@su.edu.krd

literature (Bordage, et al., 1996; Bordage and Segur, 1999; Vasenkov, 1999; Christophorou and Olthoff, 2004; Xiao and Deng, 2013; Sang-Nam, 2015; Michele, 2018). These swarm parameters are also calculated in CF_4-Ar (Kurihara, et al., 2000; Tezcan, et al., 2013), CF_4-SF_6 (Xueli and Xiao, 2007), and CHF_3-CF_4 gas mixtures (Duzkaya and Tezcan, 2019). Furthermore, the ternary mixtures SF_6-CF_4-Ar were also analyzed by solving Boltzmann's equation (Tezcan, et al., 2016; Tezcan, et al., 2016).

In the present study, the behavior of electron swarm parameters in pure tetrafluoromethane (CF_4) is studied and analyzed using the two-term approximation of the Boltzmann equation in the range of density reduced electric field strength E/N varying from 0.1 to 1000 Td (1Td=10^{-17} Vcm^2), where E is the electric field and N is neutral number density.

II. Theory

A. The Boltzmann Equation

The role of electron energy distribution function (EEDF) is an important parameter to compute the electron swarm parameters, it is difficult to measure experimentally. The EEDF calculated from a set of electron gas collision cross-section using Monte Carlo simulation method or Boltzmann equation (two-term or multi-term solution), when the electron collision frequency for inelastic collisions is much smaller than the collision frequency for elastic collision, it is the condition the two-term solution to be valid (Smith and Thomson, 1978). The steady-state distribution function is then given by the solution of the Boltzmann equation which is based on the two-term theory (Pinheiro and Loureiro, 2002). A detailed solution of Boltzmann equation used in this study to calculate electron swarm parameters may be found in the literatures (Holstein, 1946; Frost and Phelps, 1962; Smith and Thomson, 1978; Hagelaar and Pitchford, 2005). The basic of Boltzmann transport equation used in this study is given as,

$$\frac{E^2}{3}\frac{d}{d\varepsilon}\left(\frac{\varepsilon}{NQ_m^T(\varepsilon)}\frac{df_0(\varepsilon)}{d\varepsilon}\right)+\frac{2m}{M}\frac{d}{d\varepsilon}\left(\varepsilon^2 NQ_m^T(\varepsilon)f_0(\varepsilon)\right)+\frac{2mK_BT_g}{Me}\left(\varepsilon^2 NQ_m^T(\varepsilon)\frac{df_0(\varepsilon)}{d\varepsilon}\right)+\sum_J(\varepsilon+\varepsilon_J)f_0(\varepsilon+\varepsilon_J)NQ_J(\varepsilon+\varepsilon_J)-\varepsilon f_0(\varepsilon)N_J\sum_J Q_J(\varepsilon)=0 \quad (1)$$

Equation (1) is the so-called homogeneous electron Boltzmann transport equation and the isotropic component of the electron velocity distribution function, $f_o(v)$, can be expressed in terms of the electron energy $\varepsilon=0.5mv^2$, being then termed isotropic EEDF depends on the electron energy. K_B is the Boltzmann constant, T_g is the gas temperature, m/M is the ratio of electronic to atomic mass, $Q_J(\varepsilon)$ is the cross-sections for transitions from the ground state to the various excited states J, and ε_J is the threshold energy of the Jth excitation process, and $Q_m^e(\varepsilon)$ is the total effective momentum transfer cross section defined as follows,

$$Q_m^T(\varepsilon)=Q_m(\varepsilon)+\sum\nolimits_j Q_e(\varepsilon)+Q_i(\varepsilon)+Q_a(\varepsilon) \quad (2)$$

Where, $Q_m(\varepsilon)$, $Q_e(\varepsilon)$, $Q_i(\varepsilon)$, and $Q_a(\varepsilon)$ are the electron cross-sections of momentum transfer, excitation, ionization, and attachment, respectively.

The 4th term in Equation (1) expresses inelastic loss processes due to electrons of energy $(\varepsilon+\varepsilon_J)$ undergoing a collision in which they lose the energy ε_J and appear as electrons of energy ε. The last term expresses gain of energy by electrons due to the second kind collision.

Equation (1) applies to swarm of electron drifting through gas and mixtures under the influence of a uniform dc electric field E in V/cm.

B. Transport Parameters

The electron transport coefficient in given gases calculated using a two-term approximation of the Boltzmann equation is functions of the density reduced electric field strength E/N, the gas temperature, and electron collision cross-section sets. The EEDF plays an important role in the calculation of electron swarm parameters.

The EEDF can be normalized by Colonna and D'Angola, 2016,

$$\int_0^\infty f(\varepsilon)\sqrt{\varepsilon}\,d\varepsilon=1 \quad (3)$$

Taking into account, the normalization condition, $f_o(\varepsilon)$ and $f(\varepsilon)$ are linked to one another as follows,

$$f(\varepsilon)=\frac{1}{n_e}\frac{4\pi}{m}\sqrt{\frac{2}{m}}f_o(\varepsilon) \quad (4)$$

With such normalization, the Maxwellian electron distribution function at temperature T_g writes (Jiang and Economou, 1993),

$$f(\varepsilon)=\frac{2}{\sqrt{\pi}}\left(K_BT_g\right)^{-3/2}\exp\left(-\frac{\varepsilon}{K_BT_g}\right) \quad (5)$$

In terms of the EEDF, $f(\varepsilon)$, the mean electron energy is expressed as,

$$\langle\varepsilon\rangle=\int_0^\infty \varepsilon^{3/2}f(\varepsilon)\,d\varepsilon \quad (6)$$

With $\langle\varepsilon\rangle=\frac{3}{2}K_BT_g$, in the case of a Maxwellian, while the electron mobility $\mu_e=\sigma_e/en_e$, where σ_e the electron conductivity (Lee and More, 1984), is given by the equation,

$$\mu_e=-\frac{2}{3}\frac{e}{m}\int_0^\infty\frac{\varepsilon^{3/2}}{\nu_m^e(\varepsilon)}\frac{df}{d\varepsilon}d\varepsilon \quad (7)$$

Where, ν_m^e is collision frequency, making the substitution $\nu_m^e=n_oQ_m^T$, we obtain the following expression for the reduced mobility,

http://dx.doi.org/10.14500/aro.10671

$$N\mu_e = -\frac{1}{3}\sqrt{\frac{2e}{m}}\int_0^\infty \frac{\varepsilon}{Q_m^T(\varepsilon)}\frac{\partial f(\varepsilon)}{\partial \varepsilon}d\varepsilon \quad (8)$$

The electron drift velocity, diffusion coefficient, and characteristic energy are given as Smith and Thomson, 1978,

$$v_d = -\frac{\overline{E}}{3}\sqrt{\frac{2e}{m}}\int_0^\infty \frac{\varepsilon}{NQ_m^T(\varepsilon)}\frac{\partial f(\varepsilon)}{\partial \varepsilon}d\varepsilon \quad (9)$$

The transverse diffusion coefficient D_T is given by,

$$D_T = \frac{1}{3}\sqrt{\frac{2e}{m}}\int_0^\infty \frac{\varepsilon}{NQ_m^T(\varepsilon)}f(\varepsilon)d\varepsilon \quad (10)$$

$$\varepsilon_k = \frac{eD_T}{\mu_e} \quad (11)$$

From the computed drift velocity v_d, the ionization and attachment coefficients are obtained as Do, 2016,

$$\frac{\alpha}{N} = \frac{1}{v_d}\sqrt{\frac{2e}{m}}\int_i^\infty Q_i(\varepsilon)f(\varepsilon)\varepsilon^{1/2}d\varepsilon \quad (12)$$

$$\frac{\eta}{N} = \frac{1}{v_d}\sqrt{\frac{2e}{m}}\int_a^\infty Q_a(\varepsilon)f(\varepsilon)\varepsilon^{1/2}d\varepsilon \quad (13)$$

Where, $Q_i(\varepsilon)$ and $Q_a(\varepsilon)$ are ionization and attachment cross-section, here, i and a are the ionization and attachment threshold energy. The reduced limit electric field strength $(E/N)_{limit.}$ is calculated when the formation and loss electrons reach a balance, this means that the effective ionization equal to zero $(\alpha-\eta)/N = 0$ (Li, et al., 2012).

III. Collision Cross-section

The EEDF and values of transport coefficients in tetrafluoromethane (CF_4) gas calculated from the sets cross-section (elastic and inelastic) reported by Kurihara, et al., 2000. This set includes 16 collision processes: One momentum transfer cross-section (Q_m), three vibration excitations (Q_{v1}, Q_{v2}, and Q_{v3}) with threshold energy 0.0.108, 0168, and 0.077 eV, respectively, and one electronic excitation (Q_{ex}) cross-section with threshold energy of 7.54 eV, one attachment cross-section (Q_a) with threshold energy 6.4 eV, seven dissociation ionization cross-sections (Q_{i1}-Q_{i7}) with threshold energy 16, 21, 26, 24, 34, 41, and 42 eV. respectively, and three neutral dissociation cross-sections (Q_{d1}-Q_{d3}) with threshold energy 12, 17, and 18 eV, respectively.

IV. Results and Discussion

The EEDF and electron swarm parameters in pure tetrafluoromethane (CF_4) are calculated using the two-term approximation of Boltzmann equation in dc uniform fields in the range 0.1–1000 Td, at 1 Torr and 300 K. Tetrafluoromethane gas has the momentum transfer cross-section which is greater than inelastic cross-section, this is a necessary condition for the two-term approximation solution of the Boltzmann equation to be valid (Smith and Thomson, 1978). The EEDF is one of the most important parameters for gas discharge phenomena and used for calculating electron swarm parameters. The E/N values were chosen to yield mean electron energies in the range of 0.045–14.3 eV. The EEDF for a dc field with various E/N values is given in Fig. 1 (where, E is the electric field and N is the gas density).

The influence of the EEDF versus the mean electron energy for different ratios of electric field strength (E/N) is shown in Fig. 1. The EEDF is strongly affected by changing parameter E/N, the higher values of E/N lead to the extension of the EEDF curves toward higher energy tail. The distribution function is normalized by Equation (3), the outcome of EEDF curves is due to constant electron density $n_e = 1\times10^{16}$ cm^{-3}. For the lowest E/N≤ 1Td, where 1 $Td = 10^{-17}$ $V.cm^2$. The electron energy is thermal and the ionization degrees $(n_e/N) > (Q/10^{-13})\ \varepsilon^2$ (where, ε is energy in eV and Q is an elastic and inelastic cross-section in the unit of cm^2) of the order of 10^{-3}–10^{-4} can be sufficient to give Maxwellian characteristics of the EEDF as indicated by the straight line with a slope of $(-1/K_BT_g)$. In this case, the ionization degree is very small and the tetrafluoromethane (CF_4) atoms are in the ground state. However, in the range E/N>1 Td, the distribution is non-Maxwellian, the tail of the EEDF falls off rapidly as high-energy electrons are depleted due to different inelastic collisions. This behavior can be attributed to the electric field that heats the electrons and the energy of cold electrons increases. Subsequently, the mean electron energy depends on the electric field strength E/N.

Using EEDF, the electron swarm parameters have been calculated. Fig. 2 shows our calculated results for electron drift velocity as a function of E/N in comparison with the corresponding results provided by previous theoretical and experimental literatures.

The agreement between the present calculation and theoretical values (Bordage and Segure, 1999; Wu, et al., 2006; Duzkaya and Tezcan, 2019) and experimental values

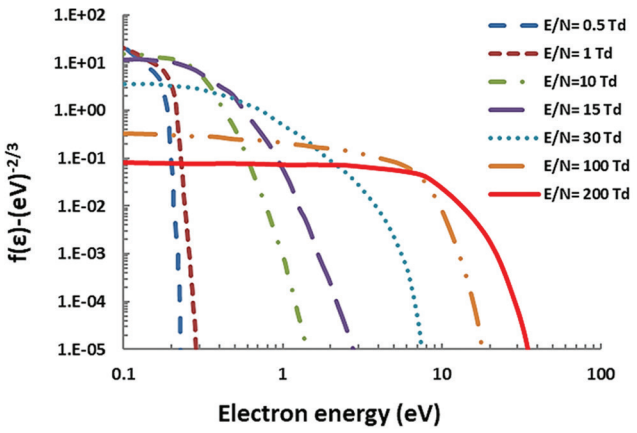

Fig. 1. Electron energy distribution functions in pure CF_4 for various E/N values.

(Hunter, et al., 1988; Nakamura, 1996; Xiao and Deng, 2013; Duzkaya and Tezcan, 2019) is excellent. The theoretical results of Sang-Nam, 2011, in range E/N >4 Td are greater than present results and theoretical results of Michele, 2018, in the range E/N ≥50 Td greater than present calculation. The drift velocity in pure CF4 showed negative differential conductivity (NDC) over the range from 15 to 60 Td, the decrease in the drift velocity was not smooth but contained a small hump. A combination of the elastic and inelastic cross-sections can occur in a tetrafluoromethane (CF_4) molecules, at low electric field strength E/N≤20 Td the drift velocity rapidly increases, and at the region of higher E/N values (20≤E/N≤100 Td), the drift velocity will decrease with increasing E/N values. NDC will occur over a range of electric field strength E/N values in CF_4 when the inelastic cross-section has a large resonant type with respect to energies, and momentum transfer cross-section rapidly increases with electron energy.

Fig. 3 shows mean electron energy which increases with increasing E/N values, it is seen that the present calculation agree well with the experimental values of Curtis, et al. 1998, and theoretical values of Kurihara, et al., 2000; Tezcan, et al., 2013; Sang-Nam, 2015.

The calculated values of the characteristic energy of electrons as a function of E/N in pure CF_4 are shown in Fig. 4.

The calculated values compared with experimental values of Curtis, et al., 1988, and theoretical values of Mašek, et al., 1987; Stefanov and Pirgov, 1993; Bordage and Segur, 1999, a very good agreement was obtained, whereas the experimental values of Christophorou and Olthoff, 2004, are lower than calculated values over the E/N range between 2 and 300 Td. The characteristic energy increases with the increase of E/N during the inelastic collision process (8 Td ≤E/N≤ 80 Td) and then starts to be approximately constant at E/N≥80 Td, where above this value, the ionization process occurs for CF_4.

Fig. 5 shows density normalized electron mobility μN, which decreases with increasing E/N value, it is seen that the present calculation agree well with the experimental values of Hunter, et al., 1988.

The product of the longitudinal diffusion coefficient and the number density ND_L (E/N) is shown in Fig. 6. The results

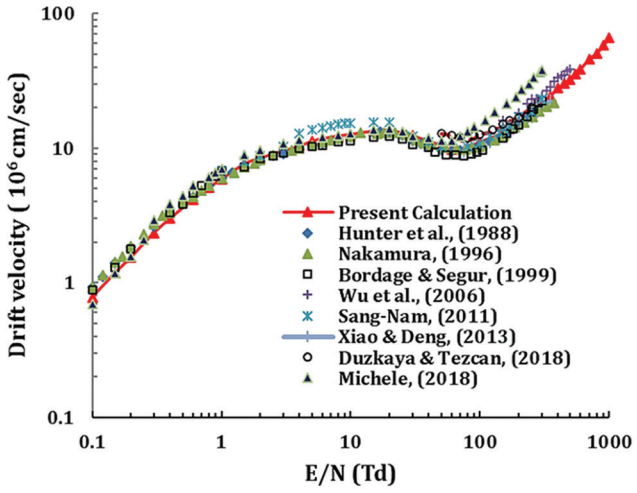

Fig. 2. Electrons drift velocity in pure CF_4.

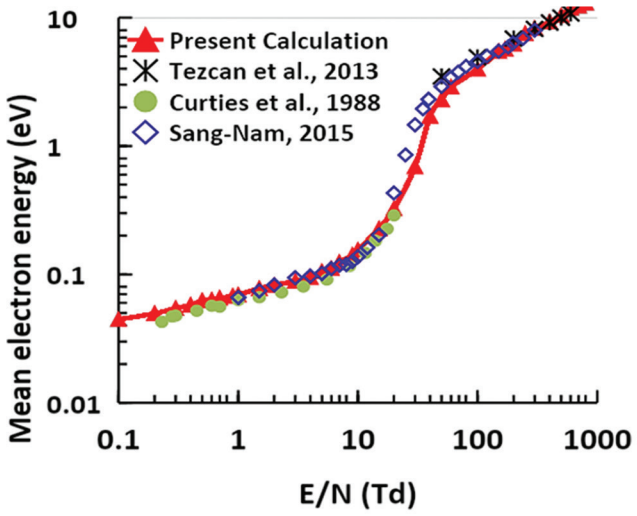

Fig. 3. Electron means energy in pure CF_4.

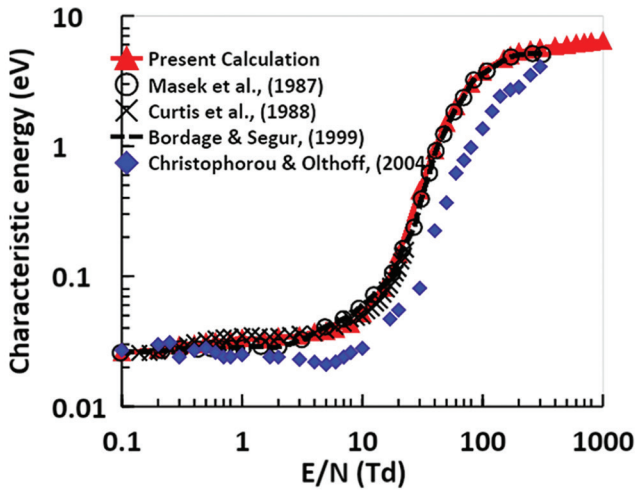

Fig. 4. Characteristic energy in pure CF_4.

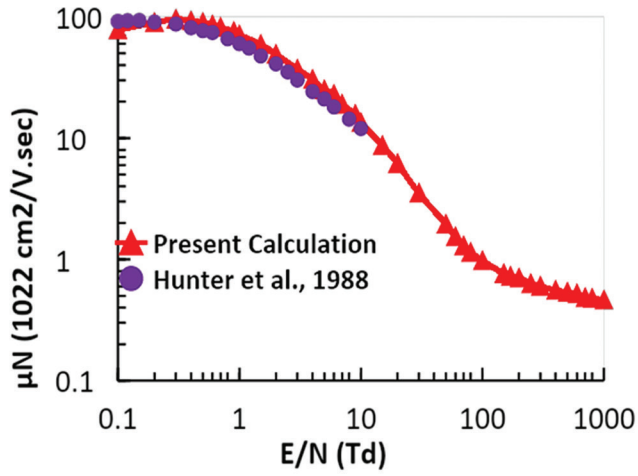

Fig. 5. Density normalized electron mobility μN in pure CF_4.

http://dx.doi.org/10.14500/aro.10671

compared with the experimental values of Nakamura, 1996; Christophorou and Olthoff, 2004, and theoretical values of Kurihara, et al., 2000; Wu, et al., 2006.

The agreement is excellent over much of the range of E/N, with discrepancies in magnitude up to 10% in the region between 150 and 500 Td between present calculation and experimental values of Xiao and Deng, 2013. The density normalized ionization coefficient α/N has been calculated for the range $80 \leq E/N \leq 1000$Td using Equation (12) and the results are shown in Fig. 7.

A good agreement has been obtained with the theoretical values of Mašek, et al., 1987; Bordage et al., 1999; San-Nam, 2012, and experimental values of Hunter, et al., 1988, for the whole range of E/N. Fig. 8 shows the density normalized attachment coefficient η/N as a function of E/N. Good agreement has been obtained with theoretical values of Bordage and Segur, 1999, and experimental values of Hunter, et al., 1988.The agreement between present data and theoretical values of San-Nam, 2012, reasonably good over the entire range of E/N, with the largest discrepancies occurring between 120 and 300 Td.

The reduced limiting electric field strength $(E/N)_{limit}$ is an important quantity calculated from ionization and attachment coefficients. It is the value of the density reduced electric field at which $(\alpha-\eta)/N=0$. This value should also be equal to the breakdown voltage of CF_4 as calculated under the uniform field, this parameter is important for some high-voltage applications. The density normalized effective ionization coefficients $(\alpha-\eta)/N=0$ in pure CF_4 are shown in Fig. 9.

The change in the attachment coefficient is more obvious than the change in the ionization coefficient, so the change of the effective ionization coefficient is more depending on the change in the attachment coefficient. The present limiting electric field strength $(E/N)_{limit}$ of pure CF_4 is evaluated as 146 Td, which is comparable with experimental values reported by Christophorou and Olthoff, 2004, and theoretical values of Liu and Xiao, 2007; Duzkaya and Tezcan, 2019, where the estimated values of $(E/N)_{limit}$ are 146, 144, and 145 Td, respectively.

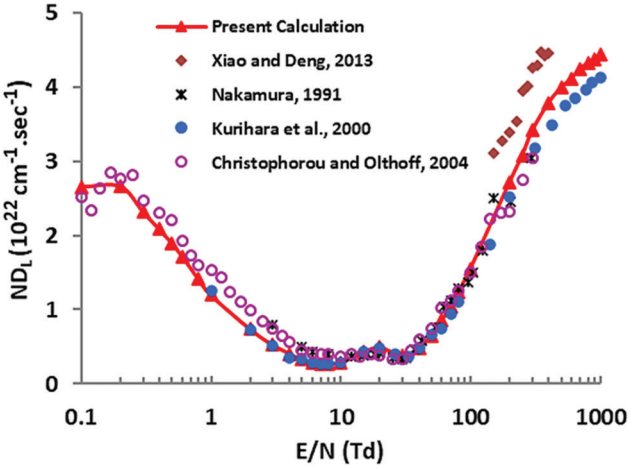

Fig. 6. The product of the longitudinal diffusion coefficient and the gas number density in pure CF_4.

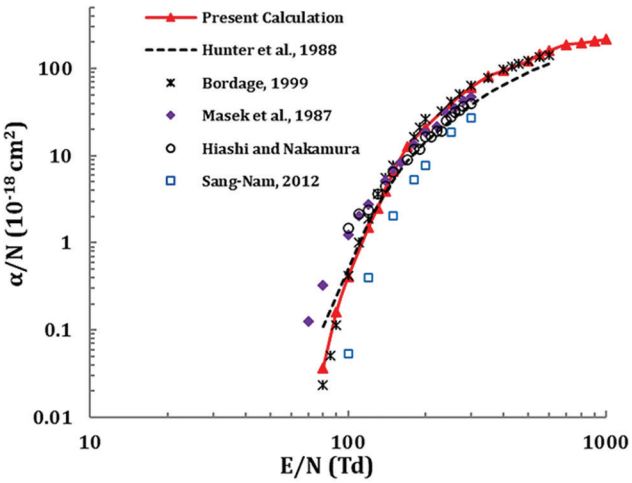

Fig. 7. Ionization coefficient in pure CF_4.

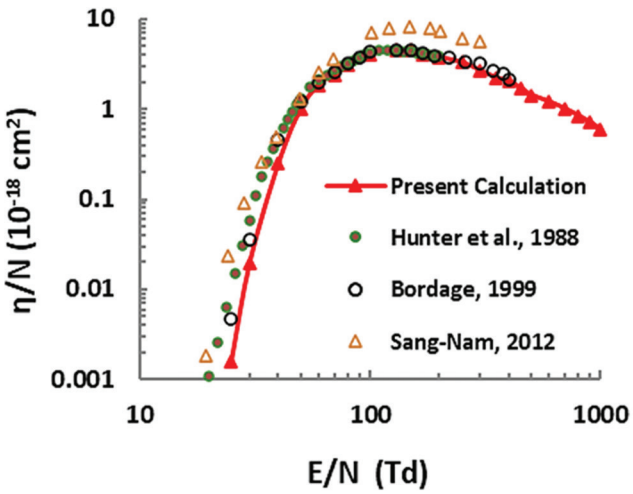

Fig. 8. Attachment coefficient in pure CF_4.

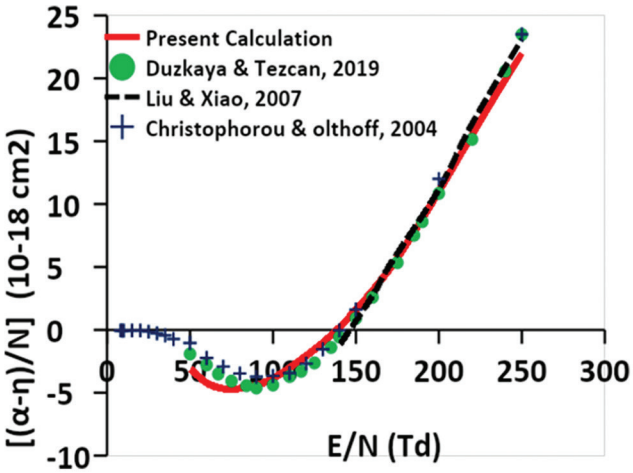

Fig. 9. Effective ionization coefficient $(\alpha-\eta)/N$ in pure CF_4.

V. Conclusion

Tetrafluoromethane (CF_4) is an electronegative and potent greenhouse gas. In this study, the EEDF, electron swarm parameters, and density normalized effective ionization coefficient of tetrafluoromethane (CF_4) are calculated using the two-term approximation solution of Boltzmann equation method for the range reduced electrical field strength varying from 0.1 Td to 1000 Td at temperature 300K. The present results based on electron collision cross-section sets for CF_4 molecules. The EEDF is strongly affected by changing the parameter E/N, we have shown that the EEDF in pure CF_4 shifts toward increasing of mean electron energy according to the increasing of E/N. The calculated swarm parameters (drift velocity, characteristic energy, mean electron energy, diffusion coefficient, electron mobility, ionization, and attachment coefficient) agree well with experimental and theoretical values. The reduced limiting electric field strength $(E/N)_{limit}$, at which the ionization and attachment rate are exactly balanced as a function of E/N, has been calculated from the effective ionization curves.

References

bordage, M.C., and Segur, P., 1999. Boltzmann analysis of electron swarm parameters in CF_4 using independently assessed electron-collision cross sections. *Journal of Applied Physics*, 86(7), pp.3558-3566.

Bordage, M.C., Segur, P., and Chouki, A., 1996. Determination of a set of electron impact cross sections in tetrafluoromethane consistent with experimental determination of swarm parameters. *Journal Applied Physics*, 80(3), pp. 1325-1336.

Christophorou, L.G., and Olthoff, J.K., 2004. *Fundamental Electron Interactions with Plasma Processing Gases*. Kluwer Academic/Plenum Publisher, New York, pp.135-218.

Colonna, G., and D'Angelo A., 2016. The Two-term Boltzmann Equation. *Plasma Modeling Methods and Applications*. Ch. 2., IOP Publishing Ltd., United Kingdom, pp.2-34.

Cox, T.I., Deshmukh, V.G.I., and Armour, D.G., 1989. Reactive ion beam etching studies of tungsten with CF4/argon mixtures using ion scattering spectroscopy and SIMS. *Vacuum*, 39(11-12), pp.1171-1173.

Curtis, M.G., Isobel, C.W., and Mathieson, K.J., 1988. Electron swarm characteristic energies (D_t/μ) in tetrafluoromethane (CF_4) at low E/N. *Journal of Physics D: Applied Physics*, 21(8), pp.1271-1274.

Do, A.T., 2016. Analysis of electron transport coefficients in binary mixtures of TEOS gas with Kr, Xe, He, and Ne gases for using in plasma assisted thin film deposition. *Journal of Electrical Engineering and Technology*, 11(2), pp.455-462.

Duzkaya, H., and Tezcan, S.S., 2017. Measurement and calculation of breakdown voltage in CF_4 gas mixtures. *Gazi Üniversitesi Journal Science Part C*, 5(3), pp.185-195.

Duzkaya, H., and Tezcan, S.S., 2019. Boltzmann analysis of electron swarm parameters in CHF_3+CF_4 mixtures. *Turkish Journal of Electrical Engineering and Computer Sciences*, 27, pp.615-622.

Frost, L.S., and Phelps, A.V., 1962. Rotational excitation and momentum transfer cross sections for electrons in H_2 and N_2 from transfer coefficients. *Physical Review*, 127(5), pp.1621-1633.

Gassman, M., 1974. Freon-14 in high-grade krypton and in the atmosphere. *Geophysics Research Letter*, 6, pp.609-612.

Hagelaar, G.J.M., and Pitchford, L.C., 2005. Solving the Boltzmann equation to obtain electron transport coefficients and rate coefficients for fluid models. *Plasma Sources Science and Technology*, 14(4), pp.722-733.

Hioki, K., Hirata, H., Nakano, N., Petrovic, Z.L., and Makabe, T., 2000. Diagnostics of an inductively coupled CF_4/Ar plasma. *Journal of Vacuum Science Technology A Vacuum Surfaces and Films*, 18(3), pp.864-872.

Holstein, T., 1946. Energy distribution of electrons in high frequency gas discharges. *Physical Review*, 70(5-6), pp.367-384.

Hunter, S.E., Carter, J.G., and Christophorou, L.G., 1988. Electron motion in the gases CF_4, C_3F_8 and n-C_4F_{10}. *Physical Review A General Physics*, 38(1), pp.58-69.

Hunter, S.R., Carter, J.G., and Christophorou, L.G., 1985. Electron transport studies of gas mixtures for use in e-beam controlled diffuse discharge switches. *Journal Applied Physics*, 58(8), pp.3001-3015.

Jiang, P., and Economou, D.J., 1993. Temporal evolution of the electron energy distribution functions in oxygen and chlorine gases under dc and ac fields. *Journal of Applied Physics*, 73(12), pp.8151-8160.

Kitajima, T., Takeo, Y., Petrovic, Z.L., and Makabe, T., 2000. Functional separation of biasing and sustaining voltages in two-frequency capacitively coupled plasma. *Applied Physics Letters*, 77(4), pp.489-491.

Kurihara, M., Petrovic, Z.L., and Makabe, T., 2000. Transport coefficients and scattering cross-sections for plasma modeling in CF4-Ar mixtures: A swarm analysis. *Journal of Physics D: Applied Physics*, 33(7), pp.2146-2153.

Lee, Y.T., and More, R.M., 1984. An electron conductivity model for dense plasmas. *Physics of Fluids*, 27(5), pp.1273-1286.

Li, X., Zhao, H., and Jia, S., 2012. Dielectric breakdown properties of SF_6-N_2 mixtures in the temperature range 300-3000K. *Journal Physics D: Applied Physics*, 45(44), p.445202.

Liu, X., and Xiao, D., 2007. Monte Carlo simulation of electron swarm parameters in the SF_6/CF_4 gas mixtures. *The Japan Society of Applied Physics*. 46(4A), pp.1664-1667.

Mašek, K., Láska, L., D'Agostino, R., and Cramarossa, F., 1987. Boltzmann equation analysis of the electron gas in CF 4 discharges plasma. *Contributions to Plasma Physics*, 27(1), pp.15-21.

Michele, R., 2018. A Monte-Carlo software tools for the characterization of gas mixtures in various detector. *Romanian Journal of Physics*, 63, pp.8-10.

Muhle, J., Ganesan, A.L., Miller, B.R., Salameh, P.K., Harth, C.M., Greally, B.R., Rigby, M., Porter, L.W., Steele, L.P., Trudinger, C.M., Krummel, P.B., O'Doherty, S., Fraser, P.J., Simmonds, P.G., Prinn, R.G., and Weiss, R.F., 2010. Perfluorocarbons in the global atmosphere: Tetrafluoromethane, hexafluoroethane, and octafluoropropane. *Atmospheric Chemistry and Physics*, 10(11), pp.5145-5164.

Nakamura, Y., 1996. Electron Swarm Parameters in Pure CF_4 and its Electron Collision Cross Sections. *Imaging Detectors in High Energy, Astroparticle and Medical Physics: Proceedings of the UCLA International Conference.* World Scientific Publishing Co Inc., Singapore, pp.75-79.

Pinheiro, M.J., and Loureiro, J., 2002. Effective ionization coefficients and electron drift velocities in gas mixtures of SF6 with He, Xe, CO_2 and N_2 from Boltzmann analysis. *Journal of Physics D: Applied Physics*, 35(23), pp.3077-3084.

Proshina, O.V., Rakhimova, T.V., Lopaev, D.V., Samara, V., Baklanov, M.R., and de Marneff, J.F., 2015. Experimental and theoretical study of RF capacitively coupled plasma in Ar-CF4-CF3I mixtures. *Plasma Sources Science and Technology*, 25, p.055006.

Reinking, G.F., Christophorou, L.G., and Hunter, S.R., 1986. Studies of total ionization in gases/mixtures of interest to pulsed power applications. *Journal Applied Physics*, 60(2), pp.499-508.

Sang-Nam, K., 2011. The drift velocity of electron in CF_4, CH_4, Ar mixtures gas. *The Transactions of the Korean Institute of Electrical Engineers P*, 60(3), pp.105-109.

Sang-Nam, K., 2012. Ionization and attachment coefficients in CF_4, CH_4, Ar mixtures gas. *The Transactions of the Korean Institute of Electrical Engineers P*, 61(1), pp.13-17.

Sang-Nam, K., 2015. Electron mean energy in CF_4, CH_4, Ar mixtures. *The Transactions of the Korean Institute of Electrical Engineers P*, 64(4), pp.241-245.

Smith, K., and Thomson, R.M., 1978. *Computer Modeling of Gas Lasers*. Plenum Press, New York.

Stefanov, B., and Pirgov, P., 1993. Semiempirical method for extracting electron molecule cross sections from experimental data: CF_4 as an example. *Plasma Chemistry and Plasma Processing*, 13(4), pp.655-671.

Tezcan, S.S., Dincer, M.S. and Bektas, S., 2016. Effective ionization coefficients, limiting electric fields, and electron energy distributions in CF_3I+CF_4+Ar ternary gas mixtures. *Physics of Plasma*, 23(7), p.073507.

Tezcan, S.S., Dincer, M.S., Bektas, S., and Hiziroglu, H.R., 2013. Boltzmann analysis of electron swarm parameters in binary CF4+Ar mixtures. *IEEE Transactions on Dielectrics and Electrical Insulation*, 20(1), pp.98-103.

Tezcan, S.S., Duzkaya, H., Dincer, M.S., and Hiziroglu, H.R., 2016. Assessment of electron swarm parameters and limiting electric fields in SF_6+CF_4+Ar gas mixtures. *IEEE Transactions on Dielectrics and Electrical Insulation*, 23(4), pp.1996-2005.

Vasenkov, A.V., 1999. Electron swarm parameters in carbon tetrafluoride. *Journal of Applied Physics*, 85(2), pp.1222-1224.

Wu, B.T., Xiao, D.M., and Zhang, L.C., 2006. Electron swarm coefficients in SF_6 and CF_4 gas mixtures from Monte Carlo method. *The European Physical Journal Applied Physics*, 35(1), pp.57-60.

Xiao, D.M., and Deng, Y., 2013. Determination of electron swarm parameters in pure CHF_3 and CF_4 by a time-resolved method. *Plasma Science and Technology*, 15(1), pp.25-29.

Xiao, D.M., Yang, J.L., and Xu, X., 2004. Electron swarm parameters in SF_6 and CF_4 gas mixtures. *Japanese Journal of Applied Physics*, 43(3A), pp.L369-L371.

Xueli, L., and Xiao, D.M., 2007. Monte Carlo simulation of electron swarm parameters in the SF_6/CF_4 gas mixtures. *Japanese Journal of Applied Physics*, 46(4A), pp.1663-1667.

Mechanical Response of PbSSe, PbSTe Ternary and PbSnSTe Quaternary Alloys at High Pressure

Mazin Sh. Othman

Department of General Science, Faculty of Education, Soran University,
Kurdistan Region – F.R. Iraq

***Abstract*— Property of the semiconductors under high pressure is investigated by the density functional theory and paralleled to the foretelling of the linear elasticity theory. In addition, ternary alloys of PbS_xSe_{1-x} and PbS_xTe_{1-x} lattice matching PbS substrate for x = 0.5 compositions are studied. Furthermore, quaternary alloys $Pb_xSn_{1-x}S_yTe_{1-y}$ lattice matching PbS substrate for x and y = 0.5 compositions are studied. The six independent elastic parameters (*Cij*) are also calculated. Meanwhile, the results data are analyzed in high pressure. The mechanical response of all alloys to pressures 0, 50 and 100 kbar increases progress to decrease in (*Cij*) in separate rates. The rapprochement between the calculated results and the available published data for these alloys demonstrate that they had worthy accordance at zero pressure and the results at high pressure may be required as an acceptable reference.**

***Index Terms*—Alloys, High pressure, Mechanical response, PbSSe, PbSTe, PbSnSTe.**

I. Introduction

The study of the mechanical response of materials is significant in both the fundamental physics and high-pressure technique. The selection of the mechanical response under pressure is extremely risky by theoretical simulations. A strong connection exists between these properties with shear rigidity of materials and with their elastic moduli (Suresh Babu, Vijayan and Devanathan, 2004). The technical significance of the PbS and PbSSe groups of semiconductor compounds and alloys as detectors of infrared radiation has been a powerful parallel stimulus.

They are chiefly used in infrared lasers in fiber optics, including thermoelectric materials, in solar energy panels, and in window coating (Othman, Mishjil and Habubi, 2012; Othman, et al., 2019). Their narrow fundamental energy band gap is one of their effective properties (Gopal, et al., 2015). Thus, IV-VI semiconductor alloys are worthwhile in optoelectronic devices such as lasers (McCann, 2006; Hutter, et al., 2014). Countless studies, theoretically and experimentally, related to these materials are available (Lebedev and Sluchinskaya, 1994) and explored the samples of $PbS_xSe_yTe_{1-x-y}$ quaternary solid solutions at low temperatures using electrical and X-ray methods (Weyand, 2007); ab initio study of cubic alloys (Kacimi, et al., 2008); structure, electronic, and optical properties of $PbS_{1-x}Se_x$ (Labidi, et al., 2011); and simulation mechanical properties of $PbS_{0.5}Se_{0.5}$ under pressure (Othman, 2013). The existent study was performed to highlight on the studies which are done in the future by the specialists to deliver and examine these alloys in laboratories. It assists them determine the change in amounts of additives in alloys, the friendship of theoretical studies with experiments and other theoretical works.

The mechanical performance of PbS_xSe_{1-x} and PbS_xTe_{1-x} ternary, $Pb_xSn_{1-x}S_yTe_{1-y}$ quaternary alloys high pressure for x and y = 0.5 compositions changes under pressure, which in a straight line impact a variety of applications of PbS compound devices under diverse working circumstances. Concerning various application circumstances, the mechanical performance of these alloys at 0, 50, and 100 kbar is considered using density functional theory (DFT) calculations in the current work.

II. Materials and Methods

Cambridge Serial Total Energy Package (CASTEP) program is used to analyze the data (Segall, et al., 2002). Kohn–Sam formation is used to complete the calculation (McGinty, et al, 2009). Using DFT to the exchange-correlation contribution is explained within the local density approximation (LDA). A cubic unit cell is centered with atoms (S/Se) and (S/Te) of PbS_xSe_{1-x} and PbS_xTe_{1-x} ternary alloys and set up with atoms (Pb/Sn) and (S/Te) of $Pb_xSn_{1-x}S_yTe_{1-y}$ quaternary alloys for x and y compositions. It is indicated that quaternary alloys have cubic symmetry in all of the calculations for all the five systems to preserve constancy and easiness. Cubic unit cell was taken for x and y and we substituted atoms to achieve the coveted concentrations. The completion of the first step of geometry optimization is done for PbS_xSe_{1-x} and PbS_xTe_{1-x} ternary alloys and $Pb_xSn_{1-x}S_yTe_{1-y}$ quaternary alloys for x and y = 0 at constant temperature with symmetry P1. Fig. 1 displays the graph of improvement steps provided merely for $Pb_xSn_{1-x}S_yTe_{1-y}$ quaternary alloys to gain gap in journal. The calculation is perfected using Kohn–

ARO-The Scientific Journal of Koya University
Vol. VIII, No.2 (2020), Article ID: ARO.10681, 5 pages
DOI:10.14500/aro.10681
Received: 21 May 2020; Accepted: 12 August 2020
Regular research paper: Published: 03 September 2020
Corresponding author's e-mail: mazin.othman@soran.edu.iq

Sam formation, which used DFT to the exchange-correlation contribution. It is determined by LDA. The wave functions have been extended in the plane waves up to a kinetic energy cutoff of 890 eV. Atomic positions are adjusted with a density mixing scheme (Othman, Kasap and Korozlu, 2010a) including the conjugate gradient (CG) process for values minimization (Ahmed, et al., 2008). Under dissimilar pressure, the Monkhorst-Pack scheme with regular integration points is put in an application (Milman, et al., 2010; Sedighi, et al., 2020).

III. Results and Discussion

Below are the elements which acted the external forces in mechanical performance. They are also called stress. In addition, whereas the body is in equilibrium, the external stress has to be perfectly well adjusted by internal forces. Overall, the stress is a second rank tensor with nine following elements (Othman, Kasap and Korozlu, 2010b; Othman, 2016; Dar, et al., 2017):

$$\tau_{ij} = \begin{vmatrix} \tau_{11}\tau_{12}\tau_{13} \\ \tau_{21}\tau_{22}\tau_{23} \\ \tau_{31}\tau_{32}\tau_{33} \end{vmatrix} \quad (1)$$

Using the so-called virile expression, the internal stress is possibly achieved in an atomistic computation

$$\tau = \frac{1}{\acute{I}}\left\{\sum_{i=1}^{N} m_i (v_i v_i^T) + \left(\sum_{i>j} r_{ij} F_{ij}^T\right)\right. \quad (2)$$

where index indicates particles 1 by means of N, η_i, vi, and F_i symbolize the mass, velocity, and force working on character i, $\acute{v}$ means the arrangement volume. Application of a stress of body brings about a modification in the relative positions of particles in the body, directed quantitatively by way of the strain tensor:

$$\eta_{ij} = \begin{vmatrix} \eta_{11}\eta_{12}\eta_{13} \\ \eta_{21}\eta_{22}\eta_{23} \\ \eta_{31}\eta_{32}\eta_{33} \end{vmatrix} \quad (3)$$

parallelepiped (e.g., a periodic simulation cell) categorized in some references, stated by the three column vectors a_0, b_0, and c_0, and by the vectors a, b, and c in the distorted state, the strain tensor is expressed by:

$$\eta = \frac{1}{2}\left[(P_0^T)^{-1} K P_0^{-1} - 1\right] \quad (4)$$

where $\mathcal{P}_0$ points to the matrix formed from the three column vectors a_0, b_0, and c_0. $\mathcal{P}$ signifies the corresponding matrix formed from a, b, and c. T indicates the matrix interpret. $\acute{K}$ means the metric tensor $\mathcal{P}^T\mathcal{P}$. The elastic hardness coefficients concerning the various components of stress and strain are defined by:

$$C_{imnk} \frac{\partial \tau_{im}}{\partial \eta_{nk}} \left| \frac{1}{\acute{y}} \frac{\partial^2 A}{\partial \eta_{lm} \partial \eta_{nk}} \right|_{T,\eta_{lm}\eta_{nk}} \quad (5)$$

where A stands for the Helmholtz which releases energy. For small deformations, the affiliation between the stresses and strains may be stated basing on a popularized:

$$\tau_{lm} = C_{lmnk}\eta_{nk} \quad (6)$$

$$\eta_{lm} = S_{imnk}\tau_{nk} \quad (7)$$

where S_{lmnk} denotes the compliance components. Note that in both Equations (6) and (7), the summation convention is indicated. For example, η_{21} is provided in full as:

$$\tau_{21} = C_{2111}\eta_{11} + C_{2112}\eta_{12} + C_{2113}\eta_{13} + C_{2121}\eta_{21} + C_{2122}\eta_{22} + C_{2123}\eta_{23} + C_{2131}\eta_{31} + C_{2132}\eta_{32} + C_{2133}\eta_{33}$$

The popularized Hooke's law is consequently often written as:

$$\tau_i = C_{ij}\eta_j \quad (8)$$

The 6 × 6 hardness matrix C is also corresponding. Therefore, 21 coefficients are needed to completely expound the stress-strain properties of an arbitrary substance. Moreover, C is a tensor, since it does not abide by the needed transformation rules.

ρ and ς refer to the Lamé coefficients. For the isotropic case, expressions are used for the Young modulus Y and bulk modulus B which are provided as follows (Jandow, et al., 2019):

$$Y = \rho\left(\frac{3\varsigma + 2\rho}{\varsigma + \rho}\right) \quad (9)$$

$$= \varsigma + - \quad (10)$$

The finite strain method is applied to calculate the elastic constants, in which the ground-state structure is forced to unusual great effort in accordance with symmetry-dependent

TABLE I
Equilibrium Lattice Parameters (α_0), Bulk Modulus (Gpa), and Band Gap Energy (Eg) of All Alloys

Materials	Pressure (kbar)	α_0 (Å)	Eg (eV)
PbS (Se)	0	6.041	0.263
	50	5.987	0.378
	100	5.746	0.506
PbS (Te)	0	6.301	0.194
	50	6.142	0.273
	100	6.009	0.299
PbSnSTe	0	5.840	0.642
	50	5.753	0.691
	100	5.701	0.753

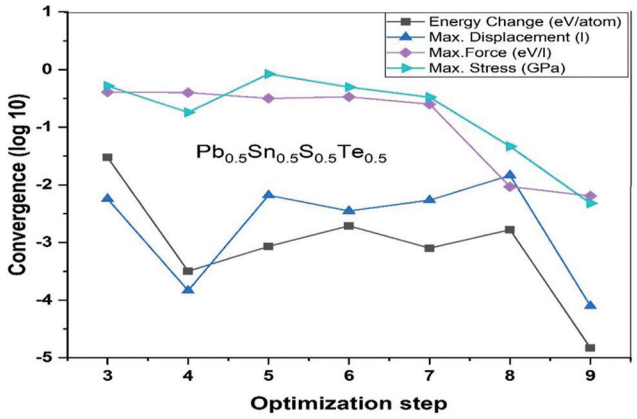

Fig. 1. The optimization step convergence of $Pb_xSn_{1-x}S_yTe_{1-y}$.

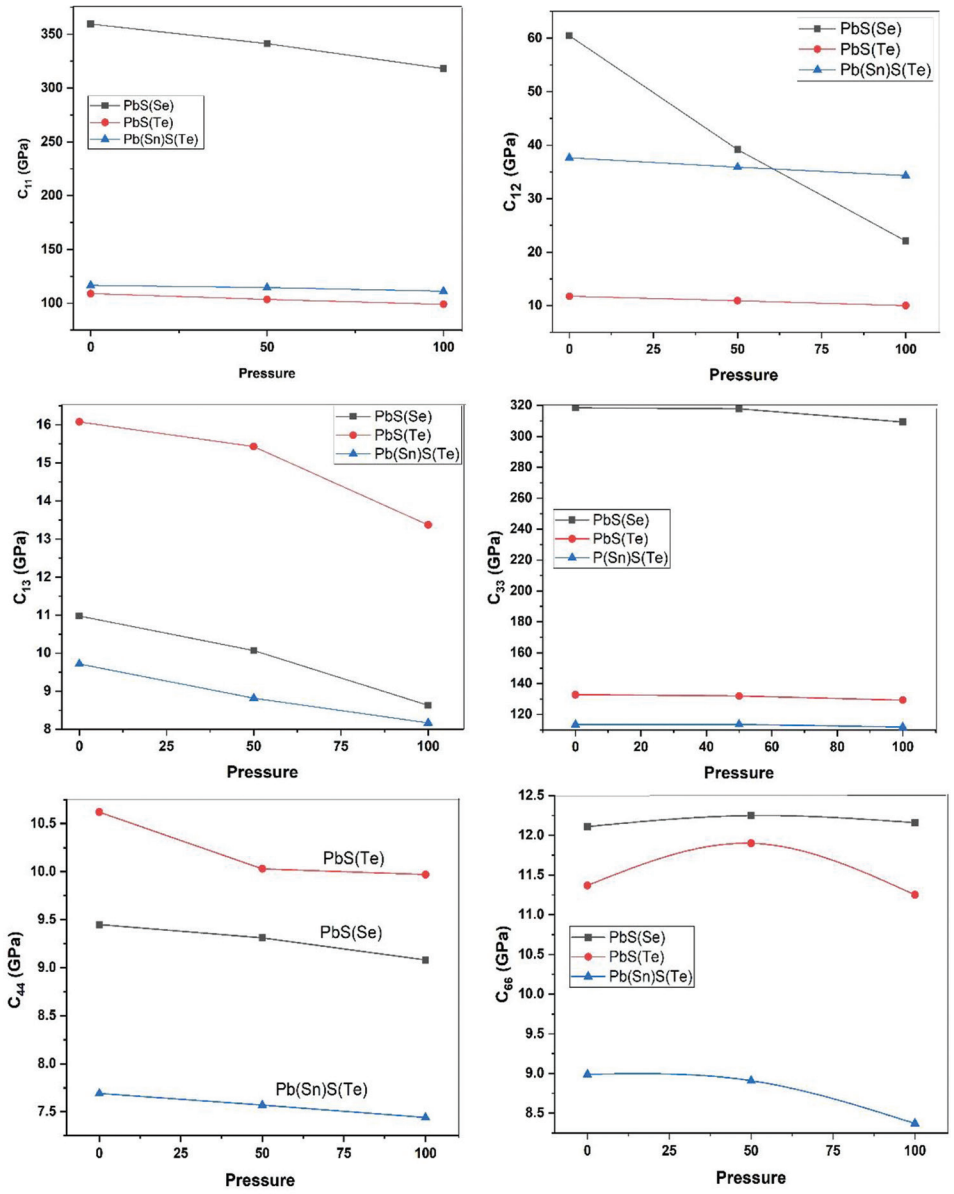

Fig. 2. Elastic constants of C_{11}, C_{12}, C_{13}, C_{33}, C_{44}, and C_{66} of PbS_xSe_{1-x} and PbS_xTe_{1-x} ternary and $Pb_xSn_{1-x}S_yTe_{1-y}$ quaternary alloys.

strain patterns with changing amplitudes and a subsequent calculation of the stress tensor after optimization of the internal structure parameters. In addition to that, the bulk modulus *B* is calculated from the elastic constants. Then, Young's modulus is computed from these values.

Table I displays lattice parameter of PbS_xSe_{1-x} and PbS_xTe_{1-x} ternary and $Pb_xSn_{1-x}S_yTe_{1-y}$ quaternary alloys for x and y compositions with increasing pressure (P = 0.50, and 100 kbar). These lattice parameters decline, as pressure rises. Moreover, whereas forbidden band gap energy goes up because of the pressure. For further information, as pressure increases, many of materials often get metallic. Furthermore, the atoms come closer, and the lattice parameter goes down. Thus, all modulus enlarge. Eventually, the referred materials get metallic than the pressure decreases (Koch, et al., 2005). A connection is provided between the mechanical characteristic of crystals by the elastic parameters of materials, which display information in terms of the nature of the forces operating in materials. Particularly, they give information about the materials' constancy and rigidity. Accurate ways and means must be applied to their first principle calculation. Since these forces and the elastic parameters are considered as the functions of the first-order and second-order derivatives of the potentials, the calculation demonstrates more detail about the accuracy of forces in materials. The second-order elastic parameters (*Cij*) are done by means of the "volume-conserving" proses (Sanati, et al., 2013) and the findings are indicated in Table II. For a stable tetragonal structure, the six independent elastic constants *Cij* should gratify the Born-Huang for constancy (Mouhat and Coudert, 2014),

$$C_{11} > 0,\ C_{33} > 0,\ C_{44} > 0,\ C_{66} > 0,\ (C_{11}-C_{12}) > 0,$$
$$(C_{11}+C_{33}-2C_{13}) > 0,$$
$$\{2\,(C_{11}+C_{12}) + C_{33} + 4C_{13}\} > 0$$

Table II indicates that elastic constants follow the stability conditions for PbS_xSe_{1-x} and PbS_xTe_{1-x} ternary and

http://dx.doi.org/10.14500/aro.10681

TABLE II
ELASTIC PARAMETERS MODULI OF THESE ALLOYS UNDER HIGH PRESSURE

Materials	Pressure (kbar)	C_{11} (GPa)	C_{12} (GPa)	C_{13} (GPa)	C_{33} (GPa)	C_{44} (GPa)	C_{66} (GPa)	Bulk modulus (GPa)	Young's modulus (GPa) $\times 10^{-2}$
PbS(Se)	0	359.43	60.47	10.98	318.43	9.45	12.11	51.42	3.708
	50	341.26	39.18	10.07	317.92	9.31	12.25	43.27	3.594
	100	317.92	22.10	8.63	309.36	9.08	12.16	28.04	3.051
PbS(Te)	0	108.92	11.75	16.08	132.84	10.62	11.37	44.51	4.625
	50	103.54	10.92	15.43	132.01	10.03	11.90	41.62	4.547
	100	99.06	10.01	13.37	129.33	9.97	11.25	38.04	4.932
Pb(Sn)S(Te)	0	116.71	37.63	9.72	113.42	7.69	8.99	39.70	5.115
	50	114.65	35.87	8.82	113.54	7.57	8.91	33.14	4.092
	100	111.23	34.31	8.17	111.89	7.44	8.37	31.69	3.304

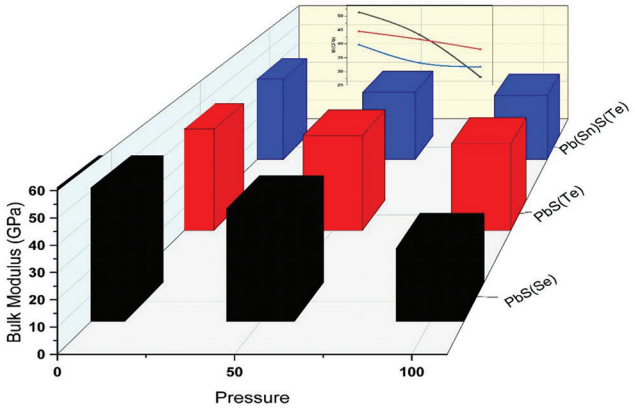

Fig. 3. Bulk modulus of the various pressures ternary and quaternary alloys.

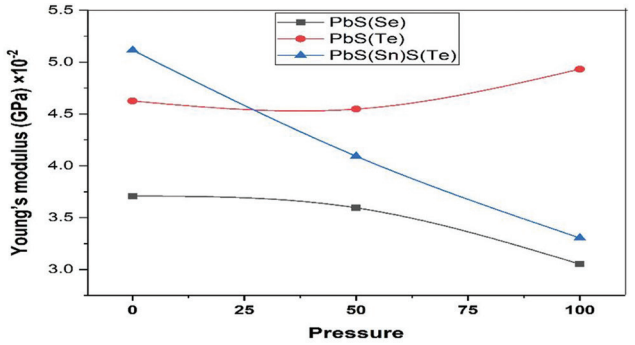

Fig. 4. Young's modulus of the ternary and quaternary alloys under various pressures.

$Pb_xSn_{1-x}S_yTe_{1-y}$ quaternary alloys. The elastic parameters C_{ij} play a significant role in some mechanical performances of the alloys, particularly in special application conditions including as internal strain and stress. Fig. 2 illustrates the findings of *Cij* of PbS_xSe_{1-x} and $PbSxTe_{1-x}$ ternary and $Pb_xSn_{1-x}S_yTe_{1-y}$ quaternary alloys for x and y = 0.5 compositions as a change of pressure from 0, 50, and 100 kbar. Experimental data for these alloys do not exist. Table II gives an explanation of that C_{11}, C_{12}, and C_{44} decrease as pressure increases. On the other side, C_{33}, C_{44}, and C_{66} decrease whereas pressure increases with different rates.

As it can be seen in Table II, the variations of bulk and young modulus of PbS_xSe_{1-x} and PbS_xTe_{1-x} ternary and $Pb_xSn_{1-x}S_yTe_{1-y}$ quaternary alloys for x and y = 0.5 as a function of pressure from 0, 50, and 100 kbar are demonstrated in Figs. 3 and 4.

In the final analysis, whereas the pressure rises, the parameters vary regularly. It displays that the varying of bulk modulus with pressure of PbS_xSe_{1-x} alloys decreases quickly and the varying of bulk modulus for $PbSxTe_{1-x}$ alloys decreases gradually with the pressure. As can be noted in Fig. 3, quaternary alloys of $Pb_xSn_{1-x}S_yTe_{1-y}$ bulk modulus decrease regularly. It can be indicated as one of the key references for the other works in the future. In Fig. 4, the young modulus parameters decline, as pressure goes up, but the varying of bulk modulus rises with the pressure in $PbSxTe_{1-x}$ alloys.

IV. CONCLUSIONS

The current study indicates the mechanical performance of PbS_xSe_{1-x} and PbS_xTe_{1-x} ternary and $Pb_xSn_{1-x}S_yTe_{1-y}$ quaternary alloys for x and y = 0.5 as a function of the pressure from 0, 50, and 100 kbar using DFT. The first principles method is used to achieve the results depending on the LDA using plane wave pseudopotentials. The traditional mechanical stability conditions for these ternary and quaternary mixed crystals are satisfied by the elastic parameters. The pressure increasing leads to a decrease in the lattice parameters. Moreover, parameter bulk and young modulus go down with pressure increasing, but young modulus parameters of PbS_xTe_{1-x} ternary go up by pressure. The results display the calculation of *Cij* of all alloys as a pressure from 0, 50, and 100 kbar. Pressure increasing progress to decrease in C_{11}, C_{12}, and C_{44} and in C_{33}, C_{44}, and C_{66} in separate rates. The data of the current study include P = 50 and 100 kbar, and it can be emphasized on in the future studies.

REFERENCES

Ahmed, R., Hashemifar S.J. and Akbarzadeh, H., 2008. First-principles study of the structural and electronic properties of III-phosphides. *Physica B: Condensed Matter*, 403(10-11), pp.1876-1881.

Dar, S.A., Srivastava, V., Sakalle, U.K., Parey, V. and Pagare, G., 2017. DFT investigation on electronic, magnetic, mechanical and thermodynamic properties under pressure of some EuMO3 (M=Ga, In) perovskites. *Materials Research Express*, 4(10), p. 11.

Gopal, P., Fornari, M., Curtarolo, S., Agapito, L.A., Liyanage, L.S.I. and Nardelli, M.B., 2015. Improved predictions of the physical properties of Zn-and

Cd-based wide band-gap semiconductors: A validation of the ACBN0 functional. *Physical Review B-Condensed Matter and Materials Physics*, 91(24), pp.1-9.

Hutter, J. Iannuzzi, M., Schiffmann, F. and VandeVondele, J., 2014. Cp2k: Atomistic simulations of condensed matter systems. *Wiley Interdisciplinary Reviews: Computational Molecular Science*, 4(1), pp.15-25.

Jandow, N.N., Othman, M., Habubi, N.F. and Chiad, S.S., 2019. Theoretical and experimental investigation of structural and optical properties of lithium doped cadmium oxide thin films. *Materials Research Express*, 6(11), p.116434.

Kacimi, S. Zaoui, A., Abbar, B. and Bouhafs, B., 2008. Ab initio study of cubic PbSxSe1-x alloys. *Journal of Alloys and Compounds*, 462(1-2), pp.135-141.

Koch, C.C., Youssef, K.M., Scattergood, R.O. and Murty, K.L., 2005. Breakthroughs in optimization of mechanical properties of nanostructured metals and alloys. *Advanced Engineering Materials*, 7(9), pp.787-794.

Labidi, M. Meradji, H., Sebti, G. and Labidi, S., 2011. Structural, electronic, optical and thermodynamic properties of PbS, Pbse and their ternary alloy pbs1-xsex. *Modern Physics Letters B*, 25(7), pp.473-486.

Lebedev, A. and Sluchinskaya, I., 1994. Ferroelectric phase transitions in iv-vi semiconductors associated with off-center ions. *Ferroelectrics*, 157(1), pp.275-280.

McCann, P.J., 2006. IV-VI semiconductors for mid-infrared optoelectronic devices. In: *Mid-infrared Semiconductor Optoelectronics*. Springer, London, pp.237-264.

McGinty, R.K., Köhn, M., Chatterjee, C., Chiang, K.P., Pratt, M.R. and Muir, T.W., 2009. Structure-activity analysis of semisynthetic nucleosomes: Mechanistic insights into the stimulation of Dot1L by ubiquitylated histone H2B. *ACS Chemical Biology*, 4(11), pp.958-968.

Milman, V., Refson, K., Clark, S.J., Pickard, C.J., Yates, J.R., Gao, S.P., Hasnip, P.J., Probert, M., Perlov, A. and Segall, A., 2010. Electron and vibrational spectroscopies using DFT, plane waves and pseudopotentials: CASTEP implementation. *Journal of Molecular Structure: THEOCHEM*, 954(1-3), pp.22-35.

Mouhat, F. and Coudert, F.X., 2014. Necessary and sufficient elastic stability conditions in various crystal systems. *Physical Review B-Condensed Matter and Materials Physics*, 90(22), pp.4-7.

Othman, M., Kasap, E. and Korozlu, N., 2010a. Ab-initio investigation of structural, electronic and optical properties of InxGa1-xAs, GaAs1-yPy ternary and InxGa1-xAs1-yPy quaternary semiconductor alloys. *Journal of Alloys and Compounds*, 496(1-2), pp.226-233.

Othman, M., Kasap, E. and Korozlu, N., 2010b. The structural, electronic and optical properties of In<inf>x</inf>Ga<inf>1-x</inf>P alloys. *Physica B: Condensed Matter*, 405(10), pp.991-1005.

Othman, M., Salih, S., Sedighi, M. and Kasapd, K., 2019. Impact of pressure and composition on the mechanical behavior of InxGa1-xAs1-yPy and AlxIn1-xSb1-yPy quaternary alloys. *Results in Physics*, 14, p.5.

Othman, M.S., 2013. Simulation mechanical properties of lead sulfur selenium under pressure. *Journal of Modern Physics*, 4(2), pp.185-190.

Othman, M.S., 2016. Theoretical analysis of linear optical properties of PbS x Se 1-x (X=0.5). *Journal of Kerbala University*, 14(2), pp.221-228.

Othman, M.S., Mishjil, K.A. and Habubi, N.F., 2012. Structural and optical properties of GaAs 0.5Sb 0.5 and In 0.5Ga 0.5As 0.5Sb 0.5: Ab initio calculations for pure and doped materials. *Chinese Physics Letters*, 29(3), p.037302.

Sanati, M., Albers, R.C., Lookman, T. and Saxena, A., 2013. First-order versus second-order phase transformation in AuZn. *Physical Review B-Condensed Matter and Materials Physics*, 88(2), pp.1-10.

Sedighi, M., Nia, B.A., Hamada, A.H., Othmana, M.S., 2020. Electronic and optical properties of SrS nanosheet in 001 and 101 directions. *Computational Condensed Matter*, 22, p.e00445.

Segall, M.D., Lindan, P.J., Probert, M.J., Pickard, C.J., Hasnip, P.J., Clark, S.J. and Payne, M.C., 2002. First-principles simulation: Ideas, illustrations and the CASTEP code. *Journal of Physics Condensed Matter*, 14(11), pp.2717-2744.

Suresh Babu, K., Vijayan, C. and Devanathan, R., 2004. Strong quantum confinement effects in polymer-based PbS nanostructures prepared by ion-exchange method. *Materials Letters*, 58(7-8), pp.1223-1226.

Weyand, S., 2007. *Purification, Crystallisation and X-ray Structure Analysis of Proteins From the Lysine Biosynthetic Pathway of Mycobacterium Tuberculosis and Structural Studies of Membrane Proteins from Deinococcus Radiodurans R1 and Escherichia coli K12'*. University of Konstanz, Konstanz.

 http://dx.doi.org/10.14500/aro.10649

Integrating Enterprise Resource Planning with the Organizations' Management Structure for Decision-Making

Diler Atrushi[1], Razwan M. Salah[1,2] and Nawzat S. Ahmed[3]

[1]Department of Computer Science, University of Duhok,
Duhok, Kurdistan Region – F.R. Iraq

[2]Department of Computer Science, Cihan University-Duhok,
Duhok, Kurdistan Region – F.R. Iraq

[3]Department of Information Technology Management, Technical College of Administration, Duhok Polytechnic University,
Kurdistan Region – F.R. Iraq

***Abstract*—*The* unstable situation of some countries in Middle East have caused several crises. Many humanitarians Non-Governmental Organizations (NGOs) intervene to provide services to the affected groups. Good information management may have an effect on the project's activities and the accuracy of decisions making, especially for organizations that have limited resource. This paper presents the integration of a Management Information System (MIS) and its' impact in a local organization operating in Duhok City, Kurdistan Region-Iraq (KRI), namely voice of older people and family (VOP Fam). The goal is to increase the quality of humanitarian work through good decision making and data management. Based on the System Usability Scale (SUS) result, the system includes many components as an Enterprise Resource Planning (ERP) and is used by the organization staff for managing and organizing their activities. This system is essential to provide knowledge and can bring together the management and the organization's senior staff members to make decisions, collect the important information, and allow the donors and the staff of the NGO to follow work timely. The importance of the research lies in its contributes to highlighting the positive impact of integrating a computer-based information system (IS) in conducting humanitarian activities of NGOs in KRI. In addition, it will add a level of reliability to the NGO's activities data and make it trustworthy. This study has concluded that Integrating IS in organizations can help in decision-making based on analyzing the aggregated data, and prepare more accurate reports in a short period.**

***Index Terms*—Decisions support system, Enterprise resource planning, Management information system, None-governmental organizations, System usability scale.**

ARO-The Scientific Journal of Koya University
Vol. VIII, No.2 (2020), Article ID: ARO.10649, 6 pages
DOI:10.14500/aro.10649
Received 21 March 2020; Accepted 30 July 2020
Regular research paper: Published 30 September 2020
Corresponding author's e-mail: diler.atrushi@uod.ac

I. Introduction

Today, information and communication technologies (ICT) and its wide applications are used by many people around the world, either by personal/group within private or public firms. Since 1991, the investment in information technology (IT) is the highest amongst all other investment sectors in many companies, such as US companies (Dewett, 2002). Furthermore, IT has helped to gathering and analyzing data of Non-Governmental Organizations (NGO), especially in the humanitarian operations. It has allowed to involve information systems (IS) and technologies in their works and activities for recording and analyzing data that have been conducted for the work. Therefore, it can be considered that it is the ICT era, where the economy depends on the valuable information to stay competitive. Hence, the organizations need well-structured information for handling work partners such as partners, stakeholders, staff, and suppliers, who are coming from other areas and covering a different geographical area.

Data gathering and analyzing using IS have become meaningful in an organization's work greatly (Stair, et al., 2018). Overall, the organization's staff can handle the data received through paper-based systems or computer-based systems (for example, tools or software) and then analyze it. Nevertheless, computer-based systems can be incompatible, because the tools or software may not be able to communicate with each other (Abeysekera, 2011). The computer knowledge and skills of staff and lack of resources can be considered as the main problems and lack of system effectivity.

At present, the integrating management information systems (MIS) and decisions support system (DSS) have a great role in improving the efficiency and productivity of the organization's manager. It can support them gaining insight into the business operations by taking into consideration providing alternatives and advice in business strategies and plans (Kohli and Devaraj, 2004).

Current paper aims to highlight the impact of integrating one or more types of IS in the operation of NGOs and their activities, especially those the organizations that have numerous of data transactions and then for making a decision for supporting the management (that is., Decision Support System). Furthermore, it is an effort to overcome the organization's weaknesses and gaps founded in the paper-based system and increasing awareness among the organizations on investing in development and integrating ICT in NGO operations.

Therefore, to reach the aims of the study, the following research questions are raised to be answered in this study:

1. For managing organizations work, is it possible to integrate IS in organizations that are located in Kurdistan Reign-Iraq to support formulating final decision and reporting it?
2. How to save time and have a better decision-making?
3. How to use and test the enterprise resource planning (ERP)?

The rest of this paper is structured as follows. In Section II, a related work is provided on how MIS can be integrated into the organizations and has supported them to make a decision. In Section III, the methodology for implementing the system is presented. The results of the SUS are discussed in Section IV. Finally, the conclusion and future work are presented in Section VI.

II. Related Work

The previous studies have highlighted the impact of integrated MIS into organizational processes for supporting the decision-making procedures. Recently, Sigala, et al., 2020, have presented a research that highlights the importance of HRP systems within Humanitarian Organizations (HO). The authors stated that each organizational IS should be formed to solve the challenges and workloads in lined with their mission and values. The research concluded that ERPs should be specifically designed to meet the specific needs of each HO. Although the study by Sigala, et al., (2020), has highlighted the importance of integrating a computerized system within the HOs, it mainly focuses on supply chain and logistics management. The current study presents a dedicated ERP package that includes project based activities and traces all the transactions involved in these projects.

A key and powerful study for this research that is aimed at using IS in within enterprise infrastructure is done by Almazán, Tovar and Quintero (2017). In their research (Almazán, Tovar and Quintero, 2017), they have used a statistical method and collected samples from 133 companies. The result obtained, indicates the information from small and medium enterprises those depend on computerized IS, can provide useful, up to date and acceptable information by users. Therefore, these enterprises have showed indications of better work performance. In the same direction, Tripathi (2011) have shed light on using computer-based systems in organizations. He clarified how the DSS contributes to the harmony and efficiency of work. Overall, Tripathi found that the reports generated by using DSS can facilitate the understanding of workflow by the management sector, help to analyses, observing the performance, and then make a well-decision to follow up the organization's work.

Nowadays, ERP systems are considered as the integrated management of the core business process by including multiple software and technology in one package that can be used to collect, store, analyze, manage, and interpret data from many organization activities (Umble, Haft and Umble, 2003). Van Nieuwenhuyse, et al. (2009) have stated "An ERP system should be able to support decisions regarding the planning and execution of the business." Meanwhile, Ali Xie and Cullinane (2013) have mentioned that ERP systems have significantly revolutionized and improved in organizations, especially in conducted activities, and have made them more productive, competitive, and integrative.

Tripathi (2011) and Ada and Ghaffarzadeh (2015) have agreed that DSS and MIS are consider the types of IS. They have recommended implementing integrating DSS and MIS in organizations operations to help the top management for decision making. Theoretically, the study that followed by Ada and Ghaffarzadeh discussed the different types of IS, which are focused on DSS and MIS. It has focused on how DSS and MIS can be similar to each other, but each one has targeted the user's group individually. Meaning, DSS can be focused on leadership and provide an innovative vision to senior management, whereas MIS can be focused on gathering and accumulating information from various transactions of activities.

In addition, Asemi et al. (2011) have presented MIS and DSS and their relation in decision-making in organizations. The MIS supports the managers in the decision-making process through the extraction of certain information from an enormous database to increase the performance of the organization, whereas DSS is the usage of computer systems by managers or user's group in an organization. These systems are intended to solve organizational problems through the generation of special or periodic reports.

III. Methodology

This research paper is focused on the benefits of integrating IS within an organization's work and its role in supporting decision-making. Several studies have been presenting integration of IS within organizations. These works were mostly focused on theories that are proposed in developed countries. In sum, each study has tackled a type of IS which are targeting a specific group of users, as shown in Fig. 1.

This study sheds light on implementing ERP that includes several systems in the organizations, which are located in KRI. The ERP has been designed and implemented to support the organizations by aggregation data from multiple activities carried out in different locations. Therefore, the research questions must be the following:

Based on the brainstorming techniques, this paper is inspired by the best known formal technique called Nominal Group Technique as presented by Hill (2019). The technique barring together all the important personnel of NGO to highlight problems in the current system and discuss the ideas and lessons learned to be reflected in the ERP.

http://dx.doi.org/10.14500/aro.10649

For following the research objective, the ERP System has been designed and implemented by including several forming. The methodology consists of stage methods: Design and implementation, which is can describe the design of the study and how the ERP System was implemented, as illustrated in Fig. 2.

A. Analysis the Current System in Voice Of Older People And Family (VOP Fam) Organization

The design phase of the system has been inspired by observing and analyzing the structure and environment of the organization. Several interviews have been made with key staff to figure out the mechanism work inside the VOP Fam organization, and then recognize the bottlenecks that happen in their traditional working processes. All in all, the observations and interviews conducted have highlighted that the process of data gathering and analyzing requires too much effort and time (Maxwell and Kaplan, 2005). Hence, the result cannot be occasionally accurate. What is more, retrieving, updating and aggregating data in the traditional process can be considered other problems and challenges for decision making. The advantages of this step lie in shaping the components and the using methods that suits the user's wishes.

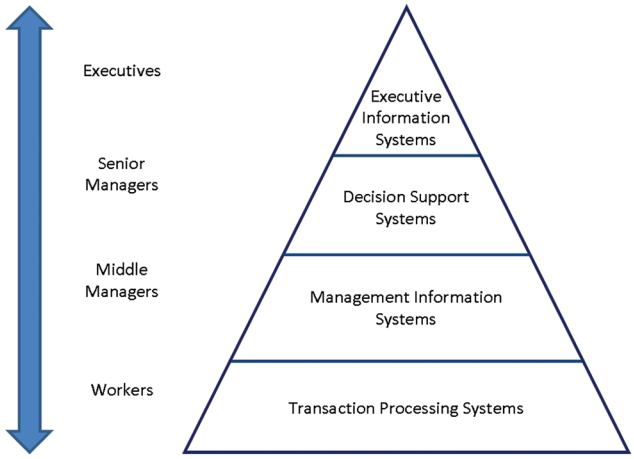

Fig. 1. Four level pyramid model based on the different levels of hierarchy in the organization ("Different Types of Information System and the Pyramid Model," no date).

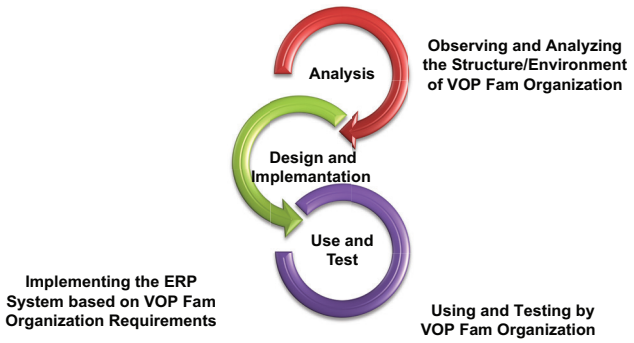

Fig. 2. Methodology used for integrating the ERP systems in voice of older people and family organization.

B. ERP System Implantation

After analyzing the structure and environment system of VOP Fam Organization, the ERP system has been designed and implemented (hence forth VOP-ERP) by including and integrating six components that are working together, as it is illustrated in Fig. 3.

The main components of VOP-ERP system:

C. Human Resources

This component of the system contains the full details of each employee/ staff, in addition to employee/staff working history record. It includes some important tools for the management, such as generating and printing employee Identification Card (ID) as it is indicated in Fig. 4, with other options for classification of the employees according to their projects and other functions.

D. Inventory

The inventory component includes the existing items of the organization in the main office and all other field locations. In addition, item status, donation, and classification have been included in this component.

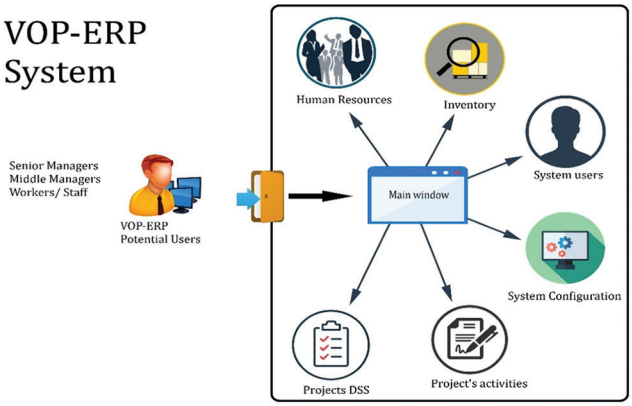

Fig. 3. Components forming of the ERP system for organization. Each component contributes to its organization activities.

Fig. 4. Staff identification (ID) generated from VOP-ERP system.

E. System Users

This component is considered a significant and vital part in VOP-ERP system because confidentiality is most demanding within the work of the humanitarian field due to the fact that the information recorded is related to other people. This component has credential access by the system's admin only and it provides the ability to give user access permissions to other users of the system separately.

F. System Configuration

This component of the system provides the ability to some users to configure some selections for avoiding errors, as much as possible, to increase the efficiency of the DSS reports that will be generated.

G. Project's Activities

This component includes the daily transactions of the workers. It means the activity that is conducted by staff must be inserted in this component. Furthermore, this component has the support for five kinds of sub-activities (for example, Narrative and Numbered Project Activities, Case Management, and Referrals) according to the work requirement and its type.

H. DSS Projects

All the data are analyzed and presented for the managers, to support the decision-making, can be found in this component. It can generate up to 20 different reports based on a variety of variables that the manager must identify. This is why this component is only available for senior staff like the project managers.

Accordingly, the system users will be grant access to VOP-ERP components, once he passes the login window to the main window as it is illustrated in Fig. 5.

This step was very important for the system users which can see all the components that have been reflected in the system for more work motivation.

I. Using and Testing ERP System

The usability method is meant to trace the user's interaction whereas they are using the system. It is not only testing the user interface of the system, but it should test the functionality of the system as well. It consists of five basic attributes: Learnability, Efficiency, user Retention over Time, Error Rate, and Satisfaction (Atrushi, Ahmed and Ahmed, 2017). According to the ISO definition, the basic elements to measure the ability to use are three elements (Ferré, Windl and Constantine, 2001): Effectiveness, Efficiency, and Satisfaction. Effectiveness means the extent of goal achievement, whereas efficiency means the effort required to complete a certain goal or a specific task. The last element, satisfaction, shows the level of satisfaction felt by the users during using the system and the extent of acceptance of the system as a tool to achieve its objectives.

IV. Results and Discussion

A. Time, Accuracy, Confidentiality, and Decision-Making

Compared with the traditional (manually) system, which has been used by VOP Fam organization previously, integrating the organization functionalities into a computerized IS resulted in many competitive advantages (Peppard and Ward, 2004). The main result is reducing and saving time of work specifically in terms of generating reports. This achievement has a direct effect on each aspect of the work sector, as illustrated in Table I.

Accordingly, several characteristics are achieved using VOP-ERP system in the organization, for instance: Saving time, Increasing Accuracy, Increasing Confidentiality, and Supporting the managers in decision-making.

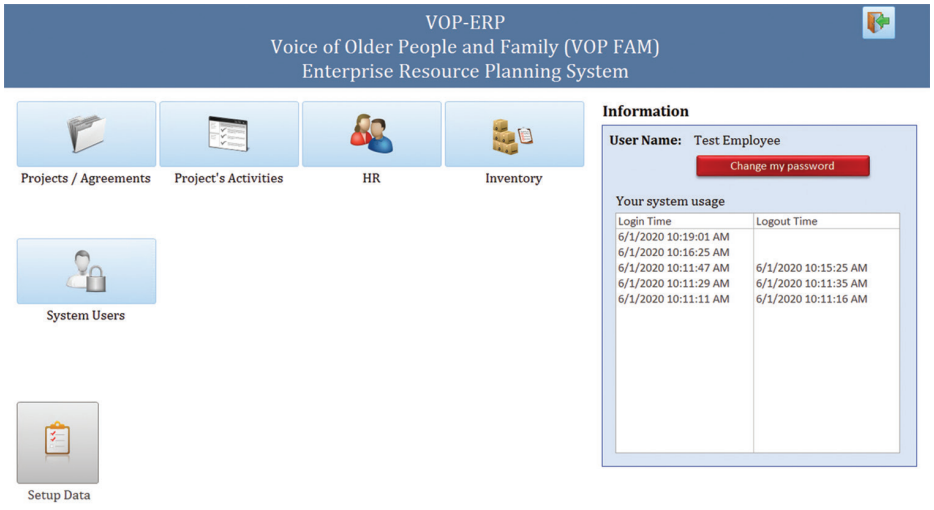

Fig. 5: VOP-ERP main window.

 http://dx.doi.org/10.14500/aro.10649

B. SUS Result

SUS as a quantitative method was developed to measure the effectiveness, efficiency, and satisfaction of the system. The SUS consists of ten adapted items (that is., Questions) with the statement on a 5 point scale: (1) Strongly disagree, (2) Disagree, (3) Normal, (4) Agree, and (5) Strongly Agree (Brooke, 1996). The odd-numbered items are formulated positively whereas even-numbered items are formulated negatively, as shown in Table II.

The odd-numbered items are formulated positively whereas the even-numbered items are formulated negatively.

As SUS can be conducted for at least two users (Sauro, 2013), the testing process of the current system ends through the contribution of (17) employees who have been using the system for more than 6 months in VOP Fam organization. The results have been analyzed, as shown in Table III. In sum, the results indicate that the minimum of the answers to SUS questions is 70%, whereas the maximum score is 95%. Therefore, the total score of SUS is 85.3% indicating that the system is generally acceptable in accordance with the rules of the SUS tool as it is a 70% acceptable ratio (Bangor, Kortum and Miller, 2009).

According to the SUS results analysis for the 17 participants in Table III, the results indicate the following:

- The result of question (1) shows that 100% of participants have agreed and would like to use the ERP system frequently and keep working on it. Furthermore, 94% of participants agree that the ERP system is easy to use basing on question (3), whereas they have disagreed that the ERP system is complex basing on question (2). In the same way, 100% of participants feel confident using the computerized system basing on question (9).
- The result of question (5) shows that 94% of participants have agreed to the various operations and activities in the ERP system are well-integrated. Similarly, the respondent answers in question (6) agree that the operations and modules in the ERP system have not been inconsistencies.

TABLE I
PAPER-BASED SYSTEM VERSUS ERP SYSTEM (BLOCK CHAIN) BASED ON TASKS ACHIEVEMENT TIME

No.	Task	Traditional system	ERP System
1	Data Collection	2 Days	2 Days
2	Data Analysis and Entry	2–3 Days	1 h
3	Project Activities Report	3 Days/Report	1 Click/Report
4	Reports for Managers	1–2 Days/ Report	1 Click/Report
5	DS Report	1–2 Days/ Report	1 Click/Report
6	HR Reports	Up to 1 Day/Report	1 Click/Report
7	Staff ID Printing	Up to 1 h/ID	1 Click/ID

TABLE II
THE SUS ITEMS (I.E. QUESTIONS)

Question No.	Items (Questions)
1	I believe that I would to use ERP system frequently.
2	I have found this system unnecessarily complex.
3	I feel that this system is easy to use.
4	I think I need assistance to use this system.
5	I found that several functions have been integrated into this system.
6	I think there are some inconsistencies in this system.
7	I believe that most people can learn to use this system quickly.
8	I found this system is cumbersome and needs a high effort to use.
9	I feel confident during using this system.
10	I need to learn a lot of things before going forward into this system.

TABLE III
SUS RESULTS BY THE PARTICIPANTS: SUS RESULTS, SCORING, CALCULATION, AND PERCENTAGES

Total agrees	17	1	16	1	16	1	16	2	17	2	
Total disagrees	0	16	1	16	1	16	1	15	0	15	
Participant	Q1	Q2	Q3	Q4	Q5	Q6	Q7	Q8	Q9	Q10	SUS Score
P1	5	2	5	1	4	1	2	1	5	1	87.5
P2	5	2	5	1	4	2	5	2	5	1	90.0
P3	5	1	5	2	5	1	5	1	4	1	95.0
P4	5	1	4	1	2	1	5	1	5	1	90.0
P5	5	2	5	1	5	2	5	1	5	1	95.0
P6	4	2	5	1	5	2	5	3	5	1	87.5
P7	5	2	4	2	4	1	5	2	4	2	82.5
P8	5	2	5	1	5	1	5	1	5	2	95.0
P9	4	2	4	2	5	2	5	1	4	1	85.0
P10	3	1	5	2	4	1	5	1	5	1	90.0
P11	4	1	3	2	5	1	3	4	3	1	72.5
P12	4	1	4	2	5	1	4	2	4	2	82.5
P13	5	3	4	1	5	1	4	2	5	3	82.5
P14	4	2	2	3	3	2	4	1	5	2	70.0
P15	4	1	3	2	5	2	5	2	4	2	80.0
P16	4	1	5	2	5	3	5	1	4	2	85.0
P17	5	2	4	1	3	1	4	2	5	3	80.0
Participant's answers percentage	100	94	94	94	94	94	94	88	100	88	
To each question	% Agree	% Disagree	% Agree	% Disagree	% Agree	% Disagree	% Agree	% Disagree	% Agree	% Disagree	
Overall results	Min score		70.0		Max score		95.0		Average score		85.3

- The result of question (Q4) and (10) indicates that the majority of the users do not need an assistant to use the system and they do not need to learn a lot of things to use it.
- The result of both questions (Q7) and (Q8) shows that 94% of participants will be able to use the system quickly, whereas only 22% of participants believe that they need a little bit of effort to use the ERP system.

V. Conclusion and Future Work

With the vast expansion of the technology and the need to keep pace with the development in the field of data analysis, it has become necessary to integrate IS in organizations due to the extensive benefits such as flexibility, productivity, and quality improvement (Melville and Kraemer, 2016). The ERP system used in VOP Fam organization is in operation currently and becomes one of the supportive to the organization seniors in decision-making and the flow up of the work. At present, it is helping the staff in tracking their activities and the managers for making decisions and generating reports. In general, it has provided more accurate and detailed results related to the operations compared with the manual system used before. On the other hand, during the system implementation phase, a challenge has appeared, namely, the wireless network structure was not helping for the communicating in this organization. This challenge has been fixed by replacing the wireless network to the wired network.

Some limitations in this work can be the relative to funding limitation, and it is still used by one local organization only, and technically it has been implemented by using commercial tools and software.

However, the following could be taken into consideration in future development of ERP system:

- Integrating extra functions so that a wider range of users can use it such as (Finance, Logistics, Monitoring, and Evaluation).
- Link the system through internet-based portal or cloud, and making it available at anytime from anywhere (24/7) to access and use the system.
- Translating the ERP system to other languages (that is, Kurdish and Arabic) for making the system clearer and understandable by local users.

References

Abeysekera, R., 2011. *Effects of System Integration in an Organization a Case Study Carried out in the Photo and Home Electronics Branch*. Linköpings Universitet, Sweden.

Ada, Ş., and Ghaffarzadeh, M., 2015. Decision making based on management information system and decision support system. *European Researcher*, 93(4), pp.260-269.

Ali, M., Xie, Y., and Cullinane, J., 2013. A decision support system for ERP implementation in small and medium-sized enterprises. In: *Sociotechnical Enterprise Information Systems Design and Integration*. IGI Global, United States, pp.97-121.

Almazán, D.A., Tovar, Y.S., and Quintero, J.M., 2017. Influence of information systems on organizational results. *Contaduría y Administración*, 62(2), pp.321-338.

Asemi, A., Safari, A., and Zavareh, A.A., 2011. The role of management information system (MIS) and decision support system (DSS) for manager's decision making process. *International Journal of Business and Management*, 6(7), pp.164-173.

Atrushi, D., Ahmed, A., and Ahmed, N.S., 2017. *The Development of an Inventory Management System using the Model-view-view Model Pattern*. University of Zakho, Iraq.

Bangor, A., Kortum, P., and Miller, J., 2009. Determining what individual SUS scores mean: Adding an adjective rating scale. *JUS*, 4(3), pp.114-123.

Brooke, J., 1996. A quick and dirty usability scale. *Usability Evaluation in Industry*, 189(194), pp.4-7. Available from: https://www.cui.unige.ch/isi/icle-wiki/_media/ipm:test-suschapt.pdf. [Last accessed on 2020 Mar 01].

Dewett, T., 2002. The role of information technology in the organization: A review, model, and assessment. *Journal of Management*, 27, pp.313–346.

"Different Types of Information System and the Pyramid Model", No Date, Available from: http://www.chris-kimble.com/Courses/World_Med_MBA/Types-of-Information-System.html. [Last accessed on 2019 Jun 08].

Ferré, X., Windl, H., and Constantine, L., 2001. Usability engineering-usability basics for software developers. *IEEE Software*, 18(1), pp.22-29.

Hill, A.V., 2019. Structured Brainstorming. *Clamshell Beach Press* CBP WP 57-03, Minnesota.

Kohli, R., and Devaraj, S., 2004. Contribution of institutional DSS to organizational performance: Evidence from a longitudinal study. *Decision Support Systems*, 37(1), pp.103-118.

Maxwell, J.A., and Kaplan, B., 2005. For evaluating computer. In: *Healthcare Information System*. Springer, Germany, pp.30-56. Available from: https://www.link.springer.com/chapter/10.1007/0-387-30329-4_2.

Melville, N., and Kraemer, K., 2016. Review : Information technology and organizational performance : An integrative model of IT business value. *MIS Quarterly*, 28(2), pp.283-322.

Peppard, J., and Ward, J., 2004. Beyond strategic information systems: Towards an IS capability. *Journal of Strategic Information Systems*, 13(2), pp.167-194.

Sauro, J., 2013. *10 Things to Know About the System Usability Scale (SUS)*. Available from: https://www.measuringu.com/10-things-sus. [Last accessed on 2020 Mar 01].

Sigala, I.F., Kettinger, W.J., and Wakolbinger, T., 2020. Digitizing the field : Designing ERP designing systems for triple-a humanitarian supply chains. *Journal of Humanitarian Logistics and Supply Chain Management*, 10(2), pp.231-260.

Stair, R.M., and Reynolds, G., 2018. Information Systems. 13th ed. CENGAGE, United States.

Tripathi, K.P., 2011. Decision support system is a tool for making better decisions in the organization. *Indian Journal of Computer Science and Engineering*, 2(1), pp.112-117.

Umble, E.J., Haft, R.R., and Umble, M.M., 2003. Enterprise resource planning: Implementation procedures and critical success factors. *European Journal of Operational Research*, 146(2), pp.241-257.

Van Nieuwenhuyse, I., De Boeck, L., Lambrecht, M., and Vandaele, N.J., 2009. Advanced resource planning as a decision support module to ERP. *Computers in Industry*, 62(1), pp.1-8.

 http://dx.doi.org/10.14500/aro.10590

Cloud Storage Protection Scheme Based on Fully Homomorphic Encryption

Mohammed A. Mohammed[1] and Fadhil S. Abed[2]

[1]Department of Computer Science, College of Science, University of Sulaimani, Sulaymaniyah, Kurdistan Region – F.R. Iraq

[2]Department of Information Technology, Kalar Technical Institute, Sulaimani Polytechnic University, Khanaqeen, Kurdistan Region – F.R. Iraq

***Abstract*— Cloud computing allows enterprises and individuals to have a less physical infrastructure of software and hardware. Nevertheless, there are some concerns regarding privacy protection which may turn out to be a strong barrier. Traditional encryption schemes have been used to encrypt the data before sending them to the cloud. However, the private key has to be provided to the server before any calculations on the data. To solve this security problem, this paper proposes a fully homomorphic encryption scheme for securing cloud data at rest. The scheme is based on prime modular operation, its security depends on factoring multiple large prime numbers ($p_1, p_2,...p_n$) up to n, which is formed from very large prime numbers up to hundreds of digits as this is an open problem in mathematics. In addition, the elements of the secret key are derived from a series of mathematical operations and the calculation of an Euler coefficient within the modular of integers. Furthermore, it adds the complexity of noise to the plaintext using the number of users of the Cloud Service Provider. Moreover, its randomness is evaluated by the National Institute of Standards and Technology statistical tests, and the results demonstrating that the best statistical performance was obtained with this algorithm.**

***Index Terms*— Cloud Computing Security, Cryptography, Fully Homomorphic Encryption, Information Security.**

I. Introduction

Cloud computing plays an important role in storing and processing huge amounts of data since the fast progress of computer networks and big data (Hashem, et al. 2015). It provides flexible and on-demand remote storage and computing capabilities to its users. Nevertheless, as Gonzales et al. (2017) stated that cloud computing is not fully trustable since its users do not have full control over their data. Privacy protection and data leakage are the main risks for individuals and enterprises when it comes to migrating their data to cloud storage. The encryption techniques that require encrypted data on the cloud to be decrypted before performing any computation is still portend the privacy of stored data. Whereas, in Homomorphic Encryption operations can be performed directly on encrypted data without decrypting it. In addition, the result of the operation on encrypted data is equivalent to the result of its corresponding plaintext operation. This paper attempts to add an extra value to the privacy protection of cloud's data through proposing a new FHE scheme based on prime modular operation, which security depends on factoring multiple large prime numbers ($p_1, p_2,...,p_n$) up to n, which is formed from very large prime numbers up to hundreds of digits as this is an open problem in mathematics. Moreover, the randomness of the proposed work is evaluated by the well-known National Institute of Standards and Technology (NIST) test suite, which is widely used as a standard battery of tests to test randomness. The results of the proposed algorithm in the NIST statistical tests show that it produces the best statistical performance through passing all the tests.

II. Problem Statement

Nowadays, individuals and enterprises are seeking to access their private information anytime and anywhere. This leads them to deploy it onto cloud storage. However, they will be facing an extra amount of risks, which makes it challenging to maintain the security of outsourced data such as confidentiality, integrity, authentication, and privacy. For example, the hacking attack on PlayStation network in 2011 led it to leak millions of user accounts' passwords, physical addresses, credit card information, and other personal information. Later, the company stated that they could have encrypted the data on their network (Sangani, 2011). In addition, as reported by the Identity Theft Resource Center on May 31, 2018, thousands of FedEx customer records were exposed due to an unsecured server; some of the documents were passports, driving licenses, and security IDs (CyberScout, 2018). Therefore, Cloud Service Providers (CSPs) are required to keep an encrypted version of user's information on their storage. There is a variety of different techniques used for data encryption. Nevertheless, as the

ARO-The Scientific Journal of Koya University
Vol. VIII, No.2 (2020), Article ID: ARO.10590, 08 pages
DOI:10.14500/aro.10590
Received: 14 November 2019; Accepted: 16 November 2020
Regular research paper: Published: 06 December 2020
Corresponding author's e-mail: mohammed.anwar@univsul.edu.iq

data resides on the cloud storage, it required to be decrypted before performing any operation on the data. This might cause privacy and confidentiality problems to the stored data. Whereas, homomorphic encryption allows performing computations on the encrypted data without decrypting it. Thus, HE solves the problems of confidentiality and privacy of the stored data inside the cloud. Therefore, this paper presents a new FHE scheme based on multiple large prime modular operation which is formed from very large prime numbers up to hundreds of digits. Hence, it makes the secret key very complicated which is difficult to retrieve it and resistance to different types of attacks.

III. Literature Review

Rivest et al. (1978) were proposed the first homomorphic encryption scheme and were partially homomorphic encryption (PHE). Then, Yao (1982) was also presented a PHE scheme. After that, RSA which was a multiplicative homomorphism introduced by Rivest et al. (1983). Afterward, several authors such as Goldwasser and Micali (1984), Elgamal (1985), and Paillier (1999) were also presented their PHE scheme. Subsequently, a fully homomorphic encryption (FHE) scheme suggested by Gentry (2009), which allows calculating of any number of addition and multiplication, hence compute arbitrary functions of encrypted data. Nevertheless, the scheme was based on Somewhat Homomorphic Encryption (SWHE), which increases the length and noise of ciphertext when calculation performs on the ciphertext. Consequently, van Dijk et al. (2010) have introduced FHE scheme that used elementary modular arithmetic and used Gentry's techniques to convert SWHE cryptosystem to FHE scheme. In addition, Smart and Vercauteren (2010) have presented an improved version of Smart-Vercauteren encryption scheme, the scheme was allowed several times decrease the ciphertext and keys lengths. In addition, IBM has released a software package named HElib in 2013, the company has implemented HE with further optimizations (Cheon, et al. 2019). Moreover, a HE scheme which is security dependent on the hardness of large integer factorization has been proposed by Xiao et al. (2012). Afterward, homomorphic encryption scheme has been worked on and improved by numerous authors, they have also tested it in a cloud computing system. Alattas and Elleithy (2013) have presented the application of algebraic homomorphic encryption mechanism and it was aiming at enhancing its security. In addition, several HE schemes such as RSA, Paillier, El-Gamal, and Gentry have been examined on a cloud computing environment by Tebaa and El Hajii (2014). In addition, Hayward and Chiang (2015) have improved Gentry's encryption in parallel processing and they have tested it in a private cloud domain. Furthermore, structured and simplified definitions in the homomorphic encryption discipline have been proposed by Armknecht et al. (2015). Moreover, SAM which is an FHE scheme over integers has been implemented by Shihab and Makki (2018). Furthermore, Li et al. (2016) constructed an efficient symmetric FHE scheme and utilized it to design a privacy-preserving-outsourced association rule mining scheme. Their proposal allows multiple data owners to jointly mine some association rules without sacrificing data privacy. The security of the HE scheme against the known-plaintext attacks was established by examining the difficulty of solving nonlinear systems. However, Wang et al. (2018) illustrated that the security of Li et al.'s HE is overvalued. They presented the retrieval and the second part can also be retrieved using a Euclidean algorithm to address the GCD problem of the first part of the secret key. Whereas, in 2019 (Li et al.) used a lookup table to propose a protocol to evaluate any function using FHE.

Moreover, Ji and Shieh (2019) presented ways to reduce the computation complexity of encrypted data by adopting the concept of aggregate plaintext and proposing an efficient scheme to handle the comparison and swap operation, which is commonly used for sorting and searching in cloud computing. In late 2019, the authors of Jubrin et al. introduced FHE as an antidote to the challenges of security and privacy of cloud data computation; they also provided insight into future research directions in the field of FHE. Furthermore, Mohammed and Abed (2019) proposed an improved FHE based on N-primes, where the proposed model's security depends on the problem of factorization the integers to their primary numbers. Mert et al. (2020) presented two hardware architectures optimized for accelerating the encryption and decryption operations of the BFV/HE scheme with high-performance polynomial multipliers. In addition, in 2020, Tan et al. presented a private comparison algorithm on encrypted integers using FHE, which scales efficiently for the length of input integers, applying techniques from finite field theory. Whereas, Mohammed and Abed (2020) proposed a novel framework and an algorithm for securing cloud data at rest. The proposed framework guarantees users' privacy protection as they are communicating with an intermediary rather than with the cloud server directly.

Despite all the works presented previously, the randomness and robustness of the secret keys remain an open problem in the area of FHE. Therefore, this paper presents a new algorithm in which the elements of the secret key are derived from a series of mathematical operations and the calculation of an Euler coefficient within the modular of integers. Furthermore, it adds the complexity of noise to the plaintext by using the number of users of the CSP. Moreover, the proposed algorithm's randomness tests prove the best statistical performance was obtained with this algorithm. Furthermore, the algorithm works on encrypting and decrypting different languages such as Kurdish, English, and Arabic.

IV. Homomorphic Encryption

In this section, HE scheme and its categories will be presented. Homomorphic encryption is divided into different categories, which are SWHE, FHE, and PHE. An encryption scheme is said to be homomorphic over an operation "+" if it supports the following equation, where ms is the plaintext message given to the encryption algorithm E:

$$E(ms_1) + E(ms_2) = E(ms_1 + ms_2),\ \forall ms_1, ms_2 \in M$$

http://dx.doi.org/10.14500/aro.10590

Algorithm 1: Key generation

Procedure

Input : n prime numbers $p_1, p_2, p_3 \dots p_n$

for i = 1 to n

Pr = Pr × p_i

L = L(p_i+1)

end for

for i = 1 to L

$M_s = M_s + p_i$

end for

Calc : $M_{avg} = M_s$ DivisibleBy L

rand := a random number $R_n \rightarrow \gcd(R_n, M_{avg}) = 1$

R_n not equal ZERO AND smaller than M_{avg}

for i = 1 to n

(Pr) = (Pr)(p_i−1)

end for

Input : U_{sr} where its ≥ 1

Calc : Q = U_{sr} ×((Pr) mod M_s)

Calc : $K_{sp} = (R_n \times Q) \bmod 256$

Output : K_{sp} as the secret key

End procedure

Algorithm 2: Encryption

Procedure

Input: N as big prime number

Input: ms the plaintext message

rand:= a random number r

for i = 1 to length(ms)

cph = ms + N(r K_{sp}+i)

end for

Output: cph as ciphertext file

End procedure

Algorithm 3: Decryption

Procedure

for i = 1 to length(cph)

ms = cph mod N

end for

Output: ms as plaintext file

End procedure

Somewhat homomorphic encryption allows addition and multiplication operations, however, both operations can be performed in a limited number Fellows and Koblitz (1994) and BNG by (Boneh-Goh-Nissim) (Dan, et al. 2005). Whereas, PHE allows one type of operation, either addition or multiplication, that is, Paillier, Goldwasser-Micali, Benaloh, El-Gamal, and RSA. On the other hand, FHE allows an unlimited number of both addition and multiplication on the ciphertext. It can be considered as ring homomorphism. As in mathematics, a ring is a set R equipped with two operations, "+" and "×" satisfying the eight axioms, known as the ring axioms. Examples of FHEs are FHE schemes Over Integers (dos Santos, et al. 2015), Simple FHE scheme (Li, et al. 2012), LWE-based FHE schemes (Regev, 2005), ideal lattice-based FHE schemes (Gentry, 2009), and NTRU-like FHE schemes (Hoffstein, et al. 1998). Fig. 1 presents the popular schemes proposed after the Gentry's discovery.

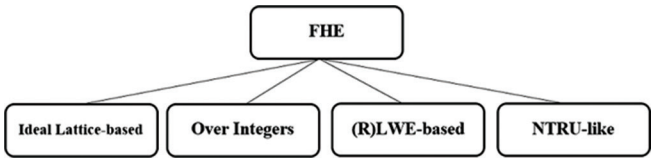

Fig. 1. Main FHE schemes after Gentry's discovery (Acar, et al. 2018).

V. The Proposed Scheme

The proposed scheme works on converting each plaintext character into its corresponding Unicode and then encrypts the derived Unicode by passing it to the encryption algorithm. In addition, the scheme also works on encrypting plaintexts in several languages such as Kurdish, English, and Arabic languages. In addition, the algorithm uses two different noises *r* as the first noise is added to make the ciphertext more digestive, whereas the counter *i* works on converting repeated characters in the text into different ciphertext values. The detailed notations used in the key generation, encryption, and decryption algorithms are presented in Table I. Subsequently, the working flow of the algorithms is illustrated in pseudocode.

Generating the Secret Key K_{sp}

At first choose multiple *P* prime numbers $p_1, p_2, p_3 \cdots p_n$ as secret keys, then calculate *P* as $P = p_1 \times p_2 \times \ldots \times p_n$, calculate *L* as $L = (p_1 + 1)(p_2 + 1)\ldots(p_n + 1)$, then calculate $M_s = \sum_{i=1}^{m} F_i$, where F_i = set of prime numbers up to *L*, and then calculate the average value of sum of all prime numbers as $M_{avg} = \frac{M_s}{L}$, then choose a random number R_n that satisfies $\gcd(R_n, M_{avg}) = 1$, $1 < R_n < M_{avg}$, then select U_{sr} as it is the number of existing users of the cloud system $\{U_{sr1}, U_{sr2}, \ldots, U_{srn}\}$, where $U_{sr} \geq 1$, calculate $\theta(P) = (p_1 - 1)\ldots(p_n - 1)$, and calculate $Q = U_{sr} \times (\theta(P) \bmod M_s)$ and finally calculate K_{sp} as:

$$K_{sp} = (R_n \times Q) \bmod 256 \quad (1)$$

Mod 255 is taken as this is because the secret key values are derived from a series of mathematical calculations that are within a certain scale between 1 and 255 so that the values resulting from the equation are not very large and prevent any slowness in the calculation process.

Encryption algorithm

$$cph = ms + N(rK_{sp} + i) \quad (2)$$

Decryption algorithm

$$\text{ms} = cph \bmod N \quad (3)$$

TABLE I
LIST OF NOTATIONS

Notations	Details
cph	Ciphertext
ms	The plaintext message
r	Noise added to the ciphertext
N	Big prime integer
K_{sp}	Secret key
i	Counter added as extra noise to the ciphertext works on converting repeated character into different ciphertext value.
$p_1, p_2, p_3 \dots p_n$	Multiple prime numbers
P	Is the multiplications of prime numbers
L	Is the multiplication of each prime number plus one
M_s	The summation of prime numbers up to *L*
M_{avg}	Average of all prime numbers
R_n	Is a random number where gcd(R_n, M_{avg}) = 1
U_{sr}	Is the number of CSP's users

CSP: Cloud service provider

A. Proof of Homomorphism

This subsection will illustrate the homomorphism of the proposed scheme, assume there are two ciphertexts cph_1 and cph_2 where $cph_1 = ms_1 + N(r_1 K_{\sup} + i)$, $cph_2 = ms_2 + N(r_2 K_{\sup} + i)$, and $cph \bmod N \equiv ms$, where $ms < N$, otherwise, we must take $(ms \bmod N)$.

Homomorphism (Addition)

Assume that the sum of two ciphertexts cph_1 and cph_2 is denoted by $(cph^+ = cph_1 + cph_2)$ so $cph^+ = cph_1 + cph_2 = (ms_1 + ms_2) + N(r_1 K_{sp} + i) + N(r_2 K_{sp} + i)$, nonetheless $N(r_1 K_{sp} + i) + N(r_2 K_{sp} + i) = NK_{sp}\begin{bmatrix}(r_1 + r_2)\\ +2i\end{bmatrix} = 0$ Then $ms^+ = (cph_1 + cph_2) \mod N = ms_1 + ms_2$

Homomorphism (Multiplication)

Assume that the sum of two ciphertexts cph_1 and cph_2 is denoted by ($cph^* = cph_1 * cph_2$) $cph^* = [ms_1 + N(r_1 K_{sp} + i)] \times [ms_2 + N(r_2 K_{sp} + i)]$ $cph^* = [ms_1 \times ms_2 + ms_1 \times N(r_2 K_{sp} + i)] + N(r_1 K_{sp} + i) \times ms_2 + N(r_1 K_{sp} + i) \times N(r_2 K_{sp} + i)]$ Then $N \times [ms_1 \times N(r_2 K_{sp} + i) + (r_1 K_{sp} + i) \times ms_2 N(r_1 K_{sp} + i) \times N(r_2 K_{sp} + i) \bmod N] = 0$ So that, $cph^* = ms_1 \times ms_2 + 0 = ms_1 \times ms_2$.

VI. Result and Analysis

In this section, the results gained from the proposed scheme will be presented through numerous tests on English, Kurdish, and Arabic languages. To test the proposed scheme, it is implemented with Java programming language and processed on a computer with the following features: Intel Core i7 processor, HDD hard drive, 16 GB RAM, and Windows 10 64-bit. At first, the generation of the secret key is illustrated then it will be used for all the tests presented in this section.

Secret key generation

Choose a set of prime numbers for as $p_1 = 31, p_2 = 59$ and $p_3 = 73$ then $\theta(P) = 30 \times 58 \times 72 = 125280$, $P = 31 \times 59 \times 73 = 133517$. Then, calculate $L = (31+1)(59+1)(73+1) = 142080$, so $M_s = 129548351731$, $M_{avg} = 911798$, assume $U_{sr} = 35$ and $R_n = 15$ then $Q = 4384800$, finally $K_{sp} = 224$.

A. Test on English Language

The proposed algorithm will be tested on an English language text of "Hello world; this is a new Fully Homomorphic algorithm." For this test, the secret key will be $K_{sp} = 224$ as generated previously, and $N = 524287$ which is big prime number, then choose a random number as $r = 62598$ the ciphertext of the given text after applying the proposed algorithm on it will be:

7351527148296 7351527672612 7351528196906
7351528721193 7351529245483 7 3 5 1 5 2 9 7 6 9 6 9 1
7351530294065 7351530818344 7 3 5 1 5 3 1 3 4 2 6 3 4
7351531866915 7351532391194 7 3 5 1 5 3 2 9 1 5 4 1 3
7351533439784 7351533964059 7 3 5 1 5 3 4 4 8 8 3 4 7
7351535012644 7351535536848 7 3 5 1 5 3 6 0 6 1 2 0 8
7351536585505 7351537109709 7 3 5 1 5 3 7 6 3 4 0 6 1
7351538158283 7351538682648 7 3 5 1 5 3 9 2 0 6 9 2 6
7351539731231 7351540255431 7 3 5 1 5 4 0 7 7 9 7 5 6
7351541304090 7351541828368 7 3 5 1 5 4 2 3 5 2 6 5 5
7351542876955 7351543401153 7 3 5 1 5 4 3 9 2 5 4 8 0
7351544449806 7351544974091 7 3 5 1 5 4 5 4 9 8 3 8 0
7351546022665 7351546546954 7 3 5 1 5 4 7 0 7 1 2 4 4
7351547595529 7351548119808 7 3 5 1 5 4 8 6 4 4 0 9 6
7351549168377 7351549692597 7 3 5 1 5 5 0 2 1 6 9 4 9
7351550741247 7351551265529 7 3 5 1 5 5 1 7 8 9 8 2 4
7351552314114 7351552838392 7 3 5 1 5 5 3 3 6 2 6 9 0
7351553886965 7351554411257

Table II and Fig. 2 illustrate the performance of the proposed algorithm tested on different file sizes that contain plaintext written in the English language.

B. Test on Kurdish Language

This test illustrates the proposed algorithm tested on a Kurdish language text of "سڵاو ئەمە ئەڵگۆریزمەکەمە بۆ تاقیکردنەوە," and the same values used for testing English language text and the ciphertext will be:

7351527149811 7 3 5 1 5 2 7 6 7 4 2 2 8
7351528198373 7351528722693 7 3 5 1 5 2 9 2 4 5 4 0 4
7351529771233735153029569 5 7 3 5 1 5 3 0 8 1 9 8 3 8
7351531344269 7351531866839 7 3 5 1 5 3 2 3 9 2 6 6 8
7351532917130 7351533441272 7 3 5 1 5 3 3 9 6 5 6 6 6
7351534489976 7351535014114 7 3 5 1 5 3 5 5 3 8 5 5 6
7351536062689 7351536586995 7 3 5 1 5 3 7 1 1 1 4 2 6
7351537635669 7351538160000 7 3 5 1 5 3 8 6 8 4 1 4 3
7351539208574 7351539731144 7 3 5 1 5 4 0 2 5 6 9 7 5
7351540781420 7351541304005 7 3 5 1 5 4 1 8 2 9 8 3 8
7351542354122 7351542878436 7 3 5 1 5 4 3 4 0 2 8 6 1
7351543927113 7351544451280 7 3 5 1 5 4 4 9 7 5 5 6 5
7351545499875 7351546024305 7 3 5 1 5 4 6 5 4 8 4 5 1
7351547072879

Table III and Fig. 3 illustrate the performance of the proposed algorithm tested on different file sizes that contain plaintext written in the Kurdish language.

http://dx.doi.org/10.14500/aro.10590

TABLE II
TESTING THE PROPOSED ALGORITHM ON DIFFERENT FILE SIZES WRITTEN IN THE ENGLISH LANGUAGE

File sizes	Encryption (ms)	Decryption (ms)
10 KB	378	414
20 KB	397	448
40 KB	413	499
80 KB	459	570
160 KB	486	625
320 KB	529	710
500 KB	599	831
1 MB	748	1081
2 MB	981	1597
4 MB	1698	2703
8 MB	2531	4843
16 MB	4234	8432

TABLE III
TESTING THE PROPOSED ALGORITHM ON DIFFERENT FILE SIZES WRITTEN IN THE KURDISH LANGUAGE

File sizes	Encryption (ms)	Decryption (ms)
10 KB	375	406
20 KB	391	438
40 KB	421	500
80 KB	437	562
160 KB	485	688
320 KB	578	766
500 KB	594	814
1 MB	734	1109
2 MB	1031	1625
4 MB	1702	2609
8 MB	2848	4582
16 MB	5471	9018

C. Test on Arabic Language

This time the proposed algorithm will be tested on an Arabic text of "مرحبا نقدم لكم خوارزمية جديدة," also the values from the first test will be used and the ciphertext is as follow:

7351527149829 7351527674096 7351528198379
7351528722661 7351529246947 7 3 5 1 5 2 9 7 6 9 6 9 1
7351530295552 7351530819835 7 3 5 1 5 3 1 3 4 4 1 0 3
7351531868412 7351532391126 7 3 5 1 5 3 2 9 1 6 9 8 5
7351533441271 7351533965560 7 3 5 1 5 3 4 4 8 8 2 7 4
7351535014111 7351535538424 7 3 5 1 5 3 6 0 6 2 6 7 8
7351536586975 7351537111263 7 3 5 1 5 3 7 6 3 5 5 6 9
7351538159861 7351538684115 7 3 5 1 5 3 9 2 0 6 8 5 7
7351539732692 7351540256982 7 3 5 1 5 4 0 7 8 1 2 9 6
7351541305556 7351541829837

The previous tests presented that the proposed algorithm can be performed on different languages, and it produces different cipher-values for all plaintext values and also for the repeated character within the same text. In addition, the rest of this section will present the performance of the proposed algorithm performed on different file sizes written in English, Kurdish, and Arabic languages. Table IV and Fig. 4 illustrate the performance of the proposed algorithm tested on different file sizes that contain plaintext written in the Arabic language.

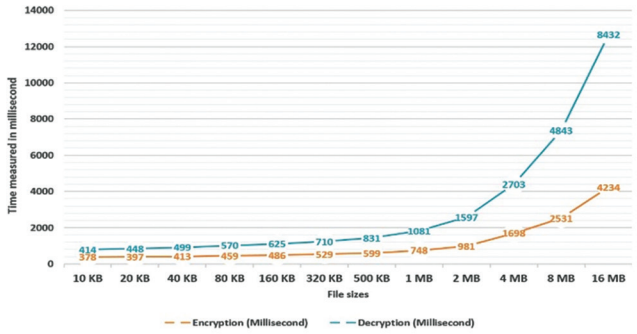

Fig. 2. Encryption and decryption time on English language plaintext file.

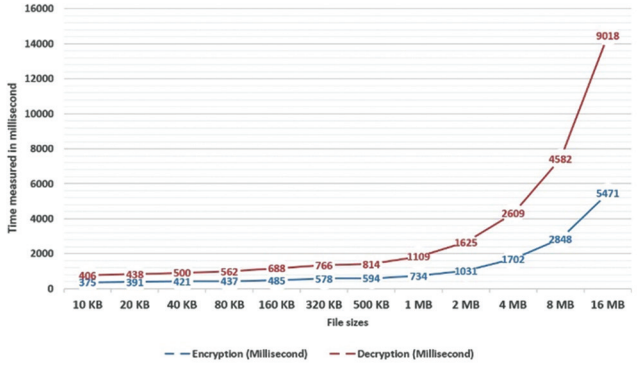

Fig. 3. Encryption and decryption time on Kurdish language plaintext file.

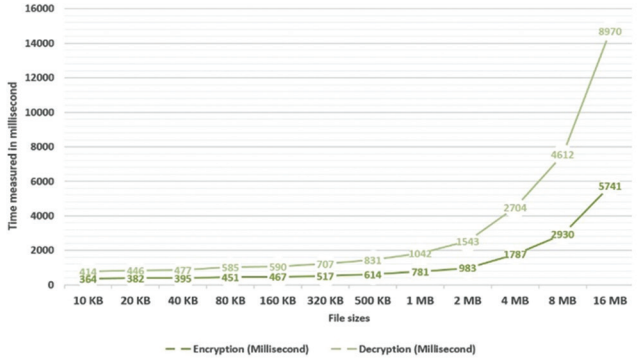

Fig. 4. Encryption and decryption time on Arabic language plaintext file.

The results of the previous tests show that the proposed algorithm is capable on encrypting plaintexts written in different languages efficiently regardless of the file size. In addition, it can be observed from the results that the algorithm performs almost the same performance on the same file sizes of various languages. Table V and Fig. 5 present a comparison of the previous tests gained from the proposed algorithm. As it is illustrated, the encryption and decryption time for all three languages are vary and almost works the same. Such as the encryption time of 20 KB Arabic text-file requires less time than the encryption time on its corresponding English and Kurdish text-file. Whereas, the encryption time of 2 MB English text-file takes less time than Kurdish and Arabic text-files.

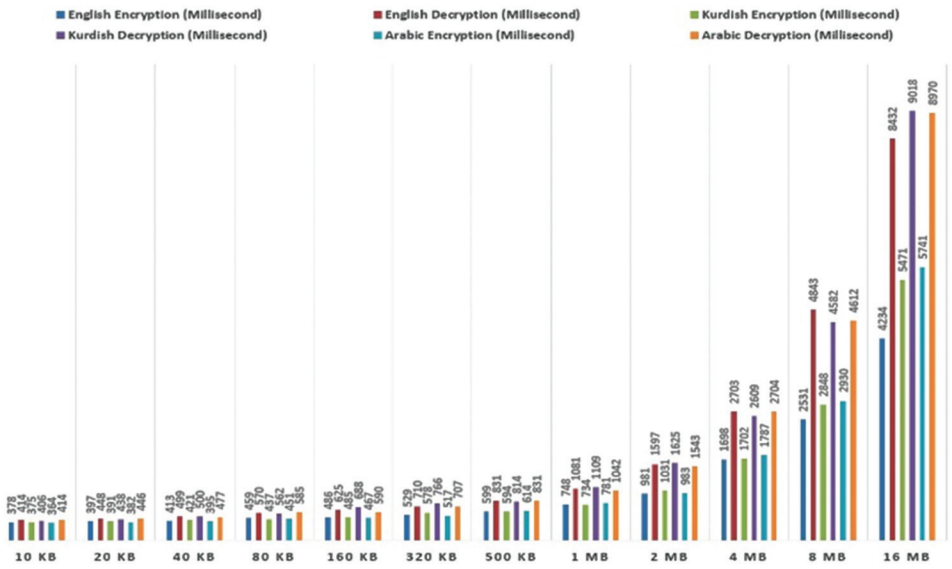

Fig. 5. Encryption and decryption time on English, Kurdish, and Arabic language plaintext file.

TABLE IV
TESTING THE PROPOSED ALGORITHM ON DIFFERENT FILE SIZES WRITTEN IN THE ARABIC LANGUAGE

File sizes	Encryption (ms)	Decryption (ms)
10 KB	364	414
20 KB	382	446
40 KB	395	477
80 KB	451	585
160 KB	467	590
320 KB	517	707
500 KB	614	831
1 MB	781	1042
2 MB	983	1543
4 MB	1787	2704
8 MB	2930	4612
16 MB	5741	8970

TABLE V
TIME COMPLEXITY OF THE BASIC ARITHMETIC OPERATIONS

Operation	Time complexity of binary integers of size n	Time complexity of decimal digits of size n
Addition x + y	O(n)	O(log(n))
Subtraction x – y	O(n)	O(log(n))
Multiplication x × y	$O(n^2)$	$O((\log(n^2))$
Division and Modular	$O(n^2)$	$O((\log(n^2))$
Inverse x^{-1}	$O(n^2\log(n))$	$O(\log(n))^3)$
Modular exponentiation x^n	$O(n^2\log(n))$	$O(\log(n))^3)$

D. Big O Notation (Time Complexity)

Searching for the "best" in algorithms is the main concern of algorithms' designers, and this can be achieved through using O-notation. The aim of studying the time complexity of an algorithm is to determine whether the algorithms' running time is *O(f(N))* for some function *f()* or not. Table VI illustrates the complexity of the basic arithmetic operations in Z_n (Sagheer, 2012).

The input numbers of encryption and decryption algorithms should be analyzed at first before performing any calculation of the time complexity. The input numbers are either binary integers or decimal digits, whereas the time complexity of the first mentioned is *O(n)* and the time complexity of decimal digits is *O(log(n))*, this excluding constant number whose complexity is *O(1)*. Since, n is the size of input numbers.

1) Time complexity of DGHV scheme

Let n be the size of input message unit.

Encryption function:

$cph = ms + 2r + p \times q$

Then: $T(cph) = O(n) + T(2r) + O(n^2)$

$T(2r) = O(n)$, by shift operation

$T(cph) = O(2n) + O(n^2) \equiv O(n^2)$ bit operation.

Decryption function:

$ms = (cph \bmod p) \bmod 2$

Then: $T(ms) = O(n^2)$ bit operation

2) Time complexity of SDC scheme

Let n be the size of input message unit.

Encryption function:

$cph = ms + p + r \times p \times q$

Then: $T(cph) = O(n) + O(n) + O(2(n^2))$

$T(cph) = O(2(n)) + O(2(n^2)) \equiv O(n^2)$ bit operation.

Decryption function:

$ms = cph \bmod p$

Then: $T(ms) = O(n^2)$ bit operation.

3) Time complexity of the proposed algorithm

Let n be the size of input message, n is decimal digit.

Encryption function:

$cph = ms + N(rK_{sp} + i)$

Then: $T(cph) = O(2(\log(n))) + O(2(\log(n))^2)$

 http://dx.doi.org/10.14500/aro.10590

TABLE VI
COMPARING THE RESULTS OF THE ALGORITHM GAINED FROM ENCRYPTING AND DECRYPTING ENGLISH, KURDISH, AND ARABIC LANGUAGE'S PLAINTEXTS

File sizes	English		Kurdish		Arabic	
	Encryption (ms)	Decryption (ms)	Encryption (ms)	Encryption (ms)	Encryption (ms)	Encryption (ms)
10 KB	378	414	375	406	364	414
20 KB	397	448	391	438	382	446
40 KB	413	499	421	500	395	477
80 KB	459	570	437	562	451	585
160 KB	486	625	485	688	467	590
320 KB	529	710	578	766	517	707
500 KB	599	831	594	814	614	831
1 MB	748	1081	734	1109	781	1042
2 MB	981	1597	1031	1625	983	1543
4 MB	1698	2703	1702	2609	1787	2704
8 MB	2531	4843	2848	4582	2930	4612
16 MB	5741	8970	5471	9018	5741	8970

$T(cph) \equiv O(\log(n)^2)$

Decryption function:

$ms = cph \bmod N$

Then: $T(ms) = O((\log(n))^2)$, Where, $(\log_2 n)$ is the number of bits of n

E. Resistance to Attacks

In this section, the resistance of the proposed algorithm to different types of attacks such as Key Generation and Character Repetition, Brute Force Attack, and Mathematical Attack are illustrated.

4) Key generation and character repetition

The proposed algorithm encrypts each file with a different key, and it depends on a variable that is different for every cloud user. In addition, the algorithm encrypts the repetition of each character into different values. Thus, the attacker cannot analyze character repetition in the file. Consequently, the combination of different keys for each file and different values for the same character allows our proposed algorithm to provide a strong encryption method.

5) Brute force attack

In the proposed algorithm, the strength of large prime numbers depends on the multiplication of n prime numbers p_1, p_2,... p_n. Thus, it is difficult to break the large prime number into multiple primes as compared to the existing algorithms. Furthermore, the multiple prime numbers increase the level of difficulty to break the security of the algorithm. In addition, the use of the addition noises makes it more difficult to break.

6) Mathematical attack

This kind of attack occurs when the attacker determines the values of p and q. In our proposed algorithm, it is reduced as the algorithm uses multiple numbers of primes, and it is hard to derive any of those primes from the multiplication result.

F. Results of NIST Statistical Tests

The randomness of this novel proposal is evaluated by the well-known NIST test suite. Table VII shows the test results of the proposed algorithm from the NIST statistical tests, demonstrating that the best statistical performance was obtained with this algorithm.

TABLE VII
NIST SP 800-22 TEST RESULTS FOR THE NAZUZ ALGORITHM

Tests	***P***-value	Result
Frequency (Monobits)	0.997743	Success
Block frequency	0.999936	Success
Cumulative sums (Cusum)	0.983782	Success
Runs	0.982544	Success
Longest run of ones	0.993900	Success
Rank	0.999594	Success
Discrete Fourier transform	0.074478	Success
Non-overlapping template matching	0.999975	Success
Overlapping template matching	0.856322	Success
Universal statistical	0.999620	Success
Approximate entropy	0.999961	Success
Random excursions	0.997529	Success
Random excursions variant	0.837424	Success
Serial	0.999995	Success
Linear complexity	0.999438	Success

VII. CONCLUSION

It has been said that homomorphic encryption is the change point of cryptography, as it protects data regardless of its situation, whether the data are in transit or at rest. This helped CSPs to use this new technique for data protection. This paper is proposed a new FHE scheme based on prime modular operation. The scheme performs encryption and decryption on plaintext values regardless of the written language of the plaintext English, Kurdish, Arabic, or any other languages as well as special characters. In addition, the scheme encrypts repeated characters of the plaintext into different ciphertext values which increases the security of the ciphertext. The randomness of the proposal scheme is evaluated by the well-known NIST test suite (widely used as a standard battery of tests to test randomness). The results of the proposed algorithm in the NIST statistical tests show that it produces the best statistical performance through passing

all the tests. Moreover, the proposed scheme demonstrates good security for the stored data on the cloud.

References

Acar A, Aksu H., Uluagac A.S. and Conti, M., 2018. A survey on homomorphic encryption schemes: Theory and implementation. *ACM Computing Surveys*, 51(4), pp.1-35.

Alattas, R. and Elleithy, K., 2013. *Cloud Computing Algebra Homomorphic Encryption Scheme Based on Fermat's Little Theorem*. The American Society of Engineering Education, Northfield, VT, USA.

Armknecht, F., Boyd, C., Carr, C., Gjøsteen, K., Jaschke, A., Reuter, C. and Strand, M., 2015. A guide to fully homomorphicencryption. *IACR Cryptology ePrint Archive*, 2015, 1192.

Cheon, J., Choe, H., Lee, D. and Son, Y., 2019. Faster linear transformations in HElib, revisited. *IEEE Access*, 7, pp.50595-50604.

CyberScout., 2018. *Data Breach Reports*. Identity Theft Resource Center, Berkeley, CA, USA.

Dan, B., Eu-Jin, G. and Kobbi, N. 2005. Evaluating 2-DNF formulas on ciphertexts. In: Proceedings of Theory of Cryptography Conference. Vol. 3378. Springer, Berlin. pp.325-341.

dos Santos, L.C., Bilar, G.R. and Pereira, F.D., 2015. Implementation of the Fully Homomorphic Encryption Scheme Over Integers with Shorter Keys. In: *2015 7th International Conference on New Technologies, Mobility and Security* (*NTMS*), Paris, France.

Elgamal, T., 1985. A public key cryptosystem and a signature scheme based on discrete logarithms. *IEEE Transactions on Information Theory*, 31(4), pp.469-472.

Fellows, M. and Koblitz, N., 1994. Combinatorial cryptosystems galore! In: *Finite Fields: Theory, Applications, and Algorithms*. American Mathematical Society, Providence, Rhode Island. pp.51-61.

Gentry, C., 2009. *A Fully Homomorphic Encryption Scheme, PhD*. Stanford University, United States.

Gentry, C., 2009. Fully Homomorphic Encryption Using Ideal Lattices. In: *Proceedings of the 41st Annual ACM Symposium on Symposium on Theory of Computing STOC '09*, Bethesda, Maryland, USA.

Goldwasser, S. and Micali, S., 1984. Probabilistic encryption. *Journal of Computer and System Sciences*, 28(2), pp.270-299.

Gonzales, D., Kaplan, J., Saltzman, E., Winkelman, Z. and Woods, D., 2017. Cloud-trust a security assessment model for infrastructure as a service (IaaS) clouds. *IEEE Transactions on Cloud Computing*, 5(3), pp.523-536.

Hashem, I., Yaqoob, I., Anuar, N., Mokhtar, S., Gani, A. and Khan, S.U., 2015. The rise of "big data" on cloud computing: Review and open research issues. *Information Systems*, 47, pp.98-115.

Hayward, R. and Chiang, C., 2015. Parallelizing fully homomorphic encryption for a cloud environment. *Journal of Applied Research and Technology*, 13(2), pp.245-252.

Hoffstein, J., Pipher, J. and Silverman, J., 1998. NTRU: A ring-based public key cryptosystem. In: *Lecture Notes in Computer Science*. Springer Science+Business Media, Berlin, Germany. pp.267-288.

Ji, J. and Shieh, M., 2019. Efficient comparison and swap on fully homomorphic encrypted data. In: *2019 IEEE International Symposium on Circuits and Systems* (ISCAS), Sapporo, Japan, pp.1-4.

Jubrin, A.M., Izegbu, I. and Adebayo, O.S., 2019. Fully homomorphic encryption: An antidote to cloud data security and privacy concems. In: *2019 15th International Conference on Electronics, Computer and Computation* (ICECCO), Abuja, Nigeria, pp.1-6.

Li, J., Song, D., Chen, S. and Lu, X., 2012. A Simple Fully Homomorphic Encryption Scheme Available in Cloud Computing. In: *2012 IEEE 2nd International Conference on Cloud Computing and Intelligence Systems*, Hangzhou, China.

Li, L., Lu, R., Choo, K.R., Datta A. and Shao J., 2016. Privacy-preserving-outsourced association rule mining on vertically partitioned databases. *IEEE Transactions on Information Forensics and Security*, 11(8), pp.1847-1861.

Li, R., Ishimaki, Y. and Yamana H., 2019. Fully homomorphic encryption with table lookup for privacy-preserving smart grid. In: *2019 IEEE International Conference on Smart Computing* (SMARTCOMP), Washington, DC, USA, pp.19-24.

Mert, A.C., Öztürk E. and Savaş, E., 2020. *Design and Implementation of Encryption/Decryption Architectures for BFV Homomorphic Encryption Scheme*. Vol. 28. IEEE Transactions on Very Large Scale Integration Systems, pp.353-362.

Mohammed, M.A. and Abed, F.S., 2019. An improved fully homomorphic encryption model based on N-primes. *Kurdistan Journal of Applied Research*, 4(2), pp.40-49.

Mohammed, M.A. and Abed, F.S., 2020. A symmetric-based framework for securing cloud data at rest. *Turkish Journal of Electrical Engineering and Computer Sciences*, 28(1), pp.347-361.

Paillier, P., n.d. Public-key cryptosystems based on composite degree residuosity classes. *Advances in Cryptology Eurocrypt*, 99, pp.223-238.

Regev, O., 2005. On Lattices, Learning with Errors, Random Linear Codes, and Cryptography. In: *Proceedings of the 37th annual ACM Symposium on Theory of Computing STOC '05*, Baltimore, Maryland, USA.

Rivest, R., Shamir, A. and Adleman, L., 1983. A method for obtaining digital signatures and public-key cryptosystems. *Communications of the ACM*, 26(1), pp.96-99.

Rivest, R.L.; Adleman, L. and Dertouzos, M.L., 1978. On data banks and privacy homomorphisms. In: *Foundations of Secure Computation*. Academia Press, Cambridge, Massachusetts. pp.169-179.

Sagheer, A.M., 2012. Elliptic Curves Cryptographic Techniques. In: *2012 6th International Conference on Signal Processing and Communication Systems*, Gold Coast, QLD, pp.1-7.

Sangani, K., 2011. Sony security laid bare. *Engineering and Technology*, 6(8), pp.74-77.

Shihab, H. and Makki, S., 2018. Design of fully homomorphic encryption by prime modular operation. *Telfor Journal*, 10(2), pp.118-122.

Smart, N. and Vercauteren, F., 2010. Fully homomorphic encryption with relatively small key and ciphertext sizes. *Public Key Cryptography*, 2010, pp.420-443.

Tan, B.H.M., Lee, H.T., Wang, H., Ren, S.Q. and Khin, A.M.M., 2020. Efficient private comparison queries over encrypted databases using fully homomorphic encryption with finite fields. *IEEE Transactions on Dependable and Secure Computing*, p.1.

Tebaa, M. and El Hajii, S., 2014. Secure cloud computing through homomorphic encryption. *Computing Research Repository*, 5, 1409.

van Dijk, M., Gentry, C., Halevi, S. and Vaikuntanathan, V., 2010. Fully homomorphic encryption over the integers. *Advances in Cryptology Eurocrypt*, 2010, pp.24-43.

Wang, B., Zhan, Y. and Zhang, Z., 2018. Cryptanalysis of a symmetric fully homomorphic encryption scheme. *IEEE Transactions on Information Forensics and Security*, 13(6), pp.1460-1467.

Xiao, L., Bastani, O. and Yen, I., 2012. *An Efficient Homorphic Encryption Protocol for Multi-user Systems*. IACR Cryptology ePrint Archive, Lyon, France.

Yao, A., 1982. Protocols for Secure Computations. In: *23rd Annual Symposium on Foundations of Computer Science* (*sfcs 1982*), Washington, DC.

 http://dx.doi.org/10.14500/aro.10739

Assessment of Curing Exposures Effect on the Long-term Engineering Properties of Novel Lightweight Aggregate Concrete

Mohammad H. Jannaty[1] and Dawood Atrushi[2]

[1]Department Of Civil Engineering, Islamic Azad University, Sanandaj Branch, Iran

[2]Department of Civil Engineering, College of Engineering, University of Duhok, Duhok, Kurdistan Region – F.R. Iraq

***Abstract*—At present, most of the generated waste expanded polystyrene (EPS) in developed countries are transported to landfill and in some developing and/or less-developed countries such as Iraq are sent to open landscapes; consequently, this inadequate waste disposal can be very dangerous to our health and environment. This study describes engineering properties of sustainable lightweight aggregate concrete (LWAC) incorporating novel aggregates of waste EPS produced by a unique recycling technique of densifying. The new recycling technique significantly improved the segregation resistance of EPS beads in concrete as these beads are ultra-light material. The novel LWA of densified EPS (DEPS) was used as partial natural aggregate replacement in the mixes. Three water/cement (W/C) ratios were used. Three different types of curing conditions of indoor full water curing, outdoor weathering exposure, and heating exposure were employed during this study to represent different conditions which concrete may be subject to. The engineering properties of concrete investigated were consistency, dry density, compressive strength, and ultrasonic pulse velocity (UPV) for long-term performance of more than one-year age. It was indicated that the properties of concrete were not only primarily influenced by the employed curing conditions but the content of DEPS in the mixtures and additionally the W/C ratio had effect on the properties of concrete. However, adequate engineering properties can be achieved using an appropriate amount of DEPS with proper W/C and curing conditions.**

***Index Terms*—Compressive strength, Curing conditions, LWAC, Ultrasonic pulse velocity, Weathering Expanded polystyrene.**

I. Introduction

Expanded polystyrene (EPS) is mostly used in the packaging industry, but it can be used in the building industry as an insulation material in concrete wall blocks and in other global industrial fields. This is due to the fact that EPS has low thermal conductivity, which makes it a very good insulating material. It has low density and almost zero compressive strength. A large quantity of EPS is disposed of in landfills as waste in developed countries. Unfortunately, in developing and less-developed countries such as Iraq and in particular in Kurdistan Region of Iraq (KRI) this waste are collected, transported, and dumped in open space areas which are dangerous for the environment and public health (Herki and Khatib, 2016; Khatib, Herki and Elkordi, 2019).

According to the literature reported to date (Table I), using unmodified shredded waste EPS directly in concrete or mortar as aggregate can be the most efficient method of utilizing and reusing waste materials from sustainability point of view. However, EPS beads are extremely light with very low densities which can cause segregation in mixes as researchers are still trying to solve this problem. In addition, EPS beads are hydrophobic, which ends in poor bonding to cement paste. Hence, some studies (Table I) have conducted experimental investigations to enhance the engineering properties and to improve segregation resistance using different techniques and materials such as adding some bonding additives such as aqueous epoxy emulsions and aqueous dispersions of polyvinyl propionate, and chemically pre-treated EPS beads. There were other techniques such as adding ultra-fine silica fume (SF) to increase the bonding between EPS beads and cement paste and using super-plasticizers to increase the workability of concrete, etc. However, these techniques might not be environmentally friendly and readily available in all countries. In addition, the reusing and recycling of waste materials in developing and less-developed countries are still in its early phases (Miled, 2004; Herki, 2017; Khatib et al., 2013). Using silica stone waste (SSW) is another waste material which can be used as a substitution for cement and contribute to a better bonding and higher mechanical properties such as compressive and tensile strength.

Some previous studies (Table I) reported mechanical and durability performance of concrete containing EPS as fine and/or coarse aggregates. The compressive strength of

ARO-The Scientific Journal of Koya University
Vol. VIII, No.2 (2020), Article ID: ARO.10739, 9 pages
DOI:10.14500/aro.10739
Received: 09 October 2020; Accepted: 24 November 2020
Regular research paper: Published: 08 December 2020
Corresponding author's e-mail: dawood.sulaiman@uod.ac

TABLE I
PREVIOUS STUDIES ON CONCRETE CONTAINING EPS

References	Mixture	Density (kg/m^3)	Compressive strength (MPa)	
			7 days	28 days
Ravindrarajah, Camporeale, and Caraballo (1996)	EPS+NA+C	1100–1920	-	8.5–37.5
Sabaa and Ravindrarajah (1997)	EPS+NA+C	1600–2000	-	8.8–21.3
Park and Chilsholm (1999)	EPS+NA+C	820	3.2	3.8
Babu (2003)	EPS+NA+SF+C	1503–1979	7.6–19.8	10.2–21.4
Chen and Liu (2004)	EPS+NA+SF+C	876–1929	7.3–21.1	9.9–25.9
Miled, 2004	EPS+NA+C	1810	-	7.6–8.5
Ganesh Babu and Saradhi Babu (2004)	EPS+NA+FA+C	582–1723	-	1.1–12.5
Ganesh Babu and Wee (2004)	EPS+NA+FA+C	582–1723	0.62–5.96	1.1–12.5
Laukaitis, Žurauskas and Kerien (2005)	EPS+C	149–275	0.1–0.75	-
Saradhi Babu, Ganesh Babu and Tiong-Huan (2006)	EPS+NA+FA+SF+C	1012–1858	4.0–30.0	5.5–34.0
Bouvard (2007)	EPS+C	432–961	0.8–11.4	-
Kan and Demirboğa (2007)	EPS+C	464–1370	-	0.11–8.5
Chen and Liu (2007)	EPS+NA+SBR+C	-	-	11.2–16.3
Tang, Lo and Nadeem (2008)	EPS+NA+C	1396–2094	11.7–32.2	13.1–39.3
Kan and Demirboğa (2009)	MEPS+NA+C	980–1734	11.8–013.4	12.6–17.6
Sadrmomtazi (2012)	EPS+SF+RHA+C	-	-	6.7–33.0
Herki (2017)	SPS+C	891–1814	0.5–7.0	1.0–10.0
Nikbin and Golshekan (2018)	EPS+SF+C	1611–2312	0.02–0.05	12.4–47.8
Present study	DEPS+NA+C	891–1961	1.81–11.26	3.0–16.43

EPS concretes was found to be directly proportional to the concrete's density. The common conclusion of these studies (Khatib et al., 2019; Nikbin and Golshekan, 2018; Herki et al., 2013) shows that an increase in the amount of EPS beads can lead to a weaker concrete integrity since EPS beads does not provide any compression strength, and this is a big disadvantage of concrete with EPS mixtures. It was also presented that water absorption of concrete by total and capillary action will increase with an increase in EPS replacement level in concrete. This is due to micro-cracks of shrinkage action in concrete incorporating EPS beads. Although, research on LWAC containing EPS has exaggerated in the past two decades as there are still gaps in the knowledge of the properties and behavior of EPS concrete. One reason is that EPS concrete properties can vary considerably depending on the type of EPS and the technique of waste EPS recycling used, and so any conclusions may only be valid for the specific cases studied indicated in the above-mentioned research sources.

Reviewing the published studies in this line reveals that there is not enough information in the literature on assessment of different curing exposures effect on the long-term (365 days) engineering properties of lightweight aggregate concrete incorporating EPS using this novel technique.

II. Experimental Plan

A. Material

For the present project, the mixed natural sand and gravel aggregates were used in the lab. For economic reasons and in line with materials that normally used in Kurdistan Region for production of concrete blocks (Rostam et al., 2016), the normal aggregate used was low-cost and it was crushed limestone. The size ranges were between 0 and 10 mm complied with the British

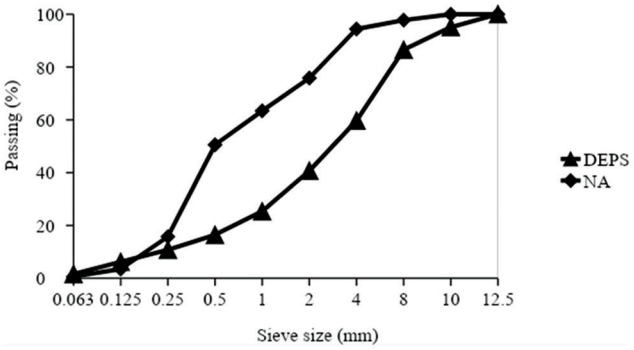

Fig. 1. Particle size distributions of natural and DEPS aggregates

standard requirements. Bulk density, specific gravity (SSD), and water absorption (24 h) of natural aggregates were 1677 kg/m^3, 2.69, and 1.2%, respectively. The particle size distributions (sieving) details of natural aggregate and the novel aggregate of densified expanded polystyrene (DEPS) complied with BS EN 933-1-2012 are presented in Fig. 1 for geometrical properties of aggregates and determination of particle size distribution. The DEPS aggregate has been made from 80% crushed waste EPS, 10% cement, and 10% red clay powder. The bulk density, SSD, and water absorption (24 h) of DEPS were 459 kg/m^3, 0.7, and 12%, respectively. It is worth mentioning here that, generally, LWAs have high porosity resulting in higher water absorption (WA) compared with natural aggregates. The cement used was ordinary Portland cement Type I. The chemical composition of cement is given in Table II.

B. Concrete Mixtures

The mix proportion of 1 (cement): Six (mixed natural sand and gravel aggregates) have been selected for the control mix. The replacement levels of natural aggregates with DEPS beads were 0, 30, 60, and 100% (by volume). The

 http://dx.doi.org/10.14500/aro.10739

TABLE II
CHEMICAL COMPOSITIONS OF PORTLAND CEMENT (SYARIF ET AL., 2018)

Constituent	SiO_2	Al_2O_3	Fe_2O_3	CaO	MgO	SO_3	K_2O	Na_2O	Cl	LOI	Compressive Strength (28-day)
Value (%)	22.8	3.8	1.4	66.5	0.8	3.3	0.7	0.1	<0.1	1.5	75.5 MPa

TABLE III
DETAILS OF CONCRETE MIXES

Series No.	W/C	Mix No.	DEPS (%)	Mixture Constituents (kg/m³)		
				Cement	Water	NA + DEPS
1	0.5	1	0 (C1)	320	192	1920 + 0
		2	30	320	192	1344 + 173
		3	60	320	192	768 + 345
		4	100	320	192	0 + 575
2	0.7	5	0 (C2)	320	256	1920 + 0
		6	30	320	256	1344 + 173
		7	60	320	256	768 + 345
		8	100	320	256	0 + 575
3	0.9	9	0 (C3)	320	320	1920 + 0
		10	30	320	320	1344 + 173
		11	60	320	320	768 + 345
		12	100	320	320	0 + 575

W/C ratios of 0.5, 0.7, and 0.9 were used for series 1, series 2, and series 3, respectively. To minimize the total cost of the present study superplasticiser has not been used. Further details about the mixes are presented in Table III.

For specimens' preparation, first DEPS aggregates were wetted with 1/3 of the mixing water. Then, the remaining materials were added to the mixer of 100 L capacity and 1/2 of the remaining water was gradually added whereas the mixing was in progress. Then, the remaining 1/2 of the mixing water was added and mixing was continued until a uniform concrete mix was obtained then slump measurement and casting of specimens was immediately started. After casting, specimens were covered and left undisturbed in the laboratory for 24 h. Then, demolding took place and specimens were placed under different curing conditions for various curing times.

C. Test Methods

Consistency and density

The consistency or workability of the fresh concrete was measured by slump-test according to BS EN 12350-2:2009 on the mixtures of Series 1, 2, and 3, and a flow test was carried out on the mixtures in Series 3 only. Usually, the flow test is used for high workability concrete (e.g., with a slump of 175 mm or more). The test is carried out in accordance with BS EN 12350-5:2009. The dry density of concrete specimens which can control many physical properties in LWC and is mainly controlled by the volume and density of LWA was measured according to BS EN 12390-7:2009.

Compressive strength

For the determination of compressive strength in conformity with BS EN 12390-3:2009, cube specimens of 100 mm size complied with BS EN 12390-2:2012 were used. Specimens were kept under different curing conditions. Curing times were 1, 7, 28, and 365 days. A testing machine of 3000 kN capacity at the loading rate of 0.6 *MPa/s* complied with BS EN 12390-4:2000 was used.

Ultrasonic pulse velocity (UPV)

For measurement of UPV values compiled with BS EN 12504-4:2004, cube specimens of 100 mm size were used. Curing times were 1, 7, 28, and 365 days. Specimens were kept under different curing conditions. The UPV as a non-destructive test method is used to evaluate concrete quality. This method can be used to detect internal cracking and other defects, as well as changes in concrete such as deterioration due to aggressive environment, freezing, and thawing (Yew, 2014). The pulse velocity was calculated from the formula:

$$V = L / T$$

where V is the pulse velocity, in *km/s*; L is the path length, in *mm*; T is the time taken by the pulse to transverse the 100 mm length, in μs.

Outdoor weathering exposure

Specimens were kept outside of the laboratory for weathering exposure effects up to 365 days age. For this type of curing, the specimens were kept outside in an open space (Fig. 2) to determine the effect of weathering on concrete properties including compressive strength and UPV. The testing ages were 7 days (September), 120 days (January), 240 days (May), and 365 days (October). At each curing time, the test was conducted at room temperature (20ºC ± 2). Table IV shows the weathering details during testing.

Heating exposure

For the heating exposure curing, the specimens were cured in water for 365 days before testing. Then, the specimens were dried at 80°C until a constant dry mass was achieved. The specimens were heated at a heating rate of 5°C/min up to 100, 200, and 300°C. (It is well known that for temperatures of 110°C and over, the uncoated EPS beads initially may shrink and finally evaporate) (Babu and Babu, 2003). The temperature of the furnace (Fig. 3) was maintained at the target temperature for 60 min. The furnace capacity was almost 0.2 m^3 and was ventilated. The duration of exposure at elevated temperatures practically guarantees that the specimens are heated uniformly and the whole sample volume is reached with adequate accuracy (Vodák, 2004). The specimens were heated in groups of 12. Then, the specimens were gradually cooled to the laboratory temperature. The UPV and compressive strength tests were carried out on the specimens.

III. RESULTS AND DISCUSSION

A. Consistency and Density

The consistency or workability (slump and flow table) values for concretes containing varying amounts of DEPS aggregate at different W/C are presented in Table V. The

Fig. 2. Outside weathering exposure

Fig. 3. Heating exposure

slump values were in the range of 3–36 mm in Series 2 which was typically used for foundations and in applications with light reinforcement, and 55–160 mm in Series 3 which these mixes are typically used for normal reinforced concrete placed with vibration and/or used in applications with tight reinforcing. None of the mixes in Series 1 recorded any slump, which means they were stiff and with appropriate mix design they can be used in some applications such as road construction. This was mainly due to the low W/C ratio and lack of any superplasticiser which would have improved the workability (Kan and Demirboğa, 2007; Le Roy, Parant and Boulay, 2005; Ferrándiz-Mas and García-Alcocel, 2013). Flow values for Series 3 (W/C=0.9) mixes were in the range of 38–48 cm. The workability for the mixes of the Series 1 was just enough to be compacted and could also be finished, but all other mixtures were flexible and easy to work with, and compaction and finishability were easy. The workability of the concrete increased with increasing the replacement level of DEPS aggregate in concrete up to 60% then decreased for 100% DEPS replacement. Further details about the workability are described in Table V.

The dry density of concretes containing varying amounts of DEPS aggregates is presented in Table V. The density values were in the range of 891–2133 kg/m^3. According to the results reported in Table V, the density of concretes

TABLE IV
WEATHERING DETAILS DURING TESTING

Month	Temperature °C				Ave. rainfall (mm)		Ave. snow days
	Average		Absolute		Daily	Monthly	
	Max.	Min.	Max.	Min.			
January	7.5	1.8	14	-10	1.4	43.5	5
February	8.1	1.5	18.1	-10.1	1.3	37.7	5
March	10.4	2.7	20.5	-8	0.8	24.8	3
April	12.7	3.6	25	-6.4	1	31.3	2
May	16.5	6.8	27	-3	0.9	26.6	0
June	19.3	9.7	31.3	-1	1.2	35.8	0
July	21.8	11.7	35	3.3	1.1	32.8	0
August	21.6	11.6	35	2.9	0.9	28.6	0
September	18.2	9.3	28	0.4	1.3	37.8	0
October	13.9	6.5	23.5	-6.8	1.5	47.6	0
November	9.9	3.7	21	-6	1.3	40	1
December	7	1.5	15.2	-13	1.3	40.2	4

TABLE V
WORKABILITY AND DENSITY OF DEPS CONCRETES AT DIFFERENT W/C RATIOS

Series No.	W/C	Mix No.	Workability		Dry density (kg/m^3)
			Slump (mm)	Flow (cm)	
1	0.5	1	0	-	2135
		2	0	-	1965
		3	0	-	1640
		4	0	-	1020
2	0.7	5	3	-	2075
		6	20	-	1815
		7	36	-	1540
		8	15	-	1010
3	0.9	9	55	46	1990
		10	140	47	1740
		11	160	48	1390
		12	70	38	895

decreased with increasing the replacement level of DEPS aggregate with natural aggregates. This is because the density of DEPS aggregates was much lower than that of natural aggregates. According to BS EN 206-1:2000, the LWC must have a dry density of not less than 800 kg/m^3 and not more than 2000 kg/m^3. Thus, the concrete containing 30% DEPS and more can be considered as LWC depending on DEPS replacement levels in concrete.

B. Ultrasonic Pulse Velocity (UPV)

Effect of water curing

This study shows an increase in DEPS in concrete leads to a decrease in UPV. This is illustrated in a comprehensive summary of UPV values of DEPS concretes for all curing conditions and series in Fig. 4. There was not a significant difference between the concrete containing 30% DEPS and control as it is interesting to see that the reduction in UPV was only 2% in series 1.

According to many recent investigations conducted on UPV of concrete (Yew, 2014; Demirboğa, Türkmen, and Karakoç, 2004), the UPV of concrete is classified into 4 types of "very good quality," "good to very good quality," "satisfactory," and "poor quality." Concrete made with 30%

http://dx.doi.org/10.14500/aro.10739

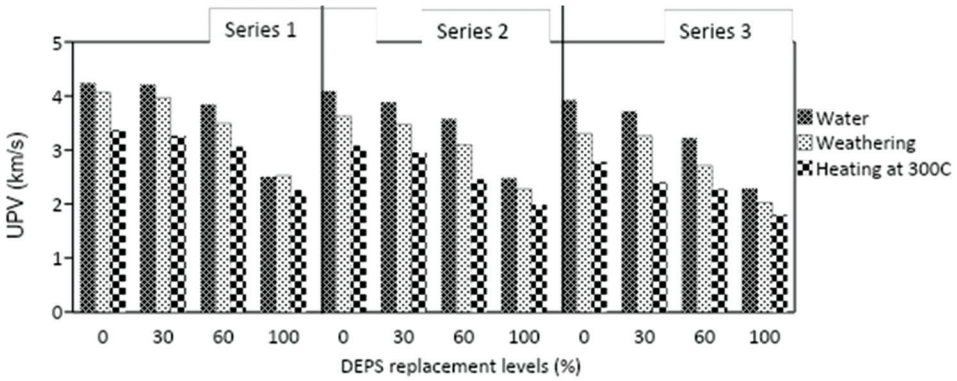

Fig. 4. Long-term study of DEPS concretes UPV values under different curing conditions

DEPS in Series 1 can comply with the Type I (very good quality) requirements. Concrete made with 60% DEPS in Series 1, and 30% DEPS in Series 2 and 3, can comply with the Type II (good to very good quality) requirements. Concrete containing 60% DEPS in Series 2 and 3 can comply with the Type III (satisfactory) requirements and 100% DEPS concretes in all three series is of poor quality based on the UPV results.

The variation of the UPV values at different curing times indicates a continuous increase for all the mixes. However, there is a high rate of increase in UPV in the early ages and as curing time rises; the increase starts to slow down until it levels off asymptotically. For example, the increase in UPV value for 30% DEPS concrete from 1 to 7 day curing time was 23%. This is due to the physical-chemical changes that happen in the concrete as a consequence of the hydration reactions increase progressively the strength and density of the material, favoring the propagation of the UPV as curing time increases (Albano, 2009).

The UPV values of the concretes with the same DEPS content decrease with an increase in W/C ratio at all curing periods (Hwang, 2012; Wang, 2009). According to the recent study (36), a change in the W/C ratio of concrete would be easily detected by UPV testing. This is due to the extra water remaining in the pores and after evaporation, leaves empty holes in the concrete structure that produces the reduction of the UPV (Albano, 2009).

Effect of outdoor weather exposure

Similar to the UPV of concrete long-term water curing, the weathering results showed that the UPV of concrete decreased as DEPS content increased. The results also showed that the UPV of concrete increased about 8% and 12% for low and high DEPS contents after 365 days of outdoor weathering exposure, respectively. The UPV of specimens continued to increase in outdoor weathering conditions due to the environment's moist and further hydration of un-hydrated or un-reacted cement particles within the specimens. Similar results have been reported elsewhere (Gunasekaran, Annadurai, and Kumar, 2012; Shi, 2012). A higher UPV shows better uniformity of the concrete. At present, in civil engineering applications, weathering studies on the degradation of concrete exposed to the environment are of great importance. Much of the knowledge on concrete deterioration comes from studies in the environment, because it is difficult to simulate the combination of conditions long-term in a laboratory. According to Amianti and Botaro (2008), microclimates can negatively affect concrete durability. They also reported that the degradation depends on the permeability, type, and geometric form of the concrete construction, as well as the type and aggressiveness of the process. Comprehensive studies into the long-term weathering performance of concrete structures exposed to severe environments for a long-term suggest that properly proportioned and placed LWC performs equal to normal-weight concrete (ACI Committee 213, 2003).

It has been reported by Neville (2008) that concrete with UPV values within the range of 3.5–4.5 km/s is considered as "Good" concrete. As long as the UPV values fall within this category, it can be deduced that the concrete does not contain any large voids or cracks which will affect its structural integrity. In the present study, the UPV values for mixes containing up to 60% DEPS at W/C of 0.5 and 30% DEPS at W/C of 0.7 fell within the above category under outdoor weathering exposure curing.

Effect of heating exposure

Measurements for UPV were carried out on the concrete samples before and after the heat treatment as explained in the methodology. A recent investigation by Biolzi, Cattaneo and Rosati (2008) reported that the UPV value, as an indicator of damage, has been used to evaluate concrete quality, as UPV is sensitive to internal cracking and other deterioration due to heating treatments. The relative properties of concrete after exposure to high temperatures during fire are of great importance in terms of the serviceability of buildings (Arioz, 2007). According to the results, in general, the UPV of concrete decreased with an increase in temperature at all DEPS percentages in all Series. The decrease in UPV with increasing temperature is a sensitive measure of the progress of cracking in the material (Savva, Manita and Sideris, 2005).

At 300°C, the reduction in UPV of all the mixtures was between 10 and 23%, 20 and 25%, and 21 and 35% in series 1, 2, and 3, respectively. The mixture with 100% DEPS content recorded the lowest reduction in UPV at 300°C in each Series. It has been reported (Neville, 2008) that concrete with UPV values within the range of 3.5–4.5 km/s is considered as "good" concrete as discussed

in the last section. The UPV for the concrete containing 0% and 30% DEPS aggregate in Series 1 at 100°C was 3.72 and 3.69 km/s, respectively. In the present study, the UPV values for all mixes containing DEPS in all Series did not exceed 3.34 km/s at 200 and 300°C; however, it is well known that obtaining high UPV values for concrete containing high DEPS (EPS beads with 95% air) are almost unexpected.

C. Compressive Strength

Effect of indoor water curing

A comprehensive summary of strength values of DEPS concrete under long-term water curing condition is shown in Fig. 5. The DEPS aggregates caused a reduction in the compressive strength of concrete as expected; depending on the level of replacement with natural aggregate the reduction was different. For example, at 28 days, age the reduction in compressive strength was between 1 and 73%, 21 and 68%, and 19 and 66% for Series 1, 2, and 3, respectively, compared to the control concrete of each series. It was interesting to see that this reduction for 30% DEPS concrete in Series 1 was not significant and it was 1% only. This reduction in compressive strength is attributed to the lack of enough bonding between EPS particles and paste in the concrete incorporating unmodified EPS particles as unmodified EPS particles have almost zero strength; however, in the case of DEPS with coating (present work) it may be different (Babu and Babu, 2004). The compressive strength of the concretes containing different DEPS contents is decreased with an increase in W/C ratio as expected. This is due to the excess of water in concrete with higher W/C causing higher porosity. Similar results have been reported elsewhere (Albano, 2009; Neville, 2008; Lo, Tang and Cui, 2007; Demirdag, Ugur and Sarac, 2008; Choi, 2005). The strength gain was different too. For example, at 7-day in Series 2 shows that concrete with 30% DEPS developed almost 63% of its 28-day strength, while that with 100% DEPS developed almost 69% of the corresponding 28-day strength. Overall, with appropriate mix design, the utilization of DEPS in lightweight concrete production, for example, lightweight blocks and bricks are possible and adequate strength can be achieved using an appropriate curing condition and DEPS replacement level. According to Rostam, Ali and Atrushi (2016), the reduced unit weight in building material such as cellular blocks makes for ease of handling, reduced floor/foundation loading, and economic. Therefore, this mix can make it relevant to creating building blocks in Kurdistan which are lighter with moderate compressive strength that makes it suitable for better building materials.

Effect of outdoor weathering exposure

As shown in Fig. 6, due to the moist environment and further hydration of unhydrated cement particles within the samples under outdoor weathering condition, strength values are similar to those for water curing at the same age explained in the previous section; this is in agreement with the results reported by Gunasekaran, Annadurai, and Kumar, 2012; Shi, 2012; Roy, Puh and Northwood, 1999. The reduction in strength was between 2 and 75%, 24 and 70%, and 7 and 70% in comparison with the control concrete for Series 1, 2, and 3, respectively. Furthermore, stresses in specimens caused by weathering exposure such as freezing and thawing, wetting and drying, and heating and cooling will damage the concrete structure over time and can cause cracking in the concrete (Roy, Puh, Northwood, 2007; ACI Committee 224, 2007). ACI 224.1R (2007) recommends protecting concrete against freezing and thawing through the use of the lowest acceptable W/C ratio, durable aggregate, and suitable air entrainment.

Effect of heating exposure

As presented in Table VI, strength values for control concrete and 30% DEPS concrete increased and for the concrete containing 60 and 100% DEPS decreased with an increase in heating temperature for all series (Vodák, 2004; Hossain, 2006). According to the recent published studies (Fraj, Kismi and Mounanga, 2010; Rashad, 2012; Noumowé, Siddique and Ranc, 2009; Al-Sibahy and Edwards 2012; Tanyildizi and Çevik, 2010; Mydin and Wang, 2012); generally, the level of water loss for the specimens heated

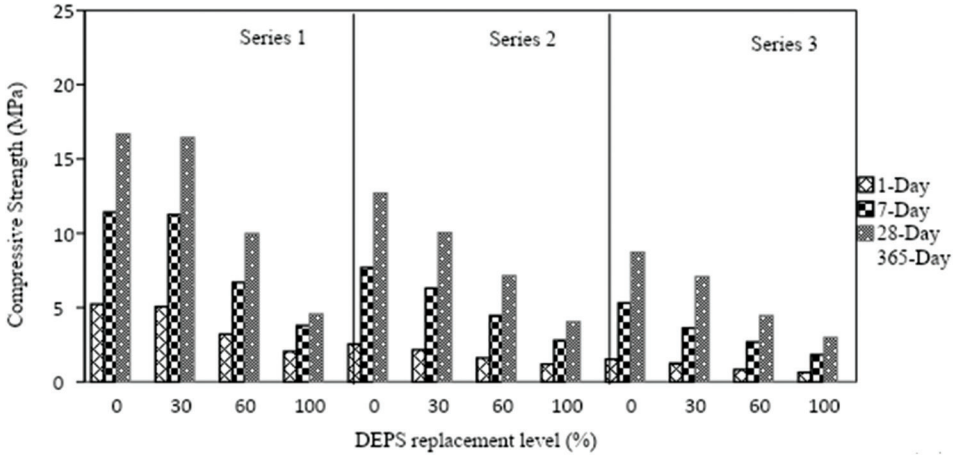

Fig. 5. Compressive strength of water cured DEPS concretes at different curing times

http://dx.doi.org/10.14500/aro.10739

TABLE VI
DEPS CONCRETES COMPRESSIVE STRENGTH AT DIFFERENT W/C RATIOS AND TEMPERATURES

Series No.	W/C	Mix No.	Compressive strength (MPa)			
			Temperatures (°C)			
			20	100	200	300
1	0.5	1	25.37	16.53	26.11	32.43
		2	24.12	24.22	27.78	28.47
		3	13.02	13.98	14.76	13.73
		4	5.86	5.77	5.50	4.64
2	0.7	5	19.12	20.82	21.96	25.13
		6	14.46	16.52	16.56	16.46
		7	11.37	10.54	11.04	10.01
		8	5.15	5.70	4.94	4.18
3	0.9	9	14.31	14.76	15.23	16.67
		10	10.63	11.45	12.16	11.85
		11	7.60	6.93	6.23	6.49
		12	3.80	3.79	3.60	3.44

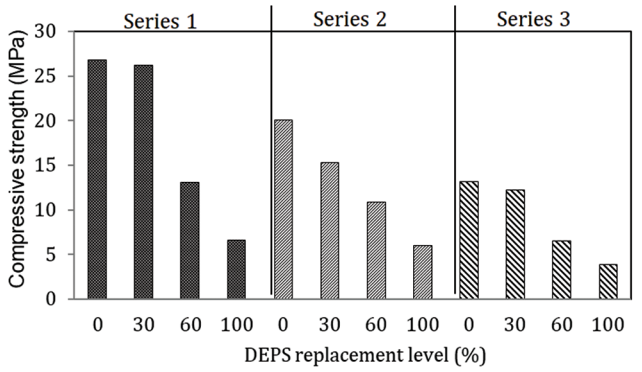

Fig. 6. Long-term study of DEPS concretes compressive strength under outdoor weathering exposure

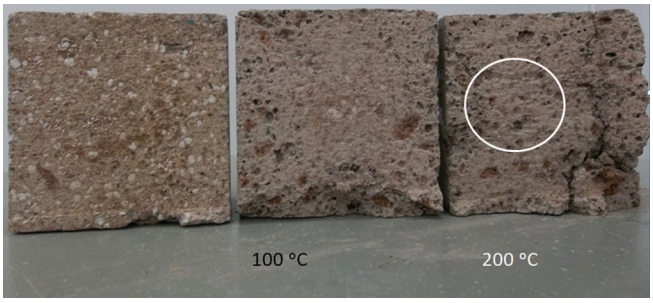

Fig. 7. Effect of different temperatures on 100% DEPS concrete

at 200 and 300°C was much higher than that measured on the specimens heated at 100°C as expected; this is confirmed that there is a small proportion of extra water in the concrete compared to the water needed for hydration.

According to the results, except for control concrete in Series 1 there was no significant difference in compressive strength obtained between 20 (lab temperature) and 100°C heating exposure. At 200°C, the EPS particles of DEPS aggregate in concrete started to evaporate as shown by the small holes which can be seen on the cross-section of specimens with 100% DEPS (Fig. 7) which resulted in increased porosity. The damage at 200°C in the center of the specimen was less but the damages at 300°C on the specimen were higher, as expected, which can be seen in Fig. 7 in the form of cracks. At high temperatures the interfacial transition zone between cement paste and aggregate will be weakened and strength and durability properties can be decreased (Hossain, 2006). The authors recommend that to reduce water loss at high temperatures concrete containing DEPS should be protected by a fire protection material as a coating layer.

IV. Conclusions

The main aim of this investigation was to study the long-term effect of different curing conditions on engineering properties of concrete incorporating a novel LWA called DEPS. The experimental study results provided the following conclusions:

- In general, the concrete containing DEPS can be used in low-strength concrete applications for example to produce lightweight bricks and blocks with low thermal conductivity. However, with appropriate mix design, the utilization of DEPS in lightweight concrete production is possible and adequate strength can be achieved using an appropriate curing condition and DEPS replacement level;
- The consistency of concrete increased with an increase in DEPS content up to 60%; beyond 60% the consistency started to decrease also the density of the concretes decreased with an increase in DEPS aggregate replacement;
- Due to the availability of water for better hydration, the UPV values of the concretes made with different DEPS percentages under water curing was higher than that of outdoor weather and heating exposure conditions;
- The compressive strength values of concrete under outdoor curing conditions were similar to that of water curing. However, the heating curing condition had a great influence on the compressive strength. The compressive strength of the control and 30% DEPS concrete increased, and of the concrete containing 60 and 100% DEPS aggregate decreased, with an increase in heating temperature; thus, a fire protection coating layer is recommended.
- For production of cellular blocks in the Kurdistan Region the use of DEPS in the concrete mix could be a good alternative and therefore it should be examined further.

REFERENCES

Abbasi, S., Jannaty, M.H., Faraj, R.H., Shahbazpanahi, S., and Mosavi, A., 2020. The effect of incorporating silica stone waste on the mechanical properties of sustainable concretes. *Materials*, 13, p.3832.

ACI Committee 213, 2003. *Guide for Structural Lightweight Aggregate Concrete*. American Concrete Institute Manual of Concrete Practice, United Kingdom.

ACI Committee 224, 2007. *Causes, Evaluation and Repair of Cracks in Concrete Structures* (*ACI 224.1R-07*), *Manual of Concrete Practice, Part 2*. American Concrete Institute, Farmington Hills.

Albano, C., Camacho, N., Hernández, M., Matheus, A., and Gutiérrez, A., 2009. Influence of content and particle size of waste pet bottles on concrete behaviour at different w/c ratios. *Waste Management*, 29(10), pp.2707-2716.

Al-Sibahy, A., and Edwards, R., 2012. Thermal behaviour of novel lightweight concrete at ambient and elevated temperatures: Experimental, modelling and parametric studies. *Construction and Building Materials*, 31, pp.174-187.

Amianti, M., and Botaro, V.R., 2008. Recycling of EPS*:* A new methodology for production of concrete impregnated with polystyrene (CIP). *Cement and Concrete Composites*, 30(1), pp.23-28.

Arioz, O., 2007. Effects of elevated temperatures on properties of concrete. *Fire Safety Journal*, 42(8), pp.516-522.

Babu, D.G., Babu, K.G., and Wee, T.H., 2005. Properties of lightweight expanded polystyrene aggregate concretes containing fly ash. *Cement and Concrete Research*, 35(6), pp.1218-1223.

Babu, D.S., Ganesh Babu, K., and Tiong-Huan, W., 2006. Effect of polystyrene aggregate size on strength and moisture migration characteristics of lightweight concrete. *Cement and Concrete Composites*, 28(6), pp.520-527.

Babu, K.G., and Babu, D.S., 2003. Behaviour of lightweight expanded polystyrene concrete containing silica fume. *Cement and Concrete Research*, 33(5), pp.755-762.

Babu, K.G., and Babu, D.S., 2004. Performance of fly ash concretes containing lightweight EPS aggregates. *Cement and Concrete Composites*, 26(6), pp.605-611.

Biolzi, L., Cattaneo, S., and Rosati, G., 2008. Evaluating residual properties of thermally damaged concrete, *Cement and Concrete Composites*, 30(10), pp.907-916.

Bouvard, D., Chaix, J.M., Dendievel, R., Fazekas, A., Létang, J.M., Peix, G., and Quenard, D., 2007. Characterization and simulation of microstructure and properties of EPS lightweight concrete. *Cement and Concrete Research*, 37(12), pp.1666-1673.

British Standards Institution, BS EN 12350-2:2009, 2009. *Testing Fresh Concrete Part 2*: *Slump-test*. British Standards Institution, United Kingdom.

British Standards Institution, BS EN 12350-5:2009, 2009. *Testing Fresh Concrete Part 5*: *Flow Table Test*. British Standards Institution, United Kingdom.

British Standards Institution, BS EN 12390-2:2012, 2012. *Testing Hardened Concrete Part 2: Making and Curing Specimens for Strength Tests*. British Standards Institution, United Kingdom.

British Standards Institution, BS EN 12390-3:2009, 2009. *Testing Hardened Concrete Part 3*: *Compressive Strength of Test Specimens*. British Standards Institution, United Kingdom.

British Standards Institution, BS EN 12390-4:2000, 2000. *Testing Hardened Concrete Part 4*: *Compressive Strength, Specification for Testing Machines*. British Standards Institution, United Kingdom.

British Standards Institution, BS EN 12390-7:2009, 2009. *Testing Hardened Concrete Part 7*: *Density of Hardened Concrete*. British Standards Institution, United Kingdom.

British Standards Institution, BS EN 12504-4:2004, 2004. *Testing Concrete Part 4*: *Determination of Ultrasonic Pulse Velocity*. British Standards Institution, United Kingdom.

British Standards Institution, BS EN 206-1:2000, 2000. *Concrete Part 1*: *Specification, Performance, Production and Conformity.* British Standards Institution, United Kingdom.

British Standards Institution, BS EN 933-1:1997, 1997. *Tests for Geometrical Properties of Aggregates. Part 1*: *Determination of Particle Size Distribution-sieving Method*. British Standards Institution, United Kingdom.

Chen, B., and Liu, J., 2004. Properties of lightweight expanded polystyrene concrete reinforced with steel fiber. *Cement and Concrete Research*, 34(7), pp.1259-1263.

Chen, B., and Liu, J., 2007. Mechanical properties of polymer-modified concretes containing expanded polystyrene beads. *Construction and Building Materials*, 21(1), pp.7-11.

Choi, Y.W., Moon, D.J., Chung, J.S., and Cho, S.K., 2005. Effects of waste PET bottles aggregate on the properties of concrete. *Cement and Concrete Research*, 35(4), pp.776-781.

Demirboğa, R., Türkmen, I., and Karakoç, M.B., 2004. Relationship between ultrasonic velocity and compressive strength for high-volume mineral-admixtures concrete. *Cement and Concrete Research*, 34(12), pp.2329-2336.

Demirdag, S., Ugur, I., and Sarac, S., 2008. The effects of cement/fly ash ratios on the volcanic slag aggregate lightweight concrete masonry units. *Construction and Building Materials*, 22(8), pp.1730-1735.

Ferrándiz-Mas, V., and García-Alcocel, E., 2013. Durability of expanded polystyrene mortars. *Construction and Building Materials*, 46, pp.175-182.

Fraj, A.B., Kismi, M., and Mounanga, P., 2010. Valorisation of coarse rigid polyurethane foam waste in lightweight aggregate concrete. *Construction and Building Materials*, 24(6), pp.1069-1077.

Gunasekaran, K., Annadurai, R., and Kumar, P.S., 2012. Long term study on compressive and bond strength of coconut shell aggregate concrete. *Construction and Building Materials*, 28(1), pp.208-215.

Herki, B.A., 2017. Absorption characteristics of lightweight concrete containing densified polystyrene. *Civil Engineering Journal*, 8(3), pp.594-609.

Herki, B.A., and Khatib, J.M., 2016. Valorisation of waste expanded polystyrene in concrete using a novel recycling technique. *European Journal of Environmental and Civil Engineering*, 21, pp.1-19.

Herki, B.A., Khatib, J.M., and Negim, E.M., 2013. Lightweight concrete made from waste polystyrene and fly ash. *World Applied Science Journal*, 21, pp.1356-1360.

Hossain, K.M.A., 2006. High strength blended cement concrete incorporating volcanic ash: Performance at high temperatures. *Cement and Concrete Composites*, 28(6), pp.535-545.

Hwang, C.L., Bui, L.A.T., Lin, K.L., and Lo, C.T., 2012. Manufacture and performance of lightweight aggregate from municipal solid waste incinerator fly ash and reservoir sediment for self-consolidating lightweight concrete. *Cement and Concrete Composites*, 34(10), pp.1159-1166.

Kan, A., and Demirboğa, R., 2007. Effect of cement and EPS beads ratios on compressive strength and density of lightweight concrete. *Indian Journal of Engineering and Materials Sciences*, 14, pp.158-162.

Kan, A., and Demirboğa, R., 2009. A novel material for lightweight concrete production. *Cement and Concrete Composites*, 31(7), pp.489-495.

Khatib, J.M., Herki, B.A., and Elkordi, A., 2019. *Use of Recycled Plastics in Eco-efficient Concrete*, *Characteristics of Concrete Containing EPS*. Woodhead Publishing, United Kingdom, pp.137-165.

Khatib, J.M., Herki, B.A., and Kenai, S., 2013. Capillarity of concrete incorporating waste foundry sand. *Construction and Building Materials*, 47, pp.867-871.

Laukaitis, A., Žurauskas, R., and Kerien, J., 2005. The effect of foam polystyrene granules on cement composite properties. *Cement and Concrete Composites*, 27(1), pp.41-47.

Le Roy, R., Parant, E., and Boulay, C., 2005. Taking into account the inclusions' size in lightweight concrete compressive strength prediction. *Cement and Concrete Research*, 35(4), pp.770-775.

Lo, T.Y., Tang, W.C., and Cui, H.Z., 2007. The effects of aggregate properties on lightweight concrete. *Building and Environment*, 42(8), pp.3025-3029.

Miled, K., Le Roy, R., Sab, K., and Boulay, C., 2004. Compressive behaviour of an idealized EPS lightweight concrete: Size effects and failure mode. *Mechanics of Materials*, 36(11), pp.1031-1046.

Mydin, M.A.O., and Wang, Y.C., 2012. Mechanical properties of foamed concrete exposed to high temperatures. *Construction and Building Materials*, 26(1), pp.638-654.

Neville, A.M., 2008. *Properties of Concrete*. 4th ed. Pearson Education Limited, Essex, UK.

Nikbin, I.M., and Golshekan, M., 2018. The effect of expanded polystyrene synthetic particles on the fracture parameters, brittleness and mechanical properties of concrete. *Construction and Building Materials*, 94, pp.160e-172.

Noumowé, A., Siddique, R., and Ranc, G., 2009. Thermo-mechanical characteristics of concrete at elevated temperatures up to 310°C. *Nuclear Engineering and Design*, 239(3), pp.470-476.

Park, S.G., and Chisholm, D.H., 1999. Polystyrene aggregate concrete. *Building Research Association of New Zealand*, *Study Report, SR 85,* Judgeford.

Rashad, A.M., Bai, Y., Basheer, P.A.M., Collier, N.C., and Milestone, N.B., 2012. Chemical and mechanical stability of sodium sulphate activated slag after exposure to elevated temperature. *Cement and Concrete Research*, 42(2), pp.333-343.

Ravindrarajah S.R., Camporeale M.J., and Caraballo C.C., 1996. Flexural Creep of Ferro Cement. In: *Polystyrene Concrete Composite*. Second International Conference on Advances in Composites, Bangalore, India.

Rostam, D., Ali, T., and Atrushi, S.D., 2016. Economical and structural feasibility of concrete cellular and solid blocks in Kurdistan region. *ARO*, *The Scientific Journal of Koya University*, 4(1), pp.1-7.

Roy, S., Puh, K.B., and Northwood, D.O., 1999. Durability of concrete-accelerated carbonation and weathering studies. *Building and Environment*, 34(5), pp.597-606.

Sabaa, B., and Ravindrarajah, R.S., 1997. *Engineering Properties of Lightweight Concrete Containing Crushed Expanded Polystyrene Waste*. Symposium MM, Advances in Materials for Cementitious Composites, United States, pp.1-11.

Sadrmomtazi, A., Sobhani, J., Mirgozar, M.A., and Najimi, M., 2012. Properties of multi-strength grade eps concrete containing silica fume and rice husk ash. *Construction and Building Materials*, 35, pp.211e-219.

Savva, A., Manita, P., and Sideris, K., 2005. Influence of elevated temperatures on the mechanical properties of blended cement concretes prepared with limestone and siliceous aggregates. *Cement and Concrete Composites*, 27(2), pp.239-248.

Shi, C., Wang, D., He, F., and Liu, M., 2012. Weathering properties of CO_2-cured concrete blocks, resources. *Conservation and Recycling*, 65, pp.11-17.

Syarif, M., Sampebulu, V., Tjaronge, M.W., and Nasruddin. 2018. Characteristics of compressive and tensile strength using the organic cement compare with Portland cement. *Case Studies in Construction Materials*, 9, p.e00172.

Tang, W.C., Lo, Y., and Nadeem, A., 2008. Mechanical and drying shrinkage properties of structural-graded polystyrene aggregate concrete. *Cement and Concrete Composites*, 30(5), pp.403-409.

Tanyildizi, H., and Çevik, A., 2010. Modelling mechanical performance of lightweight concrete containing silica fume exposed to high temperature using genetic programming. *Construction and Building Materials*, 24(12), pp.2612-2618.

Vodák, F., Trtík, K., Kapičková, O., Hošková, Š., and Demo, P., 2004. The effect of temperature on strength-porosity relationship for concrete. *Construction and Building Materials*, 18(7), pp.529-534.

Wang, H.Y., 2009. Durability of self-consolidating lightweight aggregate concrete using dredged silt. *Construction and Building Materials*, 23(6), pp.2332-2337.

Yew, M.K., Mahmud, H.B., Ang, B.C., and Yew, M.C., 2014. Effects of heat treatment on oil palm shell coarse aggregates for high strength lightweight concrete. *Materials and Design*, 54, pp.702-707.

Influence of Natural Fibers on the Performance of Hot Mix Asphalt for the Wearing Course of Pavement

Omar T. Mahmood and Sheelan A. Ahmed

Department of Civil Engineering, Faculty of Engineering, Koya University,
Daniel Mitterrand Boulevard, Koya KOY45 AB64, Kurdistan Region – F.R. Iraq

***Abstract*—Cracking in the flexible pavement is a serious problem that reduces the service life of the roads pavement unless they are treated with great care. Since flexible pavement is very weaker in tension than in compression, it is usually necessary to consider the tensile stresses and some type of additives to improve asphalt pavement performance, and one of the most effective ways of improving asphalt pavement performance is to reinforce asphalt mixtures by incorporating natural fibers. The main objective of this study is to use palm fiber, which is locally available, in hot mix asphalt mixtures. To achieve this objective, the Marshall test and indirect tensile strength test were conducted on four asphalt mixtures with different types of natural fibers (Coconut, Corn, Palm, and Sisal), added in varying percentages 0.1, 0.2, 0.3, 0.4, and 0.5% and different lengths of fiber 0.5, 1, 1.5, and 2 cm. Based on the analyzed results, it can be concluded that the use of palm fiber increased the Marshall stability by 20% as compared with the conventional mixture and raised up the retained tensile strength ratio up to 92%. Finally, the use of 0.2% content of natural fiber at 1.5 cm length gave a better performance for the mixtures.**

***Index Terms*— Coconut fiber, Corn fiber, Indirect tensile strength, Marshall flow, Marshall stability, Natural fiber, Palm fiber, Sisal fiber.**

I. Introduction

Reflection cracking is one of the major distresses that occur frequently in asphalt, concrete overlay in which the existing cracking pattern from the old pavement propagates into and through the new overlay. Cracking occurs because bituminous layers are weak in tension. Therefore, the use of fibers has received considerable attention as viable solutions to enhance flexible pavement performance (Abdelaziz and Mohamed, 2010).

Gazia and Sukhmanjit (2017) used two types of fibers (bamboo fiber and cellulose fiber) to study the resistance of permanent deformation of stone matrix asphalt mixes with four different aggregate gradations. It was observed that the bituminous mixes containing bamboo fiber as fillers are found to have Marshall properties almost the same as of cellulose fiber fillers. Where, both of them have a positive effect on the properties of bituminous mixtures by increasing its stability and voids and decreasing the flow value. In addition to filling the voids, the fillers' components interact with the binder present in the mix, potentially making it stiff and brittle. Kavalakuntle and Praveen (2016) studied the drain down analysis, static indirect tensile strength test, and static creep test to evaluate the effects of sisal fiber addition on bituminous concrete and stone mastic asphalt (SMA) performance. By Marshall method, the optimum fiber content for both mixes was found to be 0.3%. Based on the results and discussions of experimental investigations carried out, the addition of sisal fibers improves the Marshall stability, drain down characteristics, and indirect tensile strength of both mixes, especially the SMA, which gave better indirect tensile strength and creep characteristics. Furthermore, a previous study by Bindu and Beena (2015) investigated the influence of natural fibers, which were sisal, coir, and banana fibers, on the compressive strength of SMA mixture. The results showed that the maximum value of compressive strength is achieved at 0.3% fiber content. Ashraf (2012) added polypropylene and aramid fibers to the asphalt binder and mixture, with sixteen different dosages and blends of fibers. The results indicated that the blend of three dosages of polypropylene and one dosage of aramid gave the best viscosity of binder and the lowest viscosity-temperature relationships value indicating a lesser temperature susceptibility to both permanent deformation and thermal cracking. On the other hand, the aramid fiber gave better results than the polypropylene fiber to resist the indirect tensile force.

Saswat and Mahabir (2016) experimentally investigated the dense-graded bitumen mixes with bottom ash (as part of fine aggregate), fly ash (as mineral filler), and sisal fiber as an additive to enhance the engineering properties of the bituminous paving mix. Four different percentages of sisal fiber 0.25%, 0.5%, 0.75%, and 1.0% by weight of the mix were used, with different lengths (5, 10, 15, and 20 mm). The results showed that the use of fiber content up to 0.5% with fiber length 10 mm increased Marshall stability, whereas air voids and Marshall flow decreased,

ARO-The Scientific Journal of Koya University
Vol. VIII, No.2 (2020), Article ID: ARO.10710, 7 pages
DOI:10.14500/aro.10710
Received: 05 August 2020; Accepted: 07 November 2020
Regular research paper: Published: 07 December 2020
Corresponding author's e-mail: sheelan.abdulwahid@koyauniversity.org

http://dx.doi.org/10.14500/aro.10710

also indirect tensile strength increased due to the addition of emulsion coated fiber. Sigit (2013) studied the effects of short coconut fibers on the binder rheological properties and Marshall stability, moisture susceptibility, and rutting performance of asphalt mixture, the coconut fiber was cut to lengths of 5 mm, 7.5 mm, 10 mm, and 12.5 mm and added to the bitumen of grade 60/70 in levels of (0.5, 0.75, 1, 1.25, and 1.5%). The tests showed that the addition of short coconut fiber reduced the penetration grade of bitumen and ductility but increased the softening point; also, specimens prepared by 0.75% coconut fiber asphalt performed better than asphalt mixtures using virgin asphalt. Hossam and Khalifa (2005) compared the effect of palm fibers and textile fibers, in combination with styrene-butadiene rubber (SBR) polymer on the properties of open-graded friction course mixture. The results indicated that the asphalt mix containing palm fibers and SBR polymer at 5.0% and the asphalt mix containing textile fibers and SBR polymer at 6.5% asphalt content satisfied the mix design criteria. That the previous studies in this field indicate that adding fibers have a positive role in improving the performance of asphalt mixtures. As it is known that Iraq has millions of palm trees and due to the large quantities of fibers produced from them annually, it is necessary to think about using them in a way that might be economically beneficial for improving the performance of the hot asphalt mixtures used in paving roads locally. For this purpose, it was necessary to investigate the effect of adding palm fibers on the performance of asphalt mixtures by comparing them with natural fibers used in previous studies such as sisal, corn, and coconut fibers, and determining whether palm fibers behave such as these fibers in improving the performance of asphalt mixtures or do they behave in a different way.

II. Materials Characterization

All materials used in this study are locally available and currently used in road construction in northern Iraq except the fibers. Since fibers have higher tensile strengths compared to bituminous mixtures, there is a possibility that they to enhance the cohesive and tensile strength of bituminous mixes (Brown, et al., 1990)

A. Aggregates

In this study, aggregates are used an asphalt concrete mixture, in which 19 mm maximum size dense gradation has been selected according to State Corporation of Roads and Bridges (State Organization of Road and Bridges, 2007). The coarse and fine aggregate used in this investigation was brought from the Darbande Zeoi quarry near Sulaymaniyah city in Iraq and crushed at the local asphalt concrete mix plant by mechanical crusher. The aggregate gradation is shown in Table I. An ordinary Portland cement was used as mineral filler.

B. Asphalt Cement

The currently used asphalt cement with penetration grade of 40–50 from Baiji refinery. The characteristics of asphalt are meeting the standards of State Corporation of Roads and Bridges (SORB, 2007). The physical properties of the asphalt samples are given in Table II.

C. Natural Fiber

Hot mix asphalt (HMA) is strong in compression and weak in tension, then fibers reinforcement could be used to provide needed resistance to tensile stresses. For this purpose, four different types of natural fibers were used in this research coconut, corn, palm, and sisal fiber with various lengths 0.5, 1.0, 1.5, and 2.0 cm and added by five different contents 0.1, 0.2, 0.3, 0.4, and 0.5% by total weight of the mixture. The selected of these small percentages can be attributed to the lightweight of the natural fibers. Fig. 1a shows coconut fiber, which is a natural fiber extracted from the husk of coconut and used in products such as floor mats, doormats, and brushes. Coconut fiber is the fibrous material found between the hard internal shell and the outer coat of a coconut. They are naturally brown in color, having a coarse and thick nature but durable fiber, strong, and good abrasion resistance. Corn fiber shown in Fig. 1b has similar characteristics to polyester staple fiber. Corn fiber has very good flex, moisture retrieve, and good heat resistance, and it has full luster and elasticity (Reena, et al., 2009). Sisal fiber, which is shown in Fig. 1c, is one of the most widely used natural fiber and it could be can be cultivated effortlessly. It is obtained from the sisal plant. Palm fibers, which are shown in Fig. 1d, have large clearances among a mass of thick fibers are collected. These fibers being fixed to one another firmly by resin, the resultant product being reinforced by unitarily combining therewith by a resin a knitted comprising natural vegetable fiber of high tensile strength.

TABLE I
Selected Combined Gradation of Aggregate and Filler According to Sorb Specifications

Sieve size	Specification range	Selected gradation
3/4”	100	100
1/2”	90-100	95
3/8”	76-90	83
No.4	44-74	59
No.8	28-58	43
No.50	5-21	13
No.200	4-10	7

TABLE II
Physical Properties of Asphalt Cement

Properties	Unit	Specifications	Test results	Specifications limits
Penetration at (25°C, 100 g, 5 s)	0.1 mm	ASTM D5	46	40–50
Specific gravity at 25°C	----	ASTM D70	1.03	---
Softening point (Ring and Ball)	°C	ASTM D36	55.6	---
Ductility (25°C, 5 cm/min)	cm	ASTM D113	103	>100
Flash point	°C	ASTM D92	285	> 232
Fire point	°C	ASTM D92	312	---

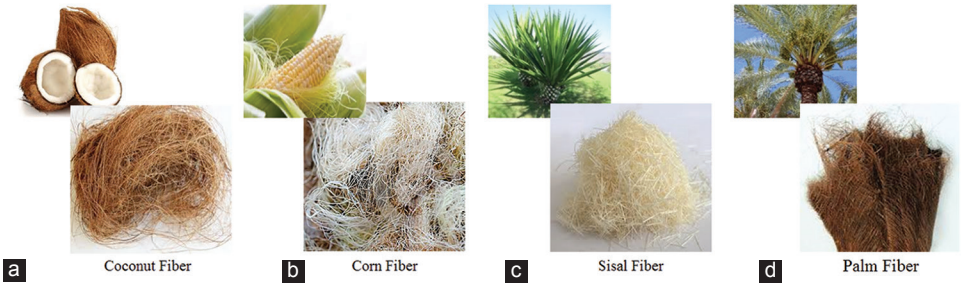

Fig. 1. Different types of natural fibers.

III. Laboratory Specimen Preparation and Test Methods

A. Optimum Asphalt Content

Marshal specimens were prepared per each type of natural fiber in accordance with the Marshall procedure specified in ASTM D6926-10 with different percentages of asphalt cement varying from 4% to 6% at an increment of 0.5% mixed with the aggregates and Portland cement filler according to the adopted gradation. The Marshall samples were extracted from the mold after the specimens were brought to room temperature and thereafter tested in accordance with ASTM D6927-15 procedure. The test results are represented in Figs. 2-5, which showed optimum asphalt contents per each mixture.

B. Effect of Natural Fiber Type

The effect of natural fiber types on the performance of HMA is evaluated through the comparisons the behavior of specimens with four different types of natural fibers (coconut, corn, sisal, and palm fiber) in which a fiber length of 1.0 cm added by 0.3% of the total weight of the mixture. Two optimum asphalt contents were used, one of them selected in correspondence with air voids 4% to compensate the absorbed asphalt by the natural fibers, and the other optimum asphalt content selected according to maximum Marshall stability to determine the optimum effect of each type of natural fibers. The results of the Marshall tests are shown in Figs. 6-9. The performance of the mixtures per each type of natural fiber showed an increment in the asphalt content, especially for the fiber with wooden texture such as palm and coconut, and also improved the Marshall properties as compared with the conventional mixture, whereas the sisal and palm fibers gave better performance.

The tensile characteristics of HMA per each type of natural fiber are evaluated by loading the Marshall specimen along a diametric plane with a compressive load at a constant rate acting parallel to and along the vertical diametrical plane of the specimen through two opposite loading strips. This loading configuration develops a relatively uniform tensile stress perpendicular to the direction of the applied load and along the vertical diametrical plane, ultimately causing the tested specimen to fail by splitting along the vertical diameter. The static indirect tensile strength of a specimen is determined using the procedure outlined in ASTM D 6931. The tensile strength ratio depending on the result of indirect tensile strength in two cases (conditioned and unconditioned)

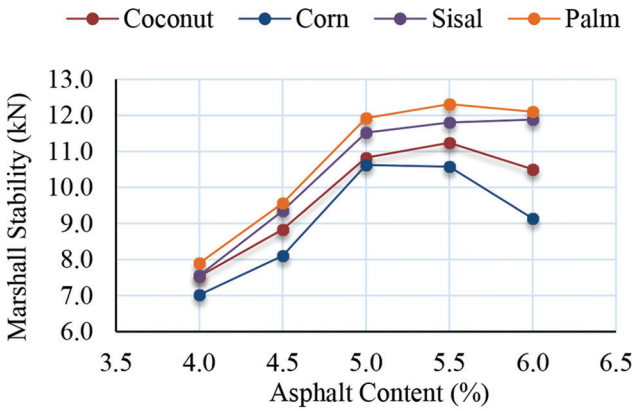

Fig. 2. Effect of asphalt content on Marshall stability of the mixture per each type of natural fibers.

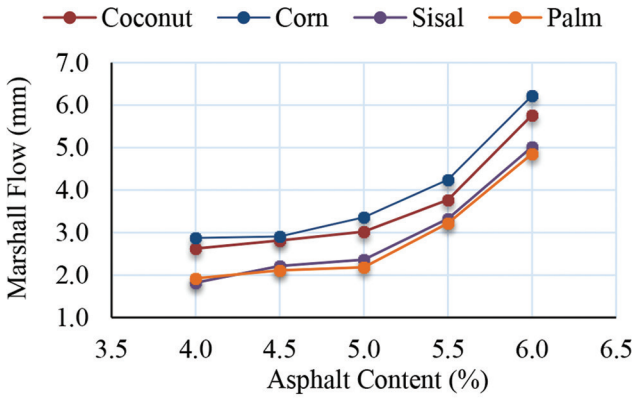

Fig. 3. Effect of asphalt content on Marshall flow of the mixture per each type of natural fibers.

as shown in Table III and represented in Figs. 10 and 11. The results indicate that adding natural fiber increases the indirect tensile strength and tensile strength ratio, especially for the sisal and palm fibers. This can be attributed to the increased amount of the asphalt content due to the effect of different texture of fibers.

C. Effect of Natural Fiber Content

Five different percentages of the sisal and coconut fibers (0.1, 0.2, 0.3, 0.4, and 0.5%) with (1.0 cm) length were added to the HMA to determine the optimum content of natural fibers. The Marshall test results represented in Figs.

http://dx.doi.org/10.14500/aro.10710

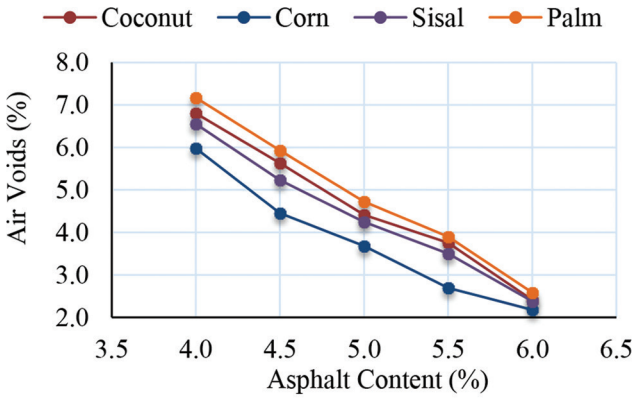

Fig. 4. Effect of asphalt content on air voids of the mixture per each type of natural fibers.

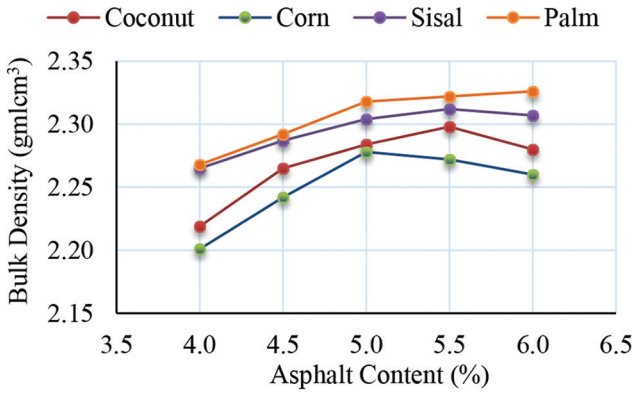

Fig. 5. Effect of asphalt content on bulk density of the mixture per each type of natural fibers.

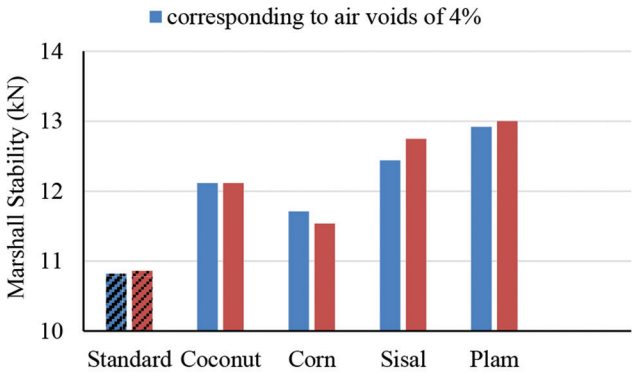

Fig. 6. Effect of fiber type on Marshall stability.

12-15 shows that when the natural fibers content is increased, the Marshall stability, Marshall flow, and the percentage of voids filled asphalt decrease, whereas the air voids increase. There existed that the optimum percentage of sisal fiber content (0.2 %) for Marshall stability; this can be attributed that the increase of fibers content in the mixture leads to reduce the contact points between aggregate, hence resulting in lower stability.

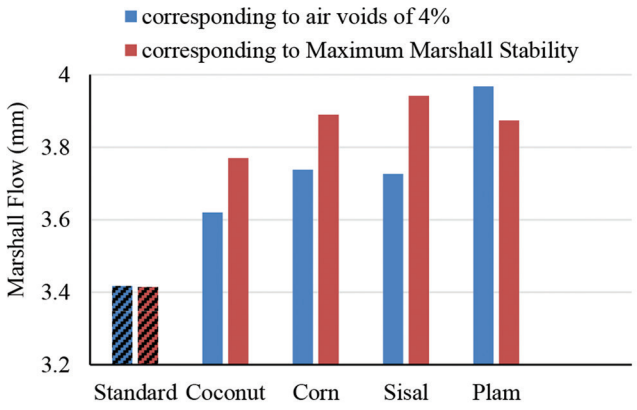

Fig. 7. Effect of fiber type on Marshall flow.

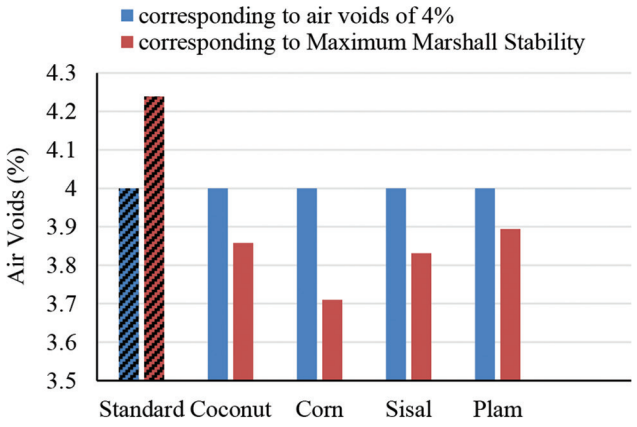

Fig. 8. Effect of fiber type on air voids.

TABLE III
INDIRECT TENSILE STRENGTH RESULTS FOR DIFFERENT TYPES OF NATURAL FIBERS

Item	Standard	Natural fiber			
		Coconut	Corn	Sisal	Palm
Asphalt content corresponding to air voids of 4%	4.9	5.5	5.3	5.6	5.7
Indirect tensile strength – unconditioned (MPa)	2.619	2.737	2.692	2.796	2.790
Indirect tensile strength – conditioned (MPa)	2.102	2.322	2.413	2.550	2.448
Tensile strength ratio (%)	80.259	84.837	89.636	91.202	87.742

The indirect tensile test results, shown in Figs. 16 and 17, indicated that adding fibers up to 0.3% into the standard mixes reasonably improves its tensile behavior as compared to the standard mix. This is probably due to the good distribution of fibers in different directions of asphalt mixture and that leads to provide a good resistance to the tensile force.

D. Effect of Natural Fiber Length

The effect of the natural fiber length on the performance of the asphalt mixture has been studied by adding the

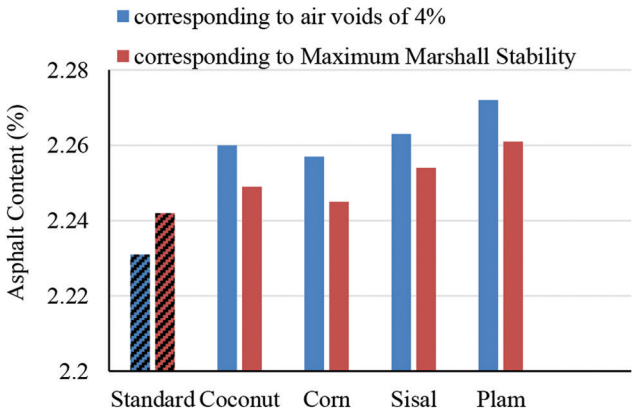

Fig. 9. Effect of fiber type on bulk density.

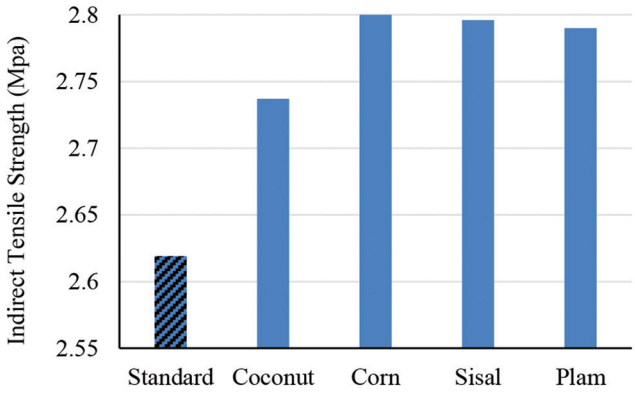

Fig. 10. Effect of natural fiber types on indirect tensile strength (unconditioned).

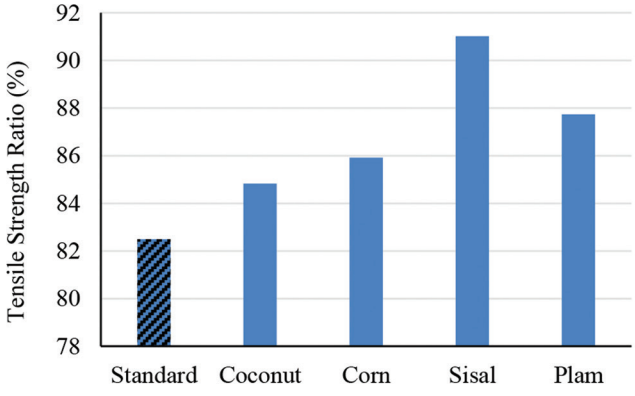

Fig. 11. Effect of natural fiber types on index of retained strength.

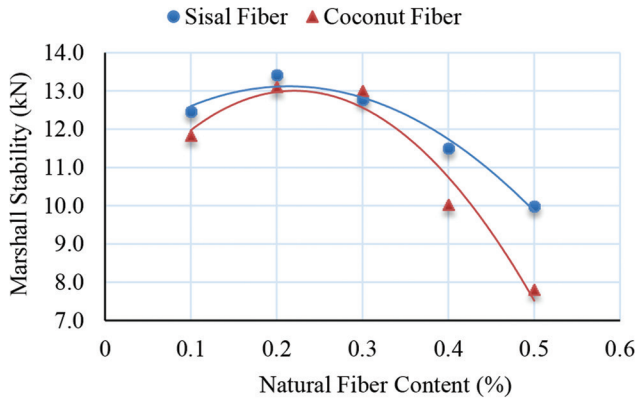

Fig. 12. Effect of fiber content on Marshall stability.

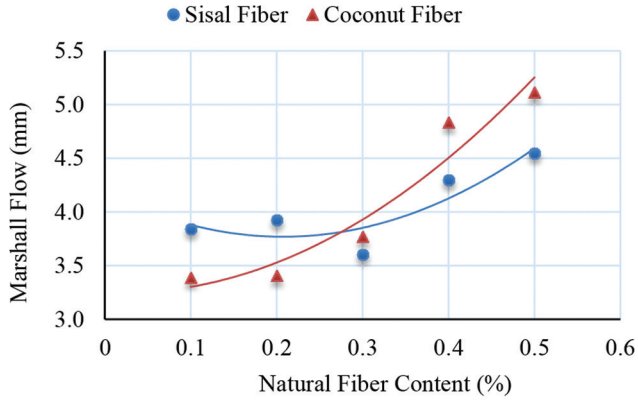

Fig. 13. Effect of fiber content on Marshall flow.

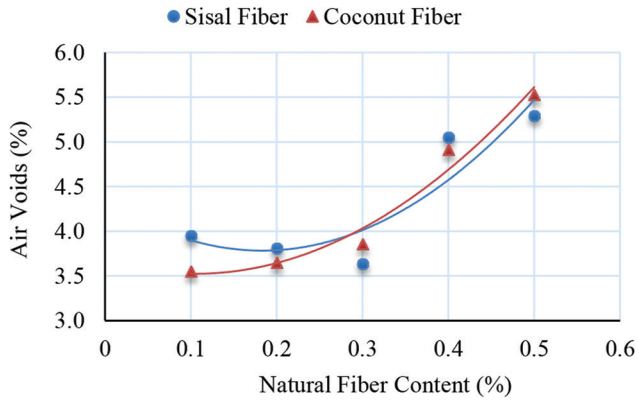

Fig. 14. Effect of fiber content on air voids.

natural fiber (sisal fiber) to the aggregate and mixed with the optimum asphalt content. The sisal fiber was cut to four different lengths of (0.5, 1.0, 1.5, and 2.0 cm) and added by 0.2 % of the total weight of the mixture, the results of the Marshall test are shown in Figs. 18-21. According to the results, using asphalt content corresponding to 4% air voids provided all the Marshall properties within the limitations. The results indicated that the air voids increased when the fiber length increase; this can be attributed that the use of too long fibers tends to "ball" in the mix.

The results of indirect tensile strength with respect to different fiber lengths are shown in Fig. 22. It can be observed that when the fiber length increases, the indirect tensile strength increases too up to some extent and starts decreasing. Fig. 23 has a similar behavior of Fig. 22, the tensile strength ratio also increases when the fiber length increases up to a certain limit and starts decreasing. Maybe this is due to the fibers

http://dx.doi.org/10.14500/aro.10710

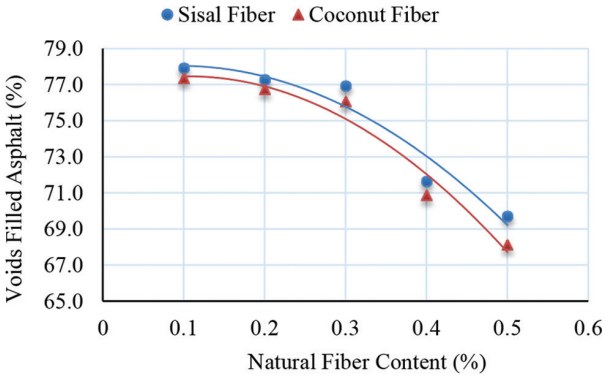

Fig. 15. Effect of fiber content on voids filled asphalt.

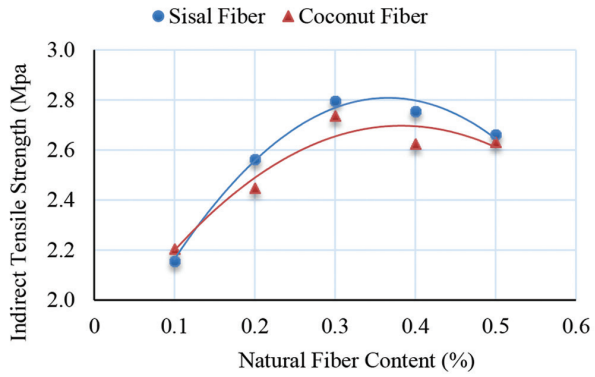

Fig. 16. Effect of natural fiber content on indirect tensile strength (unconditioned).

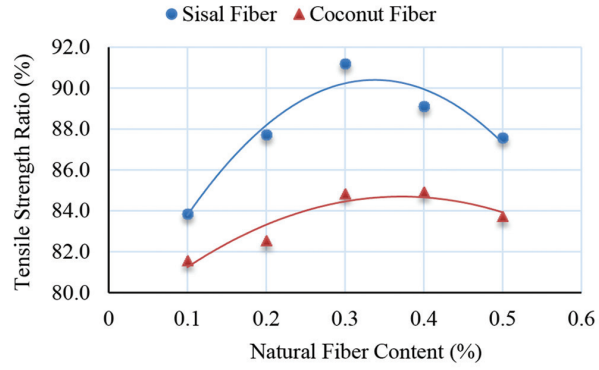

Fig. 17. Effect of natural fiber content on index of retained strength.

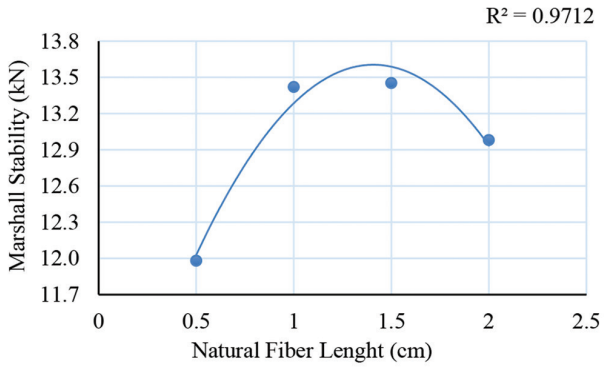

Fig. 18. Effect of natural fiber length on Marshall stability.

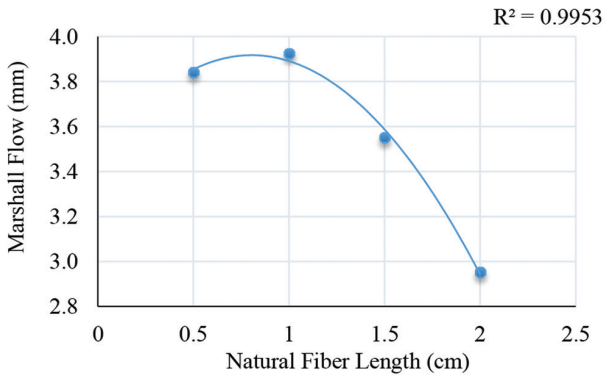

Fig. 19. Effect of natural fiber length on Marshall flow.

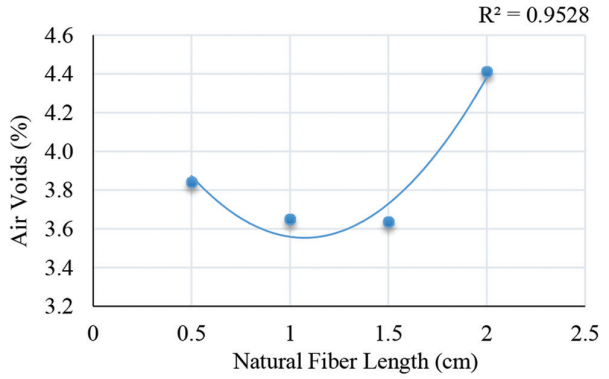

Fig. 20. Effect of natural fiber length on air voids.

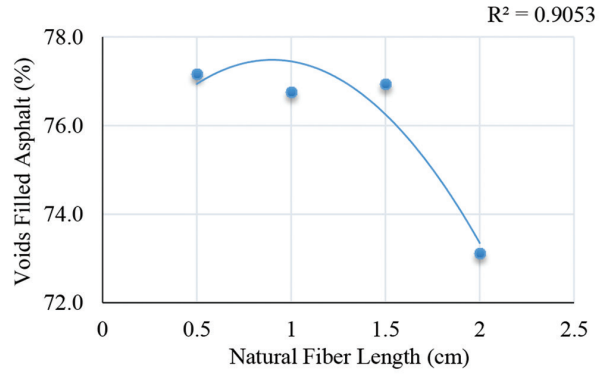

Fig. 21. Effect of natural fiber length on voids filled asphalt.

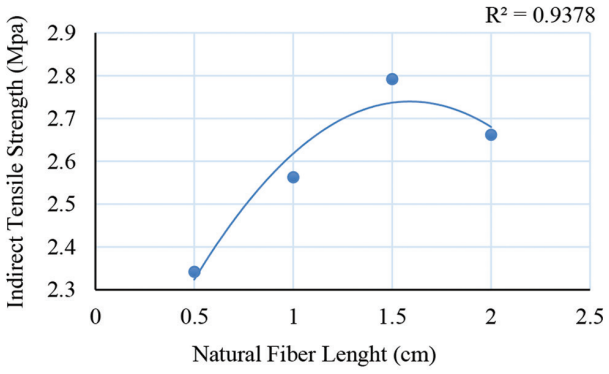

Fig. 22. Effect of natural fiber length on indirect tensile strength (unconditioned)

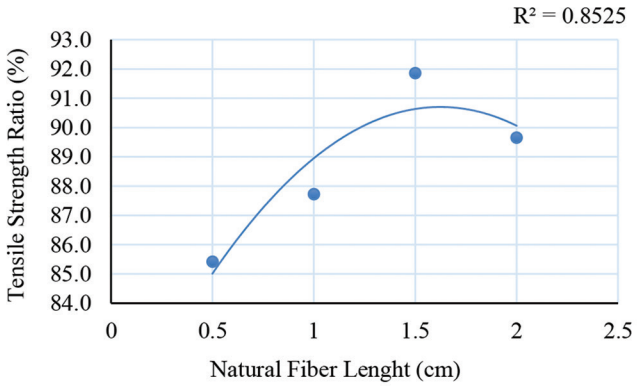

Fig. 23. Effect of natural fiber length on index of retained strength.

reinforcement, which improves the moisture sustainability by increasing the mixture resistance to cracking.

IV. Conclusions

From this research, the following conclusions can be drawn based on Marshall test properties and indirect tensile strength test, and clarify the differences between conventional mixture before and after adding the natural fibers.

1. The Marshall test results show that the sisal and palm fibers resulted best mixes considering Marshall criteria according to SORB specifications, where Marshall stability increased by 17% and 20% respectively
2. It is also observed that with an increase in fiber content up to 0.2%, air void and flow value decreases, whereas Marshall stability increased by 24% compared with the conventional mixture
3. It is further observed the use of fiber content 0.3% increases the resistance to moisture-induced damages as determined in terms of the indirect tensile strength and retained tensile strength ratio
4. The increase in fiber length up to 1.5 cm caused the Marshall stability increased by 24% and its retained tensile strength ratio increased to 92%, whereas the increase in fiber length more than 1.5 cm led to difficulties in the process of mixing the fibers with the mixture.

References

Abdelaziz, M. and Mohamed, R.K., 2010. Fatigue characteristics of stone mastic asphalt mix reinforced with fiber glass, *International Journal of the Physical Sciences*, 5(12), pp.1840-47.

Ashraf, A., 2012. Fiber Dosage Effects in Asphalt Binders and Hot Mix Asphalt Mixtures. In: *A Thesis Presented in Partial Fulfillment of the Requirements for the Degree Master of Science*. Arizona State University, Tempe, Arizona.

Bindu, C.S. and Beena, K.S., 2015. Influence of natural fibres on the compressive strength of stone matrix asphalt mixtures. *International Journal of Scientific Engineering and Applied Science*, 1(6), 445-449.

Brown, S.F., Rowlett, R.D. and Boucher, J.L., 1990. Asphalt modification. In: *Proceedings of the Conference on the United States Strategic Highway Research Program: Sharing the Benefits*, ICE, Atlanta, Georgia, United States, pp.181-203.

Reena, A., Singh, R. and Shakiya, P., 2009. *Corn Fiber: A New Fiber on Horizon, Textile Review, 2009*. Available from: https://www.fibre2fashion.com/industry-article/4455/corn-fiber-a-new-fiber-on-horizon. [Last accessed on 2020 Jul 01].

Gazia, K.K. and Sukhmanjit, A., 2017. Use of natural fibre and binder quality in stone matrix asphalt mixture. *International Journal of Latest Research in Engineering and Computing*, 5(3), 73-78.

Hossam, F.H. and Khalifa, A.J., 2005. Effect of organic fibers on open-graded friction course mixture properties. *International Journal of Pavement Engineering*, 6(1), pp.67-75.

Kavalakuntla, K.K. and Praveen, B.C., 2016. An experimental study of bituminous mixes using a natural fibre. *International Journal and Magazine of Engineering Technology, Management and Research*, 3(11), pp.906-912.

Saswat, B.D. and Mahabir, P., 2016. A study on use of natural fiber for improvement in engineering properties of dense graded bituminous mixes with coal ash, *Transportation in Developing Economies*, 2, p.4.

Sigit, P.H., 2013. Evaluation of the addition of short coconut fibers on the characteristics of asphalt mixtures. *Civil and Environmental Research*, 3(4), pp.63-73.

Standard Practice for Preparation of Bituminous Specimens Using Marshall Apparatus, ASTM D6926-10.

*Standard test method for Marshall Stability and Flow of Asphalt Mixture*s, ASTM D6927-15.

*Standard Test Method for Indirect Tensile (IDT) Strength of Bituminous Mixture*s, ASTM D6931-12.

State Organization of Road and Bridges., 2007. *Section R9, Hot-Mix Asphalt Concrete Pavement, Revised Edition by Consultant Civil Engineer Nuraddin Saeed Hussain* (*Issued in Iraq 1986*).

 http://dx.doi.org/10.14500/aro.10724

Bacterial Profile and Antimicrobial Susceptibility of Isolates Recovered from Lower Respiratory Tract Infection for Patients in Rizgary Hospital, Erbil

Mahmoud A. Chawsheen[1], Ahmed A. Al-Naqshbandi[2] and Haval H. Abdulqader[3]

[1]Department of General Sciences, Faculty of Education, Soran University, Erbil, Kurdistan Region – F.R. Iraq

[2]Department of Laboratory, Rizgary Teaching Hospital, Erbil, Kurdistan Region – F.R. Iraq

[3]Nanakali Hospital for Blood diseases and Cancer, Erbil, Kurdistan Region – F.R. Iraq

***Abstract*—Recognition of etiologies of lower respiratory tract infection (LRTI) may help in delivering effective treatment options and circumvent emergence of antibiotic resistance. This study is carried out to uncover bacterial profile and antibiotic sensitivity patterns among 310 LRTI patients attended Rizgary Hospital between January 2014 and December 2016. Standard laboratory techniques are applied in collecting, processing, and culturing sputum and bronchial wash specimens. VITEK® 2 compact systems are used to identify bacteria and their antibiotic sensitivity patterns. The results show that *Streptococcus parasanguinis* and *Acinetobacter baumannii* are the most abundant Gram-positive and Gram-negative bacteria (GPB and GNB), respectively, isolated from sputum specimens. From bronchial wash specimens, only GNB are detected and *Serratia marcescens* is the most abundant one. Antibiotic sensitivity tests reveal that *Streptococcus parasanguinis* is the most resistant GPB and *Acinetobacter baumannii* is the most resistant GNB. Sputum recovered GPB are highly resistant to ampicillin, erythromycin, levofloxacin, trimethoprim/sulfamethoxazole, and tetracycline. Bronchial wash recovered GNB are highly resistant to ampicillin, minocycline, pefloxacin, piperacillin, and ticarcillin. In conclusion, LRTIs are mainly associated with GNB rather than GPB. The recovered *Streptococcus parasanguinis* and *Acinetobacter baumannii* are found to be multidrug resistant pathogens. Ampicillin is ineffective against any of recovered pathogenic bacteria.**

***Index Terms*—*Acinetobacter baumannii*, Ampicillin, Lower respiratory tract infection, Multidrug resistance, *Streptococcus parasanguinis*.**

I. Introduction

The lower respiratory tract infections (LRTIs) are common life-threatening illnesses that frequently associated with mortalities worldwide (Madhi and Klugman, 2006; Troeger, et al., 2019). Bacterial-induced LRTI includes bronchitis and pneumonia and increases the risk of pulmonary complications (Kasper, et al., 2006). LRTIs are occurring in children and adult alike, peaking among patients in intensive care units (ICUs). The LRTI acquired in ICUs is best known as hospital-acquired LRTI (Yan, et al., 2018; Karlowsky, et al., 2020). LRTI adverse effects are not limited to population health, but they cause a tangible economic burden on the health-care systems (Ehlken, et al., 2005; Sinha, et al., 2013; Trucchi, et al., 2019).

The majority of bacterial-induced LRTIs are caused by Gram-negative bacteria (GNB), and lower case numbers caused by Gram-positive bacteria (GPB). *Pseudomonas aeruginosa* and *Haemophilus influenzae* (GNB) and *Streptococcus pneumoniae* (GPB) are among the most common bacterial isolates recovered from LTRIs (Kohlenberg, et al., 2008; Khan, et al., 2015). Viruses are also responsible for the development of LRTIs (Ren, et al., 2009; Huang, et al., 2020) and antibiotics are often unnecessarily prescribed for treating these cases that may contribute to the emergence of antibiotic resistance (Pavia, 2011; Shiley, et al., 2015).

Uncovering the etiologies of LRTI has a key role in making the right therapeutic decisions while dealing with this pathological condition (Brookes-Howell, et al., 2012; Langelier, et al., 2018). Unfortunately, in most cases, LRTI treatment is started before culture sensitivity tests are performed (Ali and Butt, 2017). Development of antibiotic resistance may also emerge once patients are given empiric therapy (Yin, et al., 2003; Fatima, et al., 2012; Claeys, et al., 2017). Hence, establishing standard guidelines to deal with LRTIs and their complications are vital to save lives, especially for those who already suffer from antibiotic-resistant bacteria. In more server cases, LRTI patients may suffer from multidrug-resistant pathogens which may make their treatment even more challenging (Woodhead, et al., 2011; Feldman and Richards, 2018).

There are guidelines in place and practiced in a few countries for LRTI management (Christiansen, 1996; Baturin,

ARO-The Scientific Journal of Koya University
Vol. VIII, No.2 (2020), Article ID: ARO.10724, 7 pages
DOI:10.14500/aro.10724
Received: 12 September 2019; Accepted: 18 November 2020
Regular research paper: Published: 07 December 2020
Corresponding author's e-mail: mahmoud.hassan@soran.edu.iq

et al., 2015; Mahashur, 2018), but these guidelines are not practiced in Iraq. Building up awareness in public and among medical societies is crucial for establishing guidelines based on etiologies explicitly associated with each region. In regard to Erbil city, there are limited data available to represent etiologies of LRTI. Because of the above-stated reasons, and the probability of emergence of new antibiotic resistance cases among the locals in Erbil city (Al-Naqshbandi, et al., 2019), this study was conducted as an attempt to uncover the current status of antibiotic sensitivity patterns of common bacterial isolates collected from LRTIs patients in Erbil city.

II. Materials and Methods

A. Specimen Collection and Transport

The LRT specimens (sputum and bronchial wash) were collected from patients attended Rizgary Teaching Hospital in Erbil city of Kurdistan Region, Iraq, for the period between January 2014 and December 2016. Sputum specimens were collected from patients after educating them to rinse their mouth with water and expectorate with the aid of a deep cough, in the first early morning and gathered directly into a labeled and sterile wide mouth screw cap container. Bronchial wash specimens were aspirated by a pulmonologist in the bronchoscopy unit and collected into a labeled and sterile screw cap container (Mahon, et al., 2014). Sputum and bronchial wash specimens were obtained separately and from different patients. After collection, 310 patients' specimens were transported to laboratories of the Microbiology Department at Rizgary Hospital for analysis.

B. Bacterial Culture and Identification

Good microbiological laboratory practice was applied to deal with sputum or a pellet of centrifuged bronchial wash specimens. Later on, specimens were inoculated separately on blood, chocolate, and MacConkey agar. The inoculum was first smeared thoroughly over the surface of the pre-poured solidified medium. Then, the loop was resterilized and drawn-out from the first site of inoculation into two or three parallel lines on fresh surfaces of the medium. A successive series of strokes were made with the loop that was sterilized between each sequence. At each step, the inoculum was derived from the most distal part of the immediately proceeded strokes. The plates were incubated overnight at 37°C. Number of colonies was counted to calculate bacterial numbers per ml of the specimens. The aerobically incubated bacterial growths were identified based on colony characteristics and outcome of Gram's staining technique (Kumar, 2016). Identification of GPB and GNB genus and species tests were performed by following VITEK® 2 compact system (bioMérieux S.A., France) protocols using the following kits: VITEK®2 GN Reference 21341, VITEK®2 GP Reference 21342, and VITEK®2 AST-GN 82 Reference 413439.

C. Antibiotics

Antimicrobial sensitivity tests were investigated in this study through VITEK® 2 compact system (bioMérieux S.A., France) kits: VITEK®2 AST-P580 Reference 22233 and VITEK®2 AST-ST01 Reference 410028. Following antibiotics were investigated in this study: AM – Ampicillin, AMC – Amoxicillin/clavulanic acid, AN – Amikacin, ATM – Aztreonam, CAZ – Ceftazidime, CIP – Ciprofloxacin, CM – Clindamycin, CRO – Ceftriaxone, CTX – Cefotaxime, CZ – Cefazolin, E – Erythromycin, ETP – Ertapenem, FA – Fusidic acid, FEP – Cefepime, FOS – Fosfomycin, FT – Nitrofurantoin, GM – Gentamicin, IPM – Imipenem, LEV – Levofloxacin, LNZ – Linezolid, MEM – Meropenem, MNO – Minocycline, MUP – Mupirocin, MXF – Moxifloxacin, OX1 – Oxacillin, P – Benzylpenicillin, PEF – Pefloxacin, PIP – Piperacillin, RA – Rifampicin, SAM – Ampicillin/sulbactam, SXT – Trimethoprim/sulfamethoxazole, TEC – Teicoplanin, TE – Tetracycline, TGC – Tigecycline, TIC – Ticarcillin, TM – Tobramycin, TZP – Piperacillin/tazobactam, and VA – Vancomycin.

D. Data Analysis

Bacterial isolates' abundancy, their distribution, and drug sensitivity were presented in percentage (%). Isolates were considered resistant toward certain antibiotic(s) when the percentile of their resistance was equal or greater than 70%. For the collective antibiotic resistance in GPB and GNB, only the resisted drugs were presented with the value equal or greater than 90%. For these calculations, Microsoft Excel 2010 was used.

TABLE I
Distribution of bacterial growth of LRTI specimen's culture

Bacterial growth	Number of growth (%)	
	Sputum No. (132) (%)	Bronchial wash No. (178) (%)
No growth of bacteria	7 (5.30)	26 (14.61)
Non-pathogenic bacteria	97 (73.49)	124 (69.66)
Pathogenic bacteria	28 (21.21)	28 (15.73)
Gram positive	7 (25)	0 (0)
Gram negative	21 (75)	28 (100)

TABLE II
Distribution of gram-positive and gram-negative bacteria isolated from LRTI specimen's culture

Gram-positive bacterial isolates	Number of bacterial isolates (%)	
	Sputum no. (7) (%)	Bronchial wash no. (0) (%)
Staphylococcus aureus	2 (28.57)	0 (0)
Streptococcus parasanguinis	3 (42.86)	0 (0)
Streptococcus pneumoniae	2 (28.57)	0 (0)
Gram-negative bacterial isolates	**Number of bacterial isolates (%)**	
	Sputum no. (21)	Bronchial wash no. (28)
Acinetobacter baumannii	7 (33.33)	2 (7.14)
Enterobacter cloacae	1 (4.76)	0 (0)
Escherichia coli	4 (19.05)	4 (14.29)
Klebsiella oxytoca	1 (4.76)	0 (0)
Klebsiella pneumonia	3 (14.29)	5 (17.86)
Proteus mirabilis	1(4.76)	1 (3.57)
Pseudomonas aeruginosa	4 (19.05)	7 (25)
Serratia marcescens	0 (0)	9 (32.14)

 http://dx.doi.org/10.14500/aro.10724

TABLE III
THE RESPONSES OF SPUTUM GRAM-POSITIVE ISOLATES TO DIFFERENT ANTIMICROBIAL AGENTS

Agents	*Staphylococcus aureus* (2) (%)	*Streptococcus parasanguinis* (3) (%)	*Streptococcus pneumoniae* (2) (%)
AM – Ampicillin	R2 (100)	R3 (100)	R2 (100)
CM – Clindamycin	R2 (100)	R3 (100)	S1 (50) R1 (50)
CRO – Ceftriaxone	R2 (100)	S2 (66.67) R1 (33.34)	S2 (100)
CTX – Cefotaxime	R2 (100)	S1 (33.34) R2 (66.67)	S2 (100)
E – Erythromycin	R2 (100)	R3 (100)	R2 (100)
FA – Fusidic acid	S2 (100)	R3 (100)	R2 (100)
FOS – Fosfomycin	S2 (100)	R3 (100)	R2 (100)
FT – Nitrofurantoin	S2 (100)	R3 (100)	R2 (100)
GM – Gentamicin	S2 (100)	R3 (100)	R2 (100)
LEV – Levofloxacin	R2 (100)	R3 (100)	R2 (100)
LNZ – Linezolid	S2 (100)	S3 (100)	S2 (100)
MUP – Mupirocin	S2 (100)	R3 (100)	R2 (100)
MXF – Moxifloxacin	S2 (100)	R3 (100)	R2 (100)
OX1 – Oxacillin	S2 (100)	R3 (100)	R2 (100)
P – Benzylpenicillin	R2 (100)	R3 (100)	S2 (100)
RA – Rifampicin	S2 (100)	R3 (100)	R2 (100)
SXT – Trimethoprim/sulfamethoxazole	R2 (100)	R3 (100)	R2 (100)
TE – Tetracycline	R2 (100)	R3 (100)	R2 (100)
TEC – Teicoplanin	S2 (100)	R3 (100)	R2 (100)
TGC – Tigecycline	S2 (100)	R3 (100)	R2 (100)
TM – Tobramycin	S2 (100)	R3 (100)	R2 (100)
VA – Vancomycin	S2 (100)	S3 (100)	S2 (100)

S: Sensitive; R: Resistant

TABLE IV
THE RESPONSES OF SPUTUM GRAM-NEGATIVE ISOLATES TO DIFFERENT ANTIMICROBIAL AGENTS

Agency	*Acinetobacter baumannii* (7) (%)	*Enterobacter cloacae* (1) (%)	*Escherichia coli* (4) (%)	*Klebsiella oxytoca* (1) (%)	*Klebsiella pneumoniae* (3) (%)	*Proteus mirabilis* (1) (%)	*Pseudomonas aeruginosa* (4) (%)
AM – Ampicillin	R7 (100)	R1 (100)	R4 (100)	R1 (100)	R3 (100)	R1 (100)	R4 (100)
AMC – Amoxicillin/ clavulanic acid	R7 (100)	R1 (100)	S1 (25) R3 (75)	R1 (100)	R3 (100)	R1 (100)	R4 (100)
AN – Amikacin	R7 (100)	S1 (100)	S2 (50) R2 (50)	S1 (100)	S3 (100)	S1 (100)	R4 (100)
ATM – Aztreonam	R7 (100)	S1 (100)	S3 (75) R1 (25)	S1 (100)	S3 (100)	S1 (100)	R4 (100)
CAZ – Ceftazidime	R7 (100)	S1 (100)	S2 (50) R2 (50)	S1 (100)	S3 (100)	S1 (100)	S1 (25) R3 (75)
CIP – Ciprofloxacin	R7 (100)	S1 (100)	S2 (50) R2 (50)	S1 (100)	S3 (100)	R1 (100)	R4 (100)
CRO – Ceftriaxone	R7 (100)	S1 (100)	S2 (50) R2 (50)	S1 (100)	S2 (66.67) R1 (33.33)	R1 (100)	R4 (100)
CZ – Cefazolin	R7 (100)	R1 (100)	S2 (50) R2 (50)	S1 (100)	S2 (66.67) R1 (33.33)	R1 (100)	R4 (100)
ETP – Ertapenem	R7 (100)	S1 (100)	S2 (50) R2 (50)	S1 (100)	S2 (66.67) R1 (33.33)	R1 (100)	R4 (100)
FEP – Cefepime	R7 (100)	S1 (100)	S3 (75) R1 (25)	S1 (100)	S3 (100)	S1 (100)	R4 (100)
FT – Nitrofurantoin	R7 (100)	R1 (100)	S3 (75) R1 (25)	R1 (100)	R3 (100)	R1 (100)	S1 (25) R3 (75)
GM – Gentamicin	R7 (100)	S1 (100)	S2 (50) R2 (50)	S1 (100)	S3 (100)	S1 (100)	S3 (75) R1 (25)
IPM – Imipenem	R7 (100)	S1 (100)	S2 (50) R2 (50)	S1 (100)	S3 (100)	R1 (100)	R4 (100)
LEV – Levofloxacin	R7 (100)	S1 (100)	S2 (50) R2 (50)	S1 (100)	S2 (66.67) R1 (33.33%)	R1 (100)	R4 (100)
MEM – Meropenem	R7 (100)	S1 (100)	S3 (75) R1 (25)	S1 (100)	S3 (100)	S1 (100)	R4 (100)
MNO – Minocycline	S1 (14.29) R6 (85.71)	R1 (100)	R4 (100)	R1 (100)	S1 (33.33) R2 (66.67%)	R1 (100)	R4 (100)
PEF – Pefloxacin	R7 (100)	R1 (100)	R4 (100)	R1 (100)	S1 (33.33) R2 (66.67%)	R1 (100)	R4 (100)
PIP – Piperacillin	R7 (100)	R1 (100)	R4 (100)	R1 (100)	R3 (100)	S1 (100)	R4 (100)
SAM – Ampicillin/ sulbactam	S2 (28.57) R5 (71.43)	R1 (100)	S1 (25) R3 (75)	S1 (100)	S2 (66.67) R1 (33.33)	R1 (100)	R4 (100)
SXT – Trimethoprim/ sulfamethoxazole	S2 (28.57) R5 (71.43)	S1 (100)	R4 (100)	S1 (100)	S3 (100)	R1 (100)	R4 (100)
TGC – Tigecycline	S2 (28.57) R5 (71.43)	S1 (100)	S2 (50) R2 (50)	R1 (100)	S2 (66.67) R1 (33.33)	R1 (100)	R4 (100)
TIC – Ticarcillin	R7 (100)	S1 (100)	R4 (100)	R1 (100)	R3 (100)	S1 (100)	R4 (100)
TM – Tobramycin	R7 (100)	R1 (100)	S3 (75) R1 (25)	S1 (100)	S3 (100)	S1 (100)	S1 (25) R3 (75)
TZP – Piperacillin/ tazobactam	R7 (100)	S1 (100)	S2 (50) R2 (50)	S1 (100)	S3 (100)	S1 (100)	R4 (100)

S: Sensitive; R: Resistant

III. Results

From different LRTIs patients, 132 sputum and 178 bronchial wash specimens were collected. Out of all sputum specimens, 5.3% showed no bacterial growth, 73.49% showed non-pathogenic bacterial growth, and 21.21% generated pathogenic bacterial growth. Our data revealed that 14.61% of bronchial wash specimens showed no bacterial growth, 69.66% produced non-pathogenic bacteria, and 15.73% generated pathogenic bacteria (Table I). About 25% of sputum pathogenic isolates were GPB (75% were GNB), and bronchial wash isolates were entirely GNB (Tables I and II).

Further analysis of sputum pathogenic isolates showed that *Streptococcus parasanguinis* was the most common GPB and *Acinetobacter baumannii* was the most common GNB. Bronchial wash specimens "entirely" generated GNB, and *Serratia marcescens* was the most detectable species (Table II). Antibiotic susceptibility tests for sputum Gram-positive isolates showed that the most resistant bacteria were *Streptococcus parasanguinis* and the most sensitive one was *Staphylococcus aureus* (Table III). Antibiotic susceptibility test also showed that *Acinetobacter baumannii* was the most resistant sputum Gram-negative isolate, and *Klebsiella pneumoniae* was the most sensitive pathogenic bacteria (Table IV). Antibiotic susceptibility testes for bronchial wash Gram-negative isolates showed that *Acinetobacter baumannii* was the most resistant, and *Klebsiella pneumoniae* was the most sensitive bacteria (Table V).

Antibiotic susceptibility tests also showed that GPB, collectively, were highly resistant to the following antibiotics: Ampicillin, erythromycin, levofloxacin, trimethoprim/sulfamethoxazole, and tetracycline. Our data also showed that all GNB isolated from sputum specimens (except for *Enterobacter cloacae*) have different responses toward studied antibiotics in comparison with the same bacteria that were isolated from bronchial wash specimens (Tables VI and VII).

Staphylococcus aureus recovered from sputum specimens were sensitive to thirteen different types of antibiotics (Table III). *Klebsiella pneumoniae* recovered from sputum specimens was sensitive toward 19 different types of antibiotics (Table IV). *K. pneumoniae* recovered from bronchial wash specimens was sensitive toward 17 different types of antibiotics (Table V).

IV. Discussion

In this study, 310 specimens were collected from patients hospitalized for LRIs treatment and then investigated for bacterial distribution patterns and antibiotic sensitivity. Our data showed no bacterial growths in 5.3% of sputum and 14.61% of bronchial wash specimens (Table I). The undetectable bacterial growth might not reflect the absence of LRIs, as some LRIs cases are due to fungal or viral infections (Troeger, et al., 2019; Barac, et al., 2018). However, this suggestion was not

TABLE V
The responses of bronchial wash gram-negative isolates to different antimicrobial agents

Agency	*Acinetobacter baumannii* (2) (%)	*Escherichia coli* (4) (%)	*Klebsiella pneumoniae* (5) (%)	*Proteus mirabilis* (1) (%)	*Pseudomonas aeruginosa* (7) (%)	*Serratia marcescens* (9) (%)
AM – Ampicillin	R2 (100)	R4 (100)	R5 (100)	R1 (100)	R7 (100)	R9 (100)
AMC – Amoxicillin/clavulanic acid	R2 (100)	S1 (25) R3 (75)	R5 (100)	S1 (100)	R7 (100)	R9 (100)
AN – Amikacin	R2 (100)	S3 (75) R1 (25)	S3 (60) R2 (40)	R1 (100)	S6 (85.71) R1 (14.29)	S5 (55.56) R4 (44.44)
ATM – Aztreonam	R2 (100)	S2 (50) R2 (50)	S3 (60) R2 (40)	R1 (100)	R7 (100)	S1 (11.11) R8 (88.89)
CAZ – Ceftazidime	R2 (100)	S3 (75) R1 (25)	S3 (60) R2 (40)	S1 (100)	S7 (100)	S4 (44.44) R5 (55.56)
CIP – Ciprofloxacin	R2 (100)	S2 (50) R2 (50)	S3 (60) R2 (40)	S1 (100)	S5 (71.43) R2 (28.57)	S5 (55.56) R4 (44.44)
CRO – Ceftriaxone	R2 (100)	S2 (50) R2 (50)	S3 (60) R2 (40)	S1 (100)	R7 (100)	S3 (33.33) R6 (66.67)
CZ – Cefazolin	R2 (100)	S2 (50) R2 (50)	S3 (60) R2 (40)	S1 (100)	R7 (100)	R9 (100)
ETP – Ertapenem	R2 (100)	S3 (75) R1 (25)	S3 (60) R2 (40)	R1 (100)	R7 (100)	S7 (77.78) R2 (22.22)
FEP – Cefepime	R2 (100)	S3 (75) R1 (25)	S3 (60) R2 (40)	S1 (100)	S6 (85.71) R1 (14.29)	S8 (88.89) R1 (11.11)
FT – Nitrofurantoin	R2 (100)	S1 (25) R3 (75)	R5 (100)	S1 (100)	S7 (100)	S4 (44.44) R5 (55.56)
GM – Gentamicin	R2 (100)	S2 (50) R2 (50)	S5 (100)	S1 (100)	S6 (85.71) R1 (14.29)	S4 (44.44) R5 (55.56)
IPM – Imipenem	R2 (100)	S4 (100)	S3 (60) R2 (40)	R1 (100)	S4 (57.14) R3 (42.86)	S7 (77.78) R2 (22.22)
LEV – Levofloxacin	R2 (100)	S1 (25) R3 (75)	S3 (60) R2 (40)	S1 (100)	S6 (85.71) R1 (14.29)	S7 (77.78) R2 (22.22)
MEM – Meropenem	R2 (100)	S3 (75) R1 (25)	S3 (60) R2 (40)	R1 (100)	S5 (71.43) R2 (28.57)	S5 (55.56) R4 (44.44)
MNO – Minocycline	R2 (100)	S1 (25) R3 (75)	R5 (100)	R1 (100)	S1 (14.29) R6 (85.71)	S1 (11.11) R8 (88.89)
PEF – Pefloxacin	R2 (100)	S1 (25) R3 (75)	R5 (100)	R1 (100)	S1 (14.29) R6 (85.71)	S1 (11.11) R8 (88.89)
PIP – Piperacillin	R2 (100)	S1 (25) R3 (75)	R5 (100)	R1 (100)	S1 (14.29) R6 (85.71)	S1 (11.11) R8 (88.89)
SAM – Ampicillin/sulbactam	R2 (100)	S1 (25) R3 (75)	S3 (60) R2 (40)	S1 (100)	R7 (100)	R9 (100)
SXT – Trimethoprim/sulfamethoxazole	R2 (100)	S1 (25) R3 (75)	S3 (60) R2 (40)	R1 (100)	S6 (85.71) R1 (14.29)	S4 (44.44) R5 (55.56)
TGC – Tigecycline	R2 (100)	S2 (50) R2 (50)	S3 (60) R2 (40)	R1 (100)	R7 (100)	S4 (44.44) R5 (55.56)
TIC – Ticarcillin	R2 (100)	S1 (25) R3 (75)	R5 (100)	R1 (100)	R7 (100)	S1 (11.11) R8 (88.89)
TM – Tobramycin	R2 (100)	S2 (50) R2 (50)	S3 (60) R2 (40)	S1 (100)	S6 (85.71) R1 (14.29)	S4 (44.44) R5 (55.56)
TZP – Piperacillin/tazobactam	R2 (100)	S2 (50) R2 (50)	S3 (60) R2 (40)	S1 (100)	S5 (71.43) R2 (28.57)	S7 (77.78) R2 (22.22)

S: Sensitive; R: Resistant

conformed since the focus of this study was only on bacteria. On the other hand, there is a possibility that some of the non-bacterial growths are due to anaerobic bacteria (Brook, 1997; Kedzia, et al., 2003), since we did not culture our specimens in anaerobic conditions we cannot confirm that.

Our data also showed that more than 73% of sputum and about 70% of bronchial wash specimens generated non-pathogenic bacterial growth, and this may indicate the presence of normal flora in the collected specimens (Budayanti, et al., 2019).

From 21.21% sputum specimens pathogenic bacteria were recovered (25% GPB and 75% GNB). *Streptococcus parasanguinis* (42.86%) was the most abundant one among GPB, and *Acinetobacter baumannii* (33.33%) was the most abundant one among GNB. Out of all bronchial wash specimens, 15.73% of them generated pathogenic bacteria (100% GNB), and *Serratia marcescens* (32.14%) was the most abundant species (Table II). In regard to bacterial genus and species, different results were reported in other studies carried out in other countries in the past few years. Khan, et al. (2015) reported that *Pseudomonas aeruginosa* and *Haemophilus influenzae* (GNB) and *Streptococcus pneumoniae* (GPB) were the most detectable bacteria in LTRIs patient. Furthermore, Tchatchouang, et al. (2019) reported in their study that *Streptococcus pneumoniae* and *Haemophilus influenzae* were the most abundant bacteria in LRTI and followed by *Klebsiella pneumoniae* and *Staphylococcus aureus* (Khan, et al., 2015; Tchatchouang, et al., 2019). Since GNB represent more than 87% of all pathogenic bacteria recovered from our specimens, they were the most LRTI associated pathogens, and this came in agreement with other studies (Kohlenberg, et al., 2008; Bali, et al., 2016).

For antibiotic sensitivity tests, our data showing that among GPB recovered from sputum specimens, *Streptococcus*

TABLE VI
Pattern of antimicrobial resistance among detected bacteria

Isolate type	No. of R.A.	Resisted antibiotics
Sputum Gram-positive isolates		
Streptococcus parasanguinis	18	Ampicillin, Clindamycin, Erythromycin, Fusidic acid, Fosfomycin, Nitrofurantoin, Gentamicin, Levofloxacin, Mupirocin, Moxifloxacin, Oxacillin, Benzylpenicillin, Rifampicin, Trimethoprim/Sulfamethoxazole, Tetracycline, Teicoplanin, Tigecycline, Tobramycin.
Streptococcus pneumoniae	16	Ampicillin, Erythromycin, Fusidic acid, Fosfomycin, Nitrofurantoin, Gentamicin, Levofloxacin, Mupirocin, Moxifloxacin, Oxacillin, Rifampicin, Trimethoprim/Sulfamethoxazole, Tetracycline, Teicoplanin, Tigecycline, Tobramycin.
Staphylococcus aureus	9	Ampicillin, Clindamycin, Ceftriaxone, Cefotaxime, Erythromycin, Levofloxacin, Benzylpenicillin, Trimethoprim/Sulfamethoxazole, Tetracycline.
Sputum Gram-negative isolates		
Acinetobacter baumannii	24	Ampicillin, Amoxicillin/clavulanic acid, Amikacin, Aztreonam, Ceftazidime, Ciprofloxacin, Ceftriaxone, Cefazolin, Ertapenem, Cefepime, Nitrofurantoin, Gentamicin, Imipenem, Levofloxacin, Meropenem, Minocycline, Pefloxacin, Piperacillin, Ampicillin/sulbactam, Trimethoprim/sulfamethoxazole, Tigecycline, Ticarcillin, Tobramycin, Piperacillin/tazobactam.
Pseudomonas aeruginosa	23	Ampicillin, Amoxicillin/clavulanic acid, Amikacin, Aztreonam, Ceftazidime, Ciprofloxacin, Ceftriaxone, Cefazolin, Ertapenem, Cefepime, Nitrofurantoin, Imipenem, Levofloxacin, Meropenem, Minocycline, Pefloxacin, Piperacillin, Ampicillin/sulbactam, Trimethoprim/sulfamethoxazole, Tigecycline, Ticarcillin, Tobramycin, Piperacillin/tazobactam.
Proteus mirabilis	14	Ampicillin, Amoxicillin/clavulanic acid, Ciprofloxacin, Ceftriaxone, Cefazolin, Ertapenem, Nitrofurantoin, Imipenem, Levofloxacin, Minocycline, Pefloxacin, Ampicillin/sulbactam, Trimethoprim/sulfamethoxazole, Tigecycline.
Enterobacter cloacae	9	Ampicillin, Amoxicillin/clavulanic acid, Cefazolin, Nitrofurantoin, Minocycline, Pefloxacin, Piperacillin, Ampicillin/sulbactam, Tobramycin.
Escherichia coli	8	Ampicillin, Amoxicillin/clavulanic acid, Amikacin, Minocycline, Pefloxacin, Piperacillin, Ampicillin/sulbactam, Trimethoprim/sulfamethoxazole.
Klebsiella oxytoca	8	Ampicillin, Amoxicillin/clavulanic acid, Nitrofurantoin, Minocycline, Pefloxacin, Piperacillin, Tigecycline, Ticarcillin.
Klebsiella pneumoniae	5	Ampicillin, Amoxicillin/clavulanic acid, Nitrofurantoin, Piperacillin, Ticarcillin.
Bronchial wash Gram-negative isolates		
Acinetobacter baumannii	24	Ampicillin, Amoxicillin/clavulanic acid, Amikacin, Aztreonam, Ceftazidime, Ciprofloxacin, Ceftriaxone, Cefazolin, Ertapenem, Cefepime, Nitrofurantoin, Gentamicin, Imipenem, Levofloxacin, Meropenem, Minocycline, Pefloxacin, Piperacillin, Ampicillin/sulbactam, Trimethoprim/sulfamethoxazole, Tigecycline, Ticarcillin, Tobramycin, Piperacillin/tazobactam.
Pseudomonas aeruginosa	12	Ampicillin, Amoxicillin/clavulanic acid, Aztreonam, Ceftriaxone, Cefazolin, Ertapenem, Minocycline, Pefloxacin, Piperacillin, Ampicillin/sulbactam, Tigecycline, Ticarcillin.
Proteus mirabilis	12	Ampicillin, Amikacin, Aztreonam, Ertapenem, Imipenem, Meropenem, Minocycline, Pefloxacin, Piperacillin, Trimethoprim/sulfamethoxazole, Tigecycline, Ticarcillin.
Escherichia coli	10	Ampicillin, Amoxicillin/clavulanic acid, Nitrofurantoin, Levofloxacin, Minocycline, Pefloxacin, Piperacillin, Ampicillin/sulbactam, Trimethoprim/sulfamethoxazole, Ticarcillin.
Serratia marcescens	9	Ampicillin, Amoxicillin/clavulanic acid, Aztreonam, Cefazolin, Minocycline, Pefloxacin, Piperacillin, Ampicillin/sulbactam, Ticarcillin.
Klebsiella pneumoniae	7	Ampicillin, Amoxicillin/clavulanic acid, Nitrofurantoin, Minocycline, Pefloxacin, Piperacillin, Ticarcillin.

R.A.: Resisted antibiotic

parasanguinis was the most resistant and *Staphylococcus aureus* was the most sensitive bacteria. For GNB recovered from sputum specimens, *Acinetobacter baumannii* was the most and *Klebsiella pneumoniae* was the least resistant one. Last but not the least, among the isolates recovered from bronchial wash specimens, *Acinetobacter baumannii* was the most resistant and *Klebsiella pneumoniae* was the most sensitive one (Table VI).

Although *Acinetobacter baumannii* that were isolated from two different types of specimens (sputum and bronchial wash), they showed identical resistance toward 24 different types of antibiotics. In contrast to *Acinetobacter baumannii*, *Pseudomonas aeruginosa* that were isolated from bronchial wash specimens were resistant to 12 types of antibiotics in comparison with the same bacteria isolated from sputum specimens that were resistant to 23 types of antibiotics. Other isolates recovered from both types of specimens showed slight differences in this regard, but not in the same patterns that we witnessed in *Acinetobacter baumannii* or *Pseudomonas aeruginosa* (Table VI).

After calculating the collective antibiotic resistance of GPB and GNB, we were able to uncover the most resisted antibiotics. Sputum detected GPB were highly resistant to ampicillin, erythromycin, levofloxacin, trimethoprim/sulfamethoxazole, and tetracycline. Sputum detected GNB were highly resistant to ampicillin and amoxicillin/clavulanic acid. Bronchial wash detected GNB were resistant to ampicillin, minocycline, pefloxacin, piperacillin, and ticarcillin. The highly resisted antibiotic that found to be ineffective against GPB and GNB from both sample types was ampicillin (Table VII). These data suggest the presence of multidrug resistant among LRIs patients in Erbil city. This may emerged as a result of antibiotic abuse, applying non-specific drugs and mismanaged regimen (Prat and Lacoma, 2016).

This study shows the necessity for developing modern and scientifically based protocols by the authorities to deal with LRTI patients and to deliver the most specific and effective antibiotics to slow down life-threatening multidrug resistance problem among the locals of Erbil city. Further investigations are required to assess bacterial profile and antibiotic sensitivity patterns in different time points to uncover the pace of antibiotic resistance among LRTI patients in Erbil city.

TABLE VII
COLLECTIVE ANTIBIOTIC RESISTANCE OF GRAM-POSITIVE AND -NEGATIVE BACTERIA ISOLATED FROM SPUTUM AND BRONCHIAL WASH SPECIMENS.

Isolates	Agent	Resistance (%)
Sputum detected Gram-positive bacteria	Ampicillin	100.0
	Erythromycin	100.0
	Levofloxacin	100.0
	Trimethoprim/ sulfamethoxazole	100.0
	Tetracycline	100.0
Sputum detected Gram-negative bacteria	Ampicillin	100.0
	Amoxicillin/ clavulanic acid	100.0
Bronchial wash detected Gram-negative bacteria	Ampicillin	100.0
	Minocycline	100.0
	Pefloxacin	100.0
	Piperacillin	100.0
	Ticarcillin	100.0

V. Conclusion

From this study, we conclude that some of LRTIs are not due to bacterial infections. LRTIs are mainly associated with GNB. This study considers *Streptococcus parasanguinis* and *Acinetobacter baumannii* to be multidrug-resistant pathogens because these two specimens collected bacteria resisted most of the tested antibiotics. The antibiotic drug ampicillin was found to be ineffective in the eradication of all types of recovered pathogenic bacteria. Consequently, there is a pronounced chance of antibiotic resistance problem among LRTI patients. As this study finding can establish a startup for LRTI, further studies are required for better detection of antibiotic resistance pattern development among the locals in Erbil city.

Acknowledgment

We would like to acknowledge Rizgary Teaching Hospital for supporting this project.

References

Ali, I. and Butt, M., 2017. Antibiotic susceptibility pattern of bacterial isolates from patients of respiratory tract infection at 43 centers in Punjab, Pakistan. *Clinical and Experimental Pharmacology*, 7, p.2.

Al-Naqshbandi, A.A., Chawsheen, M.A. and Abdulqader, H.H., 2019. Prevalence and antimicrobial susceptibility of bacterial pathogens isolated from urine specimens received in Rizgary hospital Erbil. *Journal of Infection and Public Health*, 12, pp.330-336.

Bali, N., Kakru, D., Bashir, H., Lone, S., Farhana, A. and Koul, P., 2016. Lower respiratory tract infections in intensive care units. A four year study from North India. *British Journal of Medicine and Medical Research*, 11, pp.1-9.

Barac, A., Ong, D.S.Y., Jovancevic, L., Peric, A., Surda, P., Spiric, V.T. and. Rubino, S., 2018. Fungi-induced upper and lower respiratory tract allergic diseases: One entity. *Frontiers in Microbiology*, 9, p.583.

Baturin, V.A., Shchetinin, E.V. and Malykhin, F.T., 2015. Regional specifics of microbial landscape in outpatients with lower respiratory tract infections. *The International Journal of Risk and Safety in Medicine*, 27 Suppl 1, pp.S61-2.

Brook, I., 1997. Anaerobic lower respiratory tract infections in children. *Clinical Pulmonary Medicine*, 4, pp.1-7.

Brookes-Howell, L., Hood, K., Cooper, L., Little, P., Verheij, T., Coenen, S., Godycki-Cwirko, M., Melbye, H., Borras-Santos, A., Worby, P., Jakobsen, K., Goossens, H. and Butler, C.C., 2012. Understanding variation in primary medical care: A nine-country qualitative study of clinicians' accounts of the non-clinical factors that shape antibiotic prescribing decisions for lower respiratory tract infection. *BMJ Open*, 2, p.e000796.

Budayanti, N.S., Suryawan, K., Iswari, I.S. and Sukrama, D.M., 2019. The quality of sputum specimens as a predictor of isolated bacteria from patients with lower respiratory tract infections at a tertiary referral hospital, Denpasar, Bali-Indonesia. *Frontiers in Medicine*, 6, p.64.

Christiansen, K.,1996. Treatment of common lower respiratory tract infections. *Australian Prescriber*, 16, pp.48-51.

Claeys, K.C., Zasowski, E.J., Trinh, T.D., Lagnf, A.M., Davis, S.L. and Rybak,

M.J., 2017. Antimicrobial stewardship opportunities in critically Ill patients with gram-negative lower respiratory tract infections: A multicenter cross-sectional analysis. *Infectious Diseases and Therapy*, 7, pp.135-146.

Ehlken, B., Ihorst, G., Lippert, B., Rohwedder, A., Petersen, G., Schumacher, M. and Forster, J., 2005. Economic impact of community-acquired and nosocomial lower respiratory tract infections in young children in Germany. *European Journal of Pediatrics*, 164, pp.607-615.

Fatima, A., Naqvi, S.B., Khaliq, S.A., Perveen, S. and Jabeen, S., 2012. Antimicrobial susceptibility pattern of clinical isolates of Pseudomonas aeruginosa isolated from patients of lower respiratory tract infections. *Springerplus*, 1, p.70.

Feldman, C. and Richards, G., 2018. Appropriate antibiotic management of bacterial lower respiratory tract infections. *F1000Res*, 7, p1121.

Huang, C., Wang, Y., Li, X., Ren, L., Zhao, J., Hu, Y., Zhang, L., Fan, G., Xu, J., Gu, X., Cheng, Z., Yu, T., Xia, J., Wei, Y., Wu, W., Xie, X., Yin, W., Li, H., Liu, M., Xiao, Y., Gao, H., Guo, L., Xie, J., Wang, G., Jiang, R., Gao, Z., Jin, Q., Wang, J. and Cao, B., 2020. Clinical features of patients infected with 2019 novel coronavirus in Wuhan, China. *The Lancet*, 395, pp.497-506.

Karlowsky, J.A., Lob, S.H., Kazmierczak, K.M., Young, K., Motyl, M.R. and Sahm, D.F., 2020. *In-vitro* activity of imipenem/relebactam and key β-lactam agents against gram-negative bacilli isolated from lower respiratory tract infection samples of intensive care unit patients-SMART Surveillance United States 2015-2017. *International Journal of Antimicrobial Agents*, 55, p.105841.

Kasper, D.L., Braunwald, E., Hauser, S., Longo, D., Jameson, J.L. and Fauci, A.S., 2006. *Harrison's Principles of Internal Medicine*. McGraw-Hill Education, New York.

Kedzia, A., Kwapisz, E. and Wierzbowska, M., 2003. Incidence of anaerobic bacteria in respiratory tract infections. *Pneumonologia Alergol Pol*, 71, pp.68-73.

Khan, S., Priti, S. and Ankit, S., 2015. Bacteria etiological agents causing lower respiratory tract infections and their resistance patterns. *Iranian Biomedical Journal*, 19, pp.240-246.

Kohlenberg, A., Schwab, F., Geffers, C., Behnke, M., Rüden, H. and Gastmeier, P., 2008. Time-trends for Gram-negative and multidrug-resistant Gram-positive bacteria associated with nosocomial infections in German intensive care units between 2000 and 2005. *Clinical Microbiology and Infection*, 14, pp.93-96.

Kumar, S., 2016. *Essentials of Microbiology*. Jaypee Group, Noida.

Langelier, C., Kalantar, K.L., Moazed, F., Wilson, M.R., Crawford, E.D., Deiss, T., Belzer, A., Bolourchi, S., Caldera, S., Fung, M., Jauregui, A., Malcolm, K., Lyden, A., Khan, L., Vessel, K., Quan, J., Zinter, M., Chiu, C.Y., Chow, E.D., Wilson, J., Miller, S., Matthay, M.A., Pollard, K.S., Christenson, S., Calfee, C.S. and Derisi, J.L., 2018. Integrating host response and unbiased microbe detection for lower respiratory tract infection diagnosis in critically ill adults. *Proceedings of the National Academy of Sciences*, 115, pp.E12353-E12362.

Madhi, S.A. and Klugman, K.P., 2006. Acute respiratory infections. In: Jamison, D.T., Feachem, R.G., Makgoba, M.W., Bos, E.R., Baingana, F.K., Hofman, K.J. and Rogo, K.O. (eds.) *Disease and Mortality in Sub-Saharan Africa.* The International Bank for Reconstruction and Development, The World Bank, Washington, DC.

Mahashur, A., 2018. Management of lower respiratory tract infection in outpatient settings: Focus on clarithromycin. *Lung India: Official Organ of Indian Chest Society*, 35, pp.143-149.

Mahon, C.R., Lehman, D.C. and Manuselis, G., 2014. *Textbook of Diagnostic Microbiology-E-Book*. Elsevier Health Sciences, Amsterdam, Netherlands.

Pavia, A.T., 2011. Viral infections of the lower respiratory tract: Old viruses, new viruses, and the role of diagnosis. *Clinical Infectious Diseases*, 52, pp.S284-S289.

Prat, C. and Lacoma, A., 2016. Bacteria in the respiratory tract how to treat? Or do not treat? *International Journal of Infectious Diseases*, 51, pp.113-122.

Ren, L., Gonzalez, R., Wang, Z., Xiang, Z., Wang, Y., Zhou, H., Li, J., Xiao, Y., Yang, Q., Zhang, J., Chen, L., Wang, W., Li, Y., Li, T., Meng, X., Zhang, Y., Vernet, G., Paranhos-Baccalà, G., Chen, J., Jin, Q. and Wang, J., 2009. Prevalence of human respiratory viruses in adults with acute respiratory tract infections in Beijing, 2005-2007. *Clinical Microbiology and Infection*, 15, pp.1146-1153.

Shiley, K.T., Lautenbach, E. and Lee, I., 2015. The use of antimicrobial agents after diagnosis of viral respiratory tract infections in hospitalized adults: Antibiotics or anxiolytics? *Infection Control and Hospital Epidemiology*, 31, pp.1177-1183.

Sinha, A., Kim, S., Ginsberg, G., Franklin, H., Kohberger, R., Strutton, D., Madhi, S.A., Griffiths, U.K. and Klugman, K.P., 2013. Economic burden of acute lower respiratory tract infection in South African children. *Paediatrics and International Child Health*, 32, pp.65-73.

Tchatchouang, S., Nzouankeu, A., Kenmoe, S., Ngando, L., Penlap, V., Fonkoua, M.C., Pefura-Yone, E.W. and Njouom, R., 2019. Bacterial aetiologies of lower respiratory tract infections among adults in Yaoundé, Cameroon. *BioMed Research International*, 2019, pp.1-7.

Troeger, C.E., Blacker, B.F., Khalil, I.A., Zimsen, S.R.M., Albertson, S.B., Abate, D., Abdela, J., Adhikari, T.B., Aghayan, S.A., Agrawal, S., Ahmadi, A., Aichour, A.N., Aichour, I., Aichour, M.T.E., Al-Eyadhy, A., Al-Raddadi, R.M., Alahdab, F., Alene, K.A., Aljunid, S.M., Alvis-Guzman, N., Anber, N.H., Anjomshoa, M., Antonio, C.A.T., Aremu, O., Atalay, H.T., Atique, S., Attia, E.F., Avokpaho, E.F.G., Awasthi, A., Babazadeh, A., Badali, H., Badawi, A., Banoub, J.A.M., Barac, A., Bassat, Q., Bedi, N., Belachew, A.B., Bennett, D.A., Bhattacharyya, K., Bhutta, Z.A., Bijani, A., Carvalho, F., Castañeda-Orjuela, C.A., Christopher, D.J., Dandona, L., Dandona, R., Dang, A.K., Daryani, A., Degefa, M.G., Demeke, F.M., Dhimal, M., Djalalinia, S., Doku, D.T., Dubey, M., Dubljanin, E., Duken, E.E., Edessa, D., El Sayed Zaki, M., Fakhim, H., Fernandes, E., Fischer, F., Flor, L.S., Foreman, K.J., Gebremichael, T.G., Geremew, D., Ghadiri, K., Goulart, A.C., Guo, J., Ha, G.H., Hailu, G.B., Haj-Mirzaian, A., Haj-Mirzaian, A., Hamidi, S., Hassen, H.Y., Hoang, C.L., Horita, N., Hostiuc, M., Irvani, S.S.N., Jha, R.P., Jonas, J.B., Kahsay, A., Karch, A., Kasaeian, A., Kassa, T.D., Kefale, A.T., Khader, Y.S., Khan, E.A., Khan, G., Khan, M.N., Khang, Y.H., Khoja, A.T., Khubchandani, J., Kimokoti, R.W., Kisa, A., Knibbs, L.D., Kochhar, S., Kosen, S., Koul, P.A., Koyanagi, A., Kuate Defo, B., 2019. Mortality, morbidity, and hospitalisations due to influenza lower respiratory tract infections, 2017: An analysis for the Global Burden of Disease Study 2017. *The Lancet Respiratory Medicine*, 7, pp.69-89.

Trucchi, C., Paganino, C., Orsi, A., Amicizia, D., Tisa, V., Piazza, M.F., Gallo, D., Simonetti, S., Buonopane, B., Icardi, G. and Ansaldi, F., 2019. Hospital and economic burden of influenza-like illness and lower respiratory tract infection in adults ≥50 years-old. *BMC Health Services Research*, 19, p.585.

Woodhead, M., Blasi, F., Ewig, S., Garau, J., Huchon, G., Ieven, M., Ortqvist, A., Schaberg, T., Torres, A., Van Der Heijden, G., Read, R. and Verheij, T.J.M., 2011. Guidelines for the management of adult lower respiratory tract infections summary. *Clinical Microbiology and Infection*, 17, pp.1-24.

Yan, T., Li, Y., Sun, Y., Wang, H., Wang, J., Wang, W., Liu, Y., Wu, X. and Wang, S., 2018. Hospital-acquired lower respiratory tract infections among high risk hospitalized patients in a tertiary care teaching hospital in China: An economic burden analysis. *Journal of Infection and Public Health*, 11, pp.507-513.

Yin, C.C., Huah, L.W., Lin, J.T.P., Goh, A., Ling, H. and Moh, C.O., 2003. Lower respiratory tract infection in hospitalized children. *Respirology*, 8, pp.83-89.

An Area-efficient Microstrip Diplexer with a Novel Structure and Low Group Delay for Microwave Wireless Applications

Salah I. Yahya[1,2] and Abbas Rezaei[3]

[1]Department of Communication and Computer Engineering, Cihan University-Erbil, Erbil, Kurdistan Region – F.R. Iraq

[2]Department of Software Engineering, Faculty of Engineering, Koya University, Koya KOY45, Kurdistan Region – F.R. Iraq

[3]Department of Electrical Engineering, Kermanshah University of Technology, Kermanshah, Iran

***Abstract*—In this work, a novel structure of a microstrip diplexer consisting of coupled patch cells is presented. It works at 2.5 GHz and 4.7 GHz for wireless applications. The proposed structure is well miniaturized with a compact area of 0.015 λ_g^2, fabricated on 0.787 mm substrate height. It has two wide fractional bandwidths (FBWs) of 28% and 17.9% at the lower and upper channels, respectively. Another feature of the proposed design is the low group delays, which are better than 0.4 ns for both channels. Moreover, the designed diplexer can suppress the harmonics up to 10 GHz. Meanwhile, the insertion losses at both channels are low. The design method is based on proposing an approximated equivalent *LC* circuit of a novel basic resonator. The information about the resonator behavior is extracted from the even and odd modes analysis of the proposed equivalent *LC* circuit. Finally, our introduced diplexer is fabricated and measured to verify the simulation results, where the simulated and measured results are in a good agreement.**

***Index Terms*—Fractional bandwidth, Group delay, Harmonics, Microstrip diplexer, Wireless applications.**

I. Introduction

Microstrip diplexers are attractive devices for the frequency domain multiplexing in modern communication systems (Yahya, Rezaei and Nouri, 2020a). Several types of microstrip structures have been used to design diplexers for wireless applications (Rezaei, Yahya and Jamaluddin, 2020; Rezaei, Nouri and Mohammadi, 2019; Huang, et al., 2016; Rezaei, et al., 2019a; Jun-Mei, Zhou and Cao, 2016; Peng and Chiang, 2015; Rezaei, et al., 2019b; Salehi, et al., 2016; Rezaei and Noori, 2018; Chen, 2015; Xiao, 2015; Noori and Rezaei, 2017a; Rezaei, Noori and Mohamadi, 2017, Noori and Rezaei, 2017b; Bui, et al., 2017; Guan, et al., 2014; Bukuru, Song and Xue, 2015; Yahya, Rezaei and Nouri, 2020b; Rezaei, et al., 2020). However, all of these diplexers occupy a large implementation area. Meanwhile, they do not have wide fractional bandwidths (FBWs) for broadband applications.

In (Rezaei, Yahya and Jamaluddin, 2020), engraved patch cells divided into trapezius and triangle cells have been utilized to design a microstrip diplexer. This structure is suitable for harmonic suppression with several transmission zeros (TZs) at its stopband. Two meandrous cells have been coupled to design a microstrip diplexer in (Rezaei, Nouri and Mohammadi, 2019). This diplexer could not suppress the harmonics whereas it has low frequency selectivity. In (Huang, et al., 2016), coupled stub loaded U-shape cells, in (Rezaei, et al., 2019a), coupled lines loaded by similar patch cells, in (Jun-Mei, Zhou and Cao, 2016), coupled U-shape structure, in (Peng and Chiang, 2015), meandrous close-loops connected to interdigital cells, in (Rezaei, et al., 2019b), coupled meandrous cells and in (Salehi, et al., 2016), and triangular open-loop resonators have been used to obtain dual-band band pass-band pass diplexers.

The above-mentioned diplexers could not attenuate the 4th harmonics except the introduced diplexer in (Salehi, et al., 2016), which could suppress the harmonics from 1st up to 4th harmonics. Similarly, the other designed diplexers (Rezaei and Noori, 2018; Chen, 2015; Xiao, 2015; Noori and Rezaei, 2017a; Rezaei, Noori and Mohamadi, 2017, Noori and Rezaei, 2017b; Bui, et al., 2017; Guan, et al., 2014; Bukuru, Song and Xue, 2015; Yahya) have the problem of unsuppressed harmonics. The proposed diplexer in Rezaei and Noori, 2018, which has been proposed based on novel microstrip engraved patch cells, has low insertion losses at both channels and several TZs at its stopband. Slotline-loaded microstrip ring resonators (Chen, 2015), open-loops

ARO-The Scientific Journal of Koya University
Vol. VIII, No.2 (2020), Article ID: ARO.10753, 7 pages
DOI:10.14500/aro.10753
Received: 12 September 2019; Accepted: 18 November 2020
Regular research paper: Published: 17 December 2020
Correspondent author's e-mail: salah.ismaeel@koyauniversity.org

connected by mixed electromagnetic coupling structure (Xiao 2015), coupled stub loaded microstrip lines (Noori and Rezaei, 2017a) and coupled meandrous cells (Rezaei, Noori and Mohamadi, 2017) have been used to design new microstrip diplexers.

The reported diplexers in (Chen, 2015; Xiao, 2015), occupy large areas with high insertion losses at upper and lower channels. As mentioned above, some of the reported diplexers have similar resonators. However, the designed diplexer in Noori and Rezaei, 2017b, has a novel structure. Nevertheless, the isolation between channels of this diplexer is low. Interdigital cells in (Bui, et al., 2017), two coupled E-shape structures in (Guan, et al., 2014), and coupled spiral resonators in (Bukuru, Song and Xue, 2015), have been used to design microstrip diplexers. In (Yahya, Rezaei and Nouri, 2020b), a high-performance microstrip multiplexer has been designed using computational intelligence for multi-band RF wireless communications systems. In (Rezaei, et al., 2020), a low-loss compact microstrip diplexer has been designed based on coupled meandrous open-loop resonators.

Since the diplexers with compact area, low group delay and wide FBWs are rarely designed, in this work we have designed a compact microstrip diplexer with wide FBWs and very low group delay for wireless applications. Moreover, our diplexer can attenuate from the 1st to 4th harmonics whereas it has low insertion losses at both channels, several TZs at its stopband and acceptable isolation and return loss. The designing method is based on proposing a symmetric single-mode resonator without harmonics. Then, the odd and even modes analysis is carried out to determine the microstrip cells with the most impact on the resonator behavior. Using the proposed designing method, we can miniaturize the area. Meanwhile, we show that our resonator can suppress the harmonics inherently.

II. Design and Analysis of the Proposed Structure

The proposed resonator is composed microstrip thin sections, patch cells, and coupling structure. The coupling structure creates small capacitors named coupling capacitors whereas the thin cells have inductance features. The simulation results show that using the patch cells can help to save the area. Fig. 1a shows the proposed resonator. It includes two coupled sections with a symmetric structure. As depicted in Fig. 1a, in each section there are two rectangular cells that are coupled to each other. These cells create two capacitors larger than the coupling and gap capacitors.

An approximated equivalent *LC* circuit of the proposed resonator is illustrated in Fig. 1b. The stubs with the physical lengths l_1, l_2, and l_3 are replaced with the inductors L_1, L_2, and L_3, respectively. The coupling, gap, and rectangular capacitors are C_C, C_g, and C_r, respectively. In the approximated *LC* model, the effects of bents and steps in widths are removed, as they are important only at the frequencies higher than 10 GHz (Jahanbakhshi and Hayati, 2016). Moreover, replacing the coupling effect by only three capacitors is an approximated model for the coupling structure because in the exact model the number of capacitors will be increased significantly (Rezaei and Noori, 2018).

To obtain some information about the resonator behavior, we analyzed the *LC* model. The impedance between the input and output ports (Z) is calculated as follows:

$$Z=\frac{(2j\omega L_1+Z_A)\times(2j\omega L_3+\frac{1}{j\omega C_g})}{(2j\omega L_1+Z_A)+(2j\omega L_3+\frac{1}{j\omega C_g})} \quad (1)$$

where:

$$Z_A=\frac{(\frac{1}{j\omega C_C}+\frac{2}{j\omega C_r})\times\frac{1}{j\omega C_C}}{\frac{(\frac{1}{j\omega C_C}+\frac{2}{j\omega C_r})+\frac{1}{j\omega C_C}}{(\frac{1}{j\omega C_C}+\frac{2}{j\omega C_r})\times\frac{1}{j\omega C_C}}+2j\omega L_2)\times\frac{1}{j\omega C_C}}{\frac{(\frac{1}{j\omega C_C}+\frac{2}{j\omega C_r})+\frac{1}{j\omega C_C}}{(\frac{1}{j\omega C_C}+\frac{2}{j\omega C_r})\times\frac{1}{j\omega C_C}}+2j\omega L_2+\frac{1}{j\omega C_C}}\Rightarrow$$

$$Z_A=j\frac{4\omega^2L_2(1+\frac{C_C}{C_r})-\frac{1}{C_C}-\frac{2}{C_r}}{\omega(3+\frac{4C_C}{C_r}-4\omega^2L_2C_C(1+\frac{C_C}{C_r}))}$$

In (1), ω is an angular frequency. The coupling capacitor is a small value in fF. Therefore, for $C_c \ll C_r$ we can write $1+C_C/C_r\approx 1$ and $3+4C_C/C_r\approx 3$. As a result, ZA and Z will be changed as follows:

$$Z_A=j\frac{4\omega^2L_2-\frac{1}{C_C}-\frac{2}{C_r}}{\omega(3-4\omega^2L_2C_C)}\Rightarrow$$

$$Z=j\frac{(\omega^2(6L_1+4L_2)-8\omega^4L_2C_CL_1-\frac{1}{C_C}-\frac{2}{C_r})\times(1-2\omega^2L_3C_g)}{\omega[3+\frac{C_g}{C_C}+\frac{2C_g}{C_r}-\omega^2(4L_2(C_C+C_g)+6(L_1+L_3)C_g)+8\omega^4(L_1+L_3)L_2C_gC_C]} \quad (2)$$

Similar to the coupling capacitor, the gap capacitor (C_g) is very small. Accordingly, Z will be approximated as follows:

$$Z=j\frac{\omega^2(6L_1+4L_2)-8\omega^4L_2C_CL_1-\frac{1}{C_C}-\frac{2}{C_r}}{\omega[3+\frac{C_g}{C_C}]} \quad (3)$$

For the small values of C_C, we can remove the second phrase ($8\omega^4L_2C_CL_1$) in the numerator of (3), so that:

$$Z=j\frac{\omega^2(6L_1+4L_2)-(\frac{1}{C_C}+\frac{2}{C_r})}{\omega[3+\frac{C_g}{C_C}]} \quad (4)$$

Due to the symmetry in the proposed resonator structure, we can carry out the even and odd modes analysis. To find the

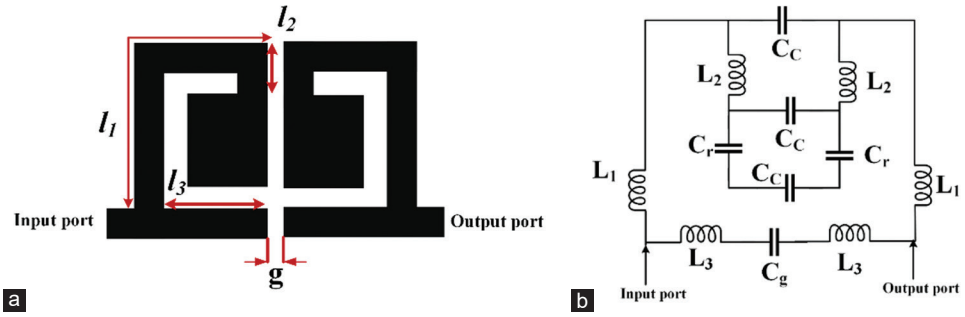

Fig. 1. (a) Layout of the proposed resonator, and (b) an equivalent *LC* circuit of the proposed resonator.

odd mode angular resonance frequency (ω_o), the numerator of the above equation must be zero. On the other hand, for calculating the even mode angular resonance frequency the denominator of the above equation should be zero. Hence, we have only an odd mode angular resonance frequency as follows:

$$\omega_o = \sqrt{\frac{C_r + 2C_C}{2C_C C_r (3L_1 + 2L_2)}} \quad (5)$$

Since we have only an odd mode resonance frequency, our proposed resonator is a single-mode resonator with the attenuated harmonics. Because, if we had more resonance frequencies they were harmonics. If we apply the approximation of the small coupling capacitor, (4) can be decreased as follows:

$$\omega_o = \sqrt{\frac{1}{2C_C (3L_1 + 2L_2)}} \quad (6)$$

According to (6), we can tune the resonance frequency by selecting the appropriate values of the inductors L_1, L_2, and a coupling capacitor. Therefore, the resonance frequency depends on the space between the coupled cells and the physical lengths l_1 and l_2, significantly. Hence, for a predetermined angular resonance frequency, we can select the space between the coupled sections and dimensions of the physical lengths l_1 and l_2 in a way that we can save the area.

If the gap between the coupled sections can be reduced, the coupling capacitor will be increased. As a result, for a constant predetermined angular resonance frequency, we can decrease the dimensions of the physical lengths l_1 and l_2 which leads to save the area. Extracting the above information about the resonator behavior leads to better optimization, easily.

By knowing the basic information, we can design two band pass filters (BPFs) (BPF1 and BPF2) with compact size and attenuated harmonics as depicted in Fig. 2a and b, respectively. In Fig. 2a and b, the dimensions of both filters are in mm. To design these BPFs, the proposed resonator is utilized. However, for BPF1 the space between cells is smaller whereas it has extra stubs that are used for better optimization. To improve the insertion losses, the patch rectangular feed structures are added to both BPFs. The bandwidths of BPF1 and BPF2 are affected by their overall sizes. Increasing the overall size of each BPF decreases the bandwidth, whereas the fractional bandwidth (FBW) remains constant.

The frequency responses of BPF1 and BPF2 are depicted in Fig. 2c and d, respectively. The simulation results are obtained using the EM simulator of ADS software on a Rogers RT/duroid 5880 substrate with ε_r = 2.2, loss tangent = 0.0009, and the substrate thickness 0.787 mm. As shown in Fig. 2, BPF1 works at 2.49 GHz whereas it has a very low simulated insertion loss of 0.02 dB and a wide FBW of 30%. It suppresses the harmonics up to 9.9 GHz with the maximum harmonic level 20 dB. Furthermore, BPF2 operates at 4.9 GHz with 0.7 dB insertion loss and an FBW of 28.7%. It suppresses the harmonics up to 18.6 GHz with the maximum harmonic level 20 dB.

To obtain a dual-band band pass-band pass diplexer, we connected BPF1 and BPF2 with the same dimensions given in Fig. 2a and b. Fig. 3 illustrates the layout configuration of the proposed diplexer. As shown in Fig. 3, there is no need to use an extra junction for connecting the BPFs and this can save the area. This is due to having several coupling structures between Ports 2 and 3, whereas there are not any paths without coupling between Ports 2 and 3. Therefore, the BPFs do not have a significant loading effect on each other.

III. Results and Discussion

We simulated the proposed diplexer using the EM simulator of Advanced Design System (ADS) software. The designed diplexer is fabricated on a Rogers RT/duroid 5880 substrate with ε_r = 2.22, loss tangent = 0.0009, and the substrate thickness 0.7874 mm. We used Agilent network analyzer N5230A to obtain the measurement results of the fabricated diplexer. The proposed diplexer occupies a very small area of 13.3 mm×10.2 mm = 0.14 λ_g × 0.11 λ_g, where λ_g is the guided wavelength calculated at the first resonance frequency.

Fig. 4a shows the simulated and measured S_{21} and S_{31}. As depicted in Fig. 4a, the designed diplexer works at f_1 = 2.5 GHz and f_2 = 4.7 GHz with two low insertion losses better than 0.2 dB at both channels. However, due to copper and junction losses, the measured losses are a little higher than the simulated losses. The first and second FBWs are 28% and 17.9%, respectively. As shown in Fig. 4a, the designed diplexer can attenuate the harmonics up to 10 GHz ($4f_1$) with the maximum harmonic level 16.2 dB. Therefore, it can attenuate 1st, 2nd, 3rd, and 4th harmonics.

Fig. 4b and c illustrate the simulated and measured isolation between channels and common port return loss, respectively. The common port return losses at the lower

http//dx.doi.org/10.14500/aro.10753

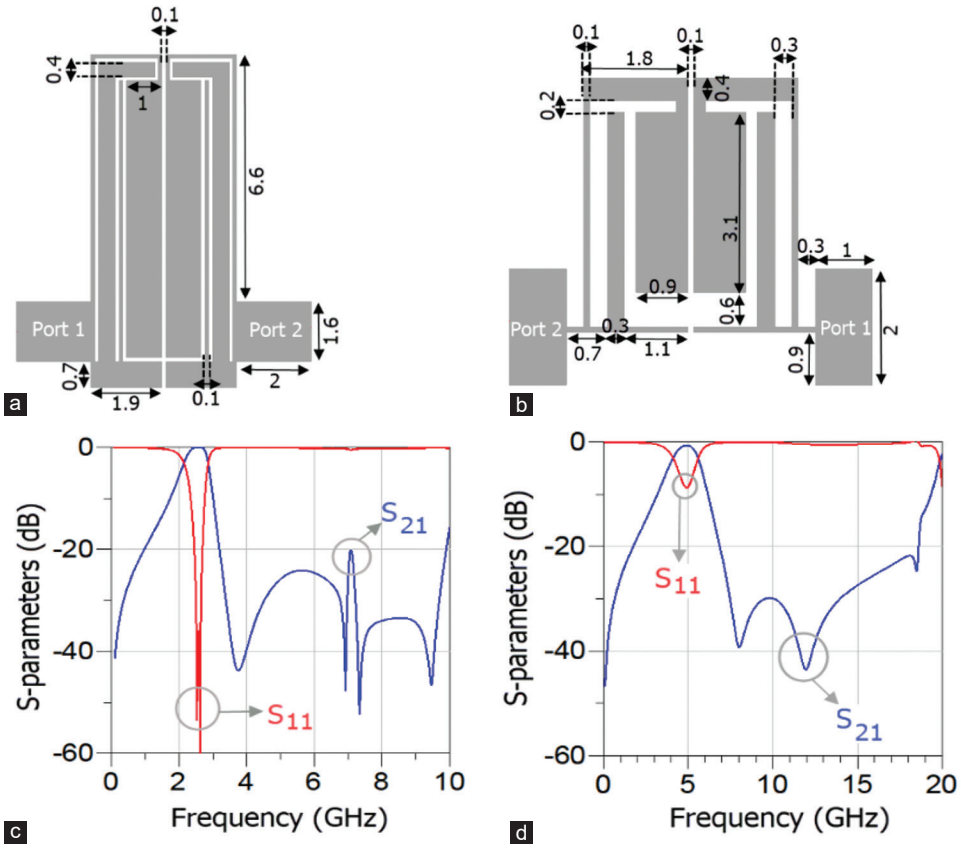

Fig. 2. (a) Layout of BPF1, (b) layout of BPF2, (c) frequency response of BPF1, and (d) frequency response of BPF2.

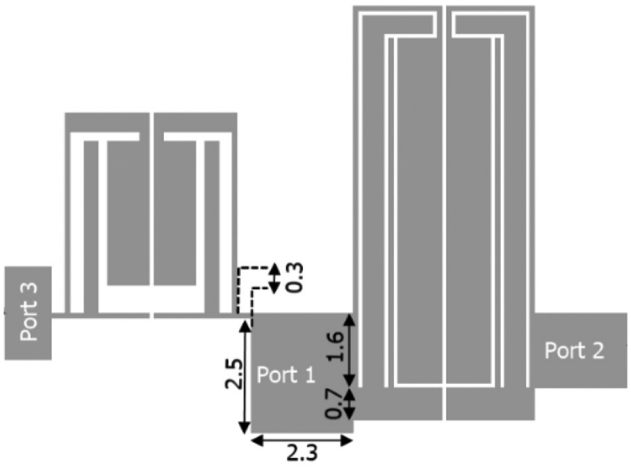

Fig. 3. Layout configuration of our diplexer (all dimensions are in mm).

and upper channels are better than 15.9 dB and 17 dB, respectively, whereas there are two transmission poles at the first channel. Meanwhile, the reasonable isolation between the channels better than 20 dB is obtained. A photograph of the fabricated diplexer is presented in Fig. 4c.

To prove the advantages of this work, we compared our diplexer with the previously reported microstrip diplexers, as shown in Table I. From Table I it can be seen that, in comparison with the previously reported diplexers, the proposed diplexer in this work has the most compact area and the widest FBWs, whereas it has low insertion losses at both channels. Moreover, it can attenuate the harmonics better than all; expect the introduced diplexers in (Rezaei, Yahya and Jamaluddin, 2020; Salehi, et al., 2016). However, these two reported diplexers occupy larger areas. Meanwhile, the channels of these diplexers are narrower than ours.

In addition to the mentioned features, the proposed diplexer has flat channels with low group delays. Fig. 5a and b show the group delays of the first and second channels, respectively. The narrowband transmission parameters of the proposed diplexer are depicted in Fig. 5c and d. The simulated group delays of the proposed diplexer are lower than 0.4 ns which are very small value for a microstrip diplexer. Despite the importance of having flat channels (a non-flat pass band with high group delay has a pulse distortion), most of the previously reported diplexers did not pay attention to this problem. Therefore, we had to compare the group delay of our work with some of the previously reported diplexers and filters, as shown in Table II. In comparison with the previous works, our diplexer has the minimum group delays at both channels.

The isolation of the proposed diplexer is a function of the gap between the first and second channels, which is depicted in Fig. 6. Using a smaller filter shifts the frequency response to the right. Accordingly to change the gap between the channels, we changed the overall dimension of the larger filter with the scales 1:1, 0.9:1, 0.8:1, and 0.7:1 so that the gap between channels are obtained 2.25 GHz, 2.22 GHz, 2.1 GHz, and 1.33 GHz, respectively. As shown in Fig. 6, by increasing the gap between channels, the isolation of the proposed diplexer will be improved.

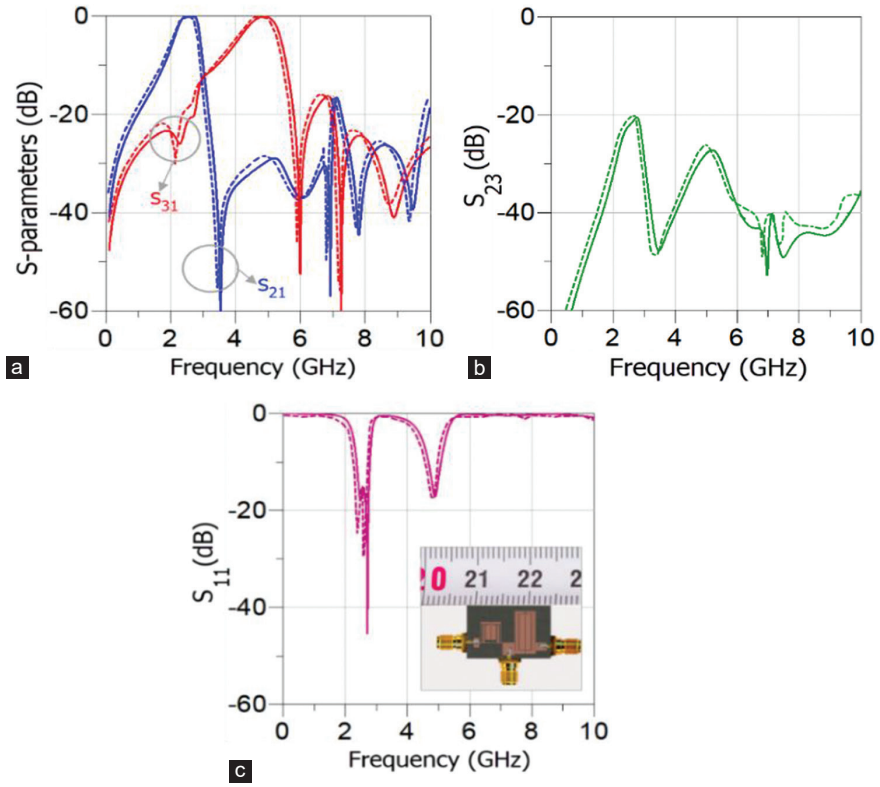

Fig. 4. (a) Simulated (solid line) and measured (dashed line) S_{21} and S_{31}, (b) simulated (solid line) and measured (dashed line) S_{23}, and (c) simulated (solid line) and measured (dashed line) S_{11} with a photograph of the fabricated diplexer.

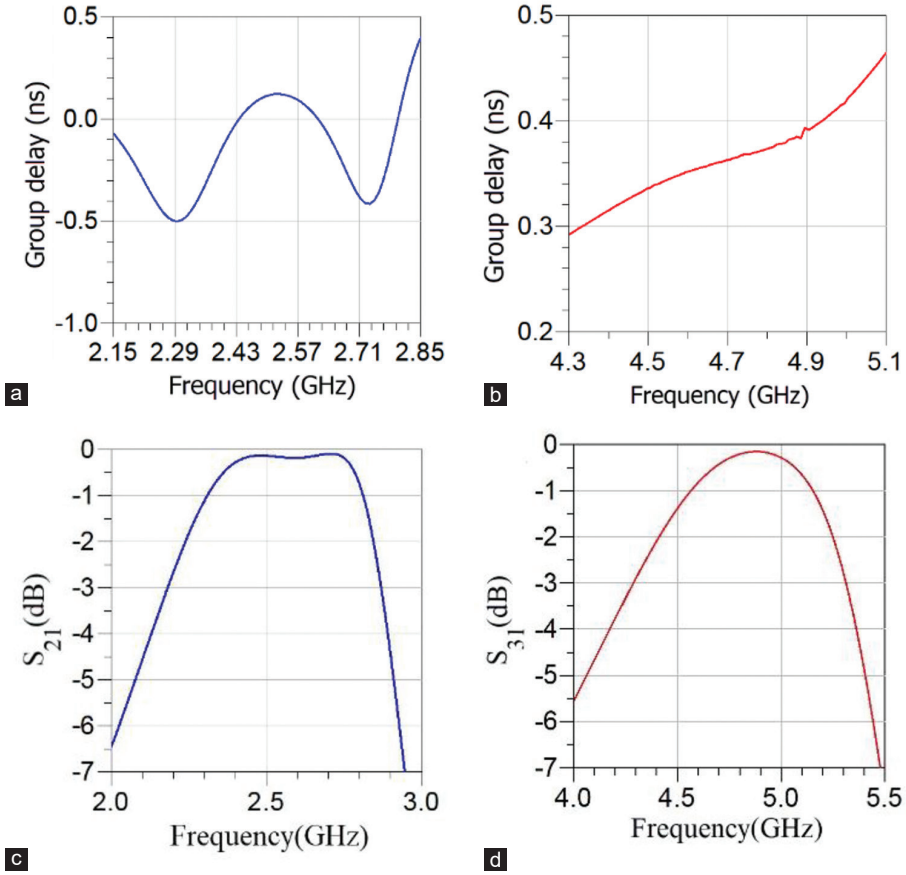

Fig. 5. (a) Simulated group delay of the first band, (b) simulated group delay of the second band (c) narrowband frequency response of S_{21}, (d) narrowband frequency response of S_{31}.

http//dx.doi.org/10.14500/aro.10753

TABLE I
COMPARISON BETWEEN THIS WORK AND THE PREVIOUSLY REPORTED MICROSTRIP DIPLEXERS

References	f_1, f_2 (GHz)	FBW_1, FBW_2	Area (λ_g^2)	IL_1, IL_2 (dB)	Last frequency with attenuated harmonics
This work	2.5, 4.7	28%, 17.9%	0.015	0.16, 0.15	10 GHz (4 ϕ_1)
Rezaei, Yahya and Jamaluddin, 2020	0.7, 1.8	12.5%, 4%	0.026	0.17, 0.30	4 GHz (5.1 ϕ_1)
Rezaei, Nouri and Mohammadi, 2019	2.8, 3.2	---	0.028	0.36, 0.44	3.5 GHz (1.2 ϕ_1)
Huang, et al., 2016	2.3, 2.7	6.1%, 5.8%	0.127	1, 0.9	4 GHz (1.7 ϕ_1)
Rezaei, et al., 2019a	1.6, 2.1	16.8%, 11%	0.054	0.10, 0.16	3.5 GHz (2.1 ϕ_1)
Jun-Mei, Zhou and Cao, 2016	1.8, 2.4	2.8%, 1.9%	0.064	2.2, 2.1	5 GHz (2.7 ϕ_1)
Peng and Chiang, 2015	1.7, 1.8	5%, 5%	0.07	2.1, 2.1	2.4 GHz (1.3 ϕ_1)
Rezaei, et al., 2019b	2.1, 3.9	---	0.038	0.25, 0.26	4.5 GHz (2.1 ϕ_1)
Salehi, et al., 2016	2.3, 2.5	3.6%, 3.4%	0.088*	0.5, 0.4	10 GHz (4.3 ϕ_1)
Rezaei and Noori, 2018	1.8, 2.4	11%, 7.1%	0.022	0.14, 0.16	6.5 GHz (3.6 ϕ_1)
Chen, 2015	1.1, 1.3	8%, 9.2%	0.705	1.83, 1.52	1.6 GHz (1.4 ϕ_1)
Xiao, et al., 2015	2.4, 3.5	---	0.282	1.43, 1.59	5 GHz (2 ϕ_1)
Noori and Rezaei, 2017a	2.3, 4	---	0.09*	0.2, 0.4	8 GHz (3.4 ϕ_1)
Rezaei, Noori and Mohamadi, 2017	2.4, 2.7	---	0.075	0.18, 0.39	5 GHz (2 ϕ_1)
Noori and Rezaei, 2017b	2.6, 6	---	0.076*	0.6, 0.9	7 GHz (2.6 ϕ_1)
Bui, et al., 2017	1.8, 2.4	---	0.095	0.4, 0.4	3 GHz (1.6 ϕ_1)
Guan, et al., 2014	1.9, 2.1	3.5%, 3.2%	0.136	1.2, 1.5	2.5 GHz (1.3 ϕ_1)
Bukuru, Song and Xue, 2015	3.6, 5.2	8.2%, 7.6%	0.05	1.35, 1.31	13 GHz (3.6 ϕ_1)
Velidi, et al., 2012	2.07, 2.3	---	0.018	1.65, 2.25	>3 GHz (1.45 ϕ_1)*
Bao, et al., 2010	0.9, 1.16	---	---	4.8, 4.9	>1.75 GHz (1.95 ϕ_1)*

Approximated values

TABLE II
THE MAXIMUM GROUP DELAY OF THIS WORK IN COMPARISON WITH THE PREVIOUSLY REPORTED MICROSTRIP DIPLEXERS AND FILTERS

References	Type	Number of channels	Maximum group delay (ns)
This work	Diplexer	2	0.4
Rezaei, et al., 2019a	Diplexer	2	2.6
Rezaei, et al., 2019b	Diplexer	2	4
Rezaei and Noori, 2018	Diplexer	2	3.14
Noori and Rezaei, 2017b	Diplexer	2	3
Sarkar, Ghatak and Poddar, 2011	Filter	2	2.5
Liu, 2010	Filter	3	8
Wibisono, Firmansyah and Syaφraditya, 2016	Filter	3	3.67
Lin, 2011	Filter	4	8

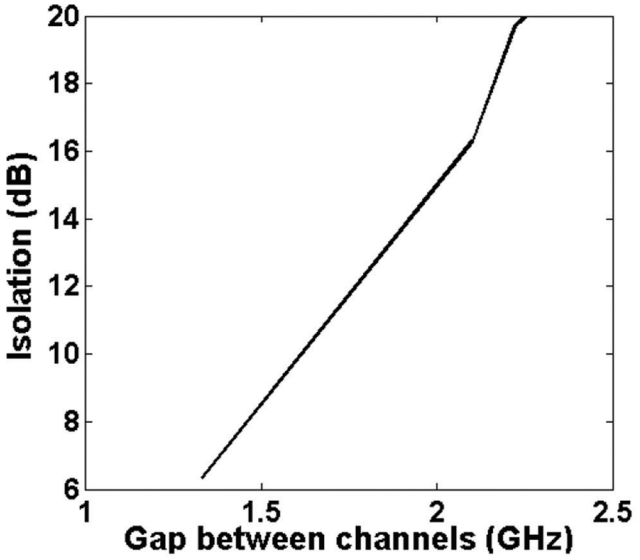

Fig. 6. Isolation of the proposed diplexer as a function of the channels spacing.

IV. CONCLUSION

A microstrip diplexer with compact size, wide fractional bandwidths (FBWs), low group delays, low insertion losses, and attenuated harmonics was designed in this work for wireless applications. Using the even and odd modes analysis of an introduced equivalent *LC* circuit, the significant microstrip sections that affect the frequency response of the proposed resonator were identified. As a result, for a predetermined angular resonance frequency, we could select the dimensions and space between the coupled sections. We obtained some information about the behavior of the introduced resonator by analyzing the proposed equivalent *LC* circuit. This information led to better optimization so that we could decrease the overall size of the proposed structure. Therefore, the proposed diplexer has a very compact area of 0.015 λ_g^2. By tuning the dimensions of the feed structures, we could improve the insertion losses, where they are better than 0.2 dB at both channels. These features were obtained whereas the isolation between channels and return losses at both channels are acceptable.

REFERENCES

Bao, Z., Chen, J., Lim, E.H. and Xue, Q., 2010. Compact microstrip diplexer with differential outputs. *Electronics Letters*, 46(11), pp.766-768.

Bui, D.H.N., Vuong, T.P., Allard, B., Verdier, J. and Benech, P., 2017. Compact low-loss microstrip diplexer for RF energy harvesting. *IET Electronic Letters*, 53(8), pp.552-554.

Bukuru, D., Song, K. and Xue, Q., 2015. Compact wide-stopband planar diplexer based on rectangular dual spiral resonator. *Microwave and Optical Technology Letters*, 57(1), pp.174-178.

Chen, D., Zhu, L., Bu, H. and Cheng, C.H., 2015. A novel planar diplexer using slot line-loaded microstrip ring resonator. *IEEE Microwave and Wireless Components Letters*, 25(11), pp.706-708.

Guan, X., Yang, F., Liu, H. and Zhu, L., 2014. Compact and high-isolation diplexer using dual-mode stub-loaded resonators. *IEEE Microwave and Wireless Components Letters*, 24(6), pp.385-387.

Huang, F., Wang, J., Zhu, L. and Wu, W., 2016. Compact microstrip balun diplexer using stub-loaded dual-mode resonators. *IET Electronic Letters*, 52, pp.1994-1996.

Jahanbakhshi, M. and Hayati, M., 2016. Design of a compact microstrip lowpass filter with sharp roll-off using combined T-shaped and L-shaped resonators. *IET Electronic Letters*, 52(23), pp.1931-1933.

Jun-Mei, Y., Zhou, H.Y. and Cao, L.Z., 2016. Compact diplexer using microstrip half- and quarter wavelength resonators. *IET Electronic Letters*, 52(19), pp.1613-1615.

Lin, S.C., 2011. Microstrip dual/quad-band filters with coupled lines and quasi-lumped impedance inverters based on parallel path transmission. *IEEE Transactions on Microwave Theory and Techniques*, 59(8), pp.1937-1946.

Liu, Y., 2010. A tri-band bandpass filter realized using tri-mode T-shape branches. *Progress in Electromagnetics Research*, 105, pp.425-444.

Noori, L. and Rezaei, A., 2017a. Design of a microstrip dual-frequency diplexer using microstrip cells analysis and coupled lines components. *International Journal of Microwave and Wireless Technologies*, 9(7), pp.1467-1471.

Noori, L. and Rezaei, A., 2017b. Design of a microstrip diplexer with a novel structure for WiMAX and wireless applications. *AEU-International Journal of Electronics and Communications*, 77, pp.18-22.

Peng, H. and Chiang, Y., 2015. Microstrip diplexer constructed with new types of dual-mode ring filters. *IEEE Microwave and Wireless Components Letters*, 25(1), pp.7-9.

Rezaei, A. and Noori, L., 2018. Compact low-loss microstrip diplexer using novel engraved semi-patch cells for GSM and WLAN applications. *AEU-International Journal of Electronics and Communications*, 87, pp.158-163.

Rezaei, A., Noori, L. and Mohamadi, H., 2017. Design of a novel compact microstrip diplexer with low insertion loss. *Microwave and Optical Technology Letters*, 59(7), pp.1672-1676.

Rezaei, A., Nouri, L. and Mohammadi, H., 2019. Design of a miniaturized microstrip diplexer using coupled lines and spiral structures for wireless and WiMAX applications. *Analog Integrated Circuits and Signal Processing*, 98, pp.409-415.

Rezaei, A., Yahya, S.I. and Jamaluddin, M.H., 2020. A novel microstrip diplexer with compact size and high isolation for GSM applications. *AEU-International Journal of Electronics and Communications*, 114, p.153018.

Rezaei, A., Yahya, S.I., Noori, L. and Jamaluddin, M.H., 2019a. Design of a novel wideband microstrip diplexer using artificial neural network. *Analog Integrated Circuits and Signal Processing*, 101(1), pp.57-66.

Rezaei, A., Yahya, S.I., Noori, L. and Jamaluddin, M.H., 2019b. Design and fabrication of a novel compact low-loss microstrip diplexer for WCDMA and WiMAX applications. *Journal of Microwaves Optoelectronics and Electromagnetic Applications*, 18(4), pp.482-491.

Rezaei, A., Yahya, S.I., Nouri, L. and Jamaluddin, M.H., 2020. Design of a low-loss microstrip diplexer with a compact size based on coupled meandrous open-loop resonators. *Analog Integrated Circuits and Signal Processing*, 102, pp.579-584.

Sarkar, P., Ghatak, R. and Poddar, D.R., 2010. A dual-band bandpass filter using SIR suitable for WiMAX band. Vol. 6, In: *2011 Proceedings of the International Conference on Information and Electronics Engineering*, pp.70-74.

Salehi, M.R., Keyvan, S., Abiri, E. and Noori, L., 2016. Compact microstrip diplexer using new design of triangular open loop resonator for 4G wireless communication systems. *AEU-International Journal of Electronics and Communications*, 70(7), pp.961-969.

Velidi, V.K., Prabhakaran, U., Subramanyam, A.V.G., Sivareddy, D. and Srinivasan, V.V., 2012. Design of compact microstrip diplexer with high selectivity. In: *2012 Proceedings of the International Conference on Signal Processing and Communications*, *Bangalore*, pp.1-4.

Wibisono, G., Firmansyah, T. and Syafraditya, T., 2016. Design of triple-band bandpass filter using cascade tri-section stepped impedance resonators. *Journal of ICT Research and Applications*, 10(1), pp.43-56.

Xiao, J.K., Zhu, M., Li, Y., Tian, L. and Ma, J.G., 2015. High selective microstrip bandpass filter and diplexer with mixed electromagnetic coupling. *IEEE Microwave and Wireless Components Letters*, 25(12), pp.781-783.

Yahya, S.I., Rezaei, A. and Nouri, L., 2020a. Design and performance of microstrip diplexers: A review. *ARO-The Scientific Journal of Koya University*, 8(1), pp.38-49.

Yahya, S.I., Rezaei, A. and Nouri, L., 2020b. Design and fabrication of a high-performance microstrip multiplexer using computational intelligence for multi-band RF wireless communications systems. *AEU-International Journal of Electronics and Communications*, 120, p.153190.

http://dx.doi.org/10.14500/aro.10738

The Effects of Amine Type and Lean Amine Temperature on Gas Sweetening Processes: A Case Study and Simulation

Ribwar K. Abdulrahman[1] and Mohammed H. S. Zangana[2]

[1]Department of Chemical Engineering, Faculty of Engineering, Koya University, Daniel Mitterrand Boulevard, Koya KOY45 AB64, Kurdistan Region – F.R. Iraq

[2]Department of Petroleum Engineering, Faculty of Engineering, Koya University, Daniel Mitterrand Boulevard, Koya KOY45 AB64, Kurdistan Region – F.R. Iraq

***Abstract*—In the North Gas Company (NGC) in Kirkuk, Iraq, sour gas stream is loaded with considerable amounts of H_2S and CO_2 of 2.95% and 2.54%, respectively. A DEA amine system is currently used to reduce these sour component concentrations below 5 ppm and 2% for H_2S and CO_2, respectively. This study used Bryan Research and Engineering's ProMax® process simulation software to optimize this amine sweetening system by adopting other amine types and blends, such as methyldiethanolamine (MDEA). It could be argued that a 50 wt% MDEA solution circulated at 414 m^3/h was determined to be the optimum operating conditions. This design met sweet gas specifications and minimized the reboiler duty to 38 MW, 30.9% reduction in steam consumption. The experimental simulation work is also examined the effects of lean solvent temperature on the gas sweetening process efficiency and performance and find out that the lean amine temperature within the range of 43–48°C in all sceneries give acceptable sweetening results.**

***Index Terms*—Gas sweetening, Lean amine temperature, Mixed amine, Natural gas industry, North gas company, Process simulation.**

I. Introduction

The raw natural gas can contain significant amounts of sour components, for instance, H_2S and CO_2 after it is produced (Abdel-Aal, Aggour and Fahim, 2003). The "sour gas" must be treated, or "sweetened," before pipeline transport to lower the risk of corrosion in the presence of water, lower toxicity from H_2S, and to increase the heating value reduced by CO_2 (Stewart and Arnold, 2011). In fact, chemical solvent absorption remains the most widely adopted technology (Sorensen, 2018).

ARO-The Scientific Journal of Koya University
Vol. VIII, No.2 (2020), Article ID: ARO.10738, 4 pages
DOI:10.14500/aro.10738
Received: 10 October 2020; Accepted: 12 December
Regular research paper: Published: 19 December 2020
Corresponding author's e-mail: ribwar.abdulrahman@koyauniversity.org

The most common form of natural gas sweetening is the use of alkanolamines in solution as a chemical solvent to absorb and remove sour gas components (Wang and Economides, 2013).

Amine molecules are similar to ammonia molecules (NH_3) with one or several of the hydrogen atoms replaced with a substituent (Bryan Research & Engineering, LLC, 2020). Amines can be classified as primary, secondary, or tertiary depending on the number of hydrogen atoms (Fig. 1).

The following chemical reaction sets show the significant interactions of amines with H_2S and CO_2 during the sweetening process (Maddox and Morgan, 1998):

H_2S:

$$H_2S \leftrightarrow H^+ + HS^- \quad (1)$$

$$HS^- \leftrightarrow H^+ + S^{2-} \quad (2)$$

$$H^+ + RH_2N \leftrightarrow RH_2NH^+ \quad (3)$$

CO_2 with primary mines:

$$CO_2 + H_2O \leftrightarrow H^+ + HCO_3^- \quad (4)$$

$$HCO_3^- + RH_2N \leftrightarrow RHNCOO^- + H_2O \quad (5)$$

$$CO_2 + RH_2N \leftrightarrow RHNCOO^- + H^+ \quad (6)$$

$$H^+ + RH_2N \leftrightarrow RH_2NH^+ \quad (7)$$

CO_2 with tertiary amines:

$$CO_2 + H_2O \leftrightarrow H^+ + HCO_3^- \quad (4)$$

$$H^+ + R_3N \leftrightarrow R_3NH^+ \quad (8)$$

Examples of primary, secondary, or tertiary amines are MEA, DEA, and MDEA, respectively.

Indeed, the amine type may consider an important factor in the gas sweetening process (Abdulrahman, et al., 2017). However, other parameters such as lean amine temperature

are also important to be examined as the parameter that used to control the absorber temperature (Sarker, 2016). In fact, the lean amine temperature might affect several factors, for example, the loading of acid gases by the lean amine (acid gases continent in sweet gas stream/ overhead), foaming that could be caused by impurities contents in the rich amine solution, for instance, condensate hydrocarbons, hydrate formation, and amine pump duty (Bryan Research and Engineering, Inc.- Technical Papers, 2020).

II. Amine Process at North Gas Company

The North Gas Company (NGC) processes the most of the associated gas in Iraq's northern oil fields. The studied NGC system in the Kirkuk Field (Fig. 2) uses a standard configuration for amine gas sweetening with an absorption section (left) and the regeneration section (right).

Absorption section: Sour gas comes in contact with the amine solution in the absorber column. Sour components are removed in the following way:

a. The bulk removal of the acid gas occurs in the bottom absorber sections where the column temperature is highest. This is commonly referred to as the absorption column's "temperature bulge."
b. The final purification, or polishing, occurs midway through the column height.
c. The column's top acts as a water wash section to prevent amine carry-over into the exiting sweet gas stream. This lost amine increases operational costs and can cause damage in following dehydration units.

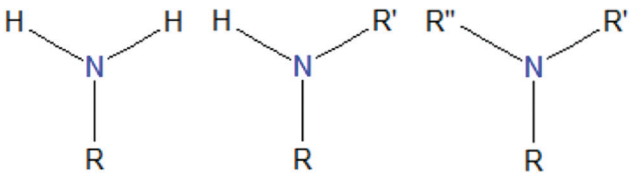

Fig. 1. Primary (left), secondary (middle), and tertiary (right) amine.

Regeneration section: Rich amine solution exits the bottom of the absorber and enters the regeneration column. Steam is used to strip the sour components from the amine solution. The lean amine solution is drawn from the regenerator's bottom and circulated back to the absorption column. The H_2S and CO_2 stream, or "Acid Gas" stream, exits the column's top and is sent to a sulfur recovery unit.

III. *NGC Gas Composition*

NGC gas stream compositions and operating conditions are shown in Tables I and II, respectively. Hexanes plus (C6+) were modeled as the n-Hexane component.

TABLE I
NGC dry basis natural gas compositions

Component	Mole%
H_2S	2.95
CO_2	2.54
Methane	71.56
Ethane	12.83
Propane	6.48
i-Butane	0.83
n-Butane	1.61
i-Pentane	0.51
n-Pentane	0.46
C_6+	0.23

TABLE II
Operation conditions (NGC)

North Gas Company (NGC) Kirkuk	
Sample No.	Stream 1000
Sample type	Natural gas
Flow rate	334.783 MMSCFD
Pressure	27.5 bar
Temperature	42 °C
DEA	28.55 wt%
DEA circulation rate	800 m^3/h
Reboiler duty	55 W

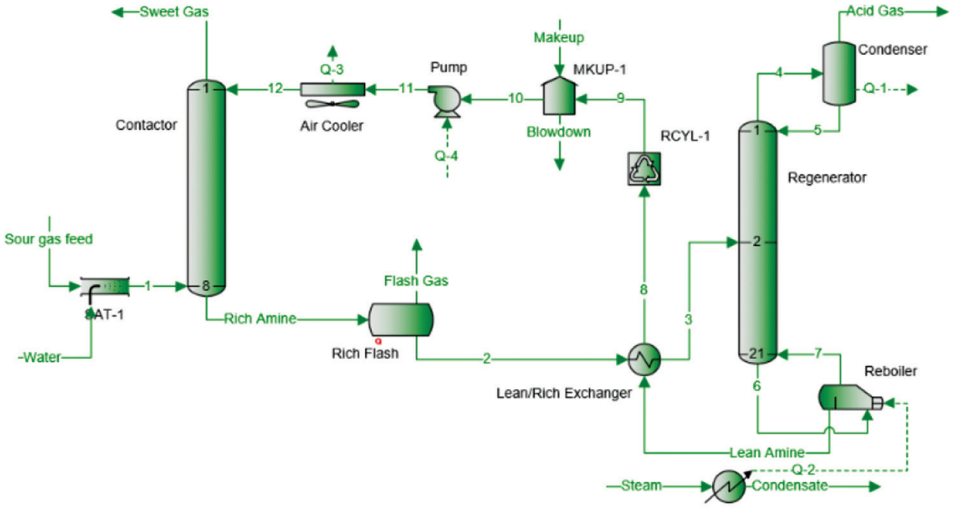

Fig. 2. ProMax® simulation of NGC amine sweetening process.

http://dx.doi.org/10.14500/aro.10738

IV. Results and Discussion

The current NGC amine gas sweetening plant is simulated using ProMax simulator V. 5. The DEA and MDEA are utilized as an aqueous absorbent to absorb acid gases from the sour gas stream. The process simulation can be done by providing the ProMax program by gas stream compositions and operation conditions from Tables I and II, respectively, and choosing amine fluid package. The installing of an inlet gas separator is an important step (Shooshtari and Shahsavand, 2013). Moreover, an amine absorber tower is also an important unit of the sweetening process and it also needs some specifications, for instance, streams temperature and pressure. Furthermore, rich amine requires to bring regenerated and that can be done by installing an amine regenerator tower (Davoudi, et al., 2014). Furthermore, the installing a flash tank for rich amine may be very useful to avoid any technical problems that might be caused by rich amine impurities. Furthermore, water makeup stream should be added with a mixer to the process. Amine concentration may be built up in the process because of water losses with sweet gas (Poe and Mokhatab, 2017). Water makeup stream will maintain the amine solution concentration during the sweetening process.

An optimization study was performed on the NGC amine sweetening unit to determine the amine type and blend that minimizes the system's energy consumption. Three different amine solvent scenarios were evaluated:

1. 28.55 wt% DEA
2. 30 wt% MDEA and 10 wt% DEA
3. 50 wt% MDEA

1) Scenario 1: 28.55 wt% DEA

The first scenario represents the current operating conditions of the NGC amine system. Fig. 3 shows the relationship between the circulation rate of the 28.55 wt% DEA solvent solution and sweet gas H_2S and CO_2 concentrations. It could be argued that using of 28.55 wt% DEA at a circulation rate of 800 m^3/h is met the gas pipeline specifications in terms of H_2S and CO_2 concentrations.

The study also examined the effect of lean amine temperature on the sweetening process efficiency in the first process optimization scenario which is 28.55wt% DEA. Fig. 4 shows the relationship between the lean amine temperature of the 28.55 wt% DEA solvent solution and sweet gas H_2S and CO_2 concentrations. It is clear from Fig. 4 that the optimum value of lean amine temperature for the current scenario of amine type is 43°C.

2) Scenario 2: 30 wt% MDEA & 10 wt% DEA

Fig. 5 shows that the 30 wt% MDEA and 10 wt% DEA amine blend are able to achieve sweet gas specifications at a 510.5 m^3/h circulation rate and a 46.9 MW reboiler duty.

The study is also examined the effect of lean amine temperature on the sweetening efficiency process in the second process optimization scenario: 30 wt% MDEA and 10 wt% DEA mixture. Fig. 6 shows the relationship between the lean amine temperature of the 30 wt% MDEA and 10 wt% DEA amine blend solvent solution and sweet gas H_2S and CO_2 concentrations. As it is shown in Fig. 6, the optimum value of lean amine temperature for the 30 wt% MDEA and 10 wt% DEA mixture amine is 42°C.

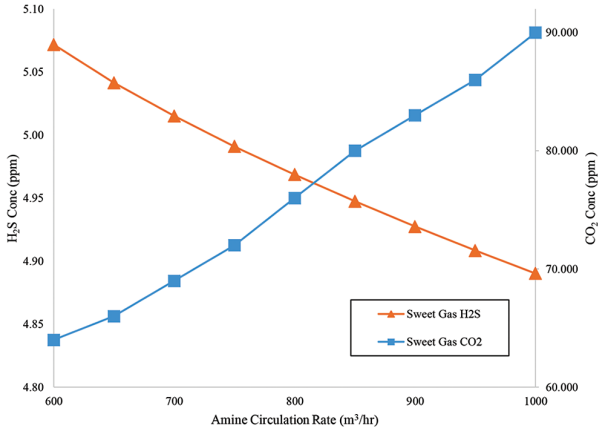

Fig. 3. H_2S and CO_2 removal with 28.55 wt% DEA.

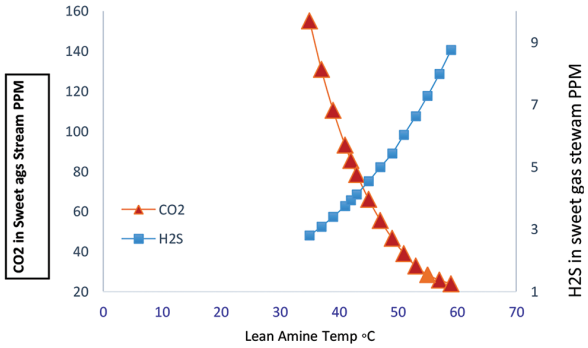

Fig. 4. The relationship between the lean amine temperature rate and the H_2S and CO_2 removal with 28.55 wt% DEA at 800 m^3/h DEA circulation rate.

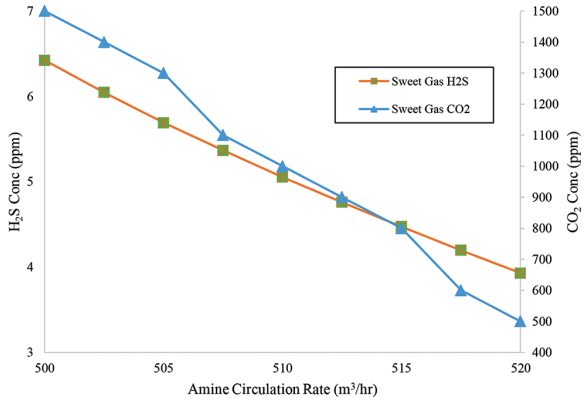

Fig. 5. H_2S and CO_2 removal with 30 wt% MDEA and 10 wt% DEA mixture.

3) Scenario 3: 50 wt% MDEA

The 50 wt% MDEA solution had the best performance of the three scenarios (Fig. 7). The 50% MDEA scenario met the sweet gas specifications at a solvent circulation rate of 414 m^3/h and a 38 MW reboiler duty.

The study also examined the effect of lean amine temperature on the third process optimization scenario which is 50 wt% MDEA. Fig. 8 shows the relationship between the lean amine temperature of the 50 wt% MDEA solvent

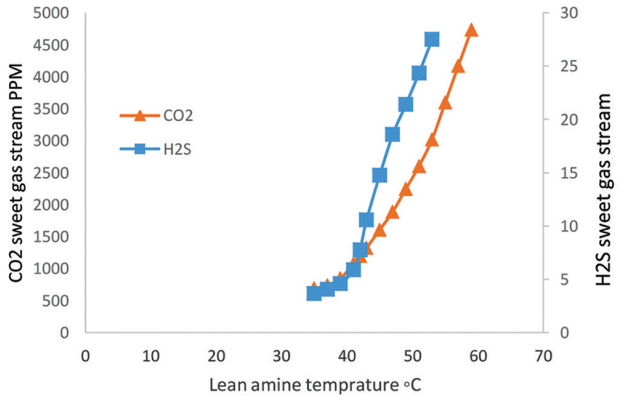

Fig. 6. The relationship between the lean amine temperature rate and the H_2S and CO_2 removal with 30 wt% MDEA and 10 wt% DEA mixture at a 510.5 m^3/h circulation rate.

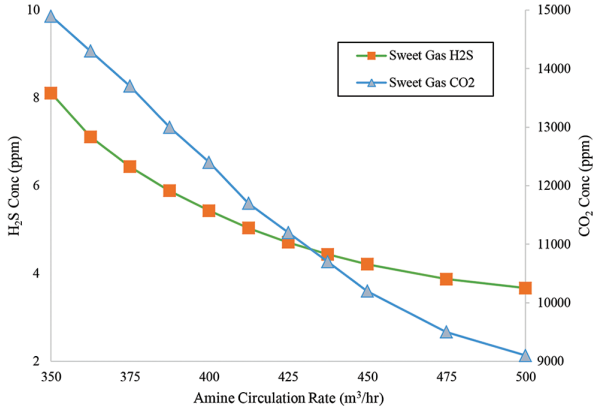

Fig. 7. H2S and CO2 removal with 50 wt% MDEA.

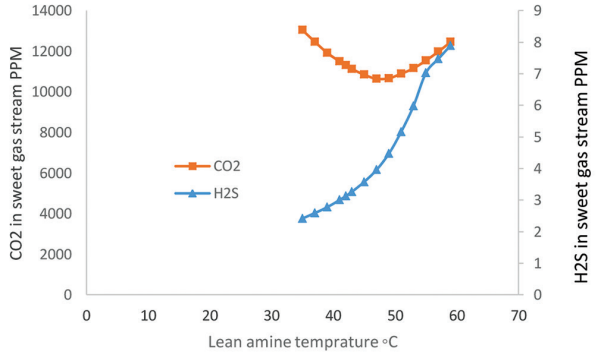

Fig. 8. The relationship between the lean amine temperature rate and the H_2S and CO_2 removal with 50 wt% MDEA at a 414 m^3/h circulation rate.

solution and sweet gas H_2S and CO_2 concentrations. It is clear from Fig. 8 that the optimum value of lean amine temperature for the 50 wt% MDEA is 45°C.

V. Conclusions

ProMax® was able to accurately model and optimize the amine system used by NGC. This work showed how the use of MDEA, can selectively absorb H_2S over CO_2 compare to DEA, a secondary amine. This was shown as required circulation rates and reboiler duties decreased with increasing MDEA concentrations. This study found that steam consumption could be reduced by 30.9% by changing from 28.55% DEA solvent to 50% MDEA solvent. Thus, it could be argued that a 50 wt% MDEA solution circulated at 414 m3/h was determined to be the optimum operating conditions. Moreover, the current study showed that the lean amine temperature also contributes to the sweetening process efficiency and performance. It can be stated that the lean amine temperature had a visible impact at all the three scenarios studied in the current work. It found that adopting lean amine temperature within the range of 43–48°C in all sceneries gives acceptable sweetening results.

Acknowledgment

The authors wish to highly acknowledge Bryan Research & Engineering, LLC, for providing the license of ProMax® process simulation software to Koya University and their continued support during the current work. The North Gas Company (NGC) also highly acknowledged for providing the necessary data for the present study, especially the help and support received from Mr. Khasraw Salih, the director of energy department at North Gas Company.

References

Abdel-Aal, H., Aggour, M. and Fahim, M., 2003. *Petroleum and Gas Field Processing*. Marcel Dekker, New York.

Abdulrahmanm, R.K., Zangana, M.H.S., Ali, K.S. and J.C. Slagle., 2017. *Utilizing Mixed Amines In Gas Sweetening Process: A Kirkuk Field Case Study And Simulation IEEE Conference Publication*. Available from: https://www.ieeexplore.ieee.org/document/8267616. [Last accessed on 2020 Dec 09].

Bre.com. 2020. Available from: https://www.bre.com/pdf/using-mixed-amine-solutions-for-gas-sweetening.pdf. [Last accessed on 2020 Feb 22].

Bre.com. 2020. *Bryan Research and Engineering, LLC*. Available from: https://www.bre.com. [Last accessed on 2020 Feb 14].

Davoudi, M., Safadoust, A., Mansoori, S.A. and Mottaghi, H., 2014. The impurities effect on thermal degradation and corrosivity of amine solution in South Pars gas sweetening plants. *Journal of Natural Gas Science and Engineering*, 19, pp.116-124.

Maddox, R. and Morgan, D., 1998. *Gas Conditioning and Processing*. Campbell Petroleum Series, Norman, Okla.

Poe, W. and Mokhatab, S., 2017. *Modeling, Control, And Optimization Of Natural Gas Processing Plants*. Gulf Professional, Amsterdam.

Sarker, N., 2016. Theoretical effect of concentration, circulation rate, stages, pressure and temperature of single amine and amine mixture solvents on gas sweetening performance. *Egyptian Journal of Petroleum*, 25(3), pp.343-354.

Shooshtari, S.R. and Shahsavand, A., 2013. Reliable prediction of condensation rates for purification of natural gas via supersonic separators. *Separation and Purification Technology*, 116, pp.458-470.

Sorensen, E., 2018. *Chemical Engineering Research and Design*. 1st ed. Institution of Chemical Engineers, London.

Stewart, M. and Arnold, K., 2011. *Gas Sweetening And Processing Field Manual*. Elsevier, Gulf Professional, Amsterdam.

Wang, X. and Economides, M., 2013. *Advanced Natural Gas Engineering*. Elsevier Science, Burlington.

http//dx.doi.org/10.14500/aro.10761

New Fluorescence Quenching Approach for Determination of Valsartan in Certain Tablets and Spiked Biological Fluids

Layth I. Abd Ali

Department of Chemistry, Faculty of Science and Health, Koya University,
Daniel Mitterrand Boulevard, Koya KOY45 AB64, Kurdistan Region – F.R. Iraq

***Abstract*—A new, simple, selective, sensitive, fast, economical, and reliable fluorescence quenching method for the quantitation of valsartan was investigated using basic fuchsin act as a fluorometric dye. The method was depended on the detection quenching influence of valsartan on the fluorescence intensity of basic fuchsin and the reaction between valsartan and basic fuchsin in a McIlvaine buffer medium at pH = 6 to yield a new basic fuchsin–valsartan non-fluorescent complex. The excitation and emission of basic fuchsin fluorescence signal were identified at 535 and 728 nm, respectively. A fluorescence quenching value (ΔF) displayed a very good linear relationship ($R^2 = 0.9992$) with valsartan concentration ranging from 0.003 to 3 μg/mL, a detection limit as low as 0.0009 μg/mL with a high precision and accuracy (RSD% <3). Significantly, no interference effect was found due to the presence of other ingredients commonly found in medical formulations. The acquired data were statistically compared with those acquired from reported chromatographic method and were observed to be in excellent agreement at a 95% confidence level; the planned fluorescence quenching procedure was subsequently utilized to detected the concentration of valsartan in spiked biological fluids and commercial medical tablets.**

***Index Terms*—Basic fuchsin, Fluorescence quenching, Pharmaceutical analysis, Valsartan.**

I. Introduction

In recent years, cardiovascular diseases have begun to be recognized as the principal causes of death in the majority of countries worldwide (Kaabipour, et al., 2020). Cardiovascular diseases are associated with heart failure, ischemic heart disease, rheumatic heart disease, cerebrovascular disease, coronary heart disease, high cholesterol levels, and high blood pressure (Kumar, et al., 2015). High blood pressure is classified as a principal reason for an array of cardiovascular diseases. The control and treatment of higher blood pressure are significant in the avoidance of the effects of cardiovascular diseases (Shah, et al., 2017).

Valsartan is taken by mouth as well as highly active is a non-peptide angiotensin II receptor antagonist and potentials through preventing the actions of angiotensin II, beside a high ability to suppress the type I angiotensin receptor (Azadi and Ahmadi, 2019), so is utilized as an antihypertensive drug (Gadepalli, et al., 2014; Shah, et al., 2017). Chemically, Valsartan is labeled as"*N*-(1-oxopentyl)-*N*-[[2′-(1H-tetrazol-5-yl)[1,1′-biphenyl]-4-yl]methyl]-L-aline"($C_{24}H_{29}N_5O_3$) (Gadepalli, et al., 2014; Qader, Salih and Tahir, 2018), as shown in Fig.1.

In a review of associated scientific articles, numerous previous analytical methods have been developed and used for the quantitation of valsartan in samples containing biological fluids and pharmaceutical products. Published methods involve the separation and determination of valsartan by various analytical approaches either with or without other drugs such as high-performance liquid chromatography (HPLC) through different detectors such as UV detectors (Kumar, et al., 2015; Pebdani, et al., 2016; Babarahimi, et al., 2018; Shaikh, et al., 2020; Marghany, et al., 2020), fluorescence detection (Macek, Klima and Ptacek, 2006; del Rosario Brunetto, et al., 2009), as well as diode-array detection (Farajzadeh, Khorram and Pazhohan, 2016); a modern class of separation system based on "ultra-high-performance liquid chromatography" (UPLC) (Krishnaiah, et al., 2010; Vojta, et al., 2015; Moussa, et al., 2018); liquid chromatography–tandem mass spectrometry (LC–MS/MS) (Selvan, et al., 2007, Koseki, et al., 2007 , Annadi, El Sheikh and Mohamed, 2019); electroanalytical voltammetry methods (Eisele, et al., 2014; Mansano, et al., 2015); and UV-vis spectrophotometry (Satana, et al., 2001; Erk, 2002; Lotfy, et al., 2015; Eissa and Abou Al Alamein 2018; Meselhy, et al., 2020; Kamal, Marie and Hammad 2020). As well the fluorescence determination of valsartan, several procedures have been described in previous articles for its determination were including native fluorescence, a first derivative fluorescence and the synchronous fluorescence (Cagigal, et al., 2001; Shaalan and Belal, 2010; El-Shaboury, et al., 2012; El-Kosasy, et al., 2015; Dinc, Ertekin and Buker, 2017; Ragab, et al., 2017).

ARO-The Scientific Journal of Koya University
Vol. VIII, No.2 (2020), Article ID: ARO.10761, 9 pages
DOI:10.14500/aro.10761
Received: 03 November 2020; Accepted: 20 December 2020
Regular research paper: Published: 27 December 2020
Corresponding author's e-mail: layth.imad@koyauniversity.org

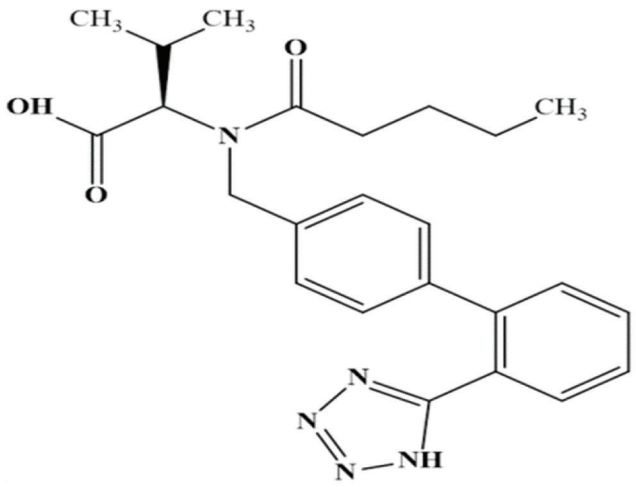

Fig. 1. Chemical structure of valsartan.

Basic fuchsin dye is recognized as a member of triphenylmethane group, with a chemical formula of $C_{20}H_{20}ClN_3$; it is also known as Magenta II because it is also known as Magenta II because it is a mix of pararosaniline, rosaniline, as well as Magenta II dyes. Fuchsin itself is inflammable, as well as having various properties such as being bactericidal, fungicidal and an anesthetic. It is commonly employed as coloring reagent for different industrial products such as textile, leather, fibers, paper, and cotton; it can also be used to stain collagen, muscle, mitochondria, and the tubercle bacillus (Pathrose, et al., 2014; Pathrose, et al., 2014; Pathrose, et al., 2016; Graham, et al. 2017; Ning, et al., 2018).

To the best of our knowledge, basic fuchsin has not been applied before for the analysis of drugs. In the current paper, a new quenching spectrofluorimetric procedure has been developed for the quantitative analysis of valsartan employing basic fuchsin as a fluorescence reagent. The developed method is simple, inexpensive, accurate, selective, and highly sensitive. It was applied for the determination of valsartan in pharmaceutical tablets and spiked biological fluids. Furthermore, the experimental conditions for an advanced spectrofluorimetric method were optimized.

II. Experimental

A. Apparatus

The fluorescence spectra and measurements were carried out using a Cary Eclipse fluorescence spectrophotometer (Agilent Technologies, USA) equipped with a xenon flash lamp, where the slit width was fixed at 5 nm. All fluorescence measurements were achieved in 1 cm quartz cell. The pH of the buffer systems was determined through an S-25 pH meter (Wincom Company Ltd., China).

B. Chemicals and Reagents

Valsartan standards were provided from Awamedica Drugs Company, Erbil-K. R. of Iraq, where a standard solution of 1 mg/mL was prepared by dissolving 50 mg of standard valsartan powder in 50 mL ethanol (Merck, Germany) with carefully mixing, and was subsequently stored in a refrigerator. Every day, working standard solutions of valsartan were prepared using the appropriate dilution of the standard solution with ethanol.

Basic fuchsin was purchased from Sigma-Aldrich, USA. Solutions of basic fuchsin were prepared at a concentration of 5×10^{-4} mol/L by dissolving 8.4 mg of basic fuchsin in 50 mL ethanol (Merck, Germany).

According to a previous procedure reported (El-Kosasy, et al., 2015), diverse buffer systems with pH values ranging from 1 to 11 were prepared, respectively. For pH 1, the standard Citrate buffer solution was created through 0.1 mole/L sodium citrate (Sigma-Aldrich, USA), then regulated for desired pH using 0.1 mole/L hydrochloric acid (Sigma-Aldrich, USA). For a pH scale between 2 and 8, the standard McIlvaine buffer solutions were preparation by mixing numerous volumes from 0.2 mol/L disodium hydrogen phosphate solution (Merck, Germany) as well as 0.1 mol/L citric acid solution (Merck, Germany). For a pH scale between 11 to 9, borate buffer solutions were created, by mixing several volumes from 0.1 mol/L sodium hydroxide solution (Sigma-Aldrich, USA) with several volumes of 0.05 mol/L sodium tetraborate solution (Sigma-Aldrich, USA).

All reagents and solvents were of extra pure grade. Valsartan tablets, Diovan® (Novartis International AG. Switzerland), Valsartan Awa® (Awamedica Drugs Company, Erbil-K. R. of Iraq), and Arbiten® (JOSWE medical. Jordan) containing 160 mg of active ingredient were purchased from a local pharmacy.

C. Sample Preparation

Ten tablets from three different brands of pharmaceutical products were carefully weighed, ground, and mixed to produce appropriate powders, after which exact weights of powders were placed in 50 mL volumetric flasks and dissolved using 40 mL of ethanol and sonication for 15 min. The solutions so obtained were filtrated by Whatman® quantitative filter paper, ashless, Grade 41 (Merck, Darmstadt, Germany), before washing and diluting to 50 mL using ethanol.

D. Procedure for Spiked Urine and Serum Samples (Gong and Zhu, 2013)

Initially, the drug-free serum and urine samples were obtained from Rizgary Hospital (Erbil-K. R. of Iraq) and kept at −20°C until analysis and thawed to lab temperature before use. The serum and urine samples were individually diluted by 1000- and 500-fold using deionized water. A 1 mL serum or urine sample was spiked with an appropriate concentration of valsartan standard solution, giving final valsartan concentrations of 0.5, 1, and 3 μg/mL.

E. Recommended Procedure

To detect a content of valsartan, 1.5 mL basic fuchsin (5×10^{-4} mol/L), 2 mL McIlvaine buffer solution (pH 6), and Aliquot volumes of the working standard or sample solutions over concentration range 0.003–3 μg/mL of

http//dx.doi.org/10.14500/aro.10761

valsartan were diluted to 10 mL, then mixed thoroughly for 15 min at lab temperature. The fluorescence intensity of basic fuchsin was recorded versus a blank solution at an excitation wavelength of 535 nm as well as emission at 728 nm.

III. Results and Discussion

A. Quenching Excitation and Emission Spectra of Basic Fuchsin with Valsartan

Basic fuchsin has high native fluorometric signal with excitation/emission wavelengths of 535/728 nm (Fig. 2a), whereas valsartan does not appear to have any fluorescence emission properties. Furthermore, under experimental conditions the fluorescence spectra of basic fuchsin were acquired from reaction with a 1 μg/mL concentration of valsartan (Fig. 2b). From Fig. 2, it can be observed that the fluorescence signal of basic fuchsin was quenched rapidly when a drug was added though no change to both the position and shape of the emission peak. The acquired data showed that there was an interaction between valsartan and basic fuchsin. Hence, basic fuchsin could be used as a quenching fluorescent reagent for spectrofluorimetric determination of valsartan.

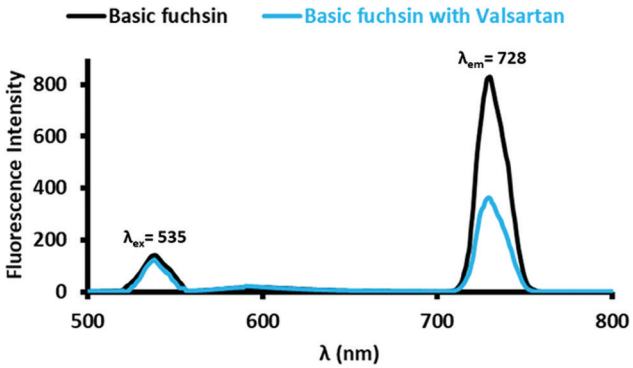

Fig. 2. Fluorescence excitation as well emission spectra of (a) Basic fuchsin (5 × 10−5 mol/L). (b) Basic fuchsin (5 × 10−5 mol/L) in the presence of valsartan (1 μg/mL), McIlvaine buffer solution (pH 6).

B. Influence of the Type and Volume Buffer Systems

The influence of the buffer solutions from pH = 1 to 11 on fluorescence quenching (ΔF) was assessed. For pH1 was utilized citrate buffer solution, whereas for the pH range 2–8 was used McIlvaine buffer solutions, finally for the pH range 9–11 was used borate buffer solutions. The acquired data exhibited that the ΔF reached a maximum value when the McIlvaine buffer (pH 6) solution was used (Fig. 3a). The McIlvaine buffer and pH 6 were selected as optimum values for further studies. From Fig. 3b, it can be seen that ΔF reached a maximum when the volume of buffer solution was 2 mL; accordingly, a 2 mL volume of McIlvaine buffer medium was nominated as the best volume for the optimized fluorescence method.

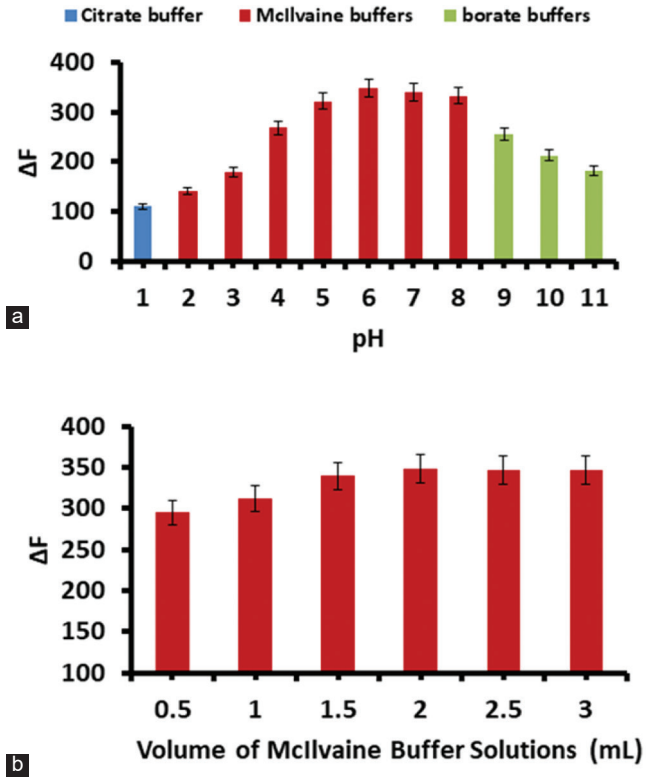

Fig. 3. Influences of (a) various buffer systems on fluorescence quenching (ΔF). (b) McIlvaine buffer volume on fluorescence quenching (ΔF) of the Basic fuchsin (5 × 10−5 mol/L) in the presence of valsartan (1 μg/mL).

C. Influence of Basic Fuchsin Concentration

The influence of different concentrations of basic fuchsin reagent (1, 2, 3, 4, 5, and 6 × 10^{-5} mol/L) on fluorescence quenching (ΔF) signal was determined. The fluorescence quenching was maximum signal after the molar concentration of basic fuchsin = 5 × 10^{-5} mol/L (Fig. 4); hence, this molar concentration was selected for following optimization tests.

D. Influence of the Time Reaction

The optimized reaction time was investigated by following the fluorescence intensity at 728 nm at lab temperature. From Fig. 5, it was determined that the complex formed and was stabilized after 5 min of mixing, and the associated fluorescence quenching, ΔF, remained stable for at least 150 min.

E. Fluorescence Quenching Spectrum and the Standard Calibration Curve for Determination of Valsartan

Under optimum experimental conditions, the fluorescence quenching value, ΔF, of the basic fuchsin reactions with different concentrations of valsartan (0.003–3 μg/mL) were determined. From Fig. 6a, it can be observed that fluorescence quenching decreased progressively with increase of valsartan concentrations in the solution, in a manner proportional to the concentration of the valsartan. Thus, basic fuchsin can be used to determine the concentration of valsartan.

Under optimum fluorescence experimental conditions, a standard calibration curve was created using various external standard concentrations (Fig. 6b). The correlation coefficient was 0.9992, demonstrating excellent linearity

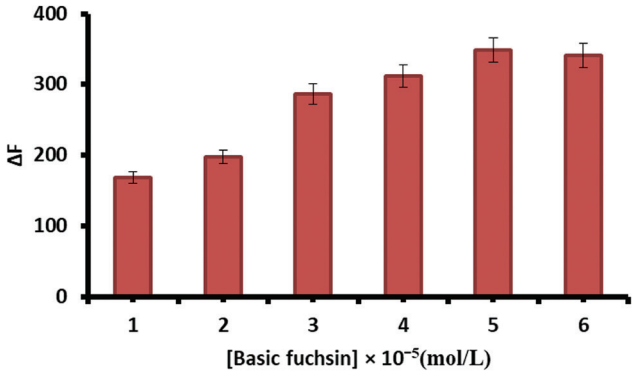

Fig. 4. Influence of various molar concentrations of basic fuchsin (1, 2, 3, 4, 5, and 6 × 10−5 mol/L) on fluorescence quenching (ΔF) in the presence of valsartan (1 µg/mL), McIlvaine buffer solution (pH 6).

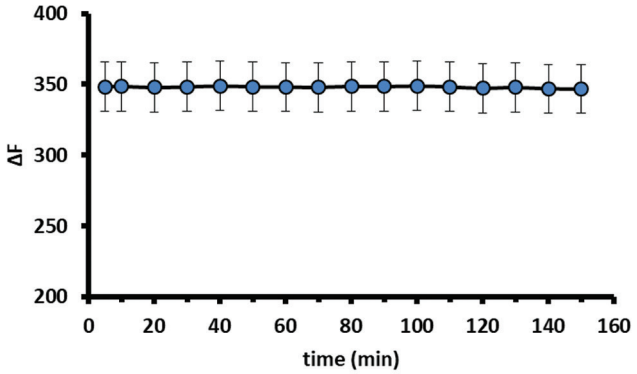

Fig. 5. Influence of the time reaction on fluorescence quenching (ΔF) of basic fuchsin (5 × 10−5 mol/L) in the presence of valsartan (1 µg/mL), McIlvaine buffer solution (pH 6).

over a concentration range of 0.003–3 µg/mL, as achieved through the equation ΔF = 104.6 C_{VAL} (µg/mL) + 100.63. According to the "International Union of Pure and Applied Chemistry (IUPAC) principles," a detection limit (DL) term correspond with a formula (3.3 × SD_{blank} /F) and quantification limit (QL) term correspond with a formula (10 × SD_{blank}/F), respectively, wherein SD_{blank} represents a standard deviation of six blank determinations, whereas F represents a slope of the constructed calibration graph. From optimum quenching method, the DL value of valsartan was 0.0009, whereas the QL value of valsartan was 0.0028 µg/mL.

F. Selectivity of the Proposed Procedure

The selectivity of the planned fluorescence procedure was assessed through determining the standard solution of valsartan (1 µg/mL) in the presence of pharmaceutical tablet materials such as citric acid, glucose, sucrose, lactose, silica, and other coexisting ionic species, the results of which are displayed in Table I. It was established that the limit of the concentrations of pharmaceutical tablet excipients that could be tolerated should produce an error of < ± 4% in the analysis of the valsartan. Furthermore, these results

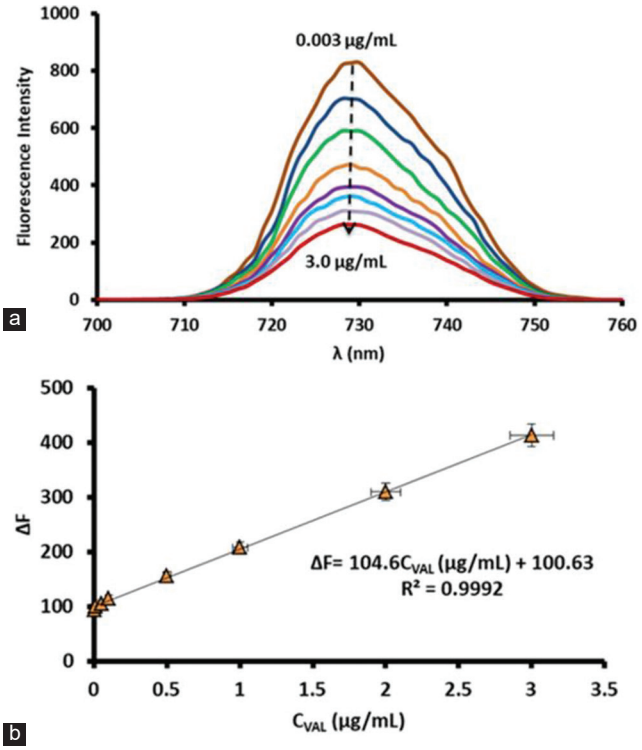

Fig. 6. (a) Influence of diverse standard concentrations of valsartan (0.003, 0.01, 0.05, 0.1, 0.5, 1.2, and 3 µg/mL) on a quenching signal (ΔF) of basic fuchsin (5 × 10−5 mol/L), McIlvaine buffer solution (pH 6). (b) Standard calibration graph for the spectrofluorometric determination of valsartan using basic fuchsin.

TABLE I
SELECTIVITY IN THE ANALYSIS OF VALSARTAN BY BASIC FUCHSIN

Tablet excipients species	Tolerance conc. (µg/mL)	Error [a]%
Citric acid	500	−3.10
Glucose	500	2.11
Sucrose	500	1.85
Lactose	500	−1.50
silica	500	1.34
Ca^{2+}	25	1.26
Mg^{2+}	100	1.47
Zn^{2+}	15	1.18
SO_4^{2-}	400	−1.83
CH_3COO^-	500	−1.66

[a]Average of five analyses

indicate no significant interference from that pharmaceutical tablet excipients and that the proposed procedure is highly selective.

G. Precision and Accuracy of the Proposed Procedure

Six measurements at three different concentrations of valsartan representing low, medium, and high concentrations from a range of the linearity were taken. The low value of the relative standard deviation percentage (RSD % < 3) points to high precision of the recommended procedure for quantitative measurements of the fluorescence quenching intensity of valsartan. Likewise, the very good percentage of recoveries of standard valsartan indicates the high accuracy of the method (Table II).

http//dx.doi.org/10.14500/aro.10761

H. Stoichiometry of the Spectrofluorimetric Reaction

The molar ratio procedure was applied to conclude the composition ratio of the fluorescence reaction between valsartan and basic fuchsin was represented as a fluorometric dye. Fig. 7 shows a plot of molar ratio [BF]/[VAL] against ΔF. From this, it was established that the stoichiometry ratio of the valsartan:basic fuchsin complex was 1:1. Correspondingly, the planned mechanism for fluorescence quenching reaction through a construction of a basic fuchsin–valsartan complex was illustrated by Scheme 1.

TABLE II
PRECISION AND ACCURACY FOR THE DETERMINATION OF VALSARTAN VIA BASIC FUCHSIN

Conc. of VAL (µg/mL)	Found Conc. (µg/mL)	Recovery	RSD [a]%
0.5	0.48	94.00	2.58
1.0	1.06	106.0	1.94
3.0	3.08	102.6	1.57

[a]*Average of six determinations*

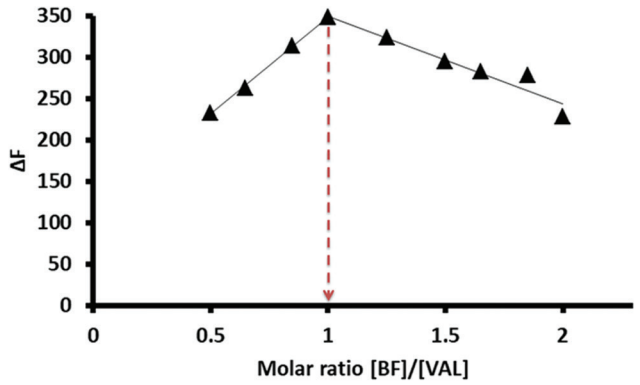

Fig. 7. Molar ratio plot for the stoichiometry of reaction quenching between basic fuchsin and valsartan.

I. The type of Fluorescence Quenching and Effect of Temperature

Often, fluorescence quenching types generally contain dynamic and static modes of quenching. The actual form of quenching process can be described by the Stern–Volmer equation (Lakowicz, 2013):

$$F_0/F = 1 + R_{sv}\,[VAL]$$

F_0 and F are characterized as the intensities of fluorescence of basic fuchsin dye with and without valsartan, respectively; R_{sv} refers to the Stern–Volmer quenching constant; whereas VAL indicate to a valsartan concentration act as the quencher.

The results obtained from the curve of the Stern–Volmer equation in linear form indicates the type of quenching that occurs in single static or dynamic mode, whereas a more curved form indicates a type of quenching that incorporates both static and dynamic modes.

However, the type of quenching cannot be discriminated from a plot of the Stern–Volmer equation, so one of the significant approaches to identifying static and dynamic

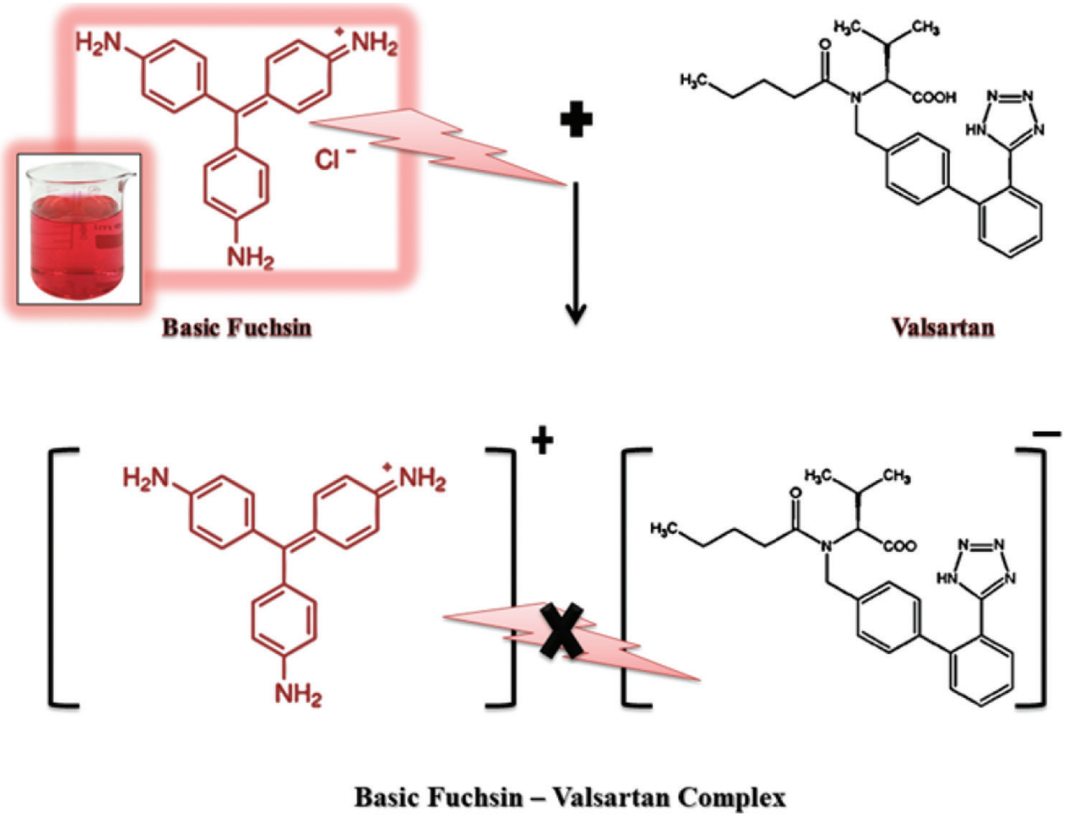

Scheme 1: Schematic illustration of fluorescence quenching of basic fuchsin by valsartan through construction of a basic fuchsin–valsartan complex.

TABLE III
QUANTITATIVE MEASUREMENTS OF VALSARTAN IN COMMERCIAL PHARMACEUTICAL TABLETS THROUGH THE PROPOSED FLUORESCENCE QUENCHING AND A REPORTED HPLC METHOD

Valsartan Brands (160 mg/tablet)	Results from Proposed method	Results from HPLC method[c]	Recovery %	Error %[a]	t and F values[b]
Diovan	162.23	159.36	101.80	1.80	t = 1.15, F = 1.02
Valsartan Awa	164.57	161.11	102.14	2.14	t = 1.76, F = 1.18
Arbiten	161.49	160.27	100.76	0.76	t = 0.94, F = 1.07

[a]Results average were obtained by five determinations. [b]Statistical analysis (t = 2.78, F = 6.39, confidence level = 95% and n = 5). [c]HPLC (Tatar and Saglik 2002)

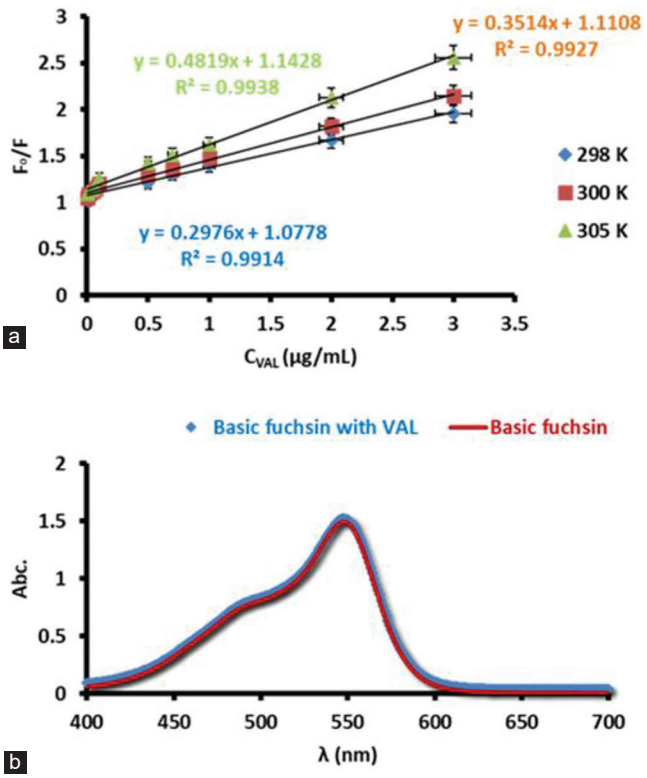

Fig. 8. (a) Stern–Volmer graphs for quenching process at various temperatures (298, 300, and 305 K), basic fuchsin (5 × 10−5 mol/L), McIlvaine buffer solution (pH 6). (b) Influence of valsartan (1 µg/mL) on UV absorption spectra of basic fuchsin (5 × 10−5 mol/L), McIlvaine buffer solution (pH 6).

modes comes from the study of the effect of temperature and the assessment of quenching constant values (R_{sv}). For the dynamic mode, the values of R_{sv} are improved with an enhanced quenching reaction temperature, whereas for the static mode the opposite influence was detected (Lakowicz, 2013).

The R_{sv} constants at three temperatures (298, 300, and 305 K) are presented in Fig. 8a. The linear function of F_0/F against [VAL] showed whether a quenching mode was dynamic or static through a single process. Fig. 8a shows that the values of R_{sv} were increased with increasing reaction temperature, demonstrating the probable fluorescence mechanism of basic fuchsin through valsartan was taking place via a dynamic quenching process.

The validation of a dynamic quenching process was establishing by the ultraviolet (UV) spectra of basic fuchsin in the presence of valsartan as a quenching reagent (Fig. 8b).

For the dynamic mode, there were no observed changes to the UV spectra of basic fuchsin dye with or without valsartan at pH 6 (Gong and Zhu, 2013).

The investigation proved that there was practically no change between the absorption spectra of basic fuchsin fluorescence dye alone and that of basic fuchsin in combination with valsartan. From this study, it can be construed that the fluorescence quenching of basic fuchsin fluorescence dye introduced using valsartan is dynamic in nature.

TABLE IV
QUANTITATIVE MEASUREMENTS OF VALSARTAN IN SPIKED SERUM AND URINE SAMPLES USING THE PROPOSED FLUORESCENCE QUENCHING METHOD

Sample	VAL spiked (µg/mL)	VAL found (µg/mL)	Recovery (%)[b]	RSD (%)
Serum	0.0	N.D[a]	–	–
	0.5	0.52	104.00	3.67
	1.0	1.06	106.00	2.26
	3.0	3.17	105.66	1.79
Urine	0.0	N.D	–	–
	0.5	0.54	108.00	3.84
	1.0	0.97	97.000	2.94
	3.0	3.23	107.66	2.13

[a]ND: No determined. [b]The average value from five measurements

J. Application of the Fluorescence Quenching Method

A fluorescence quenching method through basic fuchsin as a fluorometric dye was effectively utilized to determine valsartan concentrations in various pharmaceutical products. To validate the suggested procedure, a data listed in Table III were compared with those gained by a reference HPLC method (Tatar and Saglik, 2002), and the comparison data were analyzed using statically theoretical factors (t test and F test), where these data indicate good agreement with the reference method.

The proposed quenching procedure was also applied to the detection of valsartan concentrations in spiked serum and urine samples (Table IV) with a very good recovery percentage range (97−108%).

Table V compares valsartan drug concentrations determined in various samples in this proposed approach with those reported from the previous approaches. Compared with classical analytical approaches, the method advocated here is simple, takes very little time, and is of very low cost for an analytical system, and which returns very good precision and accuracy.

TABLE V
COMPARISON OF THE PROPOSED METHOD WITH OTHER PREVIOUS ANALYTICAL METHODS FOR VALSARTAN DETERMINATION

Analytical Method	DL (µg/mL)	QL (µg/mL)	REF.
HPLC[a]	1.0	-	(Carlucci, Carlo and Mazzeo, 2000)
HPLC	0.0148	0.0449	(Kumar, et al. 2015)
LC–MS/MS[b]	0.005	-	(Shah, et al. 2017)
LC–ESIMS/ MS[c]	0.0005	0.001	(Gadepalli, et al. 2014)
HPLC	-	0.098	(Macek, Klima, and Ptacek 2006)
HPLC	0.001	0.003	(del Rosario Brunetto, et al. 2009)
SB-DLLME–HPLC–DAD[d]	0.0003	0.001	(Farajzadeh, Khorram, and Pazhohan, 2016)
HPLC–UV	0.15	0.50	(Ibrahim, et al., 2018)
HPLC–UV	8.01	24.2	(Shaikh, et al., 2020)
HPLC–UV	0.053	0.16	(Marghany, et al., 2020)
UV Spectrophotometry	0.51	1.70	(Satana, et al., 2001)
Ratio derivative spectrophotometry	0.628	2.09	(Dinc, Uslu, and Özkan 2004)
Spectrofluorimetric	0.40	0.50	(Cagigal, et al., 2001)
Spectrofluorimetric	0.001	0.004	(Shaalan and Belal, 2010)
Spectrofluorimetric	0.002	0.005	(El-Shaboury, et al., 2012)
Spectrofluorimetric	0.004	0.013	(El-Kosasy, et al., 2015)
First derivative fluorimetry (D1)	0.0435	0.1318	(Ragab, et al., 2017)
Direct Spectrofluorimetric	0.0442	0.1339	(Ragab, et al., 2017)
First Derivative Synchronous Spectrofluorimetric	0.027	0.083	(Shalan, El-Enany and Belal, 2015)
Voltammetry	0.0033	0.01002	(Ragab, et al., 2019)
Fluorescence Quenching	0.0009	0.0028	This work

[a]HPLC: High-performance liquid chromatography. [b]LC–MS/MS: Liquid chromatography–tandem mass spectrometry. [c]LC–ESIMS/MS: Liquid chromatography–electro spray ionization/tandem mass spectrometry. [d]SB-DLLME–HPLC–DAD: Solid based-disperser liquid–liquid micro-extraction–high-performance liquid chromatography–diode array detector

IV. Conclusion

In this research, a newly advanced fluorescence quenching procedure using basic fuchsin as a fluorescence dye was devised and confirmed for the determination of valsartan. The interaction of the valsartan with basic fuchsin resulted in the production of an ion-associated complex related to the quenching of basic fuchsin fluorescence dye using a dynamic quenching mode. By the utilize of optimized model for studding the essential empirical variables, to acquire experimental results and assessment valsartan recovery value. Furthermore, the significant benefits of the new quenching method are that it is sensitive, simple, cheap, and fast, permitting the effective determination of valsartan at a parts-per-million concentration with a DL of 0.0009 and QL 0.0028 (µg/mL). An advanced procedure was employed for the quantitative measurement of valsartan in various brands of medical tablets, with a very good recovery percentage of between of 100.76 and 102.14, without any significant interference from common tablet excipients. Further, this fluorescence quenching method was applied to determine the concentration of valsartan in spiked human serum and urine samples. Hence, the results suggest that basic fuchsin could act as an efficiently type of a fluorometric dye for applications in clinical and pharmacological fields.

Acknowledgment

This research has been supported by Koya University, Science and Health Research Center, Faculty of Science and Health, and by Chemistry Department. The author wish to acknowledge and appreciate to “Dr Mark Watkins,” University of Leicester, for English language editing and proofreading this article.

References

Annadi, A.M., El Sheikh, R. and Mohamed, A.A., 2019. Development and validation of a LC-MS/MS method for the determination of valsartan in human plasma after protein precipitation or liquid-liquid extraction. *Analytical Chemistry Letters*, 9(4), pp.504-517.

Azadi, A. and Ahmadi, S., 2019. Simultaneous magnetic dispersive micro solid phase extraction of valsartan and atorvastatin using a CMC-coated Fe_3O_4 nanocomposite prior to HPLC-UV detection: Multivariate optimization. *New Journal of Chemistry*, 43, pp.16950-16959.

Babarahimi, V., Talebpour, Z., Haghighi, F., Adib, N. and Vahidi, H., 2018. Validated determination of losartan and valsartan in human plasma by stir bar sorptive extraction based on acrylate monolithic polymer, liquid chromatographic analysis and experimental design methodology. *Journal of Pharmaceutical and Biomedical Analysis*, 153, pp.204-213.

Cagigal, E., Gonzalez, L., Alonso, R.M. and Jimenez, R.M., 200. Experimental design methodologies to optimise the spectrofluorimetric determination of Losartan and Valsartan in human urine. *Talanta*, 54(6), pp.1121-33.

Carlucci, G., Carlo, V.D. and Mazzeo, P., 2000. Simultaneous determination of valsartan and hydrochlorothiazide in tablets by high-performance liquid chromatography. *Analytical Letters*, 33(12), pp.2491-2500.

del Rosario Brunetto, M., Contreras, Y., Clavijo, S., Torres, D., Delgado, Y., Ovalles, F., Ayala, C., Gallignani, M., Estela, J.M. and Martin, V.C., 2009. Determination of losartan, telmisartan, and valsartan by direct injection of human urine into a column-switching liquid chromatographic system with fluorescence detection. *Journal of Pharmaceutical and Biomedical Analysis*, 50(2), pp.194-199.

Dinc, E., Ertekin, Z.C. and Buker, E., 2017. Multiway analysis methods applied to the fluorescence excitation-emission dataset for the simultaneous quantification of valsartan and amlodipine in tablets. *Spectrochimica Acta Part A: Molecular and Biomolecular Spectroscopy*, 184, pp.255-261.

Dinc, E., Uslu, B. and Özkan, S.A., 2004. Spectral resolution of a binary mixture containing valsartan and hydrochlorothiazide in tablets by ratio spectra derivative and inverse least square techniques. *Analytical Letters*, 37(4), pp.679-693.

Eisele, A.P.P., Mansano, G.R., de Oliveira, F.M., Casarin, J., Tarley, C.R.T. and Sartori, E.R., 2014. Simultaneous determination of hydrochlorothiazide and valsartan in combined dosage forms: Electroanalytical performance of cathodically pretreated boron-doped diamond electrode. *Journal of Electroanalytical Chemistry*, 732, pp.46-52.

Eissa, M.S. and Abou Al Alamein, A.M., 2018. Innovative spectrophotometric methods for simultaneous estimation of the novel two-drug combination: sacubitril/valsartan through two manipulation approaches and a comparative statistical study. *Spectrochimica Acta Part A: Molecular and Biomolecular Spectroscopy*, 193, pp.365-374.

El-Kosasy, A.M., Tawakkol, S.M., Ayad, M.F. and Sheta, A.I., 2015. New methods for amlodipine and valsartan native spectrofluorimetric determination, with factors optimization study. *Talanta*, 143, pp. 402-413.

El-Shaboury, S.R., Hussein, S.A., Mohamed, N.A. and El-Sutohy, M.M., 2012. Spectrofluorimetric method for determination of some angiotensin II receptor antagonists. *Journal of Pharmaceutical Analysis*, 2(1), pp.12-18.

Erk, N., 2002. Spectrophotometric analysis of valsartan and hydrochlorothiazide. *Analytical Letters*, 35(2), pp.283-302.

Farajzadeh, M.A., Khorram, P. and Pazhohan, A., 2016. Simultaneous determination of atorvastatin and valsartan in human plasma by solid-based disperser liquid-liquid microextraction followed by high-performance liquid chromatography-diode array detection. *Journal of Chromatography B*, 1017, pp.62-69.

Gadepalli, S.G., Deme, P., Kuncha, M. and Sistla, R., 2014. Simultaneous determination of amlodipine, valsartan and hydrochlorothiazide by LC–ESI-MS/MS and its application to pharmacokinetics in rats. *Journal of Pharmaceutical Analysis*, 4(6), pp.399-406.

Gong, A.Q. and Zhu, X.S. 2013. Determination of epristeride by its quenching effect on the fluorescence of L-tryptophan. *Journal of Pharmaceutical Analysis*, 3(6), pp.415-420.

Graham, J.P., Rauf, M.A., Hisaindee, S. and Alzamly, A., 2017. Spectral behavior and computational studies of fuchsin in various solvents. *Journal of Molecular Liquids*, 238, pp.193-197.

Ibrahim, F.A., El-Brashy, A.M., El-Awady, M.I. and Abdallah, N.A., 2018. Fast simultaneous quantitation of valsartan and amlodipine besylate using an eco-friendly micellar HPLC-UV method: Application to spiked human plasma and content uniformity testing for amlodipine. *Analytical Methods*, 10(43), pp.5227-5235.

Kaabipour, M., Khodadoust, S. and Zeraatpisheh, F. 2020. Preparation of magnetic molecularly imprinted polymer for dispersive solid-phase extraction of valsartan and its determination by high-performance liquid chromatography: Box-Behnken design. *Journal of Separation Science*, 43, pp.912-919.

Kamal, A.H., Marie, A.A. and Hammad, S.F., 2020. Validated spectrophotometric methods for simultaneous determination of nebivolol hydrochloride and valsartan in their tablet. *Microchemical Journal*, 155, p.104741.

Koseki, N., Kawashita, H., Hara, H., Niina, M., Tanaka, M., Kawai, R., Nagae, Y. and Masuda, N., 2007. Development and validation of a method for quantitative determination of valsartan in human plasma by liquid chromatography-tandem mass spectrometry. *Journal of Pharmaceutical and Biomedical Analysis*, 43(5), pp.1769-1774.

Krishnaiah, C., Reddy, A.R., Kumar, R. and Mukkanti, K., 2010. Stability-indicating UPLC method for determination of Valsartan and their degradation products in active pharmaceutical ingredient and pharmaceutical dosage forms. *Journal of Pharmaceutical and Biomedical Analysis*, 53(3), pp.483-489.

Kumar, L., Sreenivasa Reddy, M., Managuli, R.S. and Pai, K.G., 2015. Full factorial design for optimization, development and validation of HPLC method to determine valsartan in nanoparticles. *Saudi Pharmaceutical Journal*, 23(5), pp.549-555.

Lakowicz, J.R. 2013. *Principles of Fluorescence Spectroscopy*. Springer Science and Business Media, Berlin, Germany.

Lotfy, H.M., Hegazy, M.A., Mowaka, S. and Mohamed, E.H., 2015. Novel spectrophotometric methods for simultaneous determination of amlodipine, valsartan and hydrochlorothiazide in their ternary mixture. *Spectrochimica Acta Part A: Molecular and Biomolecular Spectroscopy*, 140, pp.495-508.

Macek, J., Klima, J. and Ptacek, P., 2006. Rapid determination of valsartan in human plasma by protein precipitation and high-performance liquid chromatography. *Journal of Chromatography B*, 832(1), pp.169-172.

Mansano, G.R., Eisele, A.P.P., Dall'Antonia, L.H., Afonso, S. and Sartori, E.R., 2015. Electroanalytical application of a boron-doped diamond electrode: Improving the simultaneous voltammetric determination of amlodipine and valsartan in urine and combined dosage forms. *Journal of Electroanalytical Chemistry*, 738, pp.188-194.

Marghany, K.A., Abdelsalam, R.A. and Haddad, G.M., 2020. HPLC method transfer study for simultaneous determination of seven angiotensin II receptor blockers. *Journal of Separation Science*, 43, pp.1398-1405.

Meselhy, E.M., Aboul Kheir, A.A., El Henawee, M.M. and Elmasry, M.S., 2020. Simultaneous determination of Nebivolol hydrochloride and Valsartan in their binary mixture using different validated spectrophotometric methods. *Spectrochimica Acta Part A: Molecular and Biomolecular Spectroscopy*, 230, pp.118083.

Moussa, B.A., Hashem, H.M.A., Mahrouse, M.A. and Mahmoud, S.T., 2018. A validated RP-HPLC method for the determination of rosuvastatin in presence of sacubitril/valsartan in rat plasma: Application to *in vivo* evaluation of OATP-mediated drug interaction potential between rosuvastatin and sacubitril/valsartan. *Microchemical Journal*, 143, pp.31-38.

Ning, J., Wang, M., Luo, X., Hu, Q., Hou, R., Chen, W., Chen, D., Wang, J. and Liu, J., 2018. SiO_2 stabilized magnetic nanoparticles as a highly effective catalyst for the degradation of basic fuchsin in industrial dye wastewaters. *Molecules*, 23(10), pp.2573.

Pathrose, B., Nampoori, V.P.N., Radhakrishnan, P., Sahira, H. and Mujeeb, A., 2016. Effect of femtosecond laser ablated silver nanoparticles in the thermo-optic properties of basic fuchsin dye. *Optik*, 127(7), pp.3684-3687.

Pathrose, B., Nampoori, V.P., Radhakrishnan, P. and Mujeeb, A., 2014. Measurement of absolute fluorescence quantum yield of basic fuchsin solution using a dual-beam thermal lens technique. *Journal of Fluorescence*, 24(3), pp.895-898.

Pathrose, B., Sahira, H., Nampoori, V.P., Radhakrishnan, P. and Mujeeb, A., 2014. Variations in fluorescence quantum yield of Basic Fuchsin with silver nanoparticles prepared by femtosecond laser ablation. *Spectrochimica Acta Part A: Molecular and Biomolecular Spectroscopy*, 128, pp.522-526.

Pebdani, A.A., Dadfarnia, S., Shabani, A.M.H., Khodadoust, S. and Haghgoo, S., 2016. Application of modified stir bar with nickel: Zinc sulphide nanoparticles loaded on activated carbon as a sorbent for preconcentration of losartan and valsartan and their determination by high performance liquid chromatography. *Journal of Chromatography A*, 1437, pp.15-24.

Qader, A., Salih, M., Tahir, T., 2018. Quantitativ e Quenching of Fluorescein Based Method for Determination of Valsartan in Some Pharmaceutical Product. In: Proceeding of the 2018 International Conference on Pure and Applied Science, Koya University, 23-24 April 2018. Available from: http://www.conferences.koyauniversity.org/index.php/pas/2018/paper/view/92>. [Last accessed on 2020 Oct 10].

Ragab, M.A.A., Galal, S.M., Korany, M.A. and Ahmed, A.R., 2017. First derivative emission spectrofluorimetric method for the determination of LCZ696, a newly approved FDA supramolecular complex of valsartan and sacubitril in tablets. *Luminescence*, 32(8), pp.1417-1425.

Ragab, M.A.A., Korany, M.A., Galal, S.M. and Ahmed, A.R., 2019. Voltammetric study of valsartan-Ni complex: Application to valsartan analysis in pharmaceuticals and in vivo human urine profiling. *Chemical Papers*, 73(5), pp.1209-1219.

Satana, E., Altinay, S., Goger, N.G., Ozkan, S.A. and Senturk, Z., 2001.

Simultaneous determination of valsartan and hydrochlorothiazide in tablets by first-derivative ultraviolet spectrophotometry and LC. *Journal of Pharmaceutical and Biomedical Analysis*, 25(5-6), pp.1009-1013.

Selvan, P.S., Gowda, K.V., Mandal, U., Solomon, W.D. and Pal, T.K., 2007. Simultaneous determination of fixed dose combination of nebivolol and valsartan in human plasma by liquid chromatographic-tandem mass spectrometry and its application to pharmacokinetic study. *Journal of Chromatography B*, 858(1-2), pp.143-150.

Shaalan, R.A. and Belal, T.S., 2010. Simultaneous spectrofluorimetric determination of amlodipine besylate and valsartan in their combined tablets. *Drug Testing and Analysis*, 2(10), pp.489-493.

Shah, J.V., Parekh, J.M., Shah, P.A., Shah, P.V., Sanyal, M. and Shrivastav, P.S., 2017. Application of an LC–MS/MS method for the analysis of amlodipine, valsartan and hydrochlorothiazide in polypill for a bioequivalence study. *Journal of Pharmaceutical Analysis*, 7(5), pp.309-316.

Shaikh, J.S.A., Raut, S., Abdul, A. and Pathan, M., 2020. High performance liquid chromatographic assay of amlodipine, valsartan and hydrochlorothiazide simultaneously and its application to pharmaceuticals, urine and plasma analysis. *Journal of Chromatography B*, 1155, pp.122295.

Shalan, S., El-Enany, N. and Belal, F., 2015. Simultaneous determination of amlodipine besylate and valsartan using a micelle-enhanced first derivative synchronous spectrofluorimetric method and application in their co-formulated tablets. *Analytical Methods*, 7(19), pp.8060-8068.

Tatar, S. and Saglik, S., 2002. Comparison of UV-and second derivative-spectrophotometric and LC methods for the determination of valsartan in pharmaceutical formulation. *Journal of Pharmaceutical and Biomedical Analysis*, 30(2), pp.371-375.

Vojta, J., Jedlicka, A., Coufal, P. and Janeckova, L., 2015. A new, rapid, stability-indicating UPLC method for separation and determination of impurities in amlodipine besylate, valsartan and hydrochlorothiazide in their combined tablet dosage form. *Journal of Pharmaceutical and Biomedical Analysis*, 109, pp.36-44.

General Information

ARO's Mission: ARO seeks to publish those papers that are most influential in their fields or across fields and that will significantly advance scientific understanding. Selected papers should present novel and broadly important data, syntheses, or concepts. They should merit the recognition by the scientific community and general public provided by publication in ARO, beyond that provided by specialty journals.

We welcome submissions from all fields of natural science and technology, and from any source. We are committed to the prompt evaluation and publication of submitted papers. ARO is published biannually; selected papers are published online ahead of print.

Submission

Manuscripts should be submitted by the correspondent authors of the manuscript via the on-line submission page. Regardless of the source of the word-processing tool, only electronic Word (.doc, .docx, .rtf) files can be submitted on-line. There is no page limit. Only online submissions are accepted to facilitate rapid publication and minimize administrative costs. Submissions by any other one but the authors will not be accepted. The submitting author takes responsibility for the paper during submission and peer review. If for some technical reason submission through the email is not possible, the author can contact aro.journal@koyauniversity.org for support. Before submitting please check ARO's guide to authors thoroughly to avoid any delay in the review and publication process.

Authors are explicitly responsible for the language of their texts. Paper should be submitted in a well written in understandable English. Authors should not expect the editor or editorial board to rewrite their paper. Prior to submission, authors should have their paper proofread by a possible academic native speaker of English.

- Submit the Article with contact Information
- File name should be your article tittle
- Don't submit your article in multiple journal, we are taking only minimum time for review process. please don't waste our time
- Once the paper is accepted, it can't be withdrawn
- Please follow publication ethics and regulation
- Avoid plagiarism and copied material
- Strictly Follow ARO's Template

Terms of Submission

Papers must be submitted on the understanding that they have not been published elsewhere and are not currently under consideration by another journal or any other publisher. ARO accepts original articles with novel impacts only. Post conference papers are not accepted "as is", however, regular papers on the same topic but with a different title can be submitted. The new paper should contain significant improvements in terms of extended content, analysis, comparisons with popular methods, results, figures, comments, etc. Please do not forget that the publication of the same or similar material in ARO constitutes the grounds for filing of an (auto) plagiarism case.

The submitting author is responsible for ensuring that the article's publication has been approved by all the other co-authors. It is also the authors' responsibility to ensure that the articles emanating from a particular institution are submitted with the approval of the necessary institution. Only an acknowledgement from the editorial office officially establishes the date of receipt. Further correspondence and proofs will be sent to the author(s) before publication unless otherwise indicated. It is a condition of submission of a paper that the authors permit editing of the paper for readability. All enquiries concerning the publication of accepted papers should be addressed to aro.journal@koyauniversity.org.

Peer Review

All manuscripts are subject to peer review and are expected to meet standards of academic excellence. Submissions will be considered by an editor and "if not rejected right away" by peer-reviewers, whose identities will remain anonymous to the authors.

Guide to Author

We welcome submissions from all fields of science and from any source. We are committed to the prompt evaluation and publication of submitted papers. Selected papers are published online ahead of print. Authors are encouraged to read the instructions below before submitting their manuscripts. This section arranged into an overview speedy guidelines below and more detailed at the bottom section of this page

Manuscript Preparation

Submitting your manuscript will be in two stages namely before final acceptance and after.

Stage one:

At the first stage manuscript needs to be prepared electronically and submitted online via the online submission page in a Word (.doc, .docx, .rtf) format of one column double-spaced page, Times New Roman font type, and 12 p font size. A pdf version of the submitted manuscript should be submitted too. All authors' names, affiliations, e-mail addresses, and mobile phone numbers should be typed on a cover page, indicating the correspondent author.

Stage two:

- File type: MS-Word version 2003 or later.
- Format: The preferred format of the manuscript two-column template with figures and captions included in the text. This template can be downloaded via the following link. Please follow instructions given in the template; http://aro.koyauniversity.org/about/submissions#onlineSubmissions
- Text: All text is in Times New Roman font. The main text is 10-point, abstract is 9-point font and tables, references and captions are 8-point font.
- Figures: Figures should be easily viewed on a computer screen.

Units of Measurement

Units of measurement should be presented simply and concisely using System International (SI) units.

Title and Authorship Information

The following information should be included;

- Paper title.
- Full author names.
- Affiliation.
- Email addresses.

Abstract

The manuscript should contain an abstract. The abstract should be self-contained and citation-free and should not exceed 200 words.

Introduction

This section should be succinct, with no subheadings.

Materials and Methods

This part should contain sufficient detail so that all procedures can be repeated. It can be divided into subsections if several methods are described.

Results and Discussion

This section may each be divided by subheadings or may be combined.

Conclusions

This should clearly explain the main conclusions of the work highlighting its importance and relevance.

Acknowledgements

All acknowledgements (if any) should be included at the very end of the paper before the references and may include supporting grants, presentations, and so forth.

References

References must be included in the manuscript and authors are responsible for the accuracy of references. Manuscripts without them will be returned. ARO is following Harvard System of Referencing. (Learn how to import and use Harvard Styling in your Microsoft Office by following this link:
http://bibword.codeplex.com/releases/view/15852)

Preparation of Figures

Upon submission of an article, authors are supposed to include all figures and tables in the PDF file of the manuscript. Figures and tables should be embedded in the manuscript. Figures should be supplied in either vector art formats (Illustrator, EPS, WMF, FreeHand, CorelDraw, PowerPoint, Excel, etc.) or bitmap formats (Photoshop, TIFF, GIF, JPEG, etc.). Bitmap images should be of 300 dpi resolution at least unless the resolution is intentionally set to a lower level for scientific reasons. If a bitmap image has labels, the image and labels should be embedded in separate layers.

Preparation of Tables

Tables should be cited consecutively in the text. Every table must have a descriptive title and if numerical measurements are given, the units should be included in the column heading. Vertical rules should not be used.

Copyright

ARO Reviewer/Associate Editor Application Form

ARO is a scientific journal of Koya University (p-ISSN: 2410-9355, e-ISSN: 2307-549X) which aims to offer a novel contribution to the study of Science. The purpose of ARO is twofold: first, it will aim to become an ongoing forum for debate and discussion across the sciences and Engineering. We hope to advance our problem solving capacity and deepen our knowledge regarding a comprehensive range of collective actions. Second, ARO accepts the challenges brought about by multidisciplinary scientific areas and aspires to expand the community of academics who are able to learn from and help to produce advances in a variety of different disciplines.

The Journal is seeking reviewers who can provide constructive analysis of papers thus enhancing overall reputation of the Journal. If any expert is interested in participating of the review process, we highly encourage you to sign up as a reviewer for our Journal and help us improve our presence in domain of your expertise. Appropriate selection of reviewers who have expertise and interest in the domain relevant to each manuscript are essential elements that ensure a timely, productive peer review process. We require proficiency in English.

How to apply

To apply for becoming a reviewer of ARO, please submit the application form by following the link:
http://aro.koyauniversity.org/user/register
To apply for becoming a member of the Editorial Board of ARO, please submit the application form by following the link: http://aro.koyauniversity.org/pages/view/AEB

Both Associate Editor and Reviewers should specify their areas of research and expertise. Applicants must have a doctorate (or an equivalent degree), and if Master degree they need to have significant publishing experience. Please note that;

- You will need to write your full official name.
- Please provide an email which reflects your official name, such as nameOne.NameTwo@... , or your institute's official email.
- All data need to be written in English.

Note: For more information, kindly visit the following websites:

1. aro.koyauniversity.org.
2. http://libweb.anglia.ac.uk/referencing/harvard.htm.
3. http://bibword.codeplex.com/releases/view/15852.

INDEXING


THOMSON REUTERS
Emerging Sources Citation Index
WEB OF SCIENCE™


Crossref


OCLC
WorldCat


PRESERVED IN
LOCKSS


INDEXED IN
DOAJ


Google
Scholar


SHERPA
RoMEO


ROAD
DIRECTORY
OF OPEN ACCESS
SCHOLARLY
RESOURCES


ResearchGATE
scientific network

Koya University is a young University established in 2003 and it is located in the city of Koya (Koysinjaq), short distance to the East of regional capital city of Erbil (Arbil, Hewlêr) in Kurdistan Region of Iraq. It is on the foothills of beautiful High Mountain. Its campus has been carefully laid out to embrace the beautiful mountainous nature. The Koya University has a Faculty system which enhances the interactions between similar academic fields. Today, Koya University has four Faculties: Engineering, Science and Health, Humanities and Social Sciences and Education in addition to the School of Medicine, which all consist of twenty-five scientific departments in different fields, such as Petroleum Engineering, Geotechnical Engineering, Software Engineering, Physics, Chemistry, Clinical Psychology, Social Science, Medical Microbiology and Sport Education.

ARO-The Scientific Journal of Koya University is a biannual journal of original scientific research, global news, and commentary in the areas of Science and Technology. ARO is a Peer-reviewed Open Access journal with CC BY-NC-SA 4.0 license. It provides immediate, worldwide and barrier-free access to the full text of research articles without requiring a subscription to the journal, and has no article processing charge (APC). ARO Journal seeks to publish those papers that are most influential in their fields or across fields and that will significantly advance scientific understanding. ARO Journal is a member of ROAD and Crossref agencies and has got ESCI, DOAJ seal, SHERPA/RoMEO deposit policy, and LOCKSS archiving policy.

The Scientific Journal of Koya University

Koya University (KOU)
University Park
Danielle Mitterrand Boulevard
Koya KOY45, Kurdistan Region - Iraq

ISSN: 2410-9355 (printed version) ISSN: 2307-549X (electronic version) ARO - DOI: 10.14500/2307-549X